

Low-variable-speed, continuous-circulating current, cycloconverter-
induction-motor drives.

Abdul-Karim Shams Hamad, M.Phil. (Eng.)

A thesis submitted to the University of Leicester for the
Degree of Doctor of Philosophy.

Department of Engineering,
University of Leicester. 1977.

UMI Number: U433580

All rights reserved

INFORMATION TO ALL USERS

The quality of this reproduction is dependent upon the quality of the copy submitted.

In the unlikely event that the author did not send a complete manuscript and there are missing pages, these will be noted. Also, if material had to be removed, a note will indicate the deletion.



UMI U433580

Published by ProQuest LLC 2015. Copyright in the Dissertation held by the Author.
Microform Edition © ProQuest LLC.

All rights reserved. This work is protected against
unauthorized copying under Title 17, United States Code.



ProQuest LLC
789 East Eisenhower Parkway
P.O. Box 1346
Ann Arbor, MI 48106-1346

THESIS
531069
9 8 77



x753009187

To the memory of my father and to my brother Khazal Shams,
without whose sacrifices my higher education would never
have been possible.

MEMORANDUM

The accompanying thesis, "Low-variable-speed, continuous-circulating current, cycloconverter-induction-motor drives" is submitted in support of an application for the degree of Ph.D. in the University of Leicester.

This work has not been submitted for another Degree in this University, nor for the award of a Degree or Diploma of any other institution. This dissertation is based on studies of the following points.

1. The problems of direct low-frequency operation of an induction motor on sinusoidal and non-sinusoidal supplies.
2. A multi-machine variable-speed drive has been designed in which the stator of an induction motor serves the dual purpose of setting up a rotating field and acting as three inter-group reactors to maintain continuous circulating current in a cycloconverter. The consequent reduction in harmonic content of the cycloconverter output voltage has extended the operating frequency range and permitted regenerative braking without gate pulse circuit modification.
3. The reactive power requirements of the system in regenerative braking have been computed and the effect on cycloconverter design discussed.
4. A small signal perturbation study has been carried out. The system has been shown to be conditionally stable and a method of achieving inherent stability has been suggested.

A.K.S. Hamad,
University of Leicester,
Department of Engineering.
1977.

CONTENTS

Page No.

Memorandum

List of principal symbols

Abstract

1. Introduction	1
2. Low-frequency performance on a sinusoidal supply.	6
3. The effect of harmonics on the low-frequency operation of an induction motor.	22
4. A phase-controlled circulating current cycloconverter-induction- motor drive using a rotating machine as an inter-group reactor.	53
5. Operation of the cycloconverter-induction-motor drive.	74
6. General conclusions.	95
7. Suggestion for future work.	97
8. Acknowledgements	99
9. References.	100
10. Appendices.	114

LIST OF PRINCIPAL SYMBOLS

B	magnetic flux density, (T).
I_1	r.m.s. stator current, A.
I_0	magnetising current, A.
I_2	r.m.s. rotor current referred to stator, A.
I_D	direct stator excitation current, A.
L_1	self-inductance of the stator.
L_2	self-inductance of the rotor.
L_0	mutual inductance.
P_g	induction generator active power, watts.
Q_g	induction generator reactive power, watts.
R_1	stator resistance, Ω /ph of educational machine.
R_2	rotor resistance referred to stator, Ω /ph of educational machine.
R_0	iron loss component of magnetising circuit referred to stator Ω /ph of educational machine.
S	slip = $\frac{(\text{synchronous speed} - \text{actual speed})}{\text{synchronous speed}}$.
S_1	slip of divided winding machine.
S_2	slip of standard machine.
T_e	gross torque, Nm.
T_{e1}	torque of divided winding machine, Nm.
T_{e2}	torque of standard machine, Nm.
V_1	applied stator phase voltage, V.
V_2	primary air-gap voltage, V.
V_m	maximum value of input voltage, V.
V_0	r.m.s. value of fundamental component of cycloconverter output voltage, V.

V_p	positive thyristor group voltage output to load.
V_N	negative thyristor group voltage output to load.
X_1	stator leakage reactance, Ω/ph , 50 Hz value of educational machine.
X_2	rotor leakage reactance referred to stator, Ω/ph , 50 Hz value of educational machine.
X_0	magnetising reactance referred to stator, Ω/ph , 50 Hz value of educational machine.
X_{00}	the combined magnetising reactance of the two machines.
Y	admittance of educational machine.
Z	impedance of educational machine, Ω/ph .
Z_g	impedance of induction generator, Ω/ph .
Z_g^*	conjugate of induction generator impedance.

... continued next page ...

$e(\omega t)$	The inverter output voltage.
f	stator frequency, Hz.
f_o	output frequency, Hz.
f_H	frequency of output voltage harmonic, Hz.
i_1	divided winding machine stator current, A.
i_2	divided winding machine rotor current referred to stator, A.
i	standard machine stator current, A.
k	harmonic order.
m	number of phases.
n	machine speed, rev/sec.
n_s	synchronous speed, rev/sec.
p	number of pole pairs.
r_1	stator resistance, Ω/ph , of the standard squirrel-cage motor.
r_2	rotor resistance referred to stator, Ω/ph , of the standard squirrel-cage motor.
s	the Laplace operator.
x_1	stator leakage reactance, Ω/ph , 50 Hz value of the standard squirrel-cage motor.
x_2	rotor leakage reactance referred to stator, Ω/ph , 50 Hz value of the standard squirrel-cage motor.
x_o	magnetising reactance referred to stator, Ω/ph , 50 Hz value of the standard squirrel-cage motor.

... continued next page ...

$\alpha = \theta_1 - \frac{\pi}{6}$	displaced thyristor firing angle.
α_P	positive thyristor group firing angle, radians.
α_N	negative thyristor group firing angle, radians.
η	efficiency.
$\theta_1 = \omega t_1$	thyristor firing angle.
θ_2	thyristor extinction angle.
ϕ_0	fundamental load current displacement angle.
ψ	magnetic flux-linkage.
ω	input angular frequency rad/sec.
ω_r	slip frequency rad/sec.
ω_2	angular speed of the motor rad/sec.
ω_0	output angular frequency rad/sec.

ABSTRACT

The cycloconverter as a direct frequency converter without a d.c. link is well known as a power amplifier in low speed a.c. drives. If continuous circulating current operation can be maintained, reversible energy flow and regenerative braking can be achieved in an induction motor drive without a change in the gate pulse sequence. Continuous circulating current operation also reduces the output harmonic content of the cycloconverter and increases the speed range of the drive.

This dissertation describes the use of an induction motor stator as an inter-group reactor maintaining continuous circulating current in the cycloconverter. The same stator winding sets up the conventional rotating air gap-flux and the reactor machine has standard torque-speed characteristics.

In the multi-machine drive designed and constructed in this work, one machine requires a special stator winding. Conventional squirrel-cage machines can then be added for tandem speed control and the utilisation of copper improved. Closed-loop speed control and air gap flux control are incorporated on the reactor machine. The standard induction motors added in addition to the reactor machine are shown to be essentially operating under open-loop conditions but a "hard supply" is maintained by closed-loop control.

CHAPTER 1INTRODUCTION

The simplicity and robustness of the squirrel-cage induction motor together with the absence of sliding contacts and slip rings makes it an ideal machine for an a.c. variable-speed drive if stable control can be achieved. A variable-speed drive must be able to operate stably at near constant speed when subjected to step and shock loading. It must also be able to accelerate or brake rapidly. At low speeds, any machine with salient poles will produce a torque which varies in amplitude around the circumference of the machine. This causes the torque to vary as a function of motor speed and rotor position.

A system designer faced with this problem may choose a higher speed of rotation and subsequently reduce the speed to the desired level with a gear box. Direct low-speed drives using synchronous motors with small pole numbers or d.c. motors are rarely used because of torque variation with rotor position.

A squirrel-cage motor with a single low-impedance cage will give good near-synchronous-speed operation, but the starting torque and acceleration are poor if the supply frequency is constant. This problem may be overcome at the expense of efficiency by the use of a double-cage rotor, but even here the torque availability will not be constant at all speeds. For ideal variable-speed operation of a squirrel-cage induction motor, a variable-frequency stator supply which produces a constant air-gap flux at all speeds is required. This is approximately obtained by the use of a variable-frequency supply in which the amplitude of the voltage varies in proportion to the frequency. At low frequencies (<5Hz), the stator voltage will have to be boosted due to the dominant effect of the stator impedance if constant air gap flux is to be maintained.

In a simple frequency converter the non-sinusoidal output introduces time-dependent, harmonics into the motor supply. Each time-harmonic so introduced will generate a further series of space harmonics which will be reduced to an acceptable level by the machine designer. The harmonics introduced into the air-gap flux by the converter will modify the torque characteristic and introduce additional heating and noise in the machine.

A stable motor drive requires a supply free of sub-harmonics and a low-harmonic-content link inverter can approach this performance if pulse-width-modulation or stepped amplitude modulation is used. In general, the d.c. link inverter is a uni-directional energy converter. Regenerative braking in an induction motor drive is only possible if a reverse link is incorporated. The link capacitance tends to make the system oscillatory when sudden changes of load occur.

Reversibility and stability are natural properties of the phase-controlled cycloconverter. Most commercial cycloconverters of any size have operated in the circulating-current-free mode. At least six thyristors per group are used to reduce the output harmonic content and regeneration is achieved by reversing the gate pulse sequence. Even so, the output frequency range is usually limited to about a third of the input frequency.

It is well known that if continuous circulating current operation can be maintained that the harmonic content of the output voltage is reduced and that the number of thyristors per group can be reduced while the same operating frequency range is maintained. Usually continuous circulating current can only be obtained by the use of an inter-group reactor rated for full-load current in each output phase. These reactors are costly and bulky.

In this work the stator of an induction motor is used both to carry out the function of the inter-group reactors and to set up the conventional rotating air-gap field. A double-layer stator winding formed into identical electrically separate thyristor-group circuits, magnetically coupled in the stator slots serves this dual purpose.

The electrically-separate, magnetically-coupled stator windings also prevent line to line short-circuits caused by spurious thyristor firing. They do, however, effectively double the stator impedance and result in a poor utilisation of copper. However, standard squirrel-cage machines can be added to the system for tandem operation and the utilisation improved. Closed-loop speed control with electronic current clamping is incorporated in the experimental system.

Applications of cycloconverter-induction motor drives include crane and hoist drives, mine winders and lifts. For these operations electrical braking is an essential feature. Three types of braking are possible, plugging, d.c. dynamic braking and low-frequency a.c. braking, which may be dynamic or regenerative. Plugging can be discounted because of the excessive currents required and the tendency to run up in the opposite direction of rotation although it is the only way of holding a dead-load stationary. D.c. dynamic braking and low-frequency regenerative a.c. braking were investigated. This d.c. excitation turns the machine into an alternator and the kinetic energy of the system is dissipated in the squirrel-cage rotor causing excessive heating. It is preferable to return the kinetic energy of the rotating machine to the supply by regenerative braking. This is possible in the closed-loop cycloconverter-induction motor system if the velocity feedback system demands the appropriate frequency from the cycloconverter. A selected control signal commands peak braking torque at any speed.

However, regenerative braking can only occur if the lagging vars demanded by the motor are provided externally. This study investigates the var demand on the cycloconverter during regeneration.

The stability of the closed-loop system is investigated qualitatively using a small-signal perturbation model. This indicates that the most stable system may be a velocity feedback system with a feed forward differentiator immediately after cycloconverter reference generator.

Overall, the system proposed is claimed to be simple and relatively economic if a speed range from zero to about a third of 50Hz synchronous speed is required. It is also claimed to be safe if spurious firing occurs and stable. However, if in applications such as diesel-electric traction, a higher-frequency source is used, the output frequency range will be correspondingly increased. The experimental cycloconverter used in this system was fed from a 400 Hz source, giving an output frequency range from zero to 133 Hz. This output range was limited by the maximum available output voltage of 115 V r.m.s. as far as induction motor drive was concerned.

CHAPTER 2Page No.Low-frequency performance on a sinusoidal supply

2.1.	Introduction	6
2.2	A variable-frequency equivalent circuit.	7
2.3	Steady-state performance with parameters assumed constant (50Hz parameters).	9
2.4	Machine parameters variation with frequency.	12
2.4a	Magnetizing parameters.	12
2.4b	Parameters from the locked-rotor test.	14
2.5	Effect of parameter variation on steady-state performance.	15
2.6	Efficiency at low frequency.	15
2.7	Steady-state stability on a low-frequency sinusoidal supply.	16 19
2.8	Conclusions.	

CHAPTER 2

Low-frequency Performance on a Sinusoidal Supply

2.1 INTRODUCTION

A variable speed drive must be able to operate stably at near constant speed when subjected to step and shock loading. At low speeds, any machine with salient poles will produce a torque which varies in amplitude around the circumference of the machine. This may cause jerky motion and cogging which may induce a system designer to choose a higher speed of rotation and to subsequently reduce the speed to the desired level with a gear box. Drives using synchronous motors or d.c. motors are rarely used directly in low speed applications for this reason.

If the effect of the space and time harmonics is insignificant, an induction motor can produce a uniform torque at any rotor position. The speed of rotation will depend directly on the frequency and inversely on the number of poles. If a sinusoidal three-phase, variable-frequency supply is available, a squirrel-cage induction motor can provide a gearless drive at low speeds.

Electronic inverters and frequency converters have inherent problems such as the introduction of harmonics into the motor field and restrictions in reversibility of energy flow. In this study, these problems will be considered in later chapters. First, a study of the problems of induction motor operation on an ideal sinusoidal supply will be made. Open-loop, steady-state performance in a fixed parameter system will be considered first, then the effect of motor parameter variation and finally, the steady state stability at low stator frequencies.

2.2 A variable-frequency equivalent circuit

The advantage of using digital computers to compute the performance of electrical machines has long been established. Computation in this context, simply implies the prediction of machine performance. Much present day analysis is in terms of generalized theory ⁽¹⁾, matrix analysis ⁽²⁾ and eigen value stability determination ⁽³⁾, but this approach is generally used in a linear system analysis, when machines are operating in large systems. This study is mainly concerned with the general effects of parameter variation and the stability of a single machine. Equivalent circuit parameters ⁽⁴⁾ are easy to measure under variable-frequency conditions over a range of current and voltage variations. The equivalent circuit of the induction motor upon which the theory of this chapter is based, is shown in Fig. (2.1a,b). If certain well-known assumptions are made the parameters of this equivalent circuit can be calculated from the results of standard locked-rotor and running-light tests. Inevitably the values of these parameters can only be approximate. If there is a significant current-displacement effect in the secondary ⁽⁵⁾, the so-called "proximity" effect, the secondary parameters may not be considered to be constant for large slip and rotor frequency variations. Brown and Grantham's investigation is concerned with wide frequency variations in the rotor, i.e. large slip changes. This thesis is mainly concerned with stator-frequency change, i.e. small slip operation at all speeds under closed-loop conditions. This means that the rotor frequencies are always small, and changes in rotor parameters have less significance. Hence the total change of parameters are investigated. In the equivalent circuit shown in Fig. (2.1a), there are six parameters to be determined. The primary resistance (R_1), primary leakage reactance (X_1), resistance representing core loss (R_0) and the magnetisation reactance (X_0) all produce reactions at supply frequency and are considered to be constant at any single frequency. R_1 was determined from a separate test (see

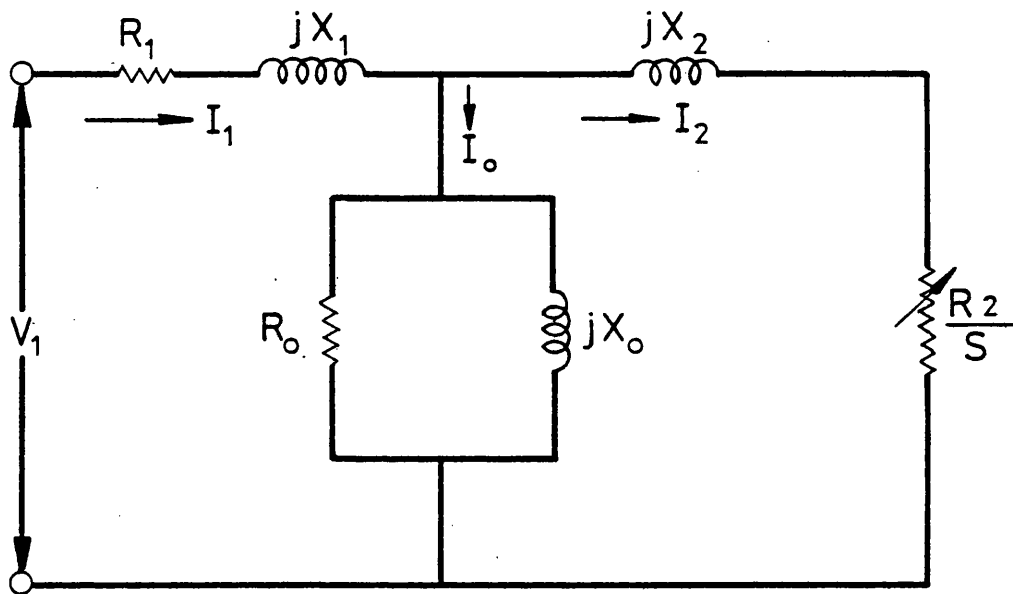


Fig 2.1a Induction motor equivalent circuit

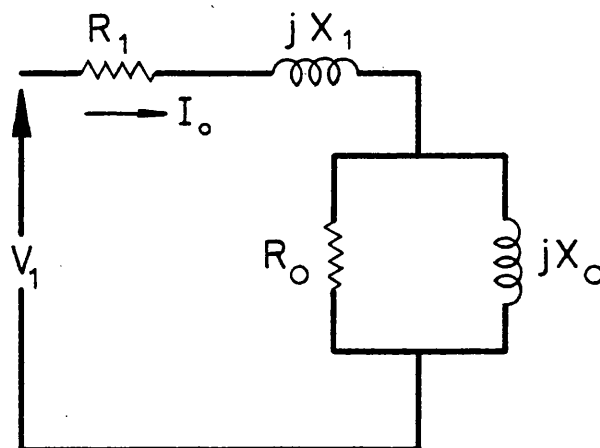


Fig 2.1b. Equivalent circuit of induction motor at synchronous speed.

Appendix A-1), while R_2 , X_1 , X_2 , R_0 and X_0 were calculated from a running-light and locked-rotor ⁽⁶⁾ test. The standard assumption that the leakage reactance is distributed equally between the primary and secondary i.e. ($X_1 = X_2$) was adopted for the purpose of this investigation.

The induction motor equivalent circuit of Fig. (2.2) allows for parameter variation with frequency. This equivalent circuit can be simplified by the use of Thevenin's theorem. $R_0 \gg X_0$ and hence R_0 has been neglected in this analysis. The equivalent circuit of Fig. (2.2) is then simplified to Fig. (2.3). V_{1A} , the equivalent source voltage, is the voltage that would appear across terminals A and B with the rotor circuit open. Hence,

$$V_{1A} = V_1 \frac{jX_0}{R_1 + jX_{11}} , V , \quad (2.1)$$

where $X_{11} = X_1 + X_0$, and is the self-reactance of one stator phase. The Thevenin equivalent stator impedance is the impedance between terminals A and B viewed toward the source with the source voltage short-circuited. ($R' + jX'$) represents this impedance which is ($R_1 + jX_1$) in parallel with jX_0 . The iron loss parameter, R_0 , has been neglected for first order torque calculation.

The torque for a machine with (m) stator phases is,

$$T_e = m \frac{1}{\omega} I_2^2 \frac{R_2}{S} , \quad (2.2)$$

where ω is the synchronous speed in rad/sec. From the Thevenin equivalent circuit, Fig. (2.3), the current I_2 referred to stator at a supply frequency of 50 Hz is

$$I_2 = \frac{V_{1A}}{\left[\left(R' + \frac{R_2}{S} \right)^2 + (X' + X_2)^2 \right]^{\frac{1}{2}}} , A . \quad (2.3)$$

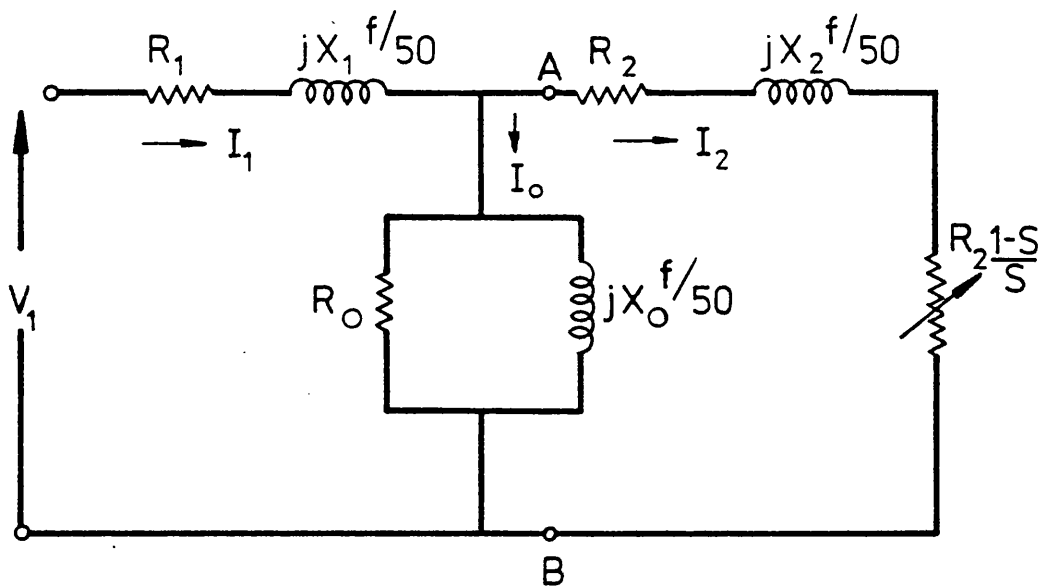


Fig.2.2 Variable-frequency equivalent circuit of induction motor with mechanical power parameter

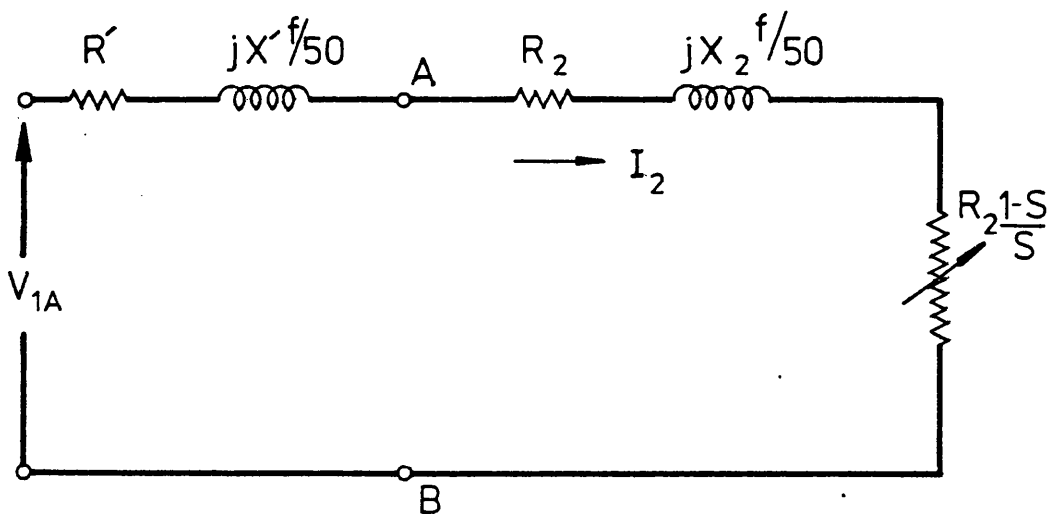


Fig 2.3 Variable - frequency equivalent circuit of induction motor simplified by the use of Thevenin theorem.

From the torque expression given by equation (2.2), substituting for I_2 , from equation (2.3),

$$T_e = \frac{1}{\omega} \frac{mV_{1A}^2 (R_2/S)}{\left[\left(R' + \frac{R_2}{S} \right)^2 + (X' + X_2)^2 \right]} \quad (2.4)$$

Equations (2.3) and (2.4) are used for the computation of steady-state characteristics in section (2.3).

2.3 Steady-state performance with parameters assumed constant (50Hz parameters)

Motor performance was investigated at frequencies from 5 to 50Hz. The machine used in this experimental investigation was a Mawdsley Educational Induction Motor ⁽⁹⁾ with a three-phase, two-pole, full-pitch stator winding in two identical layers with 36 slots, and a squirrel-cage rotor, the determination of the parameters of which is given in Appendix 1. To enable the performance characteristics of the induction motor to be measured, the machine was constrained to rotate at various speeds by means of a d.c. work motor. The work motor was separately excited and supplied from a Ward-Leonard generator as shown in Fig. (2.4). Using the d.c. work motor to control the speed of the induction motor, current and torque measurements were taken over the slip range, $0 < S < 2$. Reduced voltages were used to avoid excessive currents, at high slips and to prevent saturation. The 50Hz parameters were determined by supplying the stator from the mains through a variable transformer. Characteristics at frequencies below 50Hz were obtained with the Experimental Induction Motor fed from a 5KVA variable-frequency alternator as shown in Fig. (2.5). Fig. (2.6) shows measured results contrasted with results predicted from equation (2.3). Considering the assumptions made in deriving the equation, the predicted and measured results correlate well in the motoring region of small slip, although the experimental peak torques are less than the calculated values due to saturation. Large differences

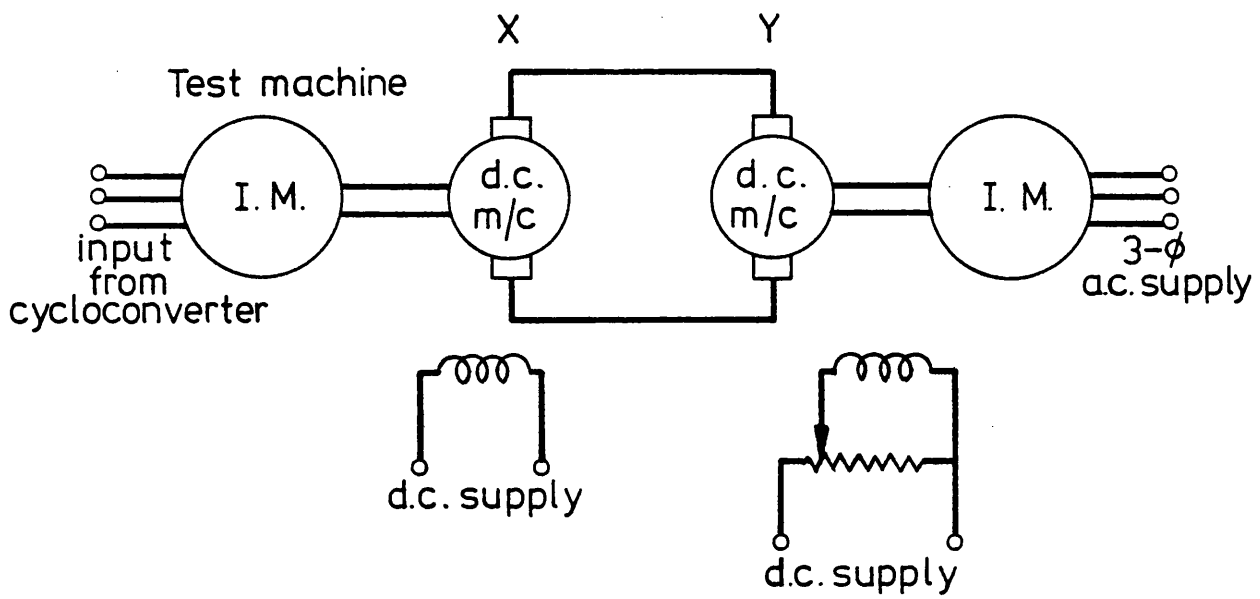


Fig. 2-4 Loading system

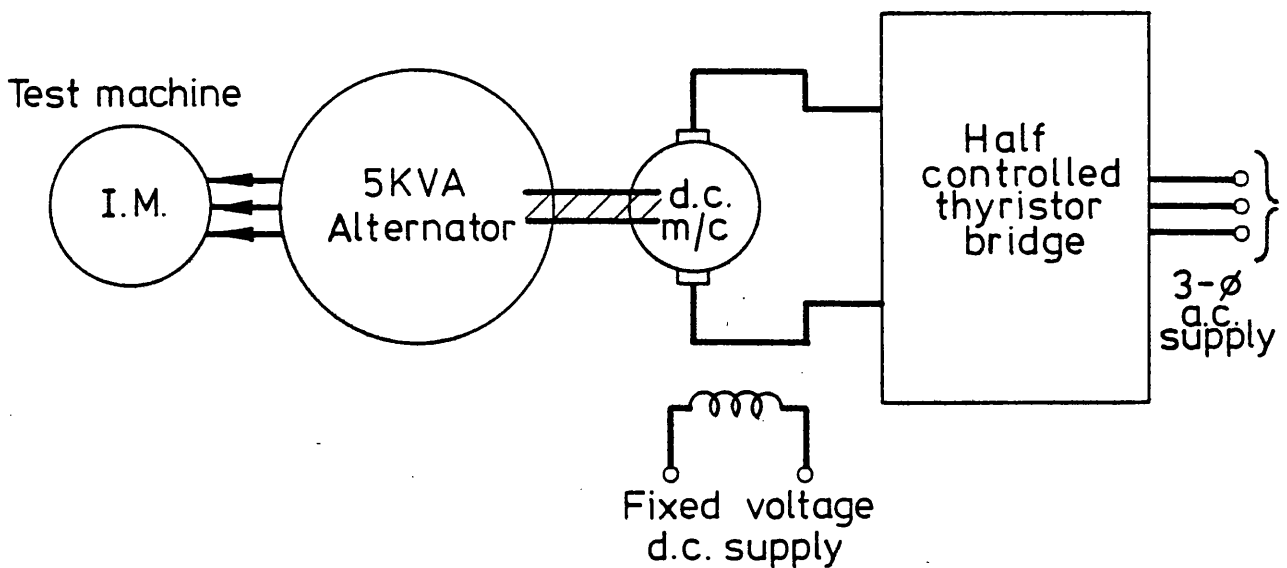


Fig. 2-5 Variable-frequency supply system from 5KVA alternator

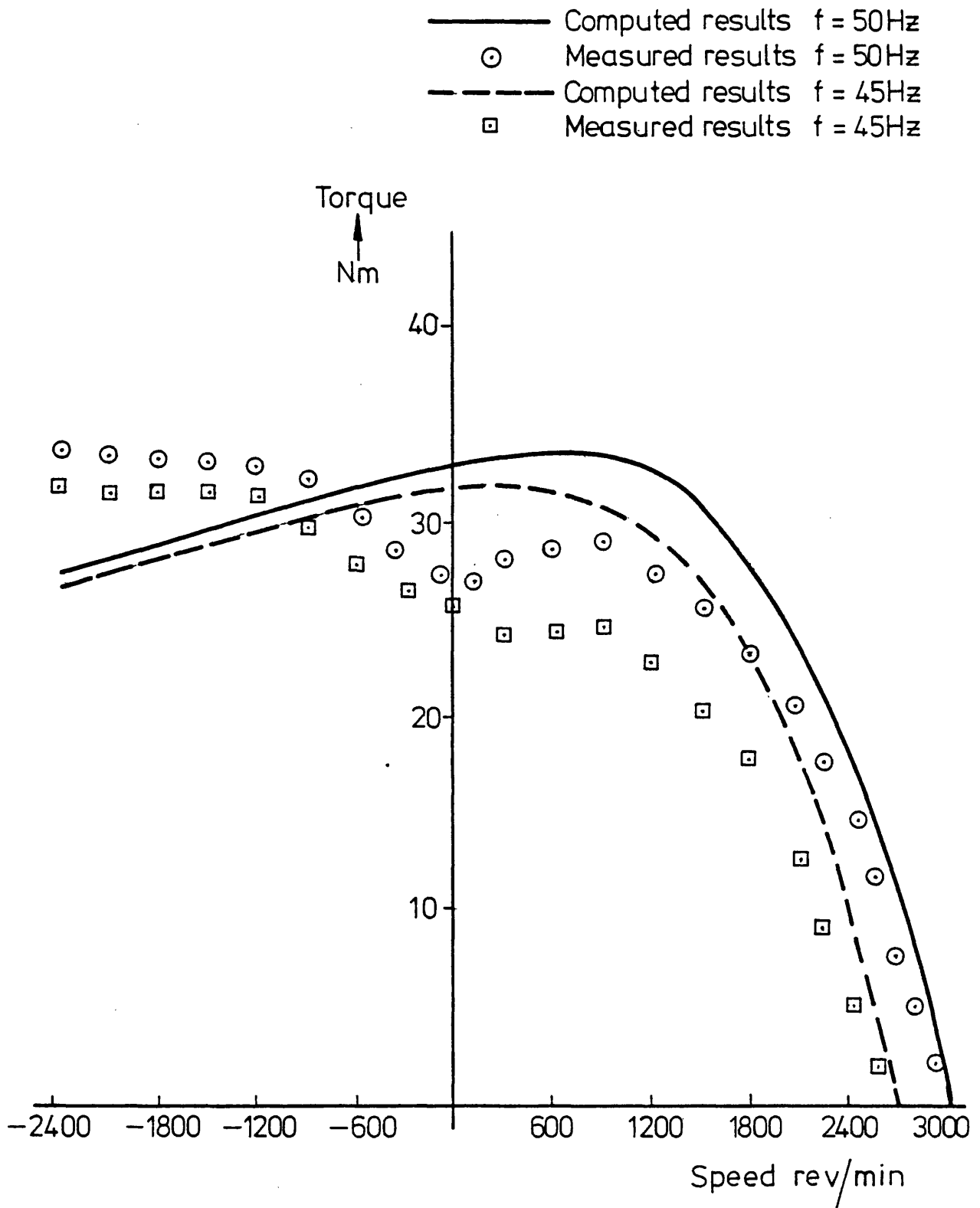


Fig. 2·6 Torque / speed characteristics at 50Hz and 45Hz.

do occur, particularly in the reverse-rotation region. The differences are due to slot-harmonics and stray-load torques ⁽⁷⁾, caused by high-frequency rotor currents at large slips. Stray-load losses make "plugging" a more acceptable form of braking than the theory suggests, but this can only be achieved at the expense of excessive current and energy dissipation.

For constant peak-torque operation of an induction motor with a variable frequency supply, a constant air-gap flux must be maintained at all frequencies. A constant air-gap flux would be obtained in an ideal system with negligible stator impedance when $\frac{V}{f}$ is constant. However, as the frequency falls, the values of leakage reactance fall, but the resistive parameters relating to the machine windings are essentially constant. The ratio of stator impedance voltage drop to the applied voltage increases and the air-gap flux decreases as the stator frequency is reduced. To maintain a constant flux the stator voltage must be increased beyond the value demanded by a simple proportionality with frequency.

The fall in peak torque with frequency when operating with a voltage proportional to frequency is illustrated experimentally and theoretically in Fig. (2.7). Here the 50Hz characteristic was obtained at 100V, just less than half the rated value, to maintain the steady state current at an acceptable level. The lower frequency, chosen as 10 Hz because a stable output from the variable-frequency supply was possible at this frequency, was maintained at a constant voltage of $(10/50 \cdot 100 = 20V$. It can be seen that the dominant effect of the stator resistance causes the peak torque to fall by about two-thirds. If the load torque remains at the 50 Hz value, the machine is operating too near to pull-out torque for stable operation. The problem will be worse at lower frequencies. Theoretical results were computed

- Computed results $f = 50\text{Hz}$
- Measured results $f = 50\text{Hz}$
- - - - Computed results $f = 10\text{Hz}$
- ▽ Measured results $f = 10\text{Hz}$

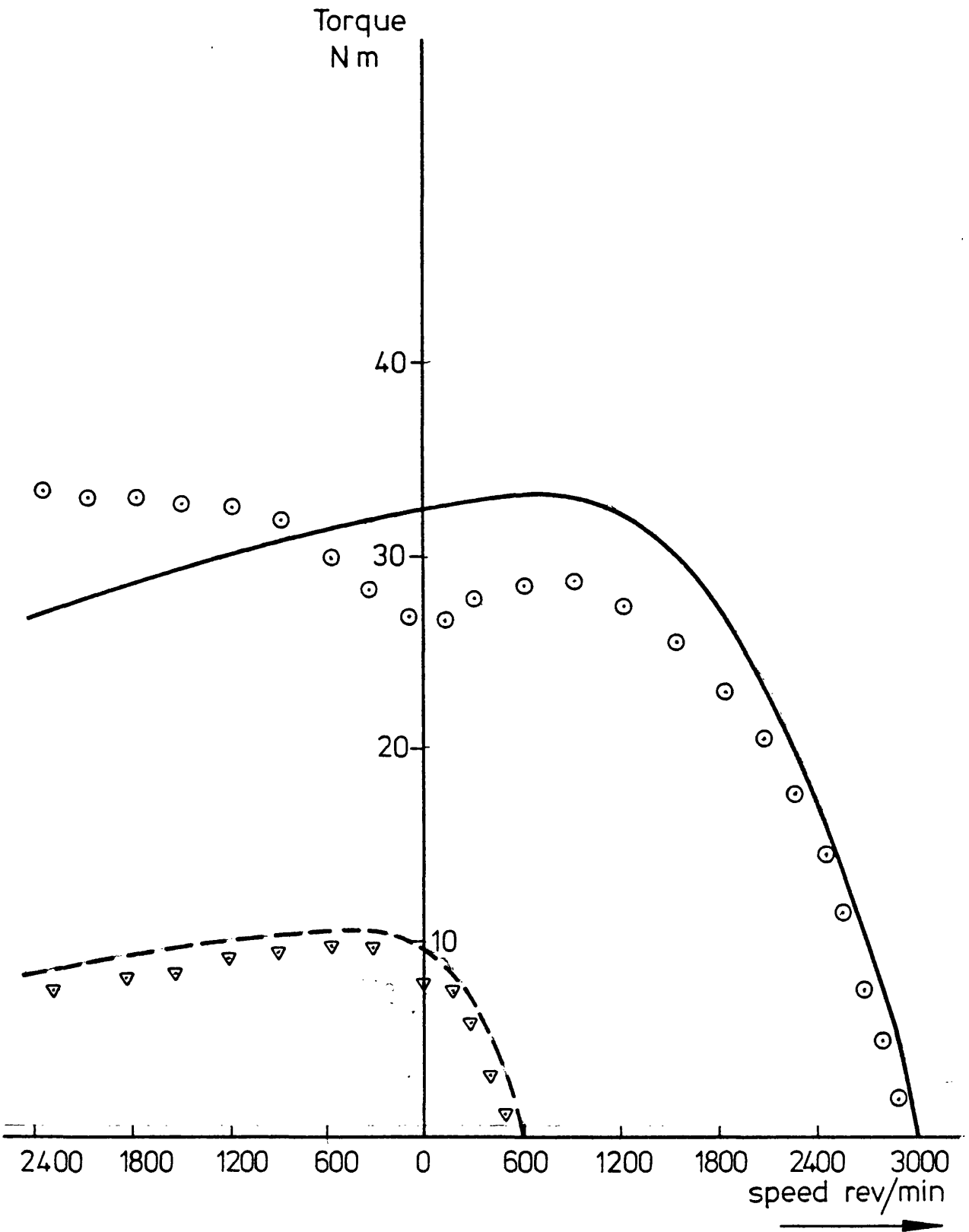


Fig.2.7 Torque/speed characteristics at 50Hz and 10Hz

from equation (2.3). Fig. (2.8) and Fig. (2.9) show calculated and measured torques and currents at 5Hz and 10Hz indicating that equations (2.3) and (2.4) give acceptable first order results. It can also be seen that the increased effect of stator resistance can be useful in limiting current at high slips.

To maintain constant peak torque at low frequencies, the terminal voltage must be increased considerably above its frequency-proportional value. It was not possible to achieve this electromechanically due to the effect of the alternator armature resistance, but it presented no problem when a cycloconverter which allowed independent adjustment of output voltage and frequency was used as described in chapters 4 and 5. It is necessary to form a new relationship between the supply voltage and frequency other than proportionality with frequency such that the peak torques are equal at all frequencies. This relation between voltage and frequency may be defined as,

$$V = F(f) \quad . \quad (2.5)$$

A simple approximate solution to the problem of defining $F(f)$ was obtained from the relationship of torque as proportional to (rotor current)², and hence to the (induced voltage)², i.e. $T = aV^2$, where a is a constant, (magnetic circuit has been neglected).

If stator impedance can be ignored, this statement will be true when V is the applied voltage. However, the stator impedance may not be neglected as indicated in Fig. (2.7), but it may be compensated for as follows;

T_{M1} , the peak torque at 50Hz, is taken as the torque value to which other torque values must be raised and V_1 the corresponding applied stator voltage. At a lower frequency, f , a voltage $V_2 = \left(\frac{f}{50}\right) V_1$ produces a peak torque, T_{M2} , then,

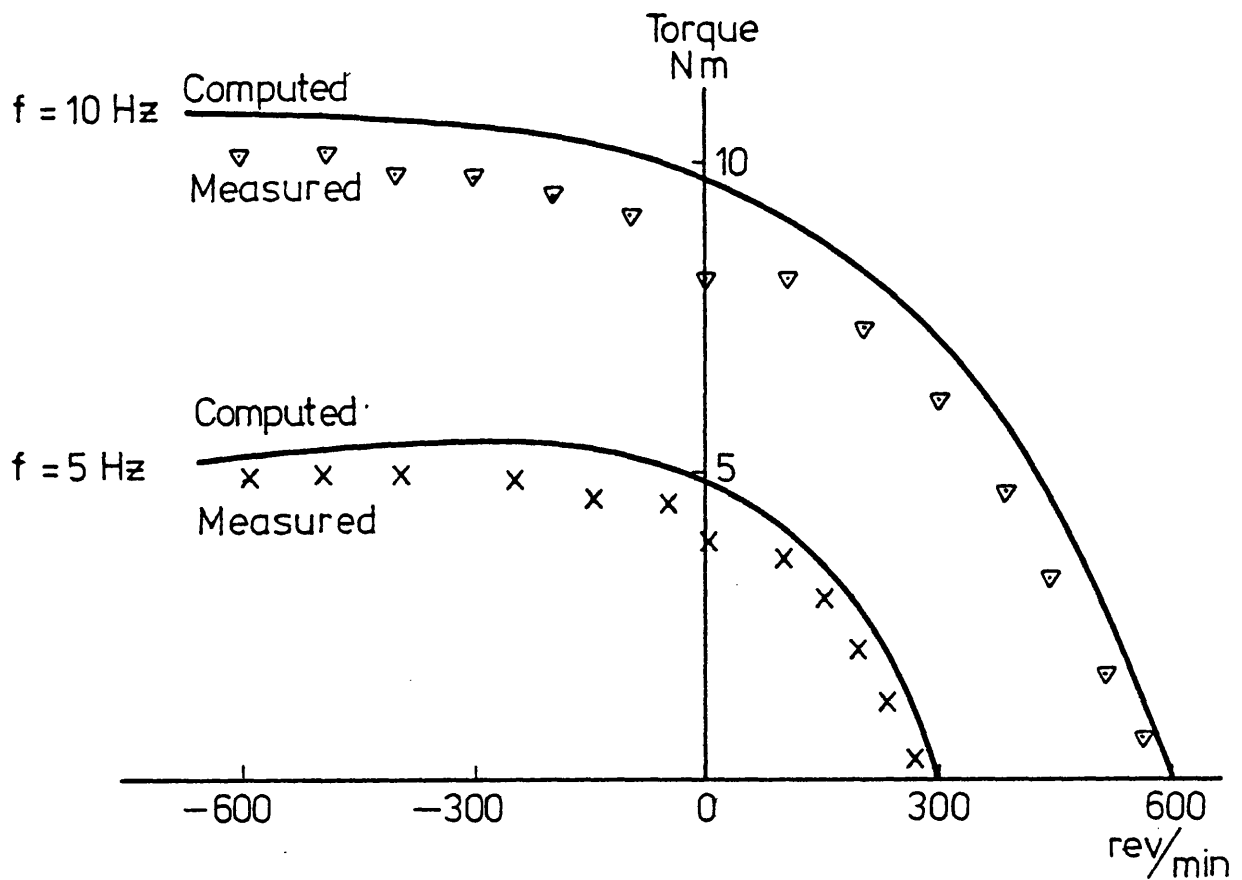


Fig.2.8 Torque/speed characteristics at 10Hz and 5Hz.

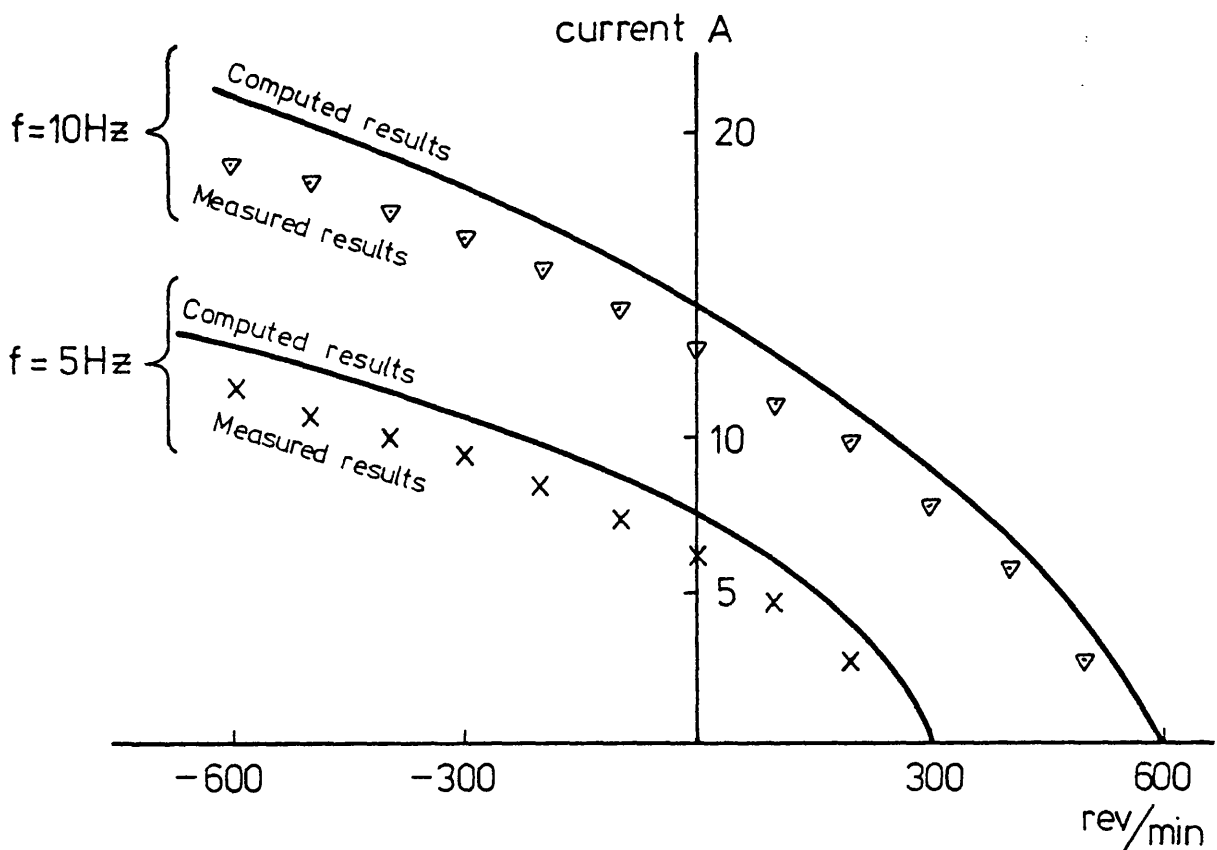


Fig. 2.9 Stator current speed at 10Hz and 5Hz.

$$T_{M2} = aV_2^2 \quad \text{gives} \quad a = \frac{T_{M2}}{V_2^2} \quad 12.$$

Hence $T_{M1} = \left(\frac{T_{M2}}{V_2^2} \right) V_f^2$, and

$$V_f = \sqrt{\frac{T_{M1}}{T_{M2}}} \times V_2, \quad (2.6)$$

which indicates the required voltage at frequency f . Fig. (2.10) shows the result of this approximation. An improved acceleration performance will be achieved if this voltage adjustment can be made in a control system. The actual voltage required as a function of frequency determined from equation (2.6) is shown in Fig. (2.11).

2.4 Machine parameter variation with frequency

The steady-state characteristics obtained in section 2.3 calculated on the assumption that the equivalent circuit parameters obtained at 50Hz are constant at all frequencies. This assumption is known to be incorrect from a knowledge of the behaviour of lamination steel under conditions of magnetisation. Also the a.c. resistance of the machine windings is known to vary with frequency. An investigation was carried out to assess the degree of error introduced by the constant parameter assumption. Running light and locked rotor tests were carried out over a frequency range of 5 to 50Hz (see Appendix 1).

2.4a Magnetising parameters

The magnetising circuit parameters R_o and X_o were determined from the open-circuit test with the unloaded machine rotating freely for each constant input frequency. Values of R_o and X_o were obtained over a frequency range $5 < f < 50$. Fig. (2.12) shows that X_o varies linearly with frequency indicating a constant inductance (L_o). R_o , representing the total iron loss, can be seen to be frequency dependent.

The total iron loss consists of two frequency dependent terms representing hysteresis and eddy current losses expressed empirically by

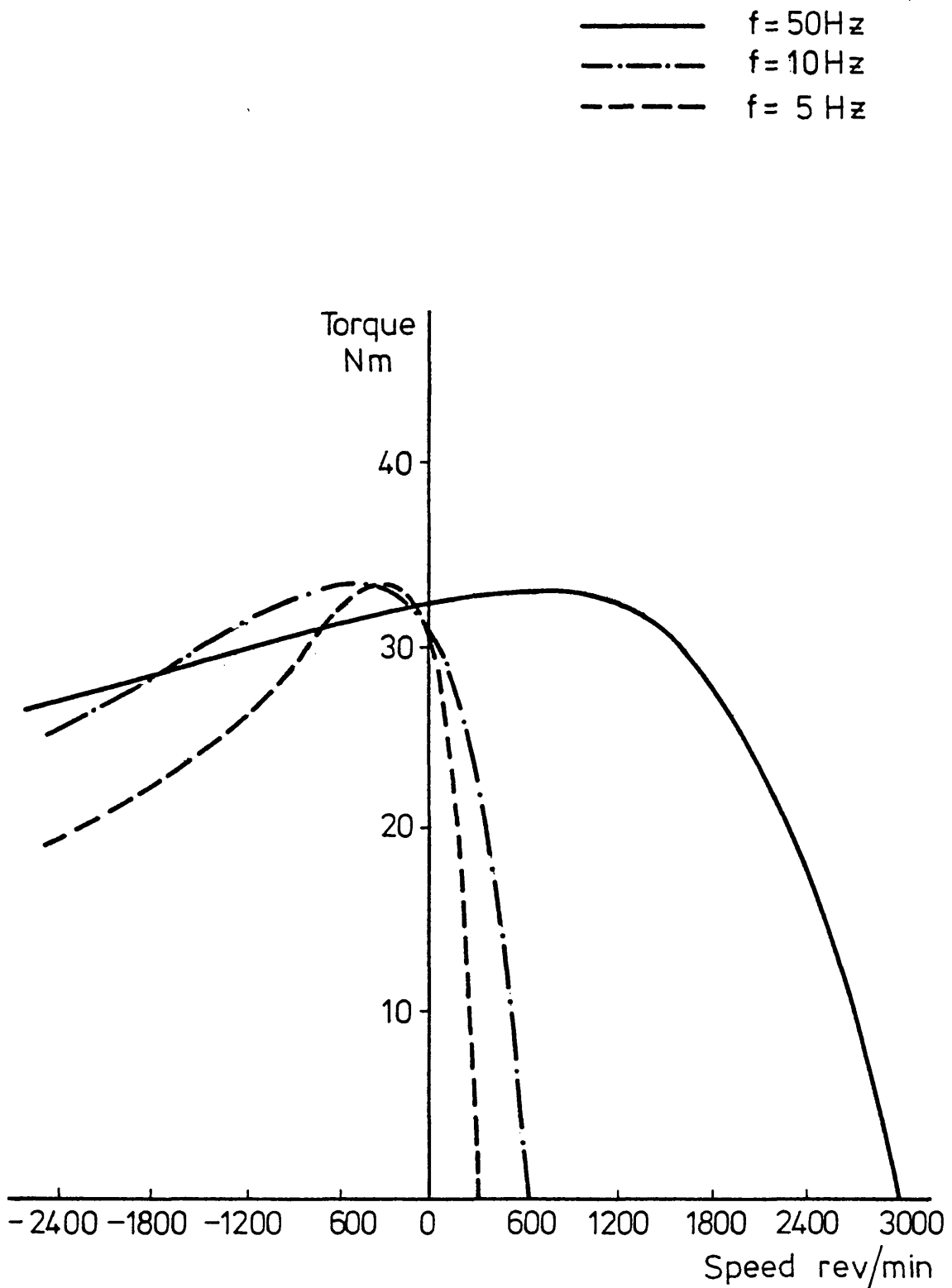


Fig. 2.10 Torque/speed characteristic at 50,10, and 5Hz with voltage adjusted such that $V = F(f)$.

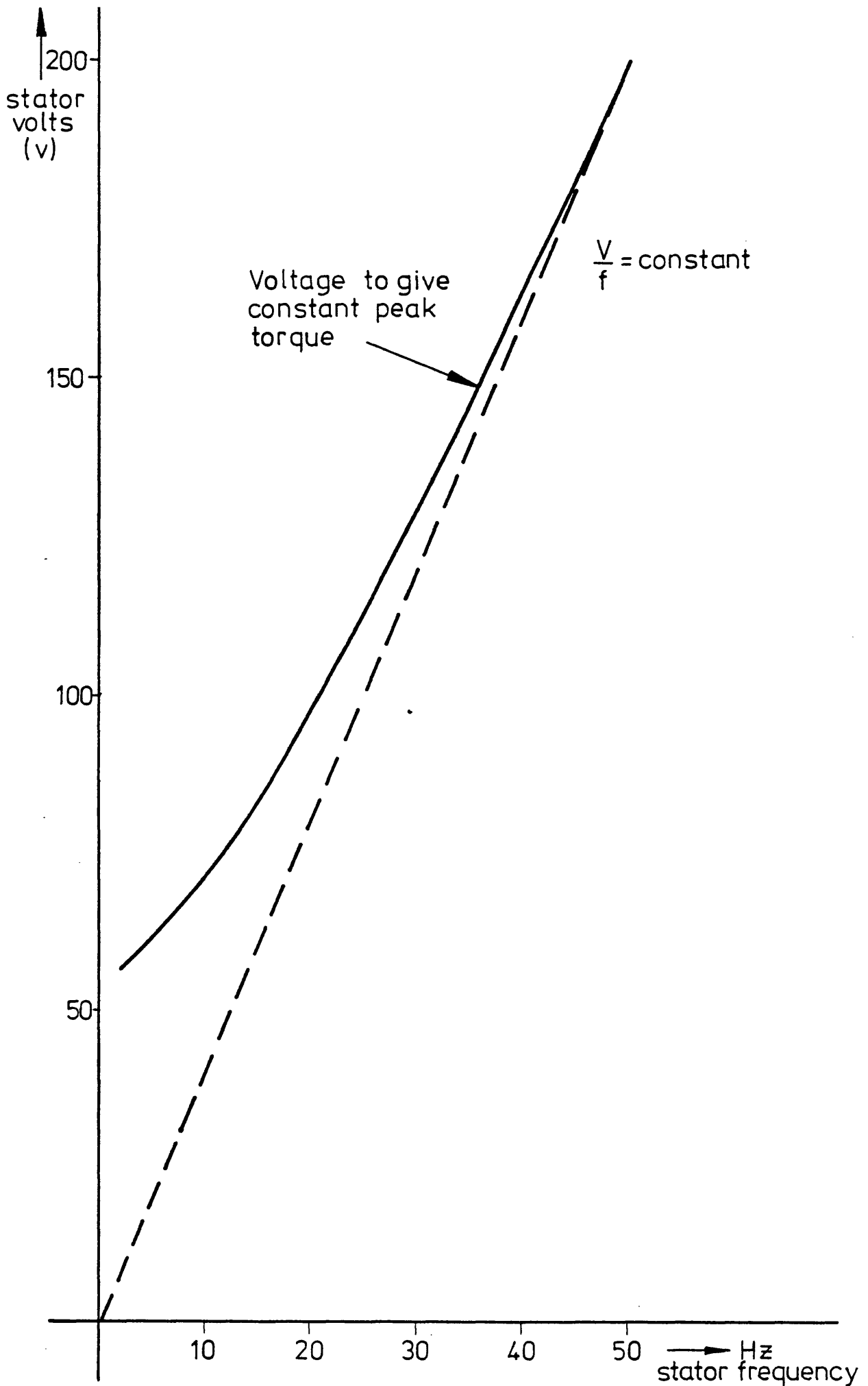


Fig. 2.11 Required stator volts / frequency for experimental induction motor.

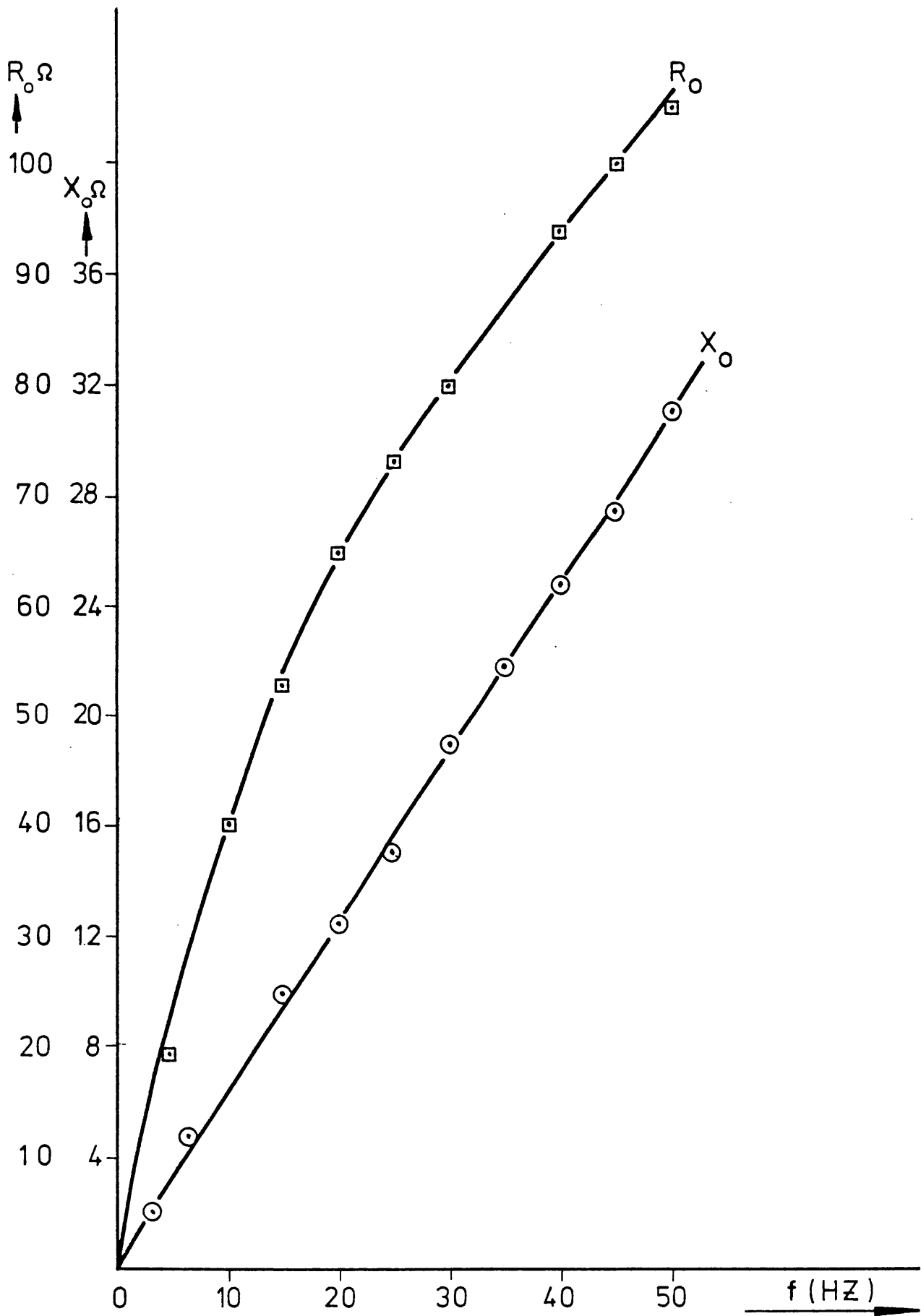


Fig.2.12 Measured magnetising circuit parameters against frequency.

Steinmetz (8) as,

$$W_I = K_h f B^{1.6} + K_e B^2 f^2, \quad (2.7)$$

where K_h and K_e are constants relating the hysteresis and eddy current components respectively and 1.6 is an index relating to soft iron laminations. B is the maximum value of flux density. The flux density B will be proportional to the applied voltage, which is, in turn, proportional to the applied frequency. Since $W_i = \frac{V^2}{R_o}$, substituting for W_I from equation (2.7) gives,

$$R_o = \frac{V^2}{K_h' f + K_e' f^2}, \quad (2.8)$$

where $K_h' = K_h B^{1.6}$ and $K_e' = K_e B^2$, for a constant flux machine, $V \propto f$, i.e. $V = af$ where $a = \text{constant}$. Equation (2.8) can be re-written as,

$$R_o = \frac{a^2 f^2}{K_h' f + K_e' f^2} = \frac{1}{\frac{a_1}{f} + a_2}, \quad (2.9)$$

where the constants are $a_1 = K_h'/a^2$, $a_2 = K_e'/a^2$. Equation (2.9) represents the variation of the iron loss parameter (R_o) with frequency. This means that the iron losses increase with frequency. Fig. (2.12) shows that equation (2.9) can be considered to be valid at frequencies above 25 Hz. Below 25 Hz, the measured value of R_o is substantially less than the predicted values and so the Steinmetz equation is invalid at low frequencies. However at low frequencies above approximately 3 Hz, R_o is substantially greater than X_o and the assumption made in section 2.2 that R_o may be neglected in the calculation of the steady state characteristic is still valid as a first order approximation.

Fig. (2.13) shows the variation of input current with frequency when running light with volts proportional to frequency. Here the magnetising current forms a substantial part of the total current and since the rate of increase of R_o with frequency falls with increasing frequency, the input current can be expected to fall at low frequencies. This input current reduction will be increased due to the reduction of friction torque ($\propto \text{speed}$) and windage torque ($\propto \text{speed}^2$) as the frequency falls.

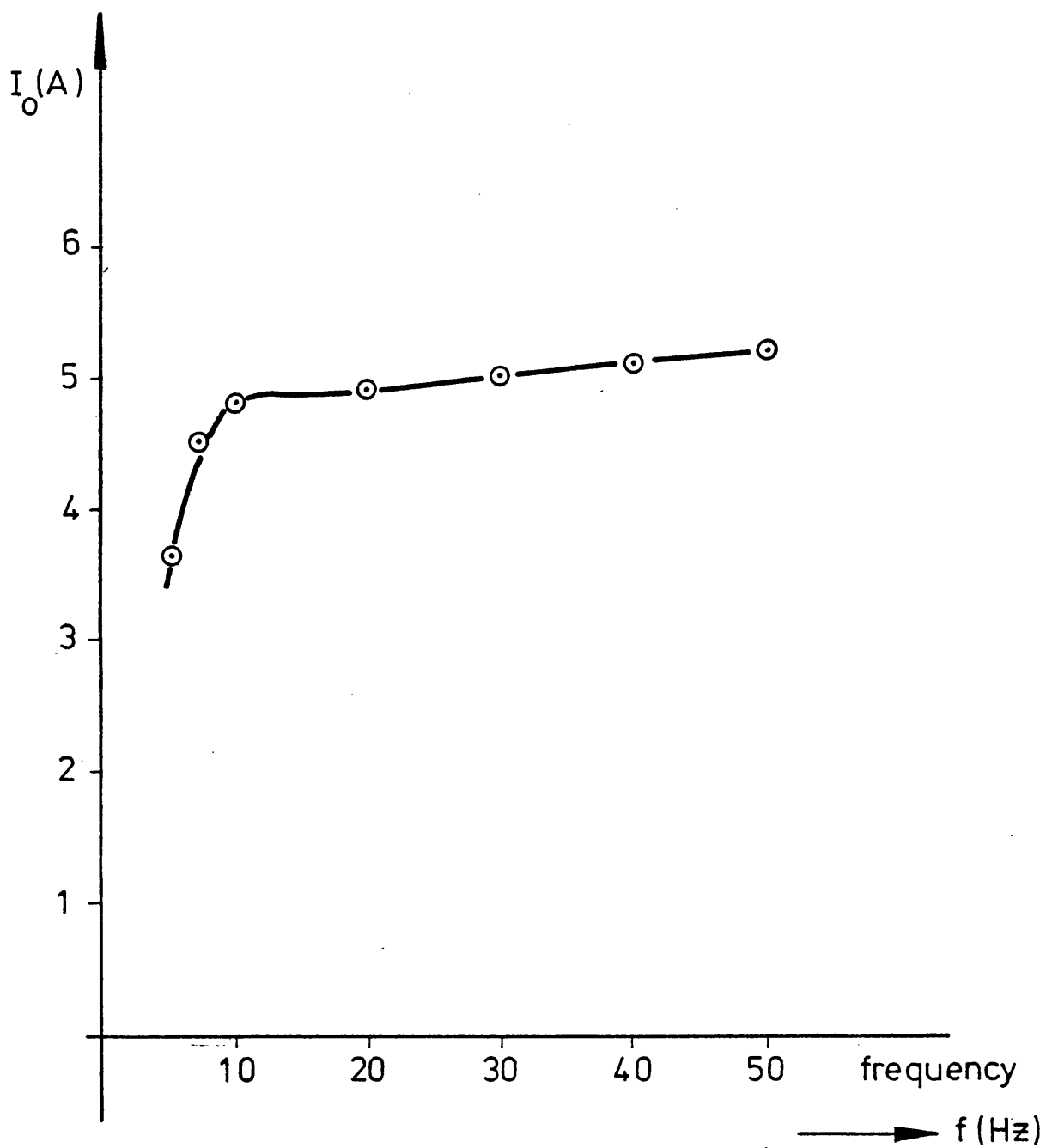


Fig. 2.13 Running Light input current against frequency.

R_o will have a substantial effect on the motor efficiency as the frequency increases. Fig. (2.14) shows a separation of losses into hysteresis, eddy current and mechanical losses. The mechanical loss was obtained by externally driving the unexcited induction machine and subtracting the known loss of the drive motor. At low frequencies, Fig. (2.14) shows that the hysteresis loss forms practically the whole of the total iron loss. Thus, at these frequencies, the iron loss can be said to increase linearly with frequency as predicted in equation (2.7).

2.4b Parameters from the locked-rotor test

Locked rotor tests were carried out over a range of frequencies between 5Hz and 50Hz. The sinusoidal variable-frequency supply was obtained from an alternator driven at a range of speeds. A rated current of 14A was used in each case, the voltage being appropriately adjusted. Fig. (2.15) shows the values of total effective resistance and reactance referred to the stator. Each parameter has a non-linear relationship with frequency.

The effective resistance, R_e increases with frequency, an expected effect accounted for by "a.c." resistance and the "skin-effect". Leakage reactance, X_e has a lower rate of increase with frequency at the higher frequencies. This indicates that the magnetic coupling is better at high frequencies and that low-frequency operation of a machine designed to operate on 50Hz can only be achieved at the expense of poor coupling and increased leakage inductance.

Each characteristic can be approximated to two straight lines, the changeover point occurring at 20Hz for R_e and 30Hz for X_e . This linearisation has been carried out in Fig. (2.15) giving the following approximate expressions for R_e and X_e ,

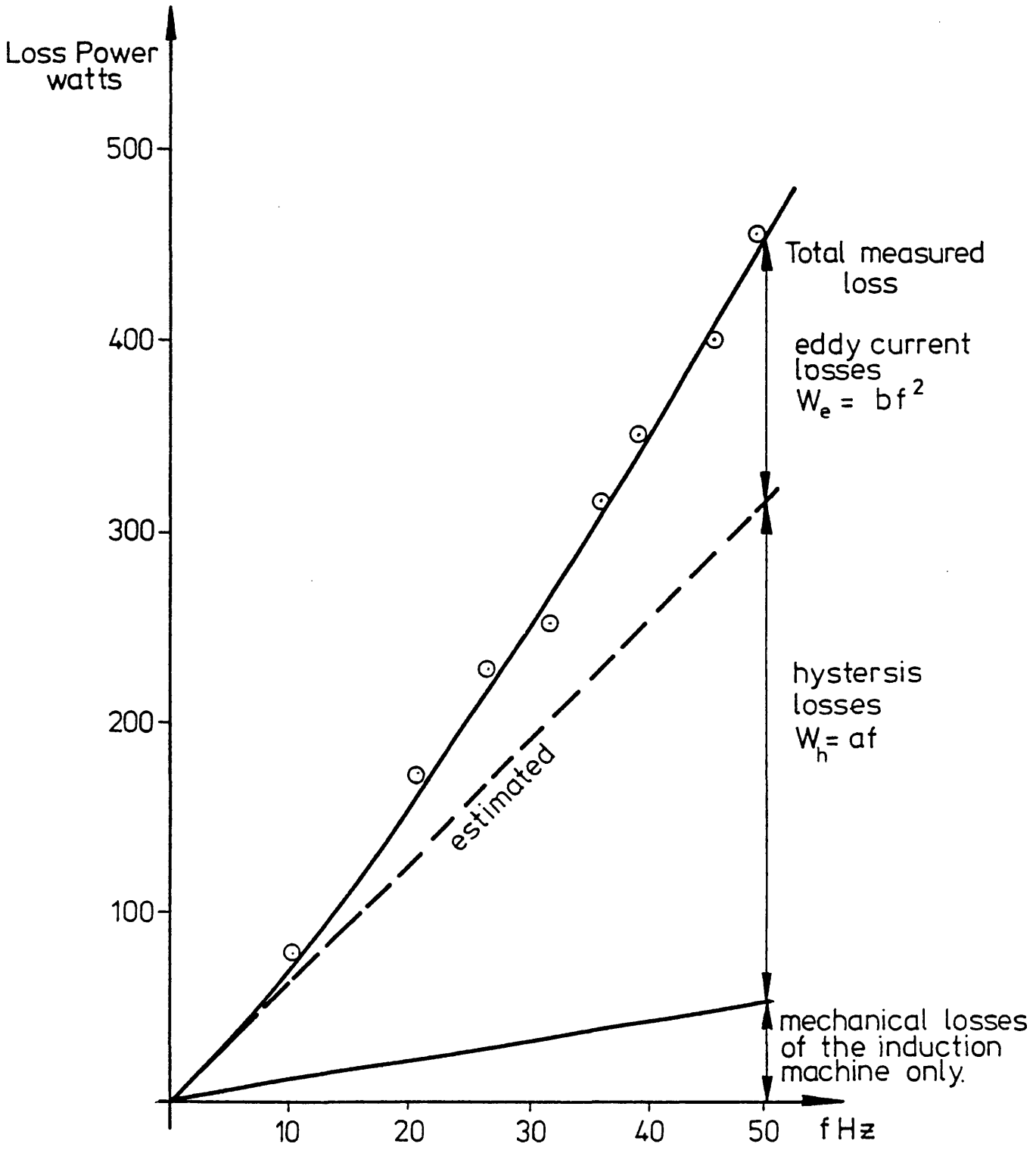


Fig. 2-14 Running light losses/frequency

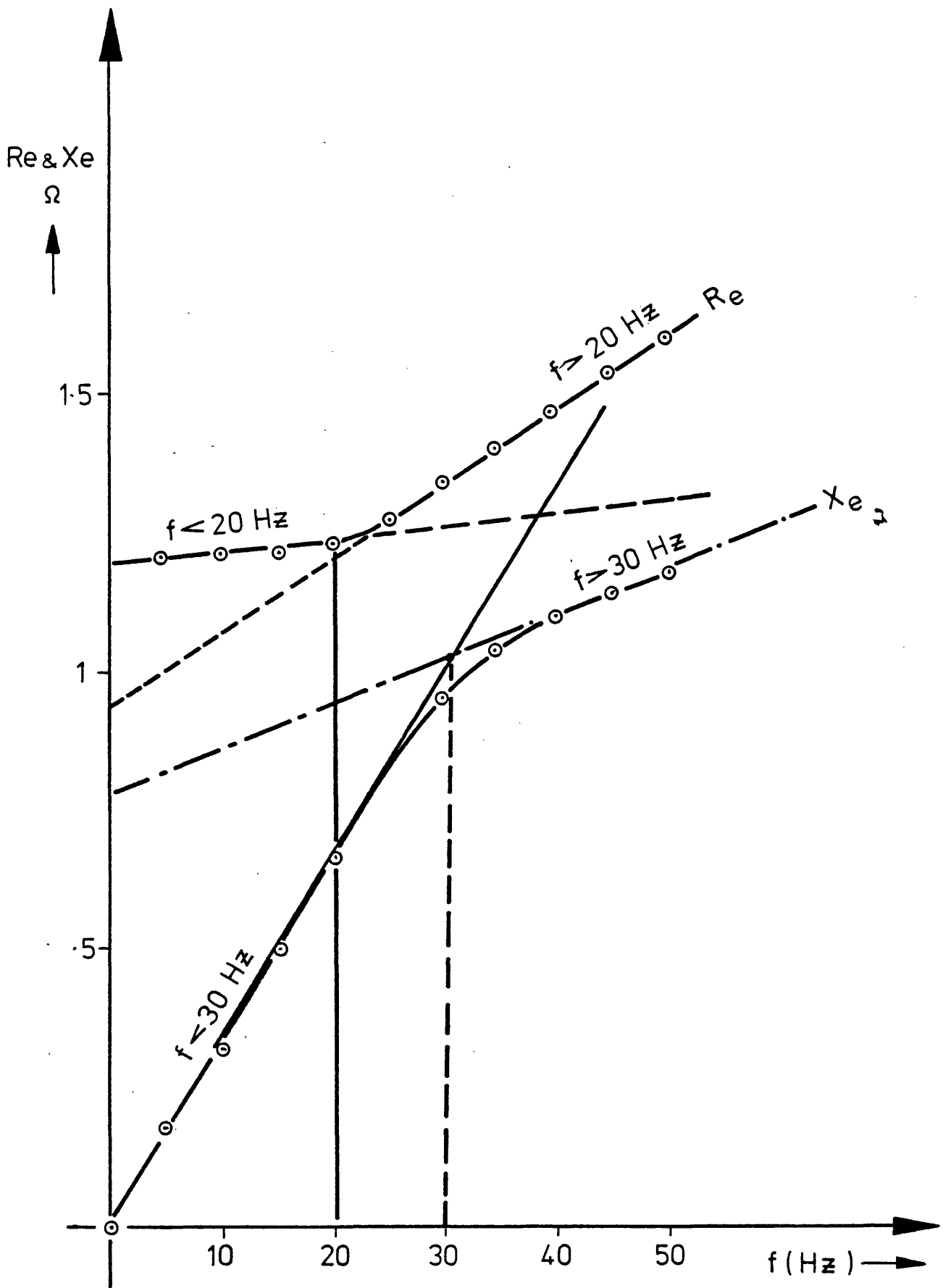


Fig.2-15 Locked rotor test parameters against frequency

$$R_e = af + b \quad f < 20\text{Hz} \quad (2.10)$$

$$R_e = cf + d \quad f > 20\text{Hz} \quad (2.11)$$

$$X_e = ef \quad f < 30\text{Hz} \quad (2.12)$$

$$X_e = Lf + g \quad f > 30\text{Hz} \quad (2.13)$$

The stator resistance R_1 was measured under d.c. conditions and hence $R_2 = R_e - R_1$. Under locked rotor conditions the frequency of both rotor and stator was that of the supply, and hence a.c. resistance effects will provide the same rate of increase of R_1 and R_2 with frequency. R_1 and R_2 are now obtainable in frequency dependent terms.

2.5 Effect of Parameter Variation on Steady-State Performance

The characteristics obtained in section 2.2 are all computed from 50Hz parameters, i.e. by using equations (2.11) and (2.13) where $f = 50$. [To investigate the effect of the parameter variation shown in Figs. (2.12) and (2.15) at low frequency, torque/speed and current/speed characteristics have been computed at frequencies of 5 and 10Hz, using equations (2.10) and (2.12). Fig. (2.16) shows the comparison between the torque/speed characteristics obtained with 50Hz parameters and parameters obtained from equations (2.10 and 2.12). This shows that the use of constant 50Hz parameters is a reasonable first order approximation and that parameter variation has little effect on performance although its effect on efficiency may be greater.

2.6 Efficiency at Low Frequency

Motor efficiency can be estimated from input and loss considerations as follows:

Motor input = input power = sum of two wattmeter readings, W_1 and W_2 .

Losses = 3 (copper loss/ph + 3 (iron loss/ph) + mechanical loss obtained from Fig. (2.14).

- Parameters obtained by equations 2.11 and 2.13
(50Hz parameters used throughout range)
- - - Parameters obtained by equations 2.10 and 2.12
(Parameter values adjusted with frequency)

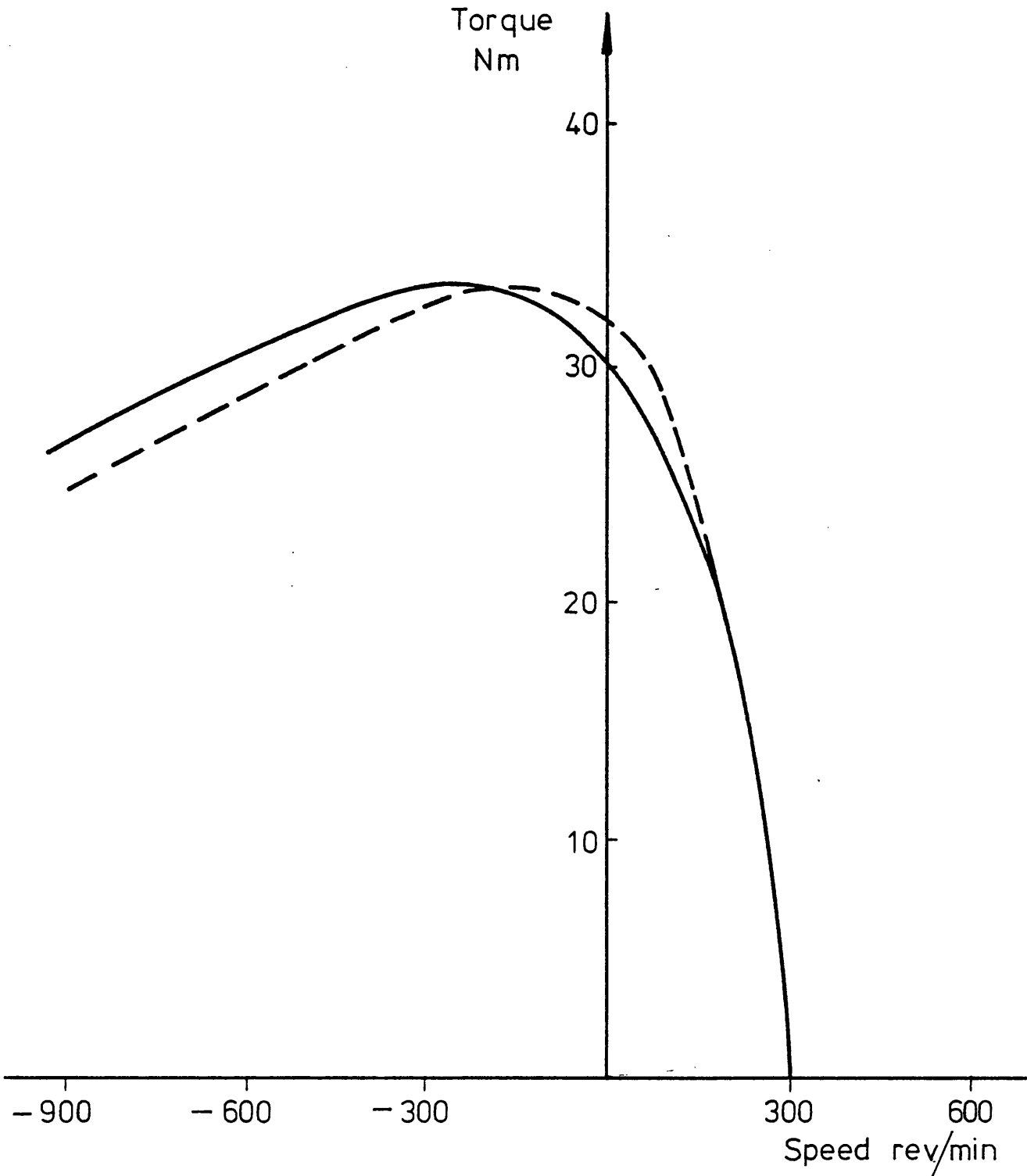


Fig. 2.16 Calculated torque speed characteristics at 5Hz
showing the effect of parameter variation with
frequency.

Hence, the motor efficiency = $\frac{(\text{Input} - \text{losses})}{\text{Input}} \times 100\%$.

Fig. (2.17) shows the efficiency obtained at full-load torque over a range of frequency when R_e and R_o vary with frequency. The overall efficiency of the experimental induction motor ⁽⁹⁾ is very low due to the comparatively high resistance of its gramme-ring winding. Efficiencies in an industrial machine would be about 10% higher at all frequencies.

It can be seen however that an induction motor designed for 50Hz operation will be very inefficient at much lower frequencies. This may necessitate forced cooling or an increased frame size for continuous operation.

2.7 Steady-state stability on a low-frequency sinusoidal supply

One of the basic problems of operating an induction motor in an open-loop system on variable low-frequency supplies is the tendency to oscillate about a mean operating point. If the torque-slip characteristic shown in Fig. (2.18) is considered, it can be seen that the maximum permitted range of slip variation will be the range between peak motoring and peak braking torque. If the load torque demand exceeds the maximum available motoring torque, the motor will stall and probably be damaged by excessive current. The slip range between peaks defined by $\frac{dT}{dS} = 0$ is,

$$\frac{+R_2}{[R_1^2 + X_e^2]^{\frac{1}{2}}} \geq S \geq \frac{-R_2}{[R_1^2 + X_e^2]^{\frac{1}{2}}} \quad (2.11)$$

As the supply frequency is reduced, equation (2.11) defines a much smaller range of speed within these slip limits. Consequently the rate of change of torque with respect to speed increases and the machine becomes much "stiffer" i.e. the restoring torque opposing a change of speed increases or decreases more rapidly and stability is reduced.

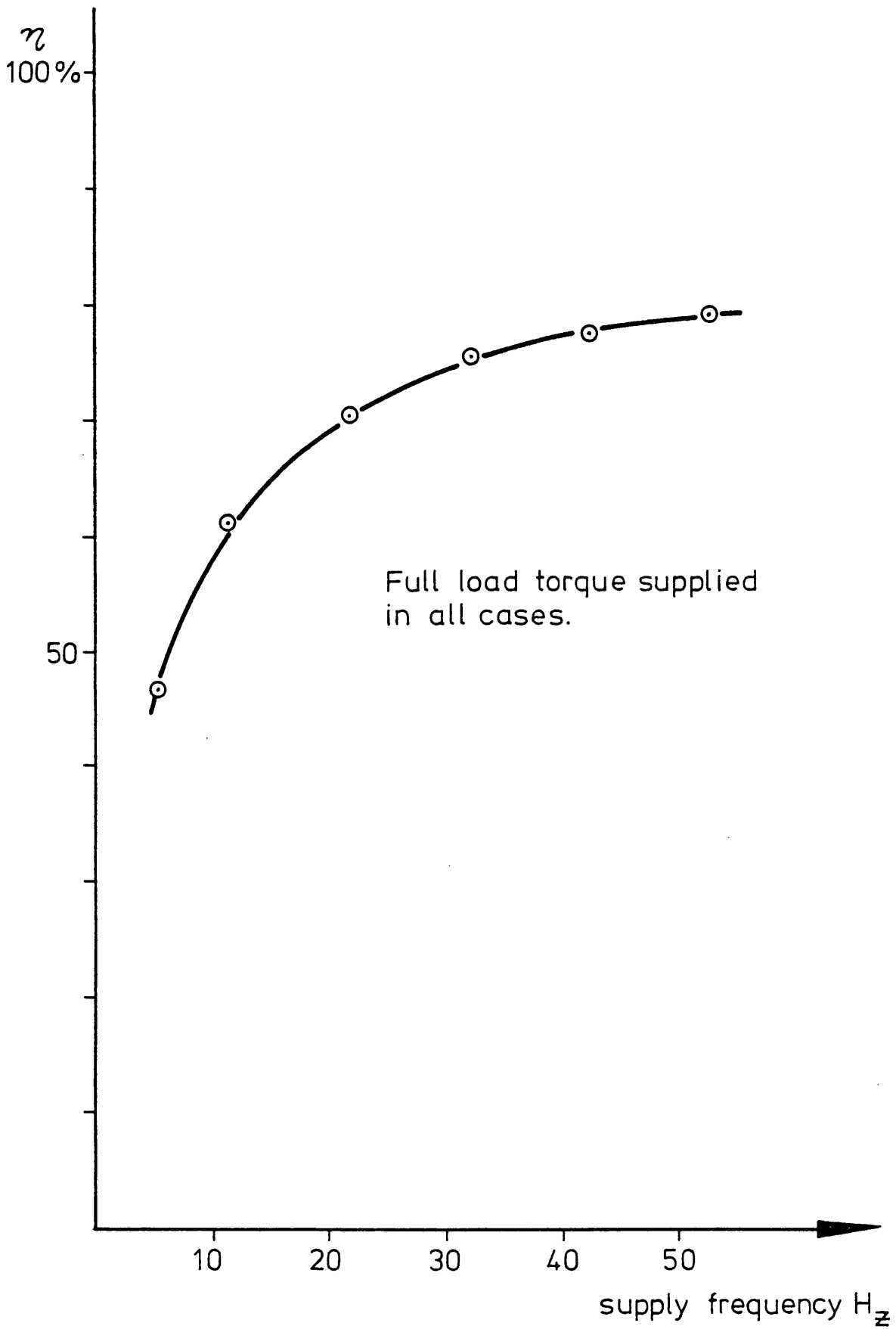


Fig. 2.17 Calculated efficiency/frequency at rated torque

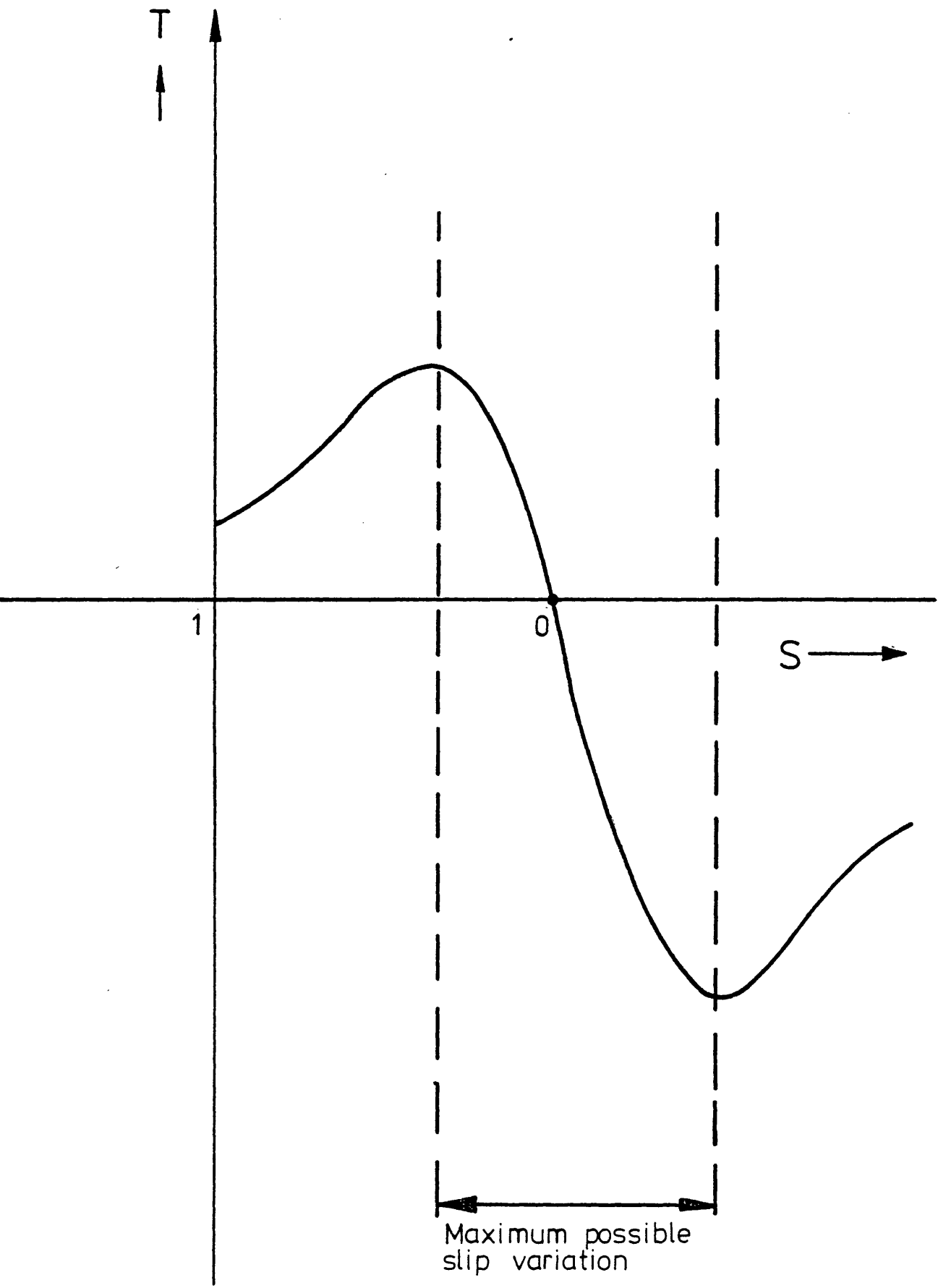


Fig. 2-18 Sketched Torque/slip characteristic showing
operating range.

Various authors (10,11) have illustrated this instability for an induction motor operating on a "stiff" sinusoidal supply, while others (12,13) discuss the instability in the context of an inverter-fed drive. Here the link capacitance is a dominant feature in the oscillatory behaviour. In this part of the current work, the inherent instability of the machine operating on a "perfect" low-frequency supply is the present problem.

Bowler and Nir in reference (11) use the equivalent circuit of Fig. (2.1a) to study the stability of the drive. They use an impedance diagram based on the equivalent circuit and its small signal derivative to define a stability criterion in terms of equivalent circuit parameters. This was presented in terms of the equivalent circuit of Fig. (2.1) as,

$$Z = R_1 + j\omega L_1 + j\omega L_0 \frac{R_2 + j\omega_r L_2}{R_2 + j\omega_r (L_0 + L_2)}, \Omega \quad (2.12)$$

where ω_r = slip frequency rad/sec. and $X_0 = \omega L_0$, $X_1 = \omega L_1$ and $X_2 = \omega_r L_2$,

and
$$T_e = \frac{I_1^2 mP\omega_r L_0^2 R_2}{[R_2 + j\omega_r (L_0 + L_2)]}, \text{ N.M.} \quad (2.13)$$

If the system is considered to be responding to small changes about a steady-state operating point, the change in impedance,

$$dZ = R_1 + j\omega L_1 + j\omega L_0 \frac{R_2 - j\omega_r L_2}{R_2 - j\omega_r (L_0 + L_2)}, \Omega. \quad (2.14)$$

The inversion of equation (2.14) gives the small signal admittance

$$dY = \frac{R_2 - j\omega_r AL_0}{(R_2 - j\omega_r AL_0)(R_1 + j\omega L_1) + j\omega L_0(R_2 - j\omega_r L_2)}, \Omega^{-1}. \quad (2.15)$$

Equation (2.15) has a real part of

$$R_e dY = \frac{R_1 R_2^2 + R_2 \omega^2 S L_0 (AL_1 + L_2) - \omega^2 L_0^2 SA (R_2 B - R_1 SA)}{[R_1 R_2 + \omega^2 S L_0 (AL_1 + L_2)]^2 + \omega^2 L_0^2 (R_2 B - R_1 SA)^2}, \Omega^{-1}, \quad (2.16)$$

where $A = 1 + \frac{L_2}{L_0}$, and $B = 1 + \frac{L_1}{L_0}$.

The bound for stability is that $R_e |dY|$ is negative and so applying this to equation (2.16),

$$\omega^2 L_o^2 S A (R_2 B - R_1 S A) > R_1 R_2^2 + R_2 \omega^2 S L_o (A L_1 + L_2) . \quad (2.17)$$

Under conditions of heavy load, the damping effect of the load will stabilise the system and so the case of greatest interest is that of light loading, where S is small. The term $R_1 S A$ in equation (2.17) becomes negligible and a single value of 'S' defines the stability boundary,

$$S_{\text{limit}} > \frac{R_1 R_2}{(\omega L_o)^2} . \quad (2.18)$$

The parameters of the machine obtained at 50Hz were then used in this expression over the frequency range (1-10Hz).

Fig. (2.19) shows the limiting value of slip related to frequency. However the very large values of slip shown at low frequencies do not represent a large permissible speed variation. Fig. (2.20) shows the permissible speed limit plotted against frequency from the relation $n_{\text{limit}} = \frac{\omega}{2\pi} (1 - S_{\text{limit}})$.

This means that the constant ratio of limit speed/frequency can be seen to be applicable at frequencies above 2Hz for the experimental machine. At low frequencies, this restriction of stable speed operation will reduce the permissible shock loading of the machine.

The importance of maintaining constant flux at all speeds is illustrated in Fig. (2.21) and (2.22). If a control system operates with voltage proportional to frequency, the stator regulation reduces the maximum or peak torque, defined here as the limit torque. Fig. (2.21) shows the limit torque plotted against limit slip and Fig. (2.22) shows the limit torque plotted against the maximum speed deviation from synchronous speed. If low speed stalling is to be avoided, a

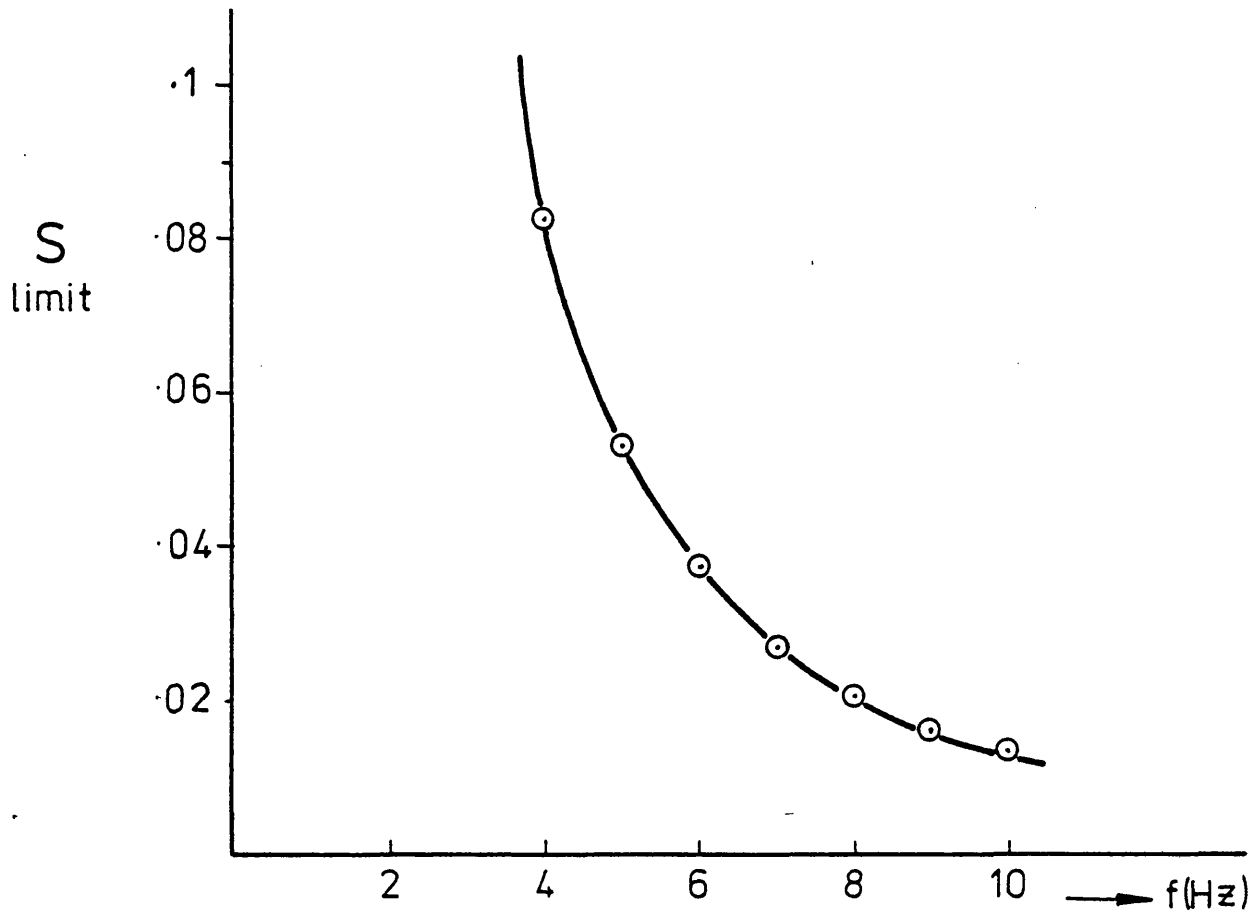


Fig.2.19 Maximum slip variation from synchronous speed/stator frequency.

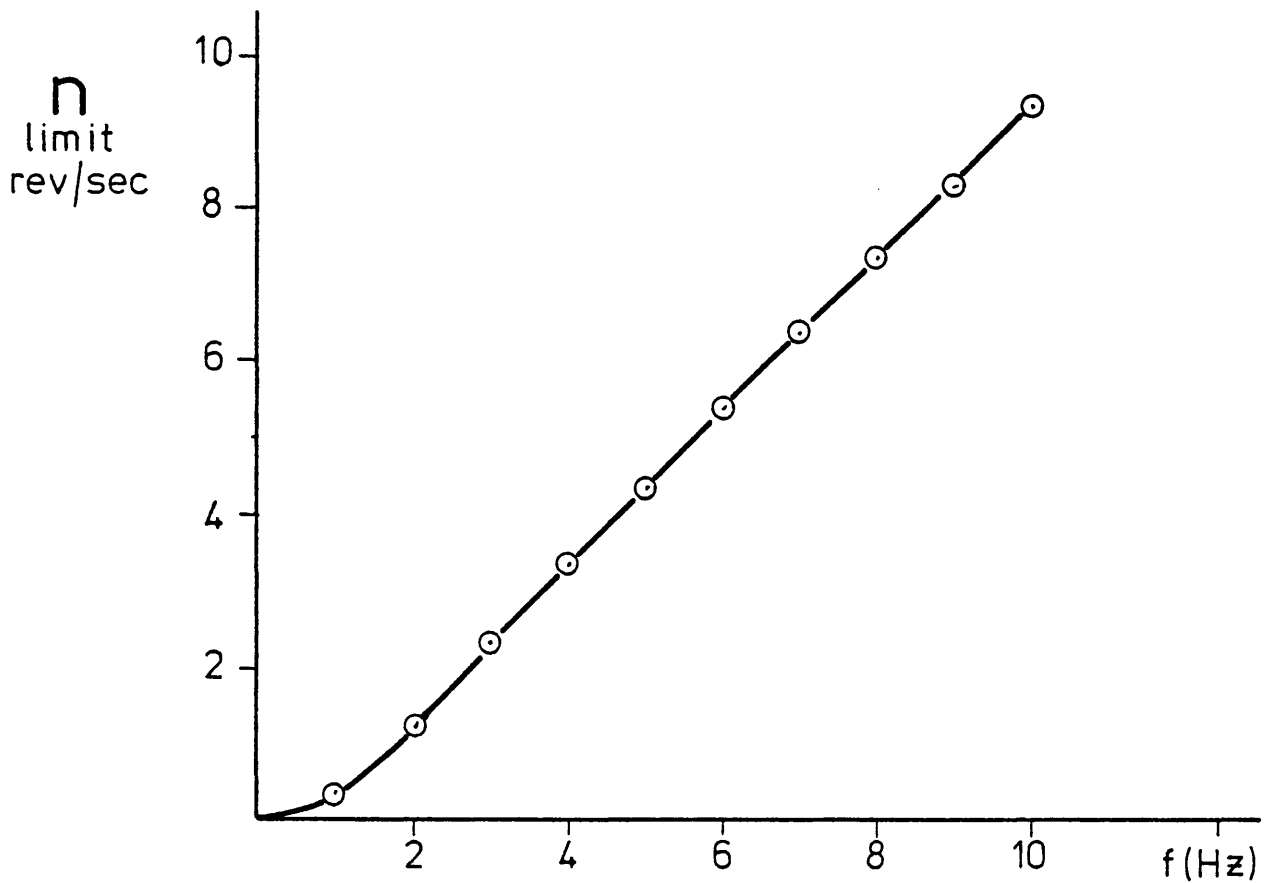


Fig.2.20 Maximum speed variation from synchronous speed/stator frequency.

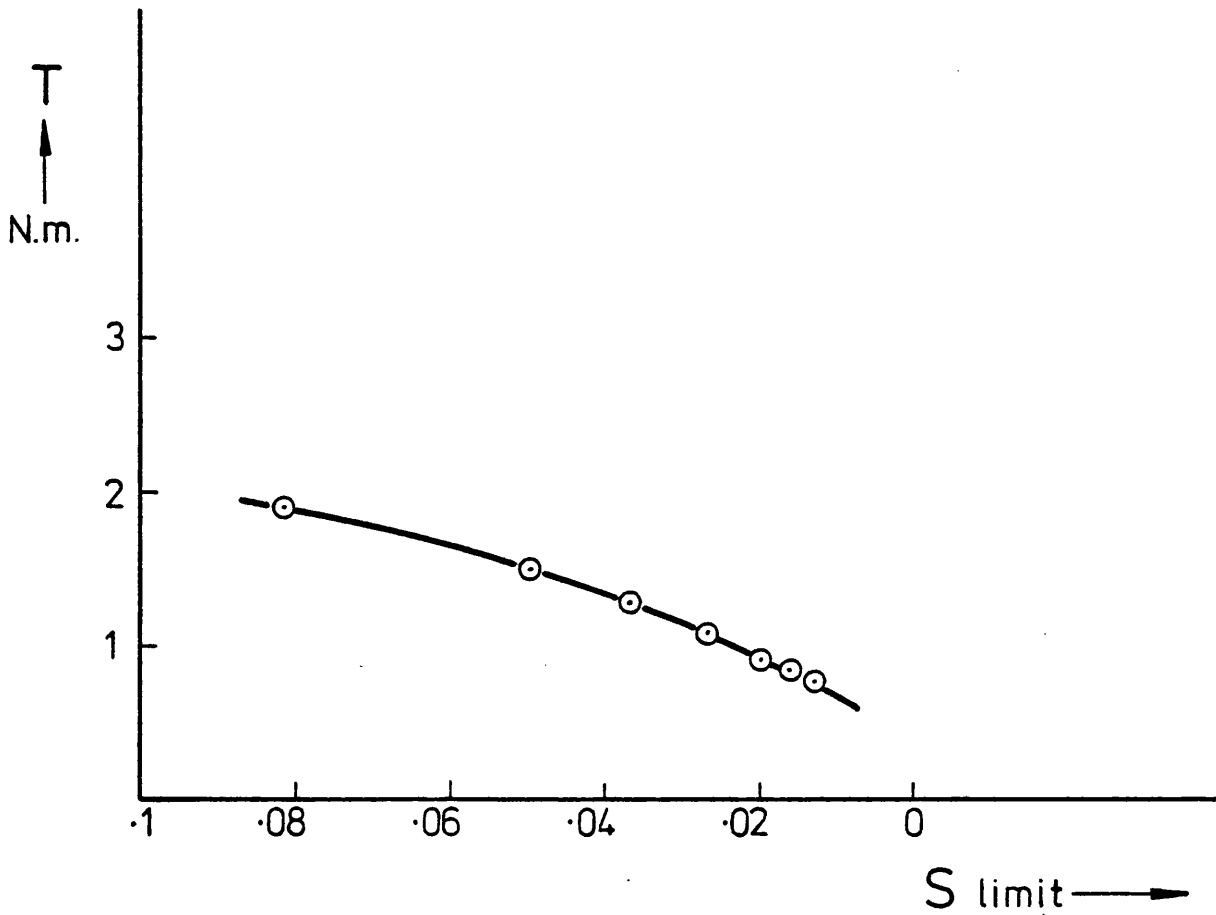


Fig.2.21 Limit torque corresponding to limit slip/limit slip in a $V \propto f$ system.

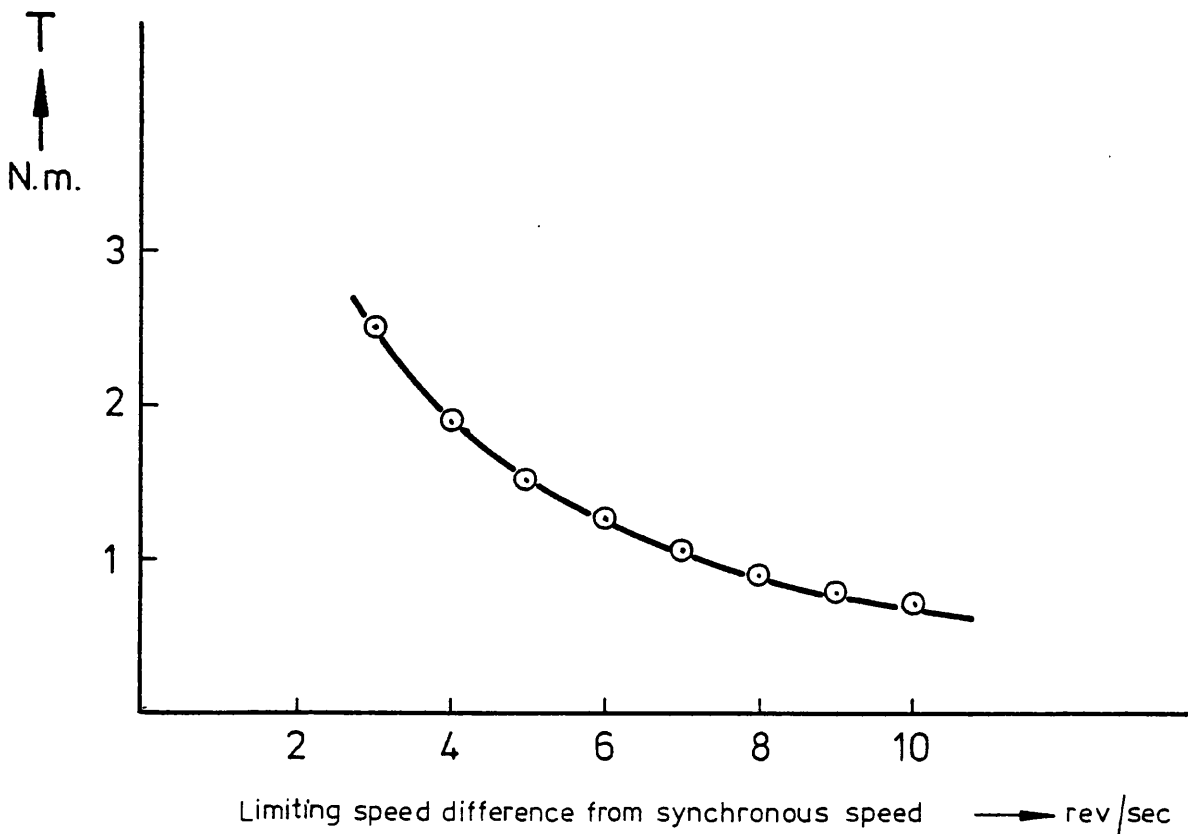


Fig.2.22 Limit torque/limit speed variation from synchronous speed $V \propto f$ system.

constant limit torque value is required. This can only be increased by an increased stator voltage as shown in section 2.3.

Figs. (2.19) and (2.22) indicate the limits of operation beyond which stalling or catastrophic failure can occur in an open-loop, sinusoidal control system. Even when operating inside these limits low frequency operation tends to result in an oscillation of the rotor about a mean operating speed. This oscillation occurs when the stator supply frequency approaches the natural frequency of the rotor. Fig. (2.23) illustrates this oscillation related to a change of load.

In the upper pen recording, a 3Hz oscillation about the steady state operating speed is continually present and a change in load with the consequent speed reduction of about 10% seems to give a slightly increased stability. The lower pen recording taken at a frequency of 4.5Hz and the same stator voltage indicates that operation before loading can be stable and that the shock of the applied load sets up a sustained oscillation. This tendency to oscillate about a steady-state speed puts the open-loop drive at a severe disadvantage when contrasted with a high motor speed geared drive. Greater stability can be achieved by closed-loop control. This is discussed in Chapter 5.

2.8 Conclusions from Chapter 2

The work described in chapter 2 shows that there are a number of problems associated with the low speed operation of induction motors even when sinusoidal supplies are available. These are:

- 1) Parameter variation with frequency. Effective resistances have been shown to vary with frequency and the "a.c." resistance values correspond with "d.c." resistance more closely as the stator frequency becomes smaller. Magnetic coupling at low frequency is worse than the coupling at 50Hz and the leakage inductances are greater at low frequency. Iron losses are

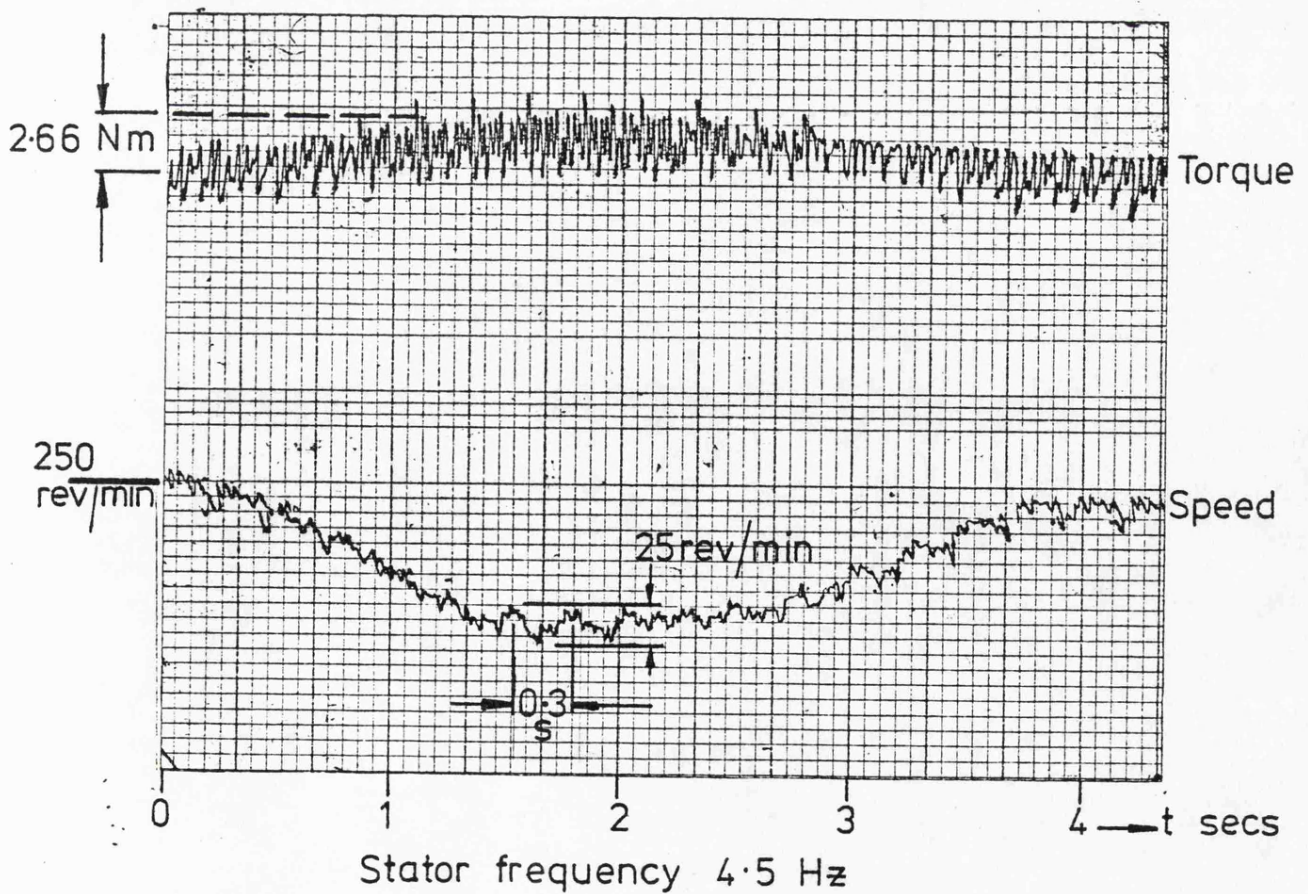
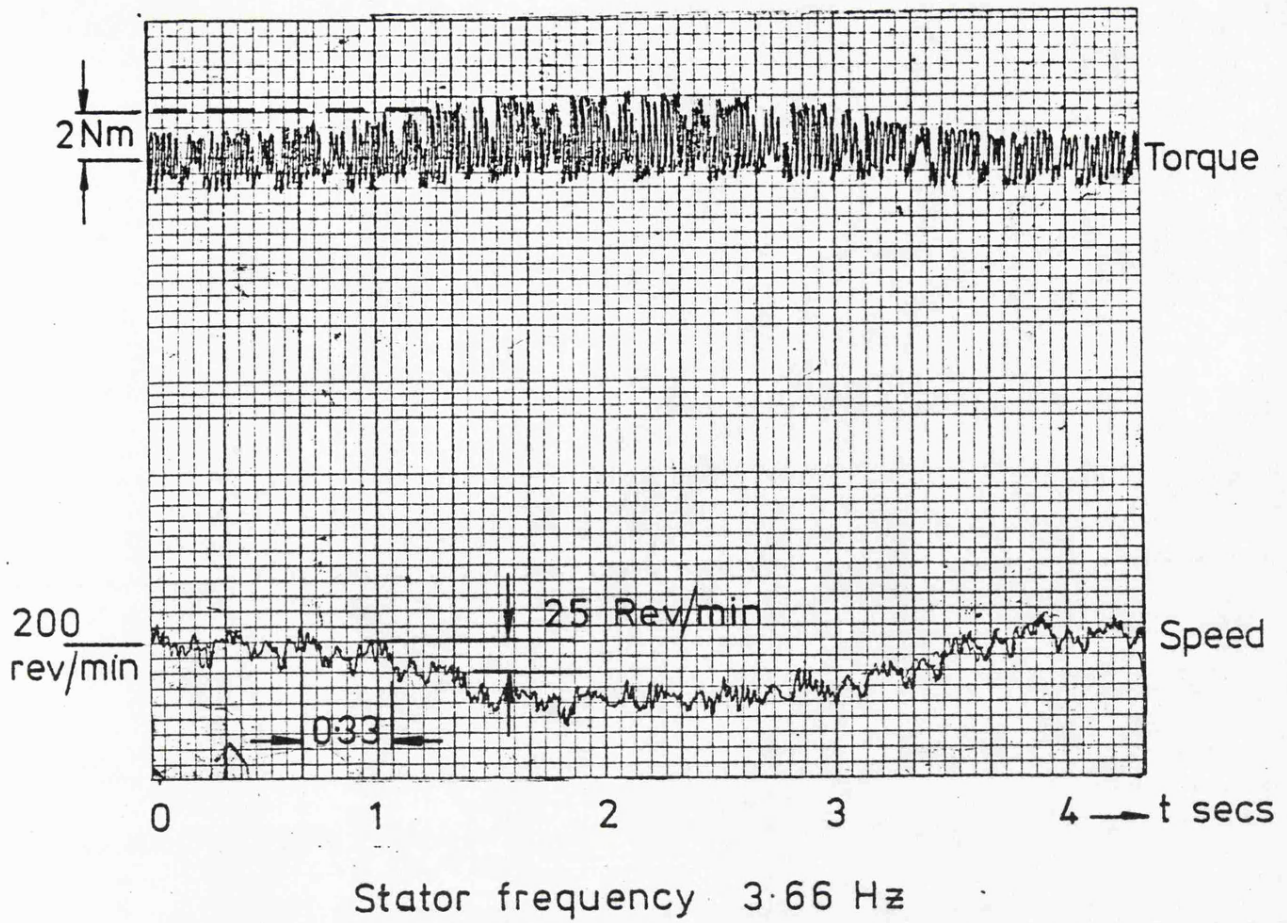


Fig.2-23. Open-loop response of induction motor to torque change.

frequency dependent and at low frequency the magnetising current is large relative to the torque producing current term. This ratio of magnetising current to torque producing current reduces the efficiency of the system at low frequencies.

- 2) Steady-state operation and characteristics are affected by parameter variation, but the variation is very much a second order effect. The difference between machine characteristics obtained from parameters measured at 50Hz and characteristics determined from parameters which allow frequency variation is always less than 5% of the torque or current concerned. It may be concluded therefore that parameter variation with frequency is important in efficiency calculations, but that the error introduced by a constant parameter assumption is less than that introduced by the approximation of the equivalent circuit. Thus a single set of parameters may be used for all first order performance calculations.
- 3) Constant flux operation is essential at all frequencies if stalling is to be avoided under acceleration or step torque increase conditions. At low frequencies, the stator resistance causes excessive voltage regulation and voltage-proportional-to-frequency operation is no longer adequate. The stator voltage must be increased by a proportion which increases as the frequency decreases to give constant peak torque operation.
- 4) The permissible speed variation about a steady-state operating condition before stalling occurs falls with frequency. This reduced speed range and the increased machine stiffness can

cause oscillations about a steady-state operating point to occur. Thus an open-loop drive may be unstable at low frequencies. In a closed-loop system a compensating network can be introduced and stable operation provided.

It may be concluded therefore, that a low-frequency direct induction motor drive is feasible and that high-speed operation through a gear box may not be necessary. Parameter variation with frequency is not significant but any control system, even with a sinusoidal supply, must be a closed-loop system incorporating stator voltage adjustment for a constant flux operation.

CHAPTER 3Page NoThe effect of harmonics on the low-frequency operation of an induction motor

3.1	Introduction	23
3.2	Harmonic analysis of the non-sinusoidal wave form.	24
3.3	Positive-sequence, negative-sequence and zero-sequence harmonics.	27
3.4	Motor equivalent circuit allowing for harmonics.	29
3.5	Harmonic effects on the induction motor steady-state performance.	31
3.5a	Positive and negative sequence harmonic effects.	32
3.5b	Zero-sequence harmonic effects.	32
3.6	Effect of sub-harmonics on motor performance.	35
3.7	Effect of harmonics on impulse torque response.	39
3.8	Effect of harmonics on run-up.	44
3.9	Effect of harmonics on losses and efficiency.	47
3.10	Conclusions.	50

CHAPTER 3

The Effect of Harmonics on the Low-frequency Operation of an Induction Motor

3.1 INTRODUCTION

The stator winding of an induction motor must be distributed in equally spaced slots around the circumference. This means that the induced emf's in the stator conductors are displaced in space. The resultant mmf will contain multiples and submultiples of the stator frequency even if the stator supply is sinusoidal. Suitable chording in a double-layer winding can eliminate a harmonic (say 3rd) and its multiples. Any machine operating from a sinusoidal supply can therefore accelerate without "cogging".

The variable-frequency supply used in an induction motor drive will generally be obtained by direct or indirect frequency conversion in a cycloconverter or a d.c. link inverter. The wave forms of these supplies are bound to be non-sinusoidal and consequently time-dependent harmonics will be introduced to the stator. Each time-harmonic so introduced will generate a further series of space harmonics, which can be reduced to an acceptable level by design features in the machine. However, the time harmonics in the air-gap flux directly will modify the torque characteristic and introduce additional heating and noise in the machine. The work described in this chapter attempts to investigate the effect of non-sinusoidal supplies on the motor performance and to define suitable operating limits.

3.2 Harmonic Analysis of the Non-sinusoidal Waveform

The operation of induction motor on a variable-frequency supply involves the use of static frequency converters. At any significant power level, the frequency converter will generate an output voltage waveform with significant harmonic content. In chapter 2, the operation of induction motor with a purely sinusoidal supply was discussed, and investigated experimentally by feeding the induction machine from an alternator. In order to investigate the operation of an induction motor on a non-sinusoidal supply, the voltage can be analysed and expressed as a series of sinusoidal voltages known as a Fourier Series. Each separate frequency will produce its own rotating field in the machine air-gap at a harmonic synchronous speed. Additional losses, heating and modification of the torque characteristic will be caused by the time harmonics produced by a non-sinusoidal supply. Additional space harmonics may be introduced by the added time harmonics, but it is assumed that the winding design will eliminate all first order effects as it does for the fundamental. This study concentrates on the effects of time harmonics.

If the positive and negative voltage envelopes are of equal size and symmetry about the zero voltage axis, all time harmonics in the supply will be of a higher frequency than the fundamental, but if asymmetry is introduced as in the case of an unsynchronised pulse-width modulated inverter or a circulating current free cycloconverter, harmonic frequencies lower than the fundamental, known as sub-harmonics, can occur.

Three main effects will occur due to the voltage harmonics produced by the frequency source.

These are:

- a) Modification of the torque characteristic due to harmonic currents and fluxes.
- b) Increased copper losses and heating due to harmonic currents,
- and c) Increased iron losses with associated vibratory noise and heating.

The simplest form of inverter output waveform is the rectangular pulse as shown in Fig. (3.1a). This rectangular waveform can be expressed by the series,

$$e(\omega t) = \frac{4V_m}{\pi} \left[\cos \omega t + \frac{1}{3} \cos 3\omega t + \frac{1}{5} \cos 5\omega t + \dots \frac{1}{n} \cos n\omega t \right] \quad (3.1)$$

This harmonic series contains a fundamental frequency ω , and a series of odd multiples of the fundamental which may produce forward, backward or stationary fields as defined in section (3.3).

If the conduction angle, γ , shown in Fig. (3.1b) is reduced and gaps between positive and negative pulses are introduced, certain harmonics of the series can be eliminated at the expense of poor utilisation of the inverter hardware. The harmonic frequencies and their relative amplitudes will be analysed as a Fourier series. Fig. (3.1b) shows that the waveform has symmetry about the y-axis which simplifies the analysis to a Fourier half-range series with only cosines present and no constant term. This waveform contains the following terms over the period T,

$$0 < t < \pm T \text{ for } y = V_m ,$$

where the amplitude, A_K , for each frequency, K , is given by

$$A_K = \frac{2}{T/2} \int_{-T/6}^{+T/6} y \cos K \omega t \cdot d(\omega t). \quad (3.2)$$

If the period, $T = 2\pi$, A_K becomes,

$$A_K = \frac{2V_m}{\pi} \left[\frac{2}{K} \sin \omega t \right]_{-\pi/3}^{+\pi/3}, \text{ which simplifies to}$$

$$A_K = \frac{4V_m}{K\pi} \cdot \frac{\sqrt{3}}{2} .$$

Therefore the series is

$$e(\omega t) = \frac{4V_m}{\pi} \cdot \frac{\sqrt{3}}{2} \left[\cos \omega t - \frac{1}{5} \cos 5\omega t + \frac{1}{7} \cos 7\omega t - \frac{1}{11} \cos 11 \omega t + \dots \right], \quad (3.3)$$

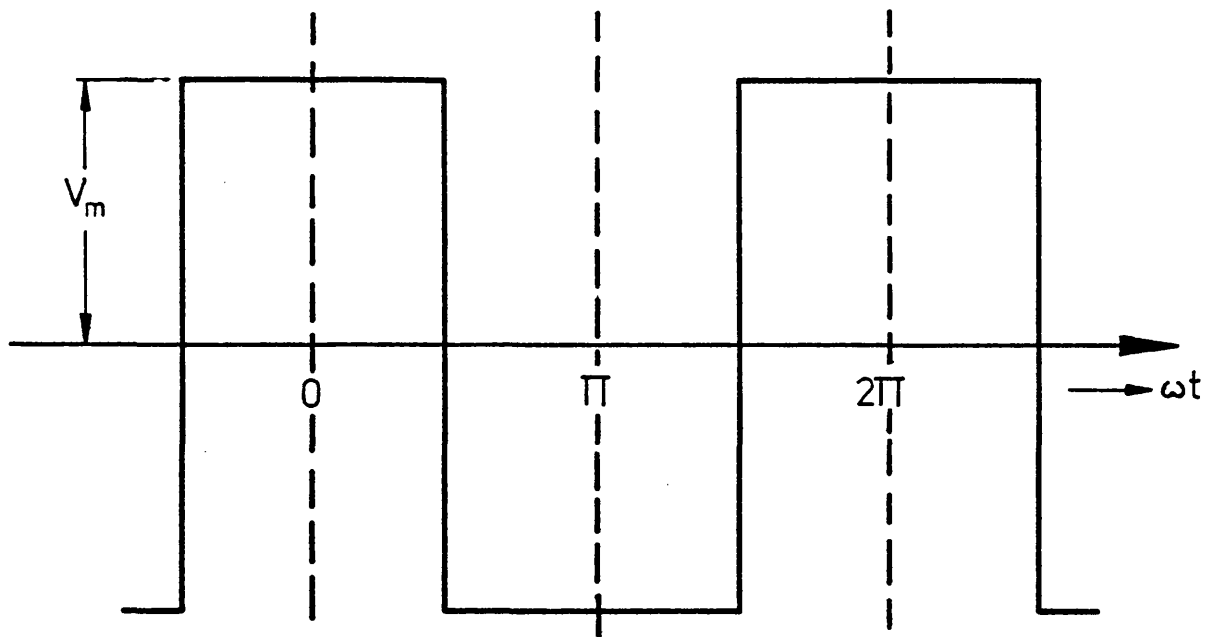


Fig. 3·1a. Square waveform.

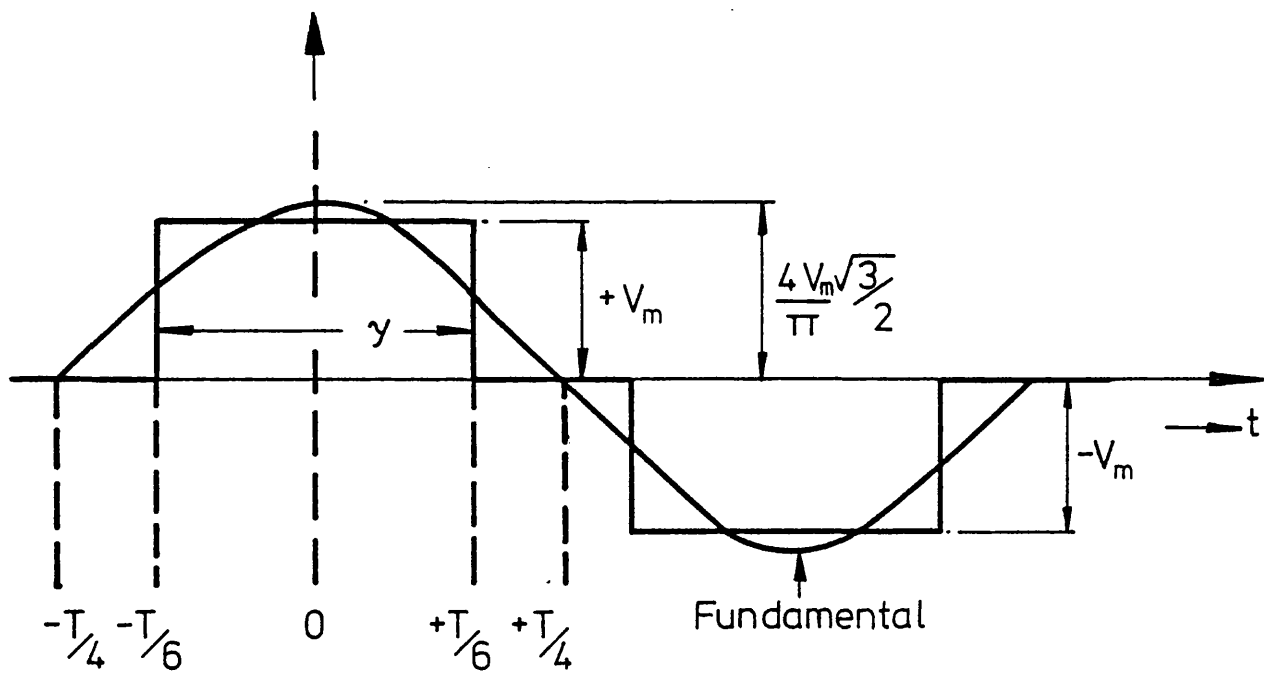


Fig. 3·1b. Waveform for voltage and harmonic analysis.

which may be expressed in a more general form as:

$$e(\omega)t = \frac{4V_m}{\pi} \sum_{K=1}^{\infty} \frac{1}{K} \sin\left(\frac{K\pi}{3}\right) \cdot \cos K \omega t . \quad (3.4)$$

The chart given in Fig.(3.2) uses equations (3.2) to (3.4) to express the harmonic amplitudes in terms of the conduction angles. It can be seen that a waveform with discontinuities has a slowly diminishing spectrum with fairly strong harmonics which should be considered when analysing the motor performance. The following table shows harmonic amplitudes related to conduction angles:

Conduction angle	γ°	30°	52°	60°	72°	80°	120°	160°
Order of Harmonic	Funda- mental	1	1	1	1	1	1	1
	K_3	0.24	0.32	0.34	0.32	0.28	0	0.29
	K_5	0.19	0.15	0.1	0	0.07	0.17	0.13
	K_7	0.14	0	0.08	0.13	0.14	0.13	0.05

Each harmonic also has a zero value at $\frac{180^\circ}{K}$ added to the zero shown in the table, where K is the order of the harmonic.

Any harmonic and its multiples can be eliminated, but it is most general practice to eliminate the triplens and zero-sequence effects. This can be achieved by making $\gamma = 120^\circ$.

Induction motor operation has been achieved with $\gamma = 180^\circ$ by McLean and Alwash ⁽¹⁴⁾, but at low frequencies the long conduction time when $\frac{dv}{dt} = 0$ can cause a flux collapse due to magnetic saturation if the peak flux is near to saturation level. They achieved stable operation by incorporating special machine windings which gave, in effect, nine-

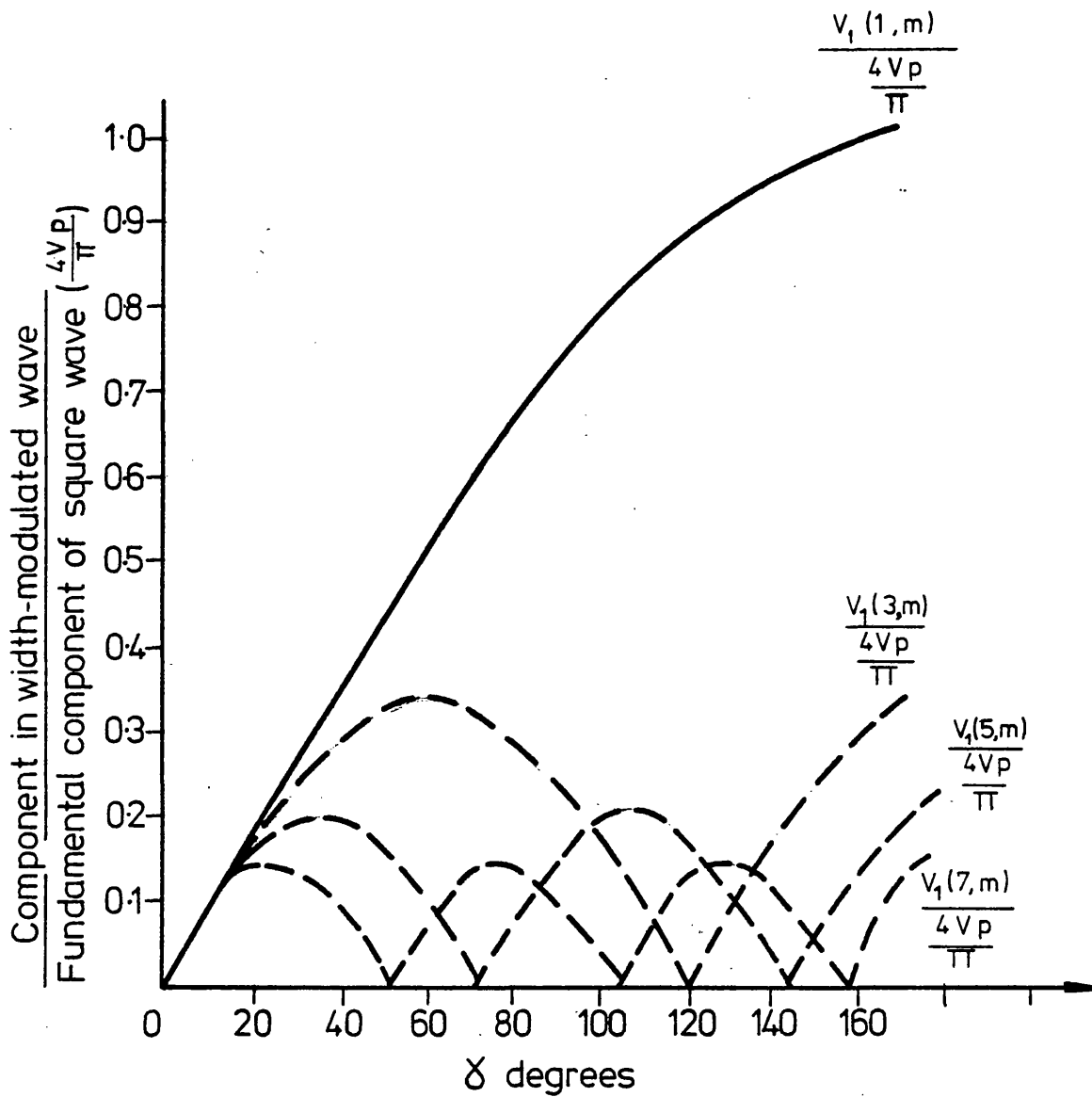


Fig. 3.2 Harmonic content, expressed as a fraction of the fundamental component in a nonsinusoidal wave related to pulse width δ

phase operation and triplen-harmonic elimination.

Many small size (<100kw) drives operate satisfactorily on rectangular pulses with triplen elimination as shown in Fig. (3.1b), but systems of a greater size require voltage waveforms nearer to the sinusoidal. Typical waves are the stepped waveforms of Figs. (3.3a) and (3.3b) ⁽¹⁵⁾ and the pulse-width modulated waveforms of Fig. (3.3c). These waveforms are much to be preferred for efficient and stable system operation, but the complexity of electronic logic required to generate the waveform is considerable and this present study is based on the simpler rectangular pulse system in which the harmonic effects will be greater.

3.3 Positive-sequence, negative-sequence and zero-sequence harmonics

The three stator voltages of the induction motor spaced by 120° are given by Fourier series analysis as:

$$V_A = \sum_{K=1}^{\infty} A_K \cos K\omega t + \sum_{K=1}^{\infty} B_K \sin K\omega t \quad , \quad (3.5)$$

$$V_B = \sum_{K=1}^{\infty} A_K \cos K\left(\omega t + \frac{2\pi}{3}\right) + \sum_{K=1}^{\infty} B_K \sin K\left(\omega t + \frac{2\pi}{3}\right) \quad , \quad (3.6)$$

$$V_C = \sum_{K=1}^{\infty} A_K \cos K\left(\omega t + \frac{4\pi}{3}\right) + \sum_{K=1}^{\infty} B_K \sin K\left(\omega t + \frac{4\pi}{3}\right) \quad . \quad (3.7)$$

It can be seen from the above equations that if $K = 3N + 1$, the phase sequence is V_A, V_B, V_C which is taken as the positive sequence, the fundamental sequence of the rotation of the field. If $K = 3N + 2$, the phase-sequence is V_A, V_C, V_B which gives resultant fields rotating in the opposite direction or a negative sequence. When $K = 3N + 3$, the three phase voltages are in phase. The resultant field is pulsating, but not rotating, and it is defined as a zero sequence.

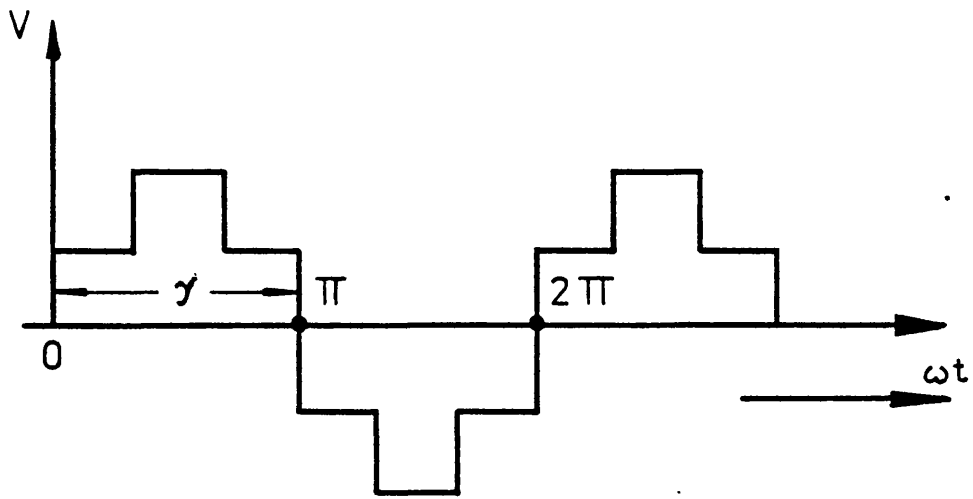


Fig.3-3 (a) Six-step nonsinusoidal waveform.

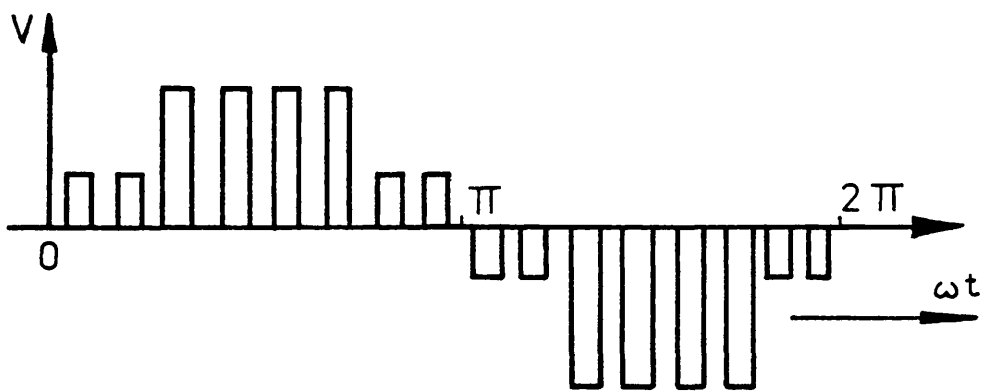


Fig.3-3 (b) Eight step waveform.

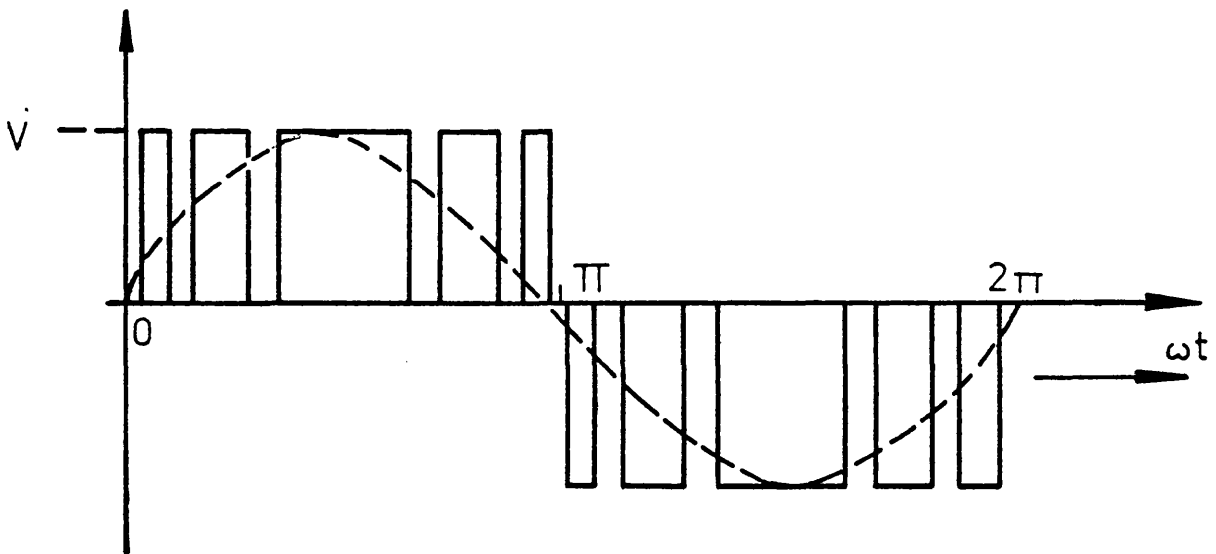


Fig.3-3 (c) Pulse width modulated waveform.

The orders of harmonic present in the general series are given in the table below. However the Fourier series of the supply voltage is an odd harmonic series and even harmonic components cannot be present in the air-gap flux.

	positive-sequence	negative-sequence	zero-sequence
N	$K=3N+1$	$K=3N+2$	$K=3N+3$
0	1	2	3
1	4	5	6
2	7	8	9
3	10	11	12
4	13	14	15
5	16	17	18
6	19	20	21
7	22	23	24
8	25	26	27
9	28	29	30
10	31	32	33
11	34	35	36

Only odd harmonics need to be considered and from the above table the harmonics can be classified according to their sequences. The fundamental frequency is defined by $K = 1$, and is of positive phase sequence.

The following systems exist for the other harmonics;

- a) Positive-sequence 7, 13, 19 etc.
- b) Negative-sequence 5, 11, 17 etc.
- c) Zero-sequence 3, 9, 15 etc.

3.4 Motor equivalent circuit allowing for harmonics

In section 3.3, the non-sinusoidal supply was seen to give positive, negative and zero sequence harmonic frequencies. This means that three equivalent circuits will be necessary, one for each sequence. All reactive components are assumed to vary linearly with frequency so that $X_{1K} = KX_1$ etc, where X_1 is the reactance at fundamental frequency. R_{1K} and R_{2K} are the a.c. values of stator and rotor phase resistance for the K^{th} harmonic and R_{oK} is the iron loss energy component at this harmonic frequency. Thus for positive sequence operation the equivalent circuit of Fig. (2.1) becomes that of Fig. 3.4a) for the K^{th} harmonic.

The slip, S_K , related to the K^{th} harmonic is:

$$S_K = \frac{K\omega - \omega_2}{K\omega} , \quad (3.8)$$

where ω is the fundamental synchronous speed and ω_2 is the rotor speed in radians per second.

If the harmonic field is counter rotating, negative sequence operation results and the slip term to be used in the equivalent circuit is $2 - S_K$. The negative sequence equivalent circuit will then be shown in Fig. (3.4b).

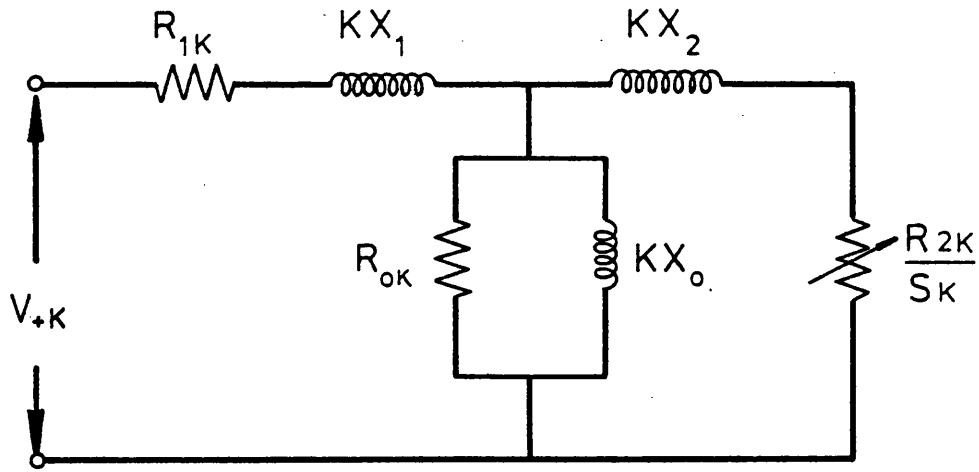


Fig. 3.4a Exact positive-sequence equivalent circuit.

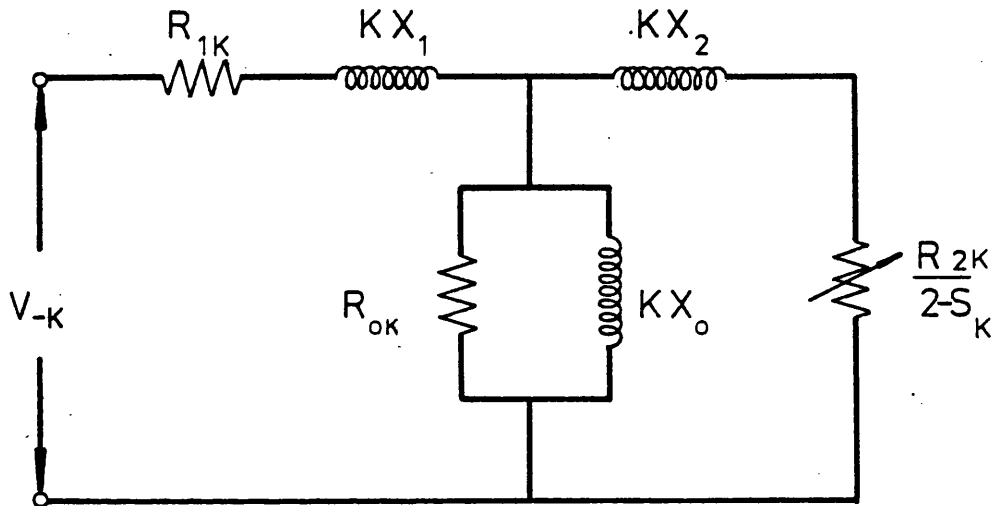


Fig. 3.4b Exact negative-sequence equivalent circuit.

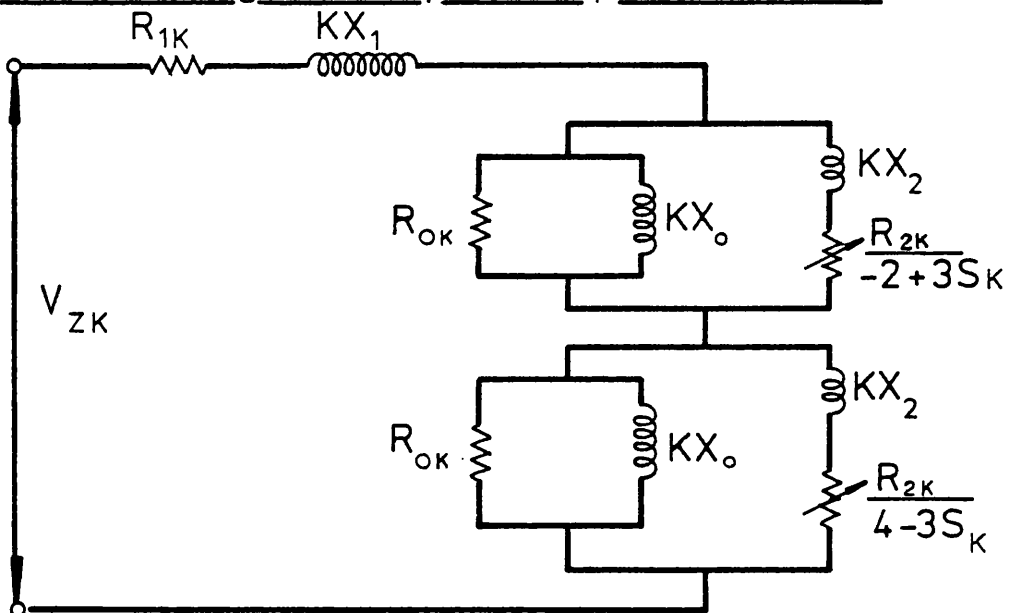


Fig. 3.4c Exact zero-sequence equivalent circuit.

A zero-sequence voltage component is simply a pulsating or single phase field. In effect all these phase windings can be considered to be connected in series to a zero-sequence voltage. The effect of this is the well-known pole trebling effect used in squirrel-cage pole-change systems. Thus the zero-sequence voltage may be assumed to consist of a half-magnitude forward rotating component, and a half-magnitude reverse rotating component. The forward component will have a slip term of $1 - 2 + 3 S_K$ and the reverse component, a slip of $4 - 3 S_K$. Both components are incorporated into the zero-sequence equivalent circuit of Fig. (3.4c).

For torque calculations, the equivalent circuits of Figs. (3.4a,b and c) must be used. This is illustrated in section 3.5. However, the other effects of harmonics, increased iron and copper losses and consequent loss of efficiency require a knowledge of the current in the appropriate equivalent circuit parameters.

If zero-sequence components have been substantially eliminated, by making the conduction angle γ such that all triplens disappear, the harmonic slip can be represented by the general expression:

$$S_K = \frac{K\omega \pm \omega_2}{K\omega} , \quad (3.8b)$$

where the + sign represents a positive-sequence harmonic and - sign, a negative-sequence harmonic. Equation (3.8) may now be re-written in terms of the fundamental slip, S, by the use of the relationship:

$$\omega_2 = (1 - S) \omega , \quad (3.9)$$

which gives,

$$S_K = \frac{K \pm (1-S)}{K} = 1 \pm \frac{(1-S)}{K} . \quad ((3.10)$$

Iron losses in the machine would normally be determined experimentally by driving the machine externally at fundamental

synchronous speed and measuring the input power. For the fundamental, $I_2 = 0$ and the equivalent circuit becomes that of Fig. (3.5a). This is an approximation, because the harmonic slips are much greater than zero, and the input power measured in the way includes harmonic copper losses, but the fundamental copper loss is eliminated and so Fig. (3.5a) is a good, simple first order approximation. Fig. (3.5a) then enables the iron loss currents to be calculated independently of machine slip, and, if the circuit parameters are correct for each harmonic K , the rms iron loss current will be given by:

$$I_o = \sqrt{\sum I_K^2} \quad (3.11)$$

Copper loss currents under load conditions will be much greater than the iron loss components and a first order estimate of the copper loss current for each harmonic will be given by the equivalent circuit of Fig. (3.5b) for any high order of harmonic, $S_K \gg 0$ and $\frac{R_{2K}}{S_K}$ can be replaced by a short-circuit, giving the approximation of Jain (16).

3.5 Harmonic effects on the induction motor steady-state performance

Additional heating caused by harmonics will be discussed more fully in section 3.7. At this stage the effect of harmonic currents on the motor torque will be considered. Equation (3.1) for the fully conducting rectangular voltage gives a series containing positive, negative and zero-sequence harmonics. The effect of each is considered in turn.

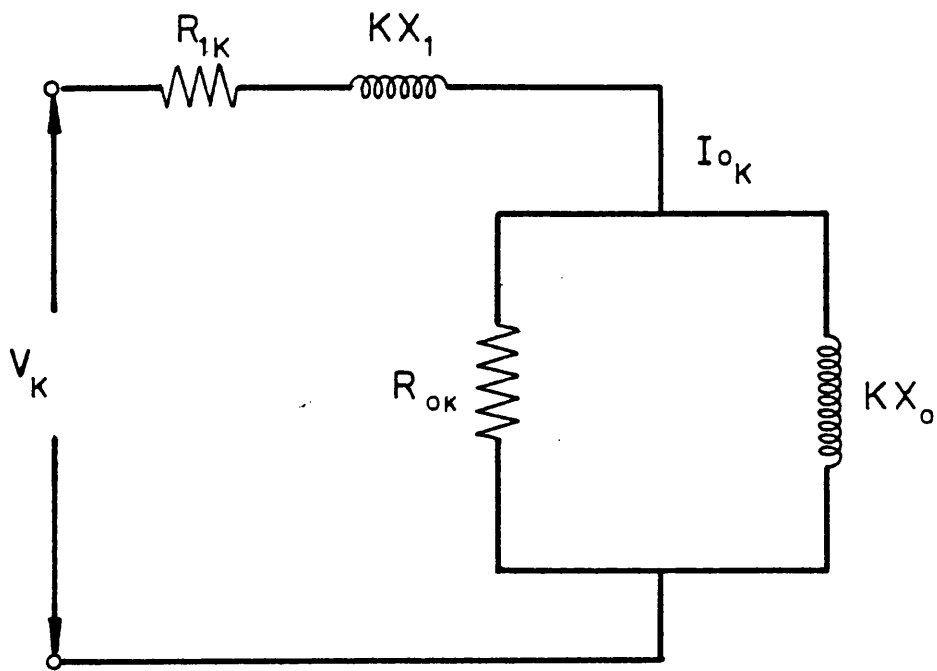


Fig. 3.5a. Equivalent circuit for iron loss calculation.

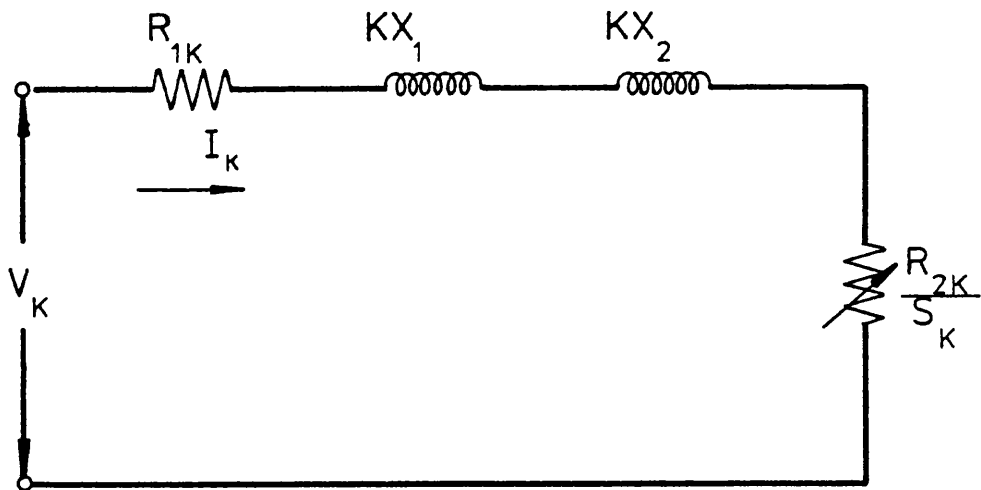


Fig. 3.5b. Equivalent circuit for copper loss calculation.

3.5a Positive and negative sequences

It has been shown that the phase sequence of the 7th, 13th and 19th harmonics is the same as that of the fundamental sequence and that the amplitude of the harmonic relative to the fundamental is inversely proportional to the order of the harmonic, i.e.

$$A_7 = \frac{A_1}{7}, \quad A_{13} = \frac{A_1}{13} \text{ etc.}$$

Fig. (3.6) shows how the fundamental torque is modified by the Kth harmonic. Motoring and plugging torques are slightly increased, while the supersynchronous braking torque is slightly reduced. Equations (3.5) to (3.7) show that the phase sequence of the 5th, 11th and 17th harmonics will be opposite to the fundamental sequence, while the amplitudes $A_5 = \frac{A_1}{5}$ etc. as before. These negative sequence torques modify the torque characteristic as shown in Fig. (3.7). Here motoring and plugging torques are slightly reduced and the supersynchronous braking torque is increased.

However, in practice, the effect of a positive or a negative time harmonic on the torque is negligible. This can be justified as follows. At harmonic frequencies, the leakage reactance is much greater than the machine resistance at substantial slips. The leakage reactance increases with frequency and the harmonic voltage amplitude falls with frequency. Hence the Kth harmonic current will be approximately $\left(\frac{1}{K}\right)^2$ x the fundamental current. The motor torque is proportional to the (current)², and hence the positive and negative sequence time harmonics have little effect on steady state performance although they may have an effect on motor losses which must be considered.

3.5b Zero-sequence harmonic effects

Equations (3.5) to (3.7) show that the harmonic voltages of the 3rd and all triplen harmonics are of equal magnitude and in phase in each phase winding of the machine. Effectively the machine phase

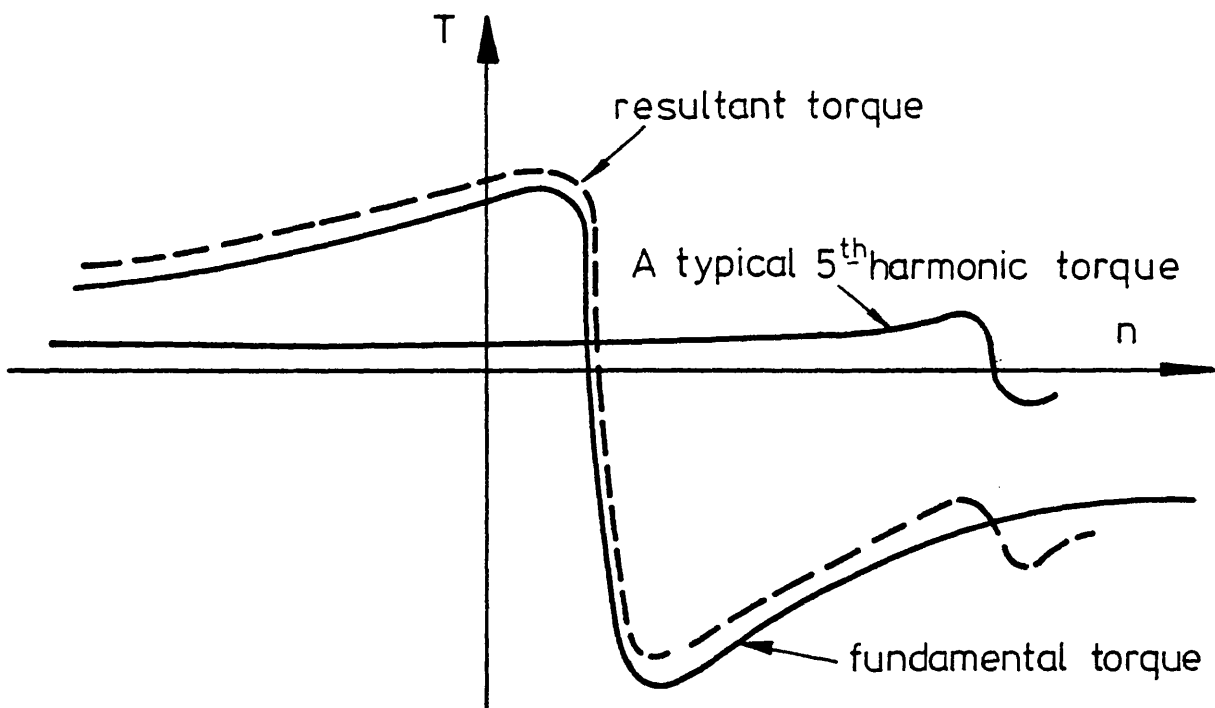


Fig. 3.6 Positive - sequence harmonic torque.

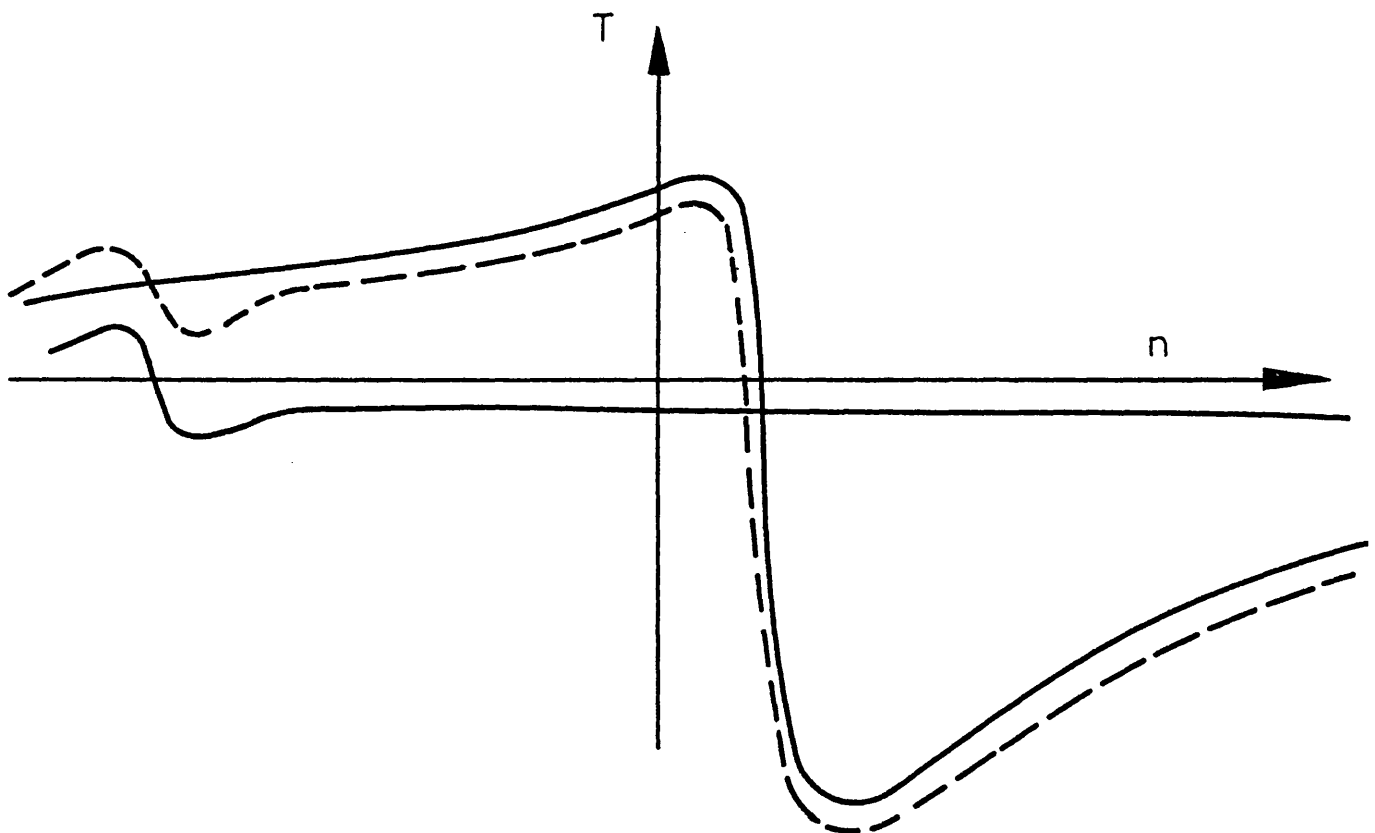


Fig. 3.7 Negative sequence harmonic torque.

windings have been connected up in series to a single phase supply of harmonic frequency. The nature of the resultant air-gap flux can be seen by a consideration of Figs. (3.8) to (3.10). For simplicity a single-layer, two slots/pole/phase winding has been chosen. When the stator is energised by a balanced 3-phase supply, at the instant $t = 0$, the air-gap mmf is as shown in Fig. (3.9). The resultant flux of constant amplitude moves around the circumference of the machine at synchronous speed. However, when the stator coils are connected in series to a single phase supply, Fig. (3.10) shows that the effective stator pole number has been trebled and that the resultant air-gap mmf is stationary and pulsating.

The air-gap fluxes were observed experimentally by exciting the stator with d.c. and rotating the machine at a constant speed of 1000 rev/min. while rotor search coil induced voltages were observed on an oscilloscope. For this experiment the squirrel-cage rotor was replaced by a 4-pole wound rotor with open-circuit slip-rings. In each case, $I = 1.0$ A d.c. Fig. (3.12a) shows the air-gap flux corresponding to the condition of Fig. (3.9) and Fig. (3.11a). If time phases are reversed as shown in Fig. (3.11b), the phase currents correspond to the same time sequence, but they are of unequal amplitudes and the "W" shaped flux of Fig. (3.12b) results. Finally, if all three phases are fed in series with the same supply as shown in Fig. (3.11c), the triple-pole air-gap flux of Fig. (3.12c) results. A comparison of Fig. (3.12a) and Fig. (3.12c) shows that a zero-sequence harmonic gives single-phase operation at one-third of the harmonic synchronous speed.

This stationary pulsating field may be considered as producing two half-amplitude, counter-rotating fields producing a single-phase motor torque. Fig. (3.13a) shows the form of this torque for a low impedance motor. The resultant torque is the sum of a positive and a negative sequence torque. Between zero and forward synchronous speed this produces a net motoring torque with zero torque

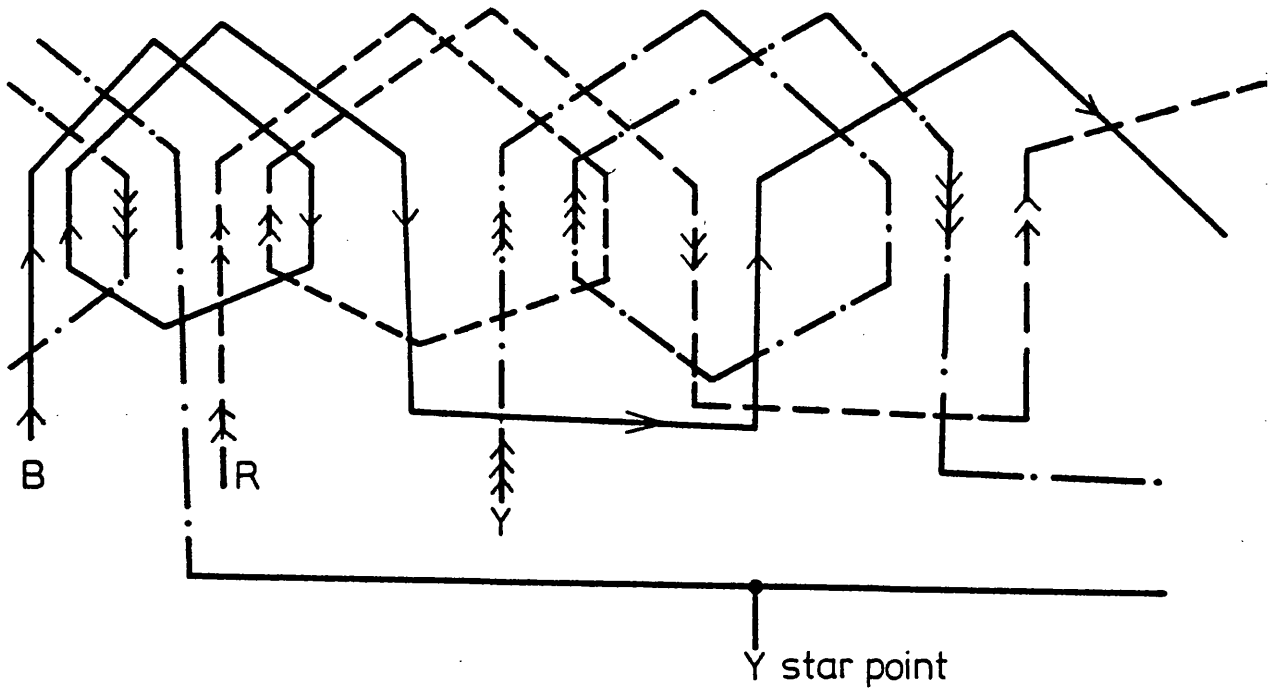


Fig.3.8 Developed 3 phase, star connected full pitch, single layer winding, 2 slots/pole/phase.

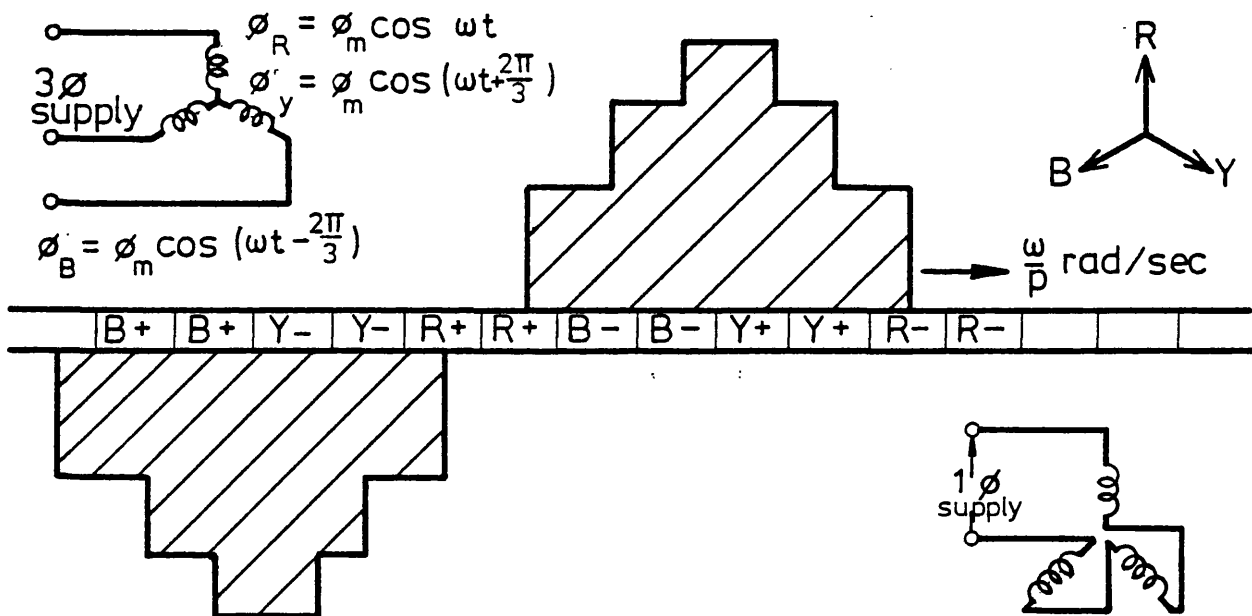


Fig.3.9 FUNDAMENTAL MMF at $t=0$

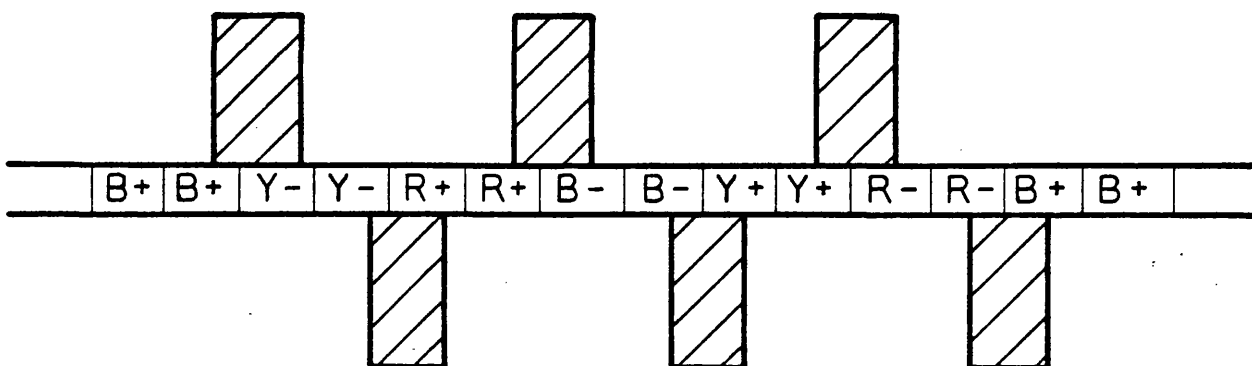
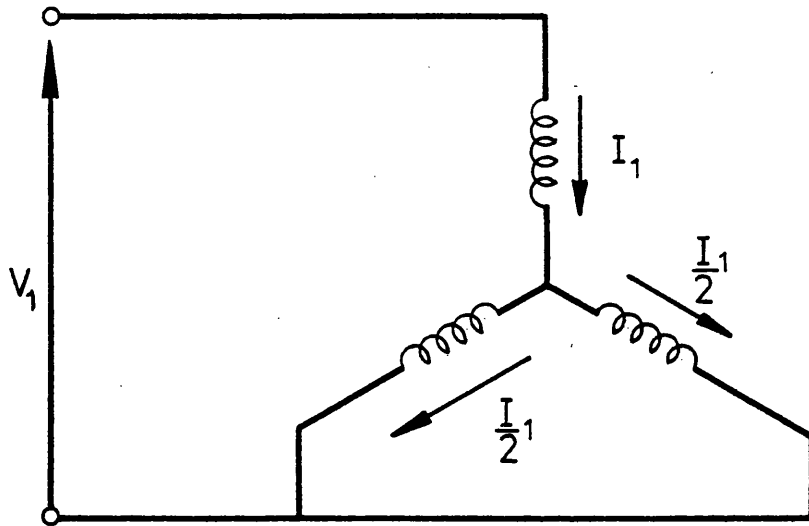
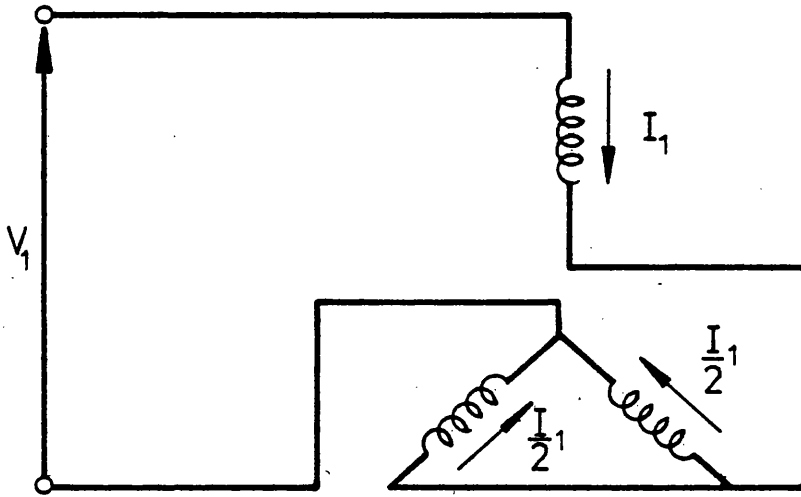


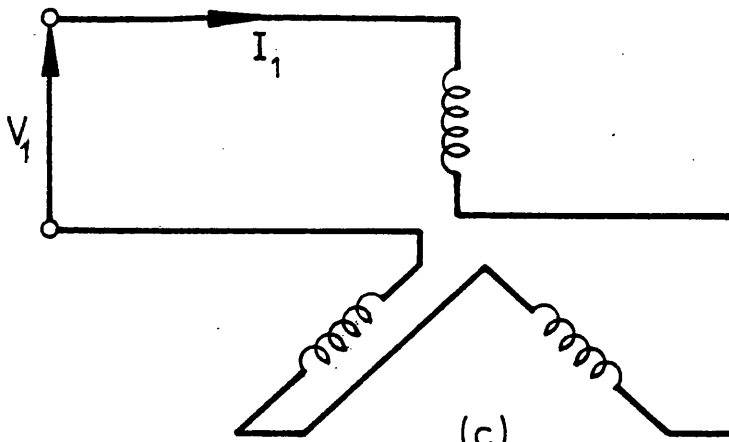
Fig.3.10 MMF due to fundamental frequency zero-sequence voltage.



(a)



(b)



(c)

Fig.3.11. Excitation connections for air gap flux observation.

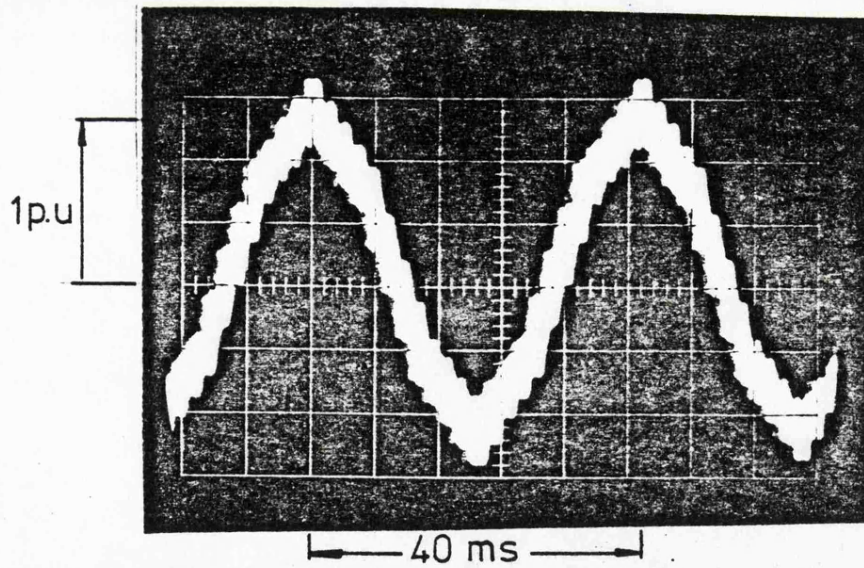


Fig. 3.12a Air gap flux in balanced 3-phase operation.

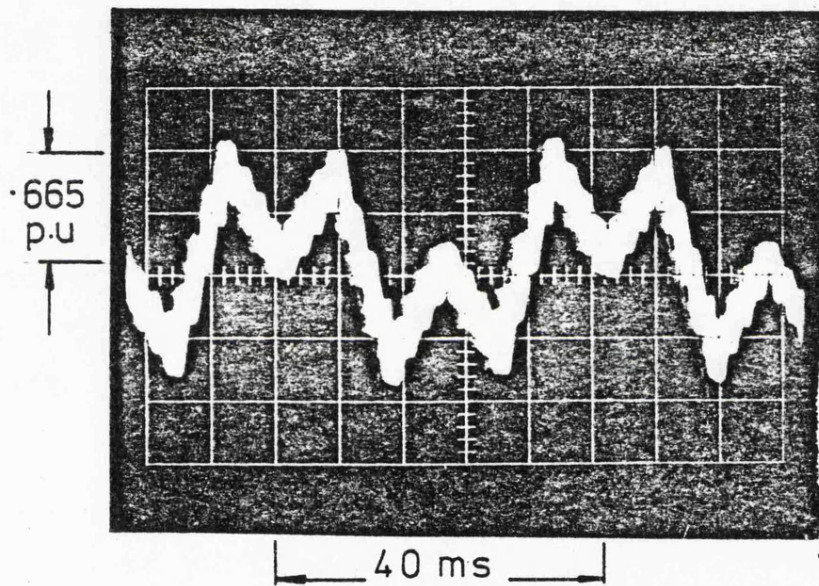


Fig. 3.12b. Air gap flux with current reversal in two phases.

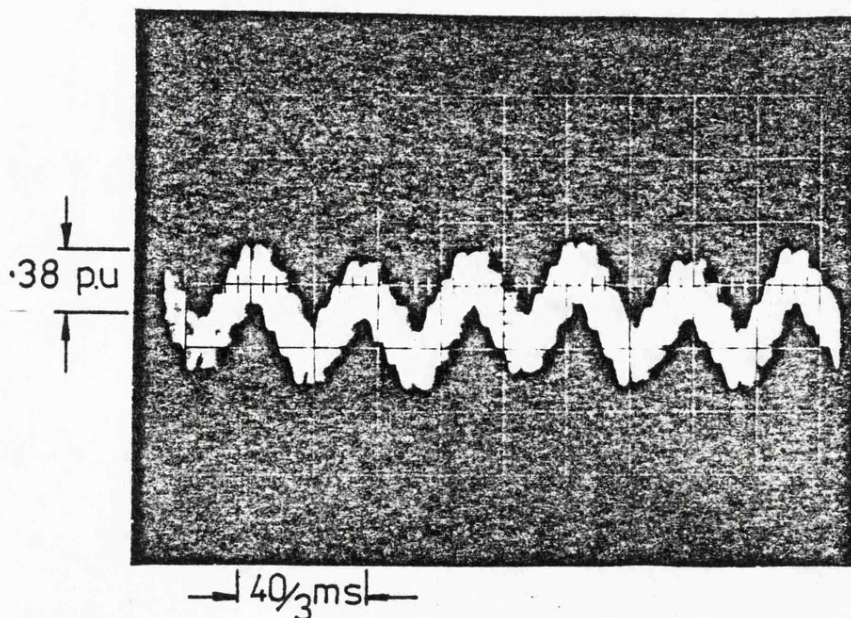


Fig. 3.12c. Zero sequence air gap flux.

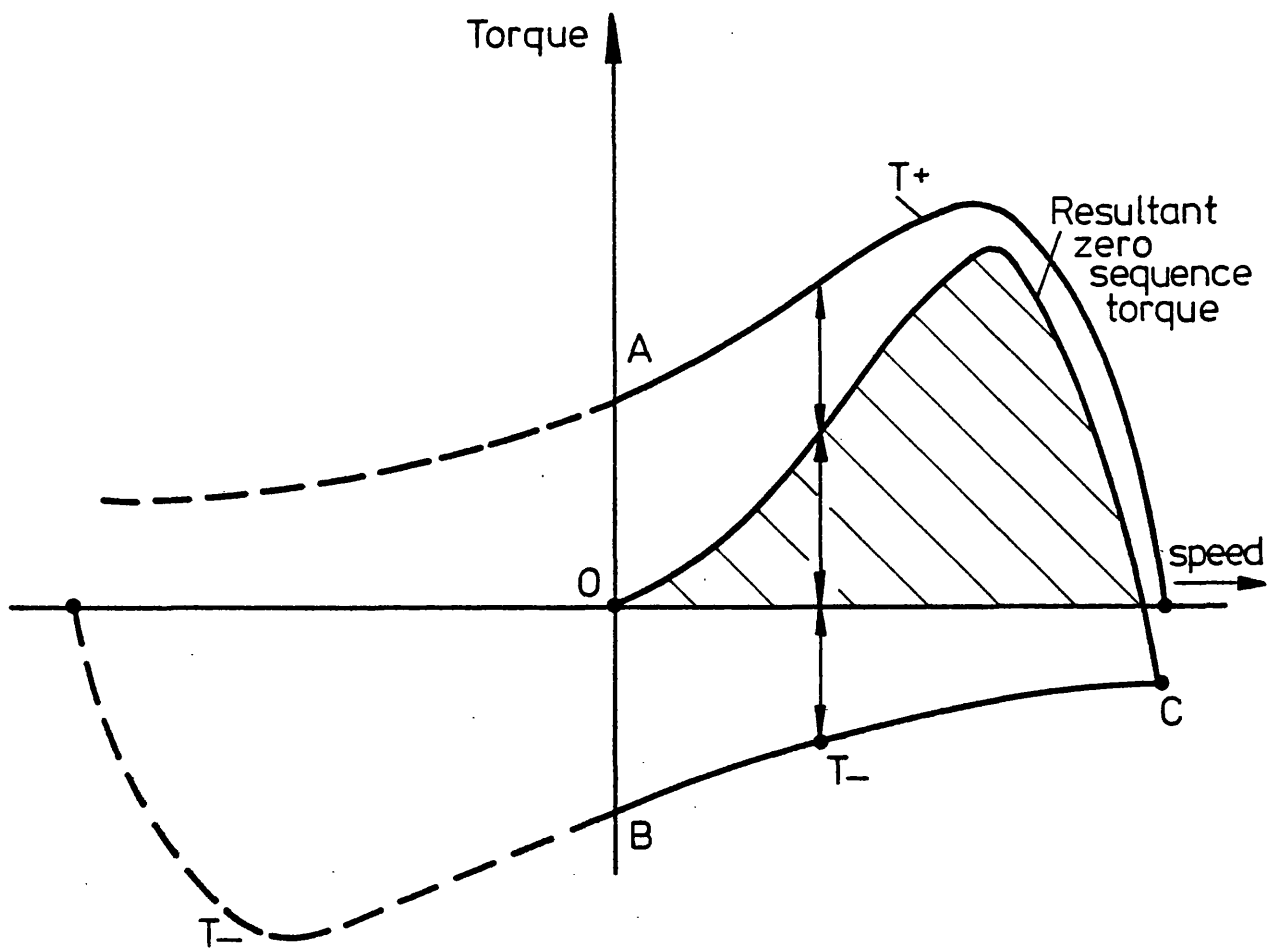


Fig 3.13a Zero sequence torque for low impedance rotor.

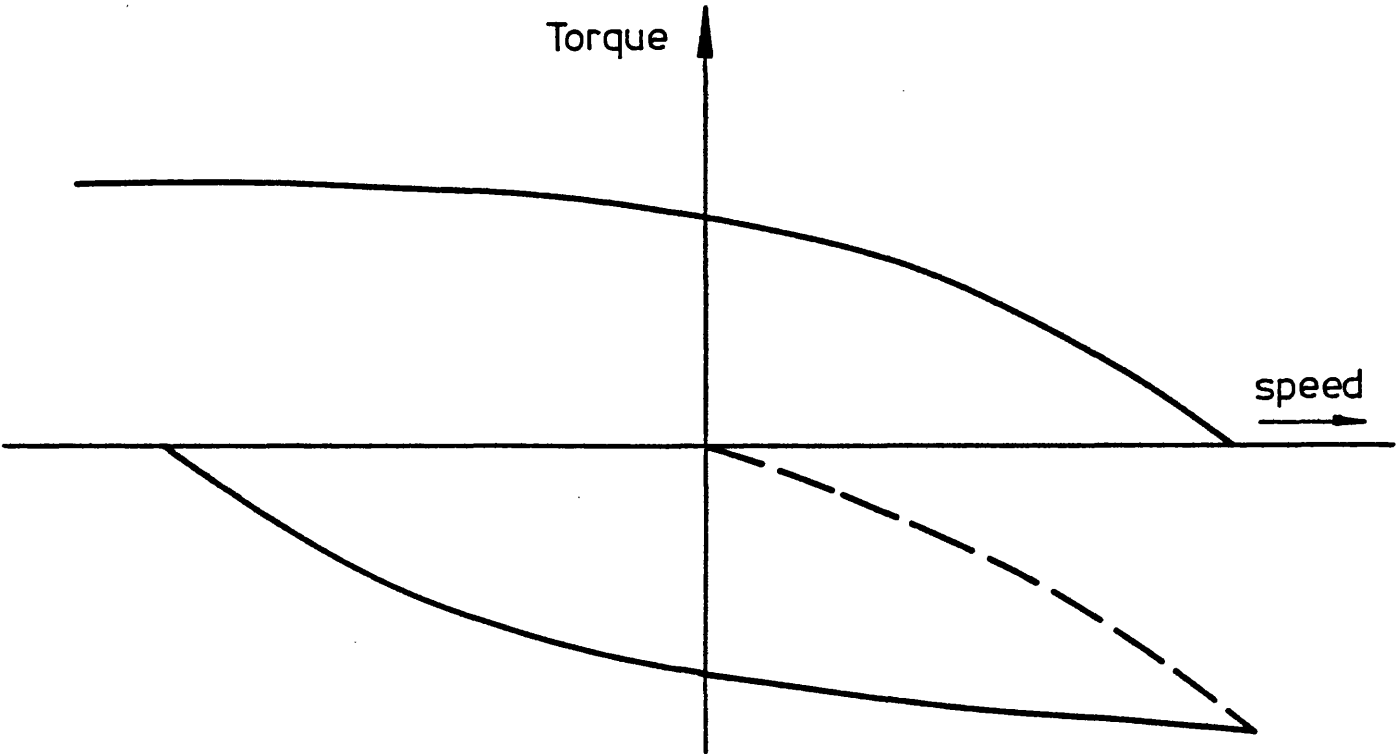


Fig 3.13 b Zero-sequence torque for high impedance rotor.

at zero and synchronous speed. When the rotor is of high impedance, a net braking torque will result as shown in Fig. (3.13b).

The effect of zero sequence torques is shown experimentally in Figs. (3.14) and (3.15) at 10 Hz and 20 Hz respectively. Predicted 3-phase and zero-sequence torques from equation (2.3) are shown for the third harmonic. The third harmonic zero-sequence currents produce a field of fundamental frequency which pulsates but does not rotate. Measured zero-sequence results corresponding to this prediction were obtained with all three stator phases connected in series to a single phase supply of three times the fundamental frequency. Each phase was excited with one-third of the fundamental voltage amplitude. Fundamental balanced 3-phase torques outside the range of speed between zero and synchronous speed were obtained with the motor supplied by an alternator generating a sinusoidal voltage. This alternator also supplied the single-phase supply.

The experimental results between zero and synchronous speed were obtained by supplying the stator by a cycloconverter fed with a square-wave reference giving a mean square output. This cycloconverter was unidirectional in conduction and unable to maintain the required output voltage under motor plugging conditions. However, it gave a good approximation to a square waveform with a pronounced third harmonic.

The resultant torque predicted between zero and synchronous speed is the graphical sum of the 3-phase and zero-sequence characteristics. Fig. (3.14) shows that at 10 Hz, the machine characteristic is that of a high resistance rotor machine, an effect becoming more pronounced at low frequencies. It can be clearly seen that the zero-sequence harmonic substantially reduces the motoring torque while increasing the total

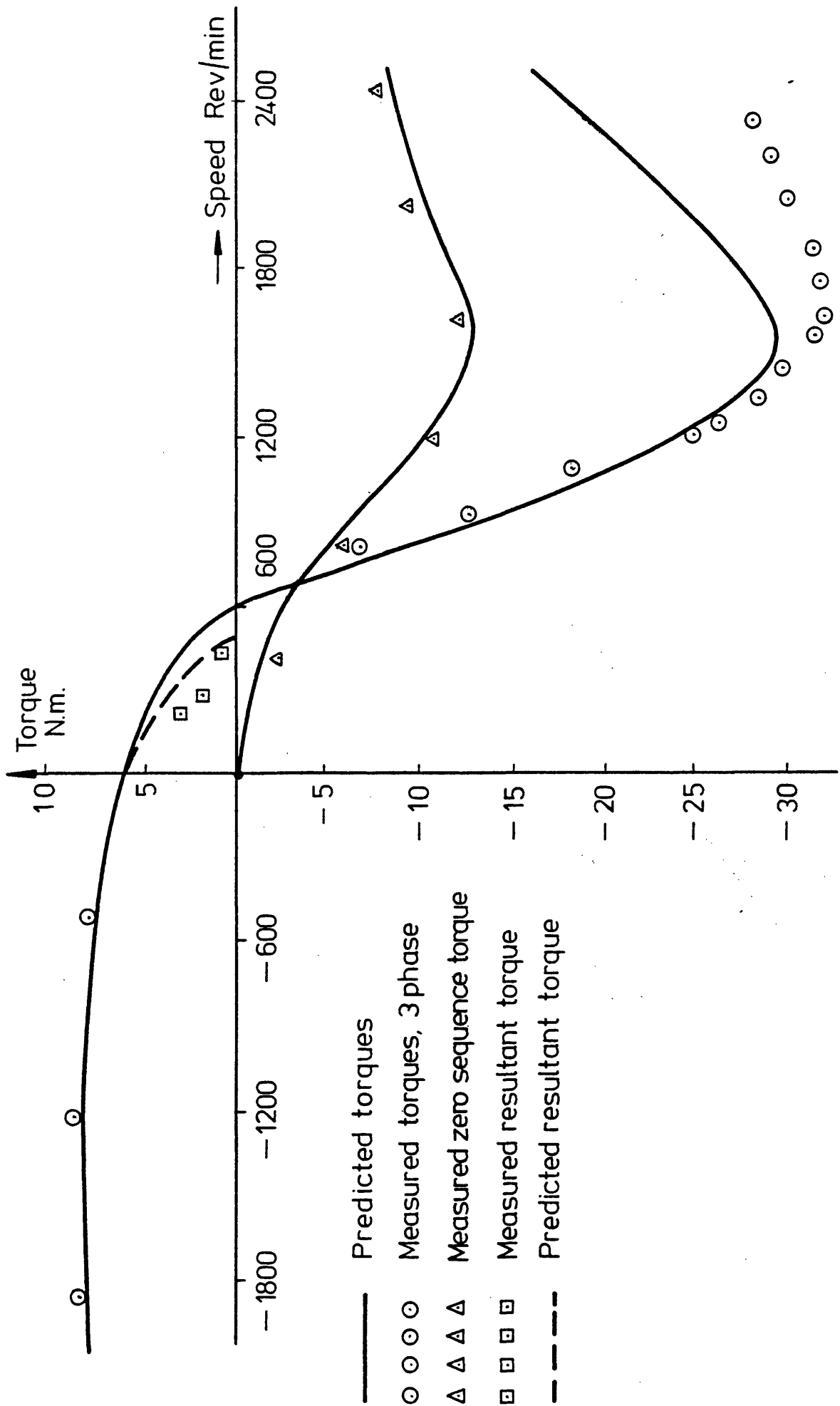


Fig. 3-14 Torque/speed characteristic, 10 Hz, V = 30V

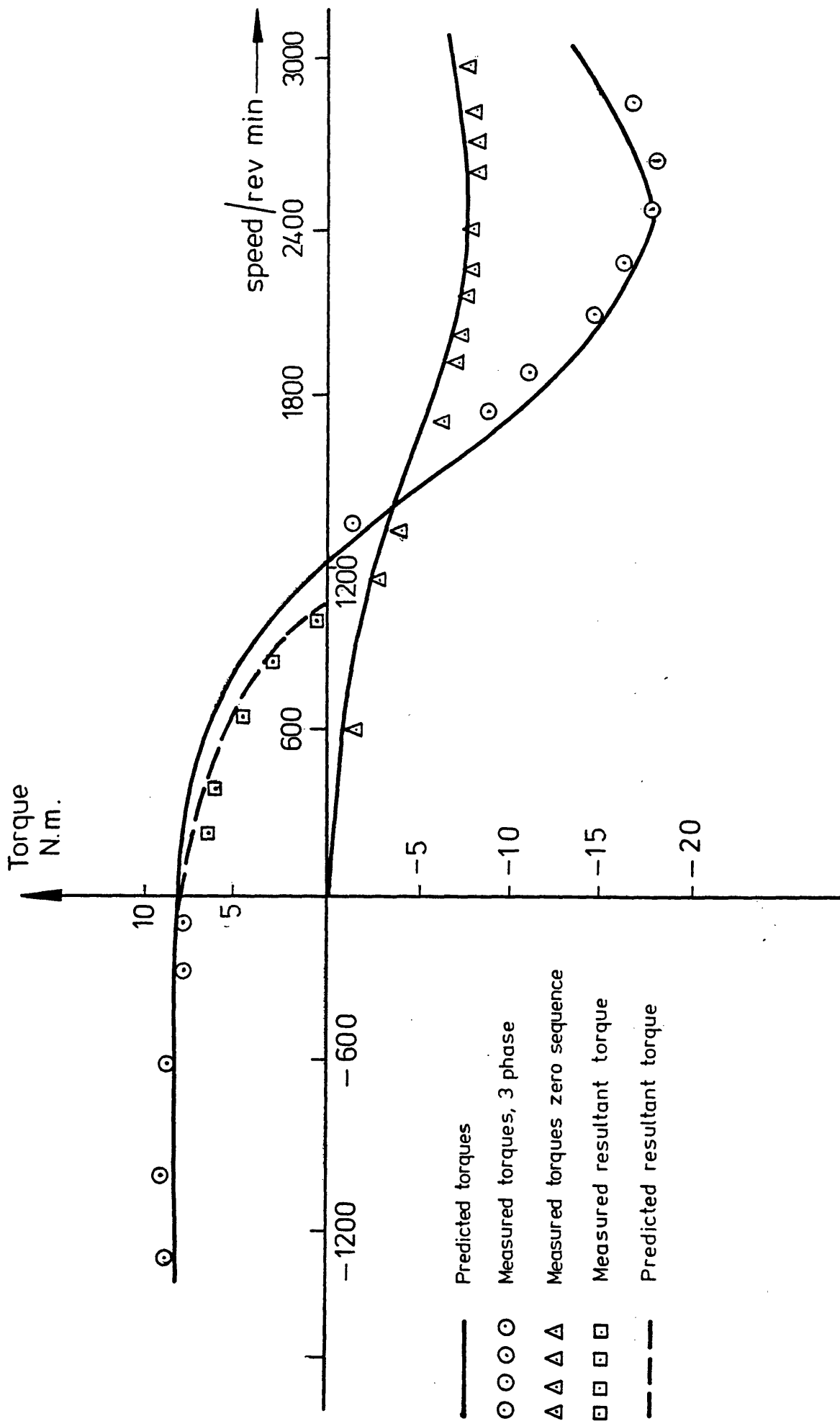


Fig. 3.15. Torque/speed characteristic, at 20 Hz, $V = 50$ V.

rms current. As the fundamental frequency is increased, the high resistance rotor effect is less pronounced and the relative motoring torque reduction is less as shown at 20Hz in Fig. (3.15)

It can be seen however that it is highly desirable to eliminate all triplen harmonics from the supply. The pulse-width limited waveform of Fig. (3.3) is highly desirable in order to achieve this, even at the expense of poor utility of electronic components.

3.6 Effect of sub-harmonics on motor performance

The previous discussion has been based on the effects of harmonics of greater frequency than the fundamental. Any symmetrical and balanced source of supply will only feed this type of harmonic into the system. However certain types of inverter operating on the pulse-width modulation principle with free-running non-synchronised thyristor pulse reference generators ^(17,18) can generate output voltages in which the positive half-cycles are not exact reflections of the negative half-cycles. In general the variation is cyclic at a frequency lower than the fundamental and sub-harmonics are introduced into the supply.

This sub-harmonic generation is also very pronounced in a circulating current free cycloconverter ⁽¹⁹⁾ operating with low input to output frequency ratios. Here the pulse inhibiting network in the cycloconverter may cause the positive and negative output half cycles to vary in size and deviation. Figs. (3.16a) and (3.16b) show how this asymmetry may occur. The deviation from the symmetrical is cyclic at a frequency lower than the fundamental. It also depends on the phase displacement of the load. This means that in an induction motor drive in which the power factor varies with load, that the sub-harmonic frequencies will vary with loading. A particular load sub-harmonic content cannot be specified. However it can be shown ⁽²⁰⁾ that with input to output cyclo-

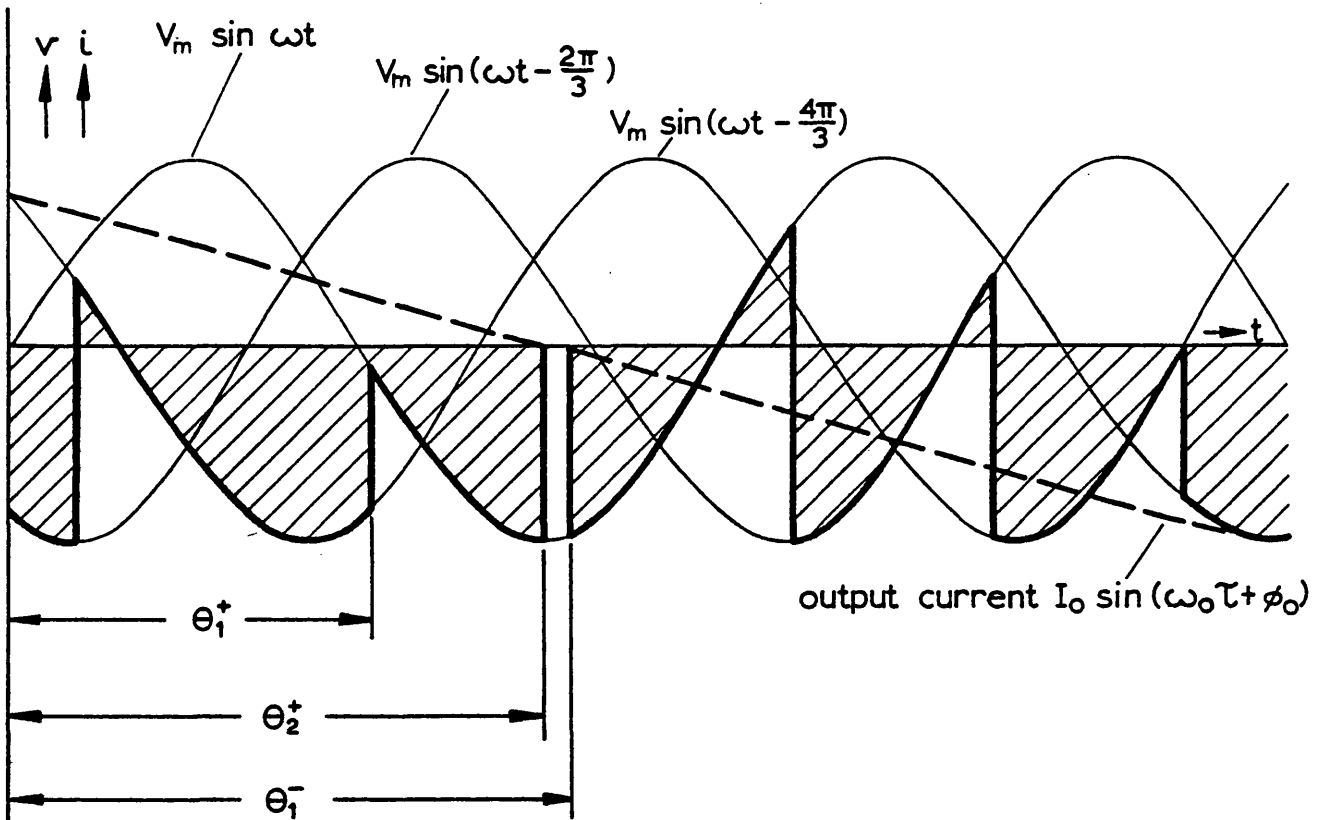


Fig. 3.16a LAGGING POWER FACTOR

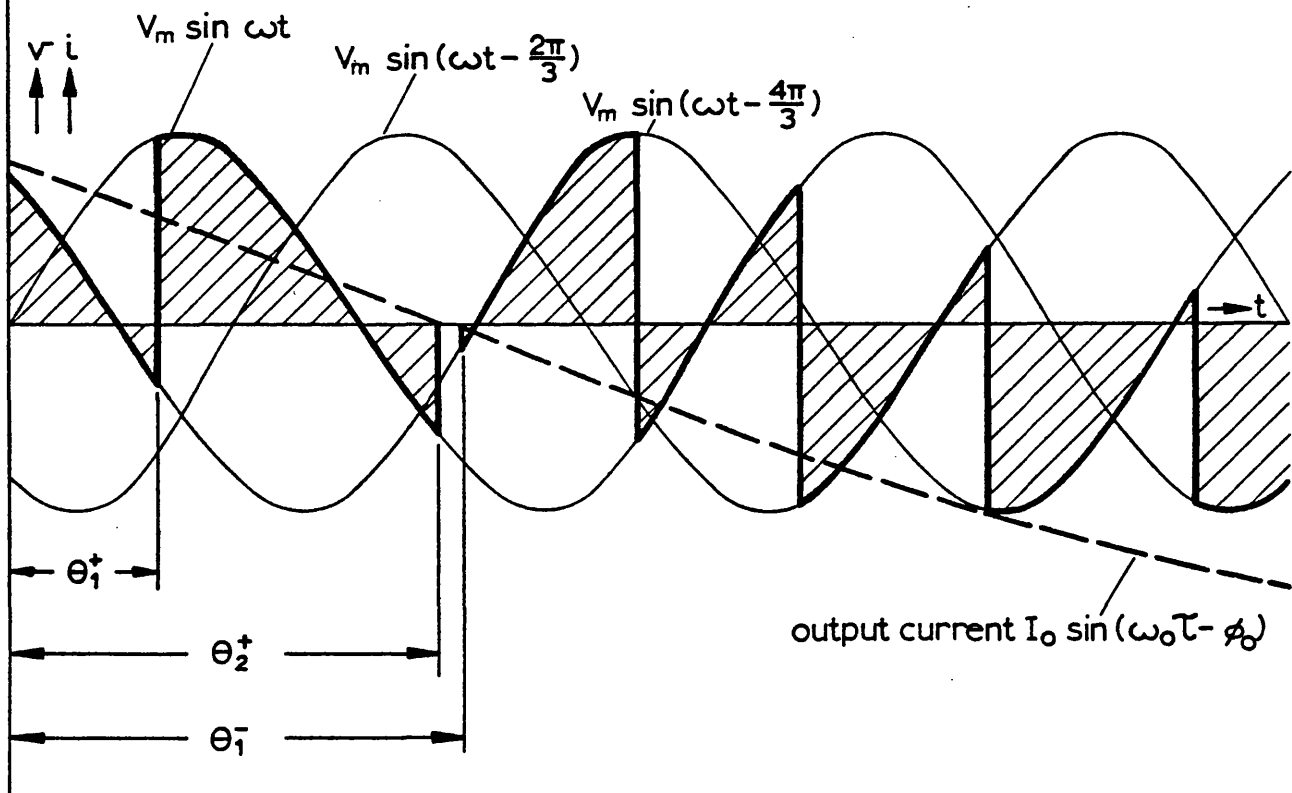


Fig. 3.16 b LEADING POWER FACTOR

CONDUCTION CHANGEOVER BETWEEN THYRISTOR GROUPS IN CIRCULATING CURRENT-FREE CYCLOCONVERTER

converter frequency ratios less than 3 and fundamental load displacement angles of 60° that the sub-harmonic amplitude at frequencies between one-fifth and one-third of the fundamental can approach a quarter of the fundamental amplitude. The effect of such sub-harmonics was investigated theoretically and experimentally.

No pulse-width modulated inverter or circulating-current-free cycloconverter was available for the experimental work and so the effect of sub-harmonics on the motor torque characteristic was investigated by injecting a sub-harmonic into the supply from an external source. First this was tried by transformer injection, as shown in Fig. (3.17). This was unsuccessful because the injected 50Hz produced induction torques in the alternator causing it to accelerate. It was impossible to load the induction motor in these circumstances.

Harmonic injection was successfully achieved in the system shown in Fig. (3.18). Here the two layers of the induction motor stator winding were kept electrically separate. Each frequency was fed into one layer of the stator winding. The two layers are coupled magnetically but separated electrically. Some transformer interaction between windings was experienced but this was not enough to change the speed of the alternator.

Sub-harmonics of one-fifth and one-third of the fundamental frequency were chosen to illustrate sub-harmonic effects. The sub-harmonic effect on the torque was exaggerated by making the sub-harmonic voltage amplitude large enough to give sub-harmonic currents of similar magnitude to the fundamental currents.

For the calculation of sub-harmonic torques the equivalent circuit expressed in terms of leakage reactances shown in Fig. (3.19a) was redrawn in terms of self and mutual-inductances as shown in Fig. (3.19b). The machine parameters in these terms are given in Appendix 1.

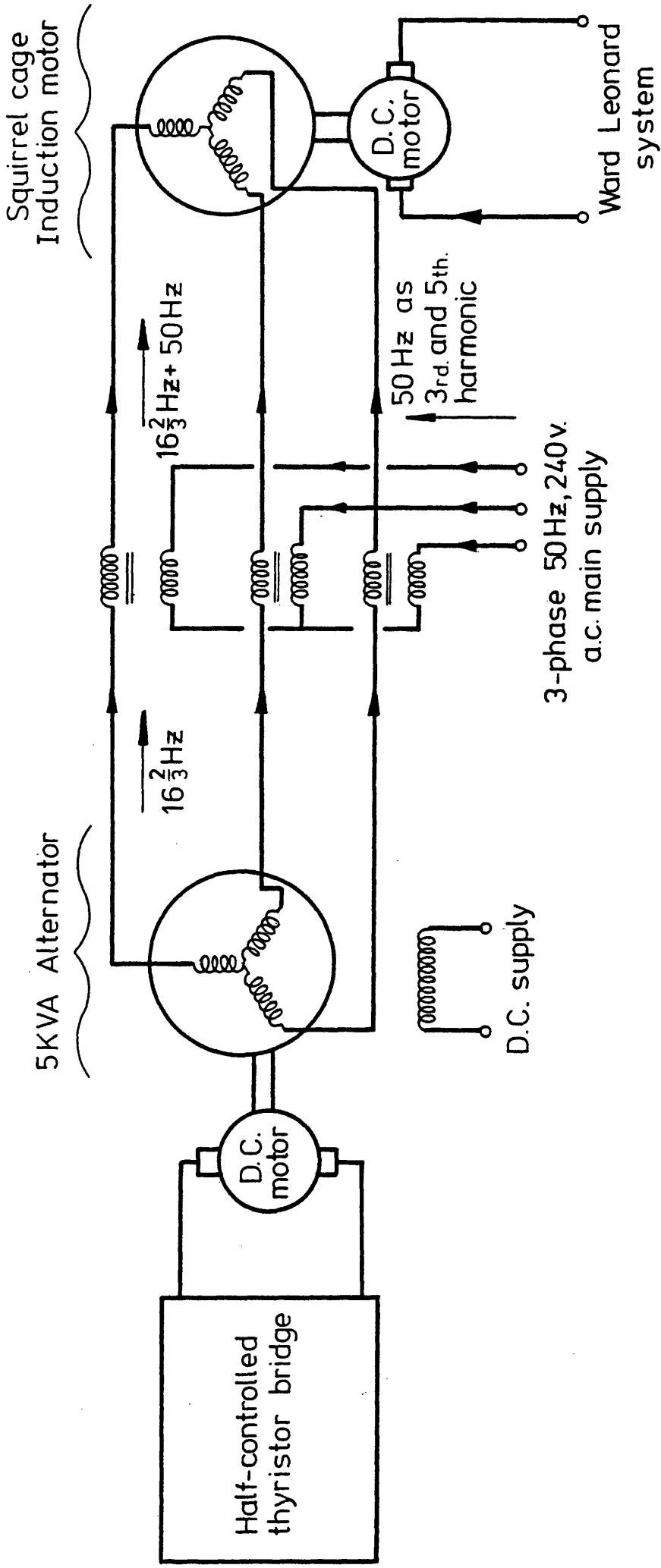


Fig. 3-17 Experimental apparatus for harmonic injection by external transformer.

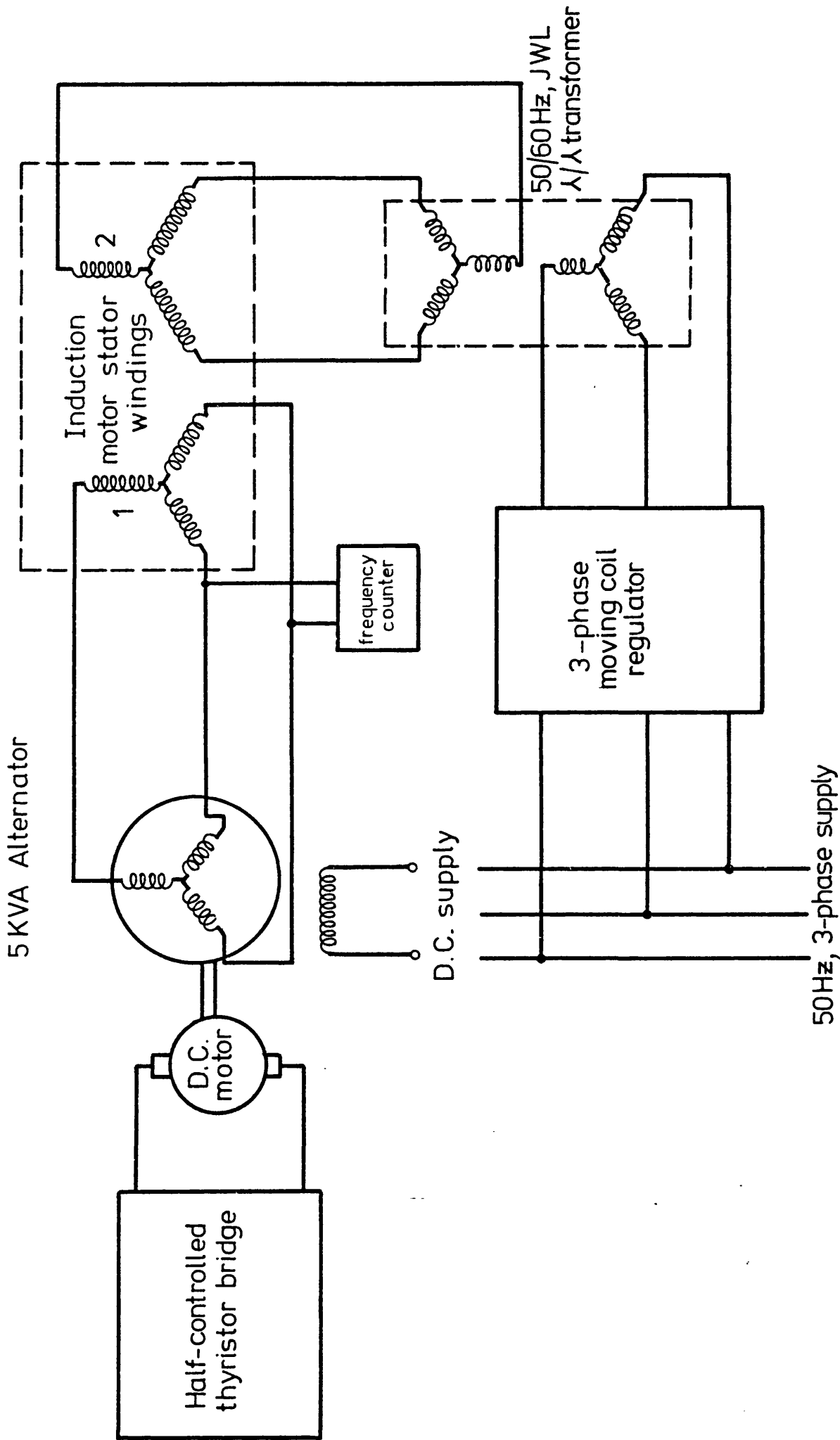


Fig. 3-18 The experimental apparatus for harmonic injection into separate stator windings.

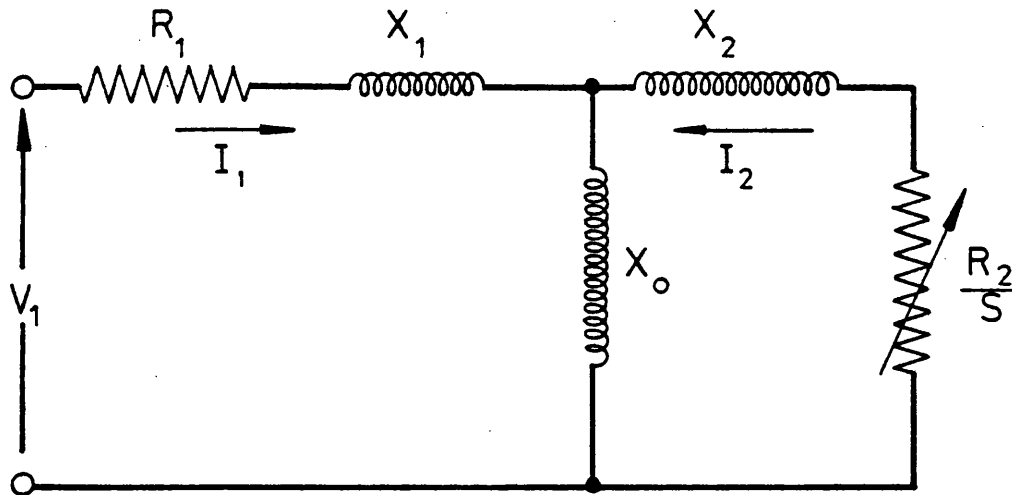


Fig.3:19a. Induction motor equivalent circuit in terms of leakage reactances.

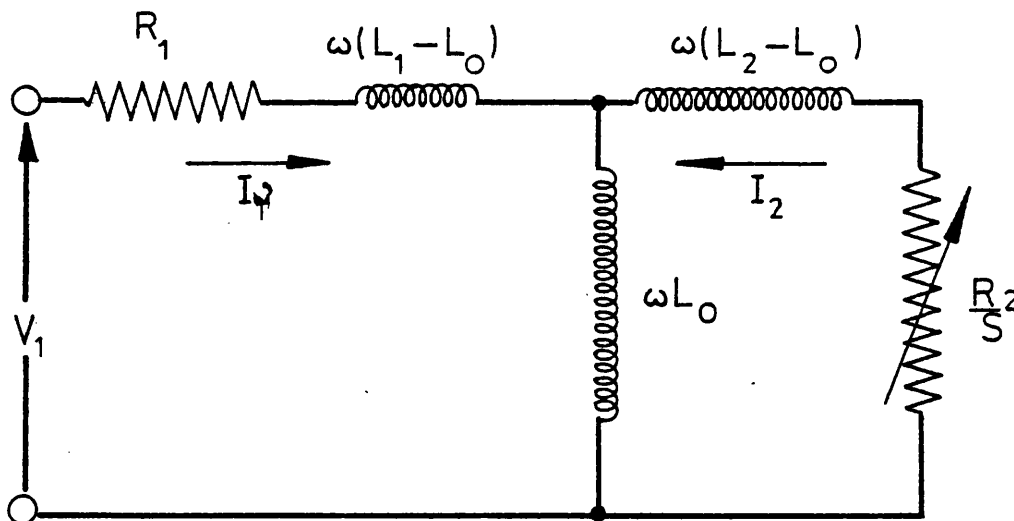


Fig.3:19b. Induction motor equivalent circuit in terms of self and mutual inductances.

The equations of the network shown in Fig. (3.19b) are as follows:

$$V_1 = [R_1 + j\omega L_1] I_1 + j\omega L_o I_2 \quad , \quad (3.12)$$

$$\text{and } 0 = j\omega L_o I_1 + \left[\frac{R_2}{S} + j\omega L_2 \right] I_2 \quad . \quad (3.13)$$

Equations (3.12) and (3.13) combine to give expressions for stator and rotor current respectively of,

$$I_1 = \frac{\left[\left(\frac{R_2}{S} \right)^2 + \omega^2 L_2^2 \right]^{\frac{1}{2}} V_1}{\left[\left\{ \frac{R_1 R_2}{S} - \omega^2 (L_1 L_2 - L_o^2) \right\}^2 + \omega^2 \left\{ -\frac{L_1 R_2}{S} + L_2 R_1 \right\}^2 \right]^{\frac{1}{2}}} \quad , \quad (3.14)$$

$$\text{and } I_2 = \frac{\omega L_o V_1}{\left[\left\{ \frac{R_1 R_2}{S} - \omega^2 (L_1 L_2 - L_o^2) \right\}^2 + \omega^2 \left\{ -\frac{L_1 R_2}{S} + L_2 R_1 \right\}^2 \right]^{\frac{1}{2}}} \quad . \quad (3.15)$$

The slip, S, may be written in general terms as:

$$1 - \frac{\omega_2 P}{\omega} \quad , \quad (3.16)$$

where ω_2 is the motor speed in rad/sec. and ω is the angular frequency of the supply. The iron loss parameter has been assumed to be of infinite value because the sub-harmonic iron losses are negligible at fundamental and lower frequencies.

The motor torque can be expressed as,

$$T_e = \frac{3I_2^2 R_2 (1-S)}{\omega_2 S} \quad , \quad (3.17)$$

which combines with equation (3.16) to give,

$$T_e = \frac{3I_2^2 R_2 P}{(\omega - P\omega_2)} \quad . \quad (3.18)$$

Resultant torques were computed from equation (3.18) after the current I_2 had been computed from equation (3.15) with S substituted from equation (3.16). The torque for each frequency was computed separately and the resultant formed from the sum of the individual frequency torques. This addition is shown graphically for positive-sequence sub-harmonics in Fig. (3.20) and negative-sequence sub-harmonics in Fig. (3.21). Cogging at sub-synchronous speeds may occur at a speed near to the sub-harmonic synchronous speed. A negative sequence sub-harmonic will drastically reduce starting torque and reduce motoring torques at higher speeds.

Fig. (3.22) shows the effect of a positive-sequence sub-harmonic in theory and practice with injected frequencies of 50 Hz and $16 \frac{2}{3}$ Hz. With this amplitude of sub-harmonic, the machine cannot run on load at a speed beyond the sub-harmonic crawling speed. With a lower sub-harmonic of 10 Hz, Fig. (3.23) shows a similar effect, although the fundamental peak motoring torque is doubled in this case.

Fig. (3.24) shows that a 10 Hz negative-sequence harmonic halves the motoring torque throughout the range compared with a 50 Hz torque. Plug-braking torques are increased. Overheating will result due to the added sub-harmonic currents.

These results show that the sub-harmonic content of a variable-frequency supply must be kept to absolute minimum if satisfactory motor operation is to be achieved. Low-speed crawling will inevitably result if the forward sub-harmonic amplitude approaches $(K) \times$ fundamental. ($K =$ order of harmonic = $1/3, 1/5$ etc.). A reverse sub-harmonic will probably prevent starting at all.

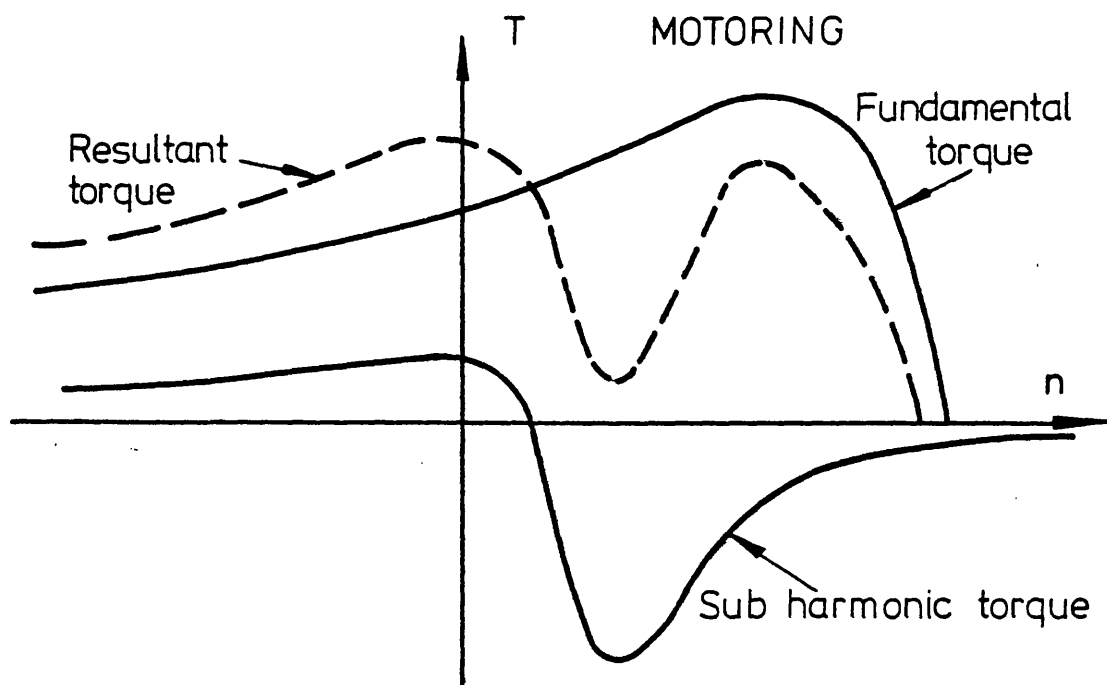


Fig.3.20. Effect of positive-sequence sub-harmonic on torque characteristic.

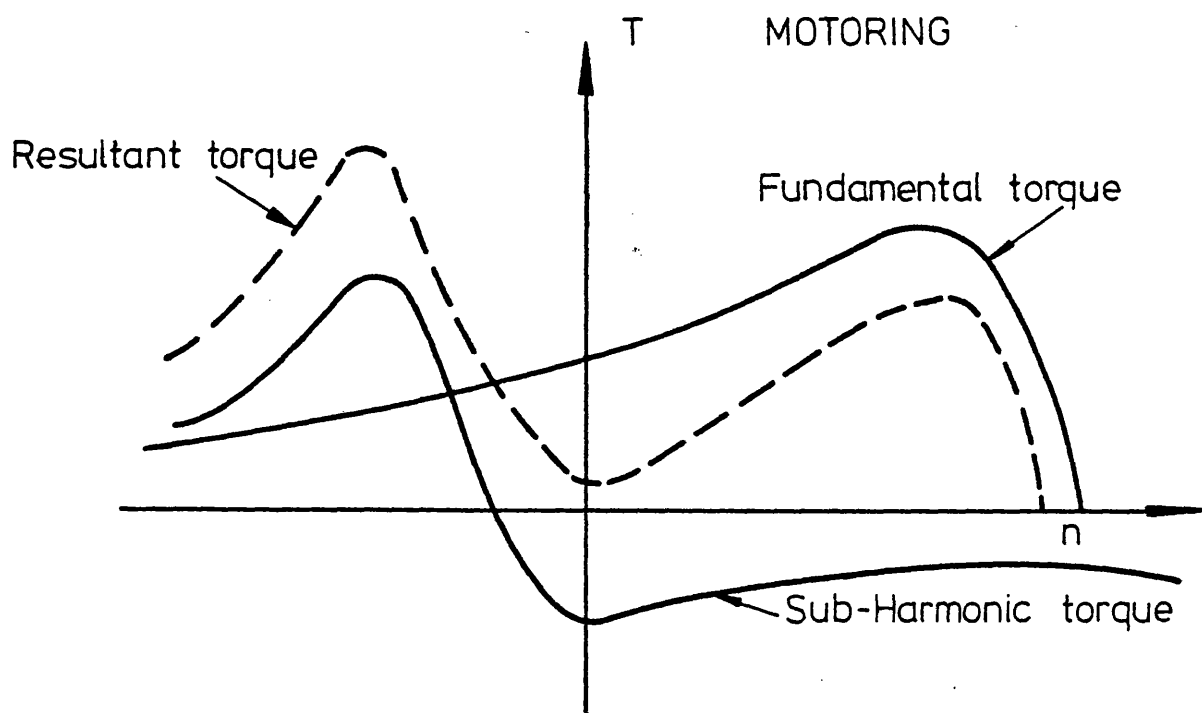


Fig.3.21. Effect of negative-sequence sub harmonic on torque characteristic.

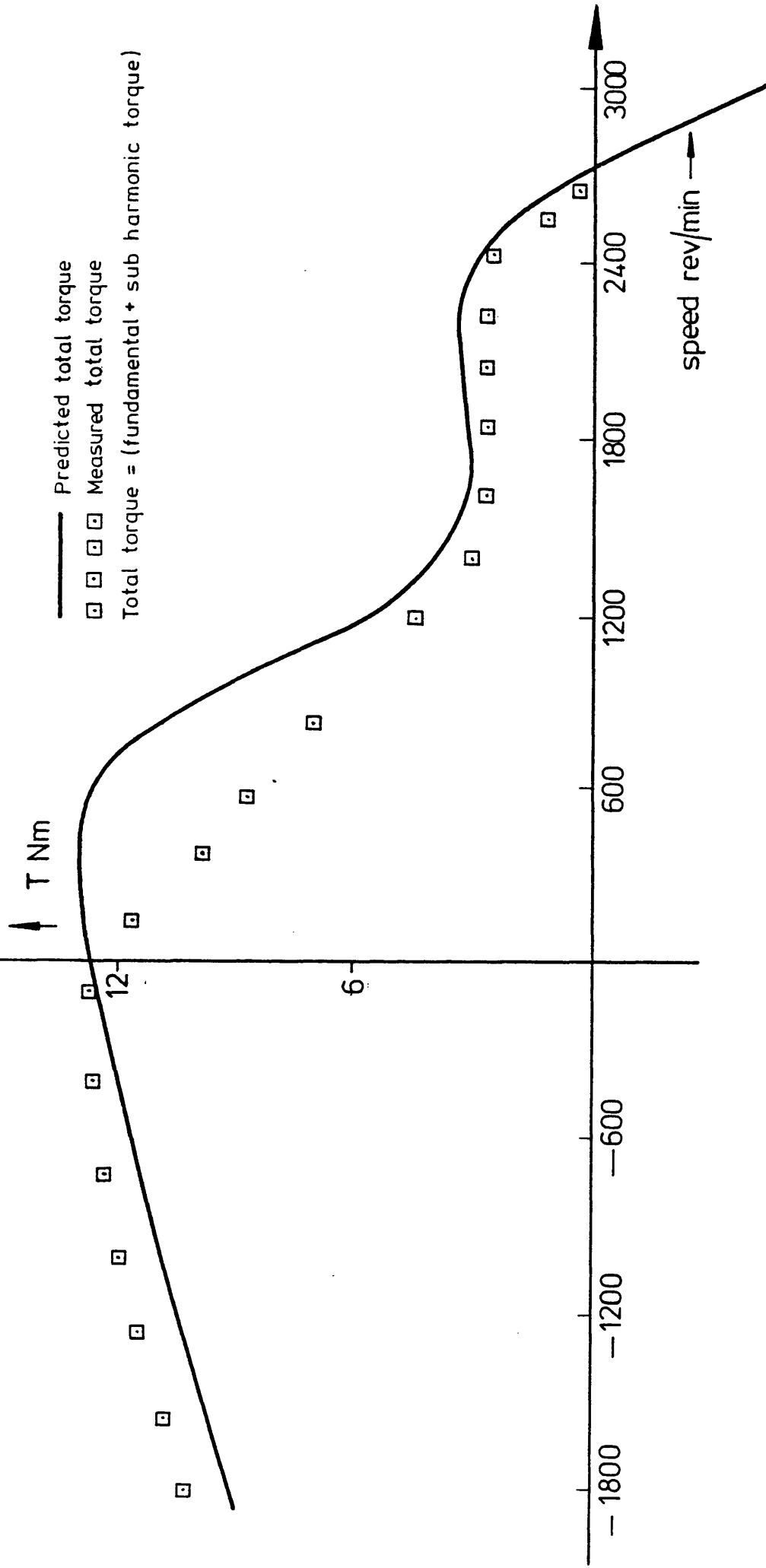


Fig.3.22 Torque/speed characteristic at $(50\text{Hz} + 16\frac{2}{3}\text{Hz})16\frac{2}{3}\text{Hz}$ injected with the same phase rotation as fundamental.

(Harmonic amplitude = $\frac{1}{3}$) Fundamental amplitude of 100V)

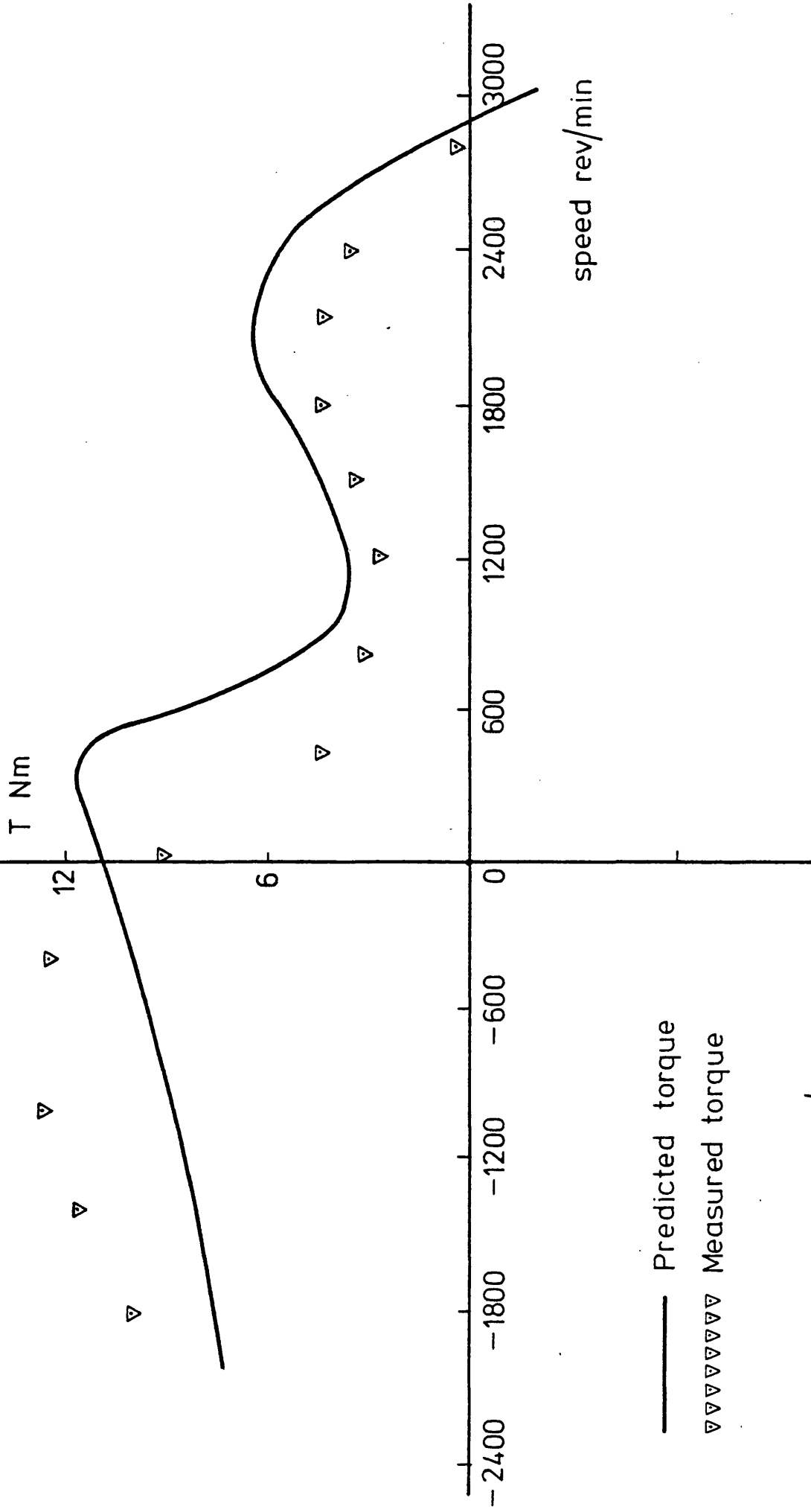


Fig. 3.23 Torque / speed characteristic at (50 Hz + 10 Hz), 10 Hz injected
with the same phase-rotation as fundamental.
(Harmonic amplitude = $\frac{1}{5}$) Fundamental amplitude of 100V)

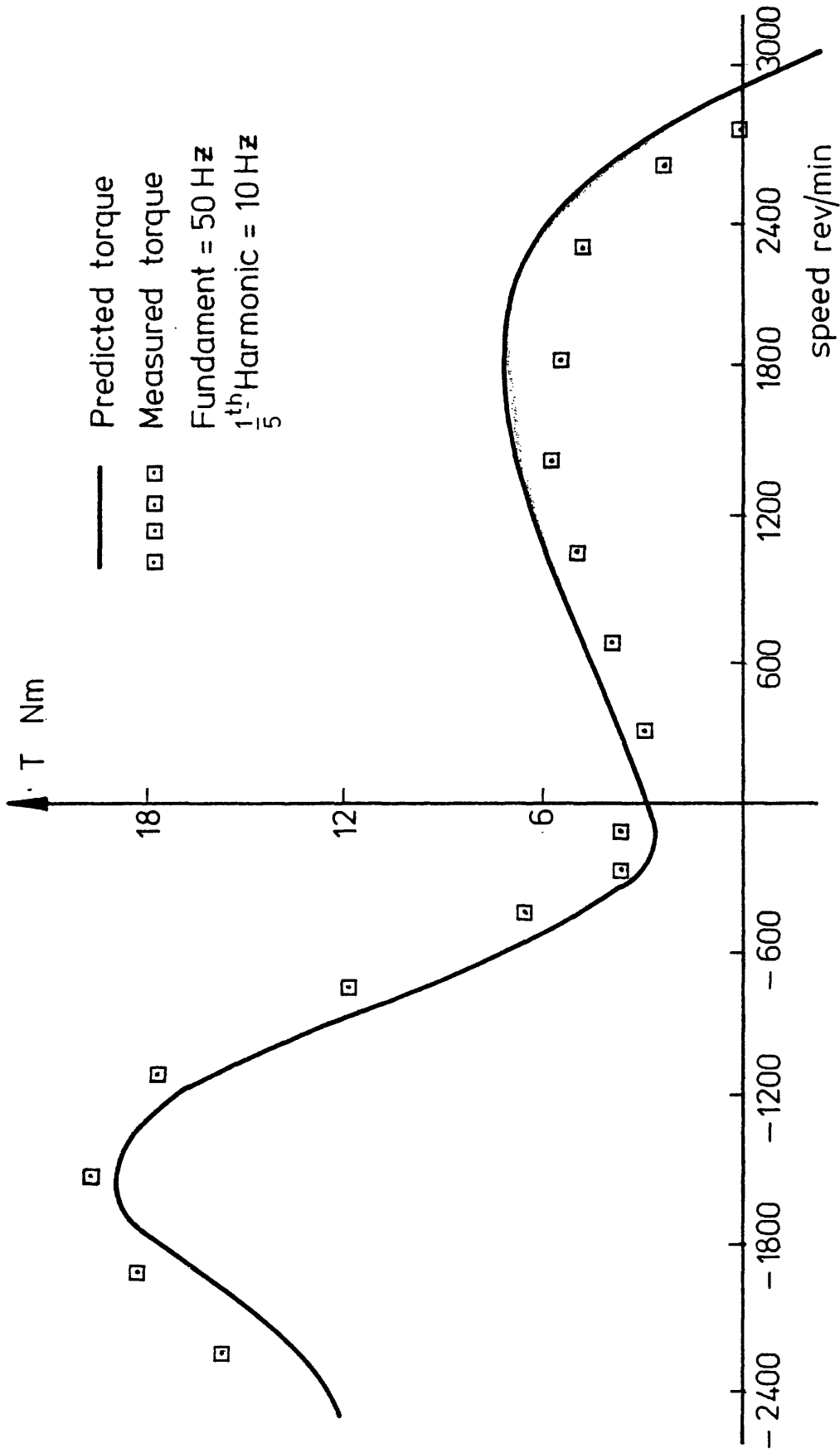


Fig. 3.24 Torque/speed characteristic at (50 Hz + 10 Hz). 10 Hz injected with opposite phase rotation to fundamental. (Harmonic amplitude = $\frac{1}{5}$ fundamental amplitude).

3.7 Effect of harmonics on harmonic torque response

When an impulse load is applied to an induction motor in an open-loop system, it will cause the slip to increase and the speed to fall. The behaviour of the system when an impulse torque is applied is generally as shown in Fig. (3.25). An impact load such as that produced by a punching mechanism or printing press will demand a torque from the motor roughly as shown in Fig. (3.25a). For analysis, this torque can be considered to be an impulse of infinite height and zero width as shown in Fig. (3.25b). For analytical purposes the impact can be considered to instantaneously reduce the speed from the steady state speed $\omega_{2.0}$ by $\Delta\omega_2$ as shown in Fig. (3.25c), and a corresponding increase of stator current as shown in Fig. (3.25d) will result. Recovery to the steady state will consist of an exponential rise in speed and an exponential fall in current as shown in Figs. (3.25c and d).

White and Woodson ⁽²¹⁾ have derived equations representing the recovery from an impact torque. This analysis, however, depends on assumed linearity and small slip operation. The previous experimental work in this study has shown that in this case neither assumption can be made if an accurate solution is to be derived. In this study, the effect of harmonics on recovery from an impulse torque was examined experimentally under known harmonic conditions produced by harmonic injection.

Figs. (3.26a and c) show the effect of a one-third sub-harmonic of forward rotation on the system response. The current recovery in sinusoidal 50 Hz operation without a harmonic shows the exponential current response. An exponential rise of current contrasts in Fig. (3.26a) with the instantaneous rise is shown in Fig. (3.25d). This is because the field time-constants of the Ward-Leonard loading system prevents the application of a time impulse torque. Torques were applied by manual adjustment of a field rheostat in the Ward-Leonard loading system. Fig. (3.26b) shows the effect of an added one-third sub-harmonic ($16 \frac{2}{3}$ Hz) in steady state conditions. The current profile

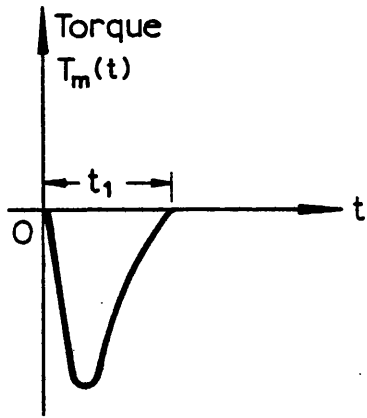


FIG. 3-25a ACTUAL TORQUE IMPULSE

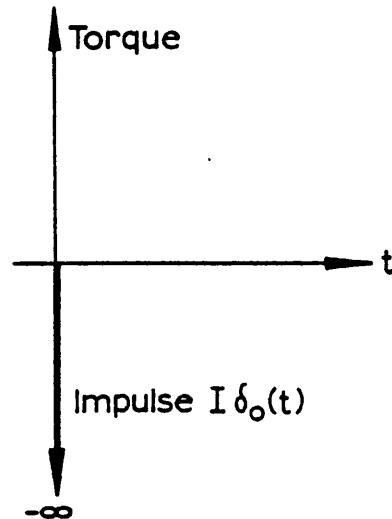


FIG. 3-25b IMPULSE APPROXIMATION

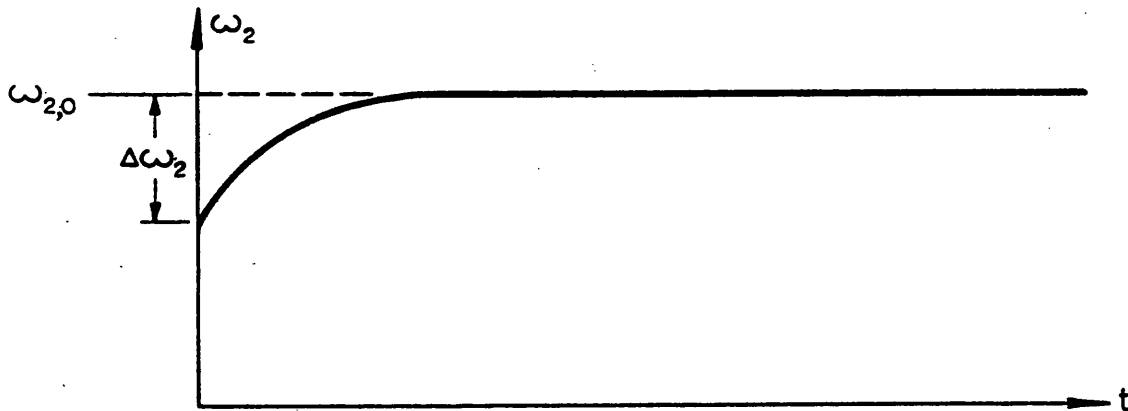


FIG. 3-25c. INDUCTION MOTOR RESPONSE TO IMPACT LOAD

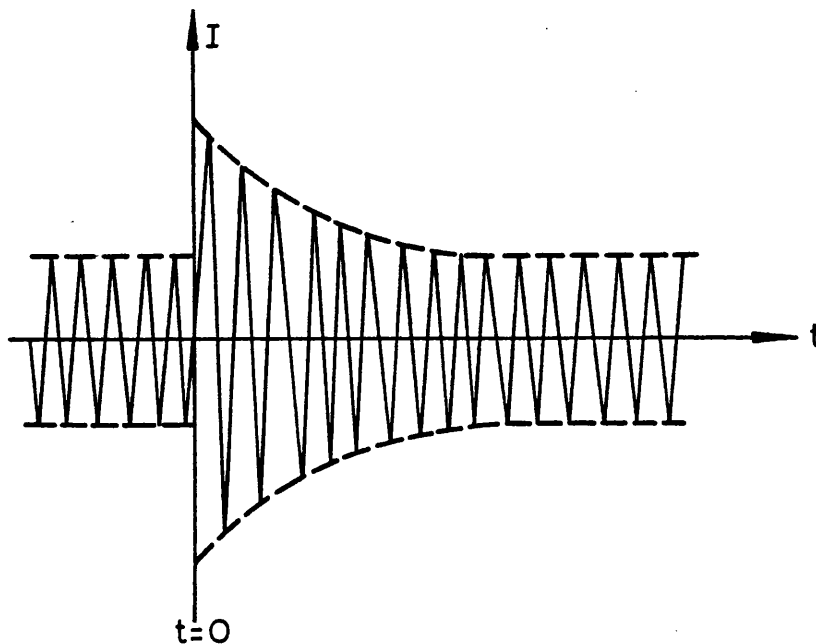


FIG. 3-25d. STATOR CURRENT RESPONSE TO IMPACT LOAD

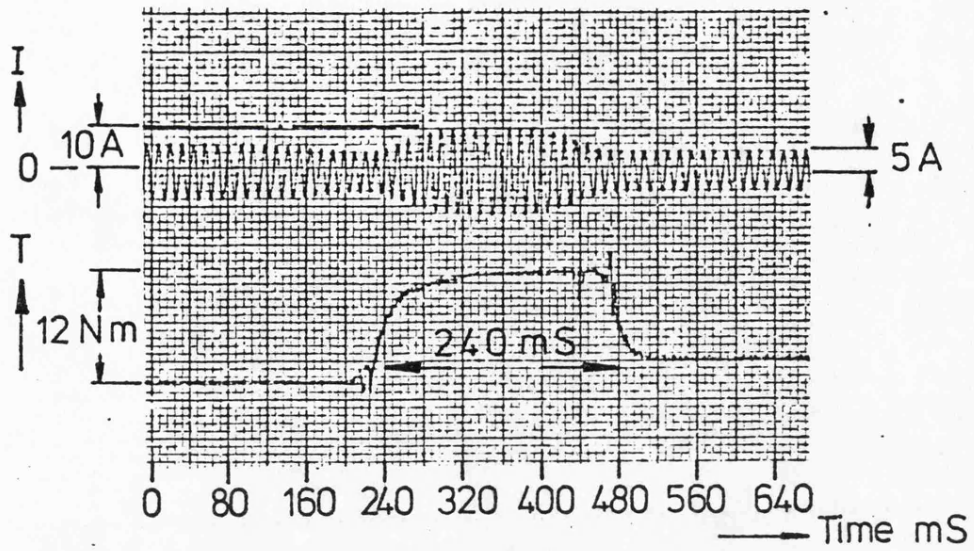


Fig.3-26a. Impulse torque at 50 Hz

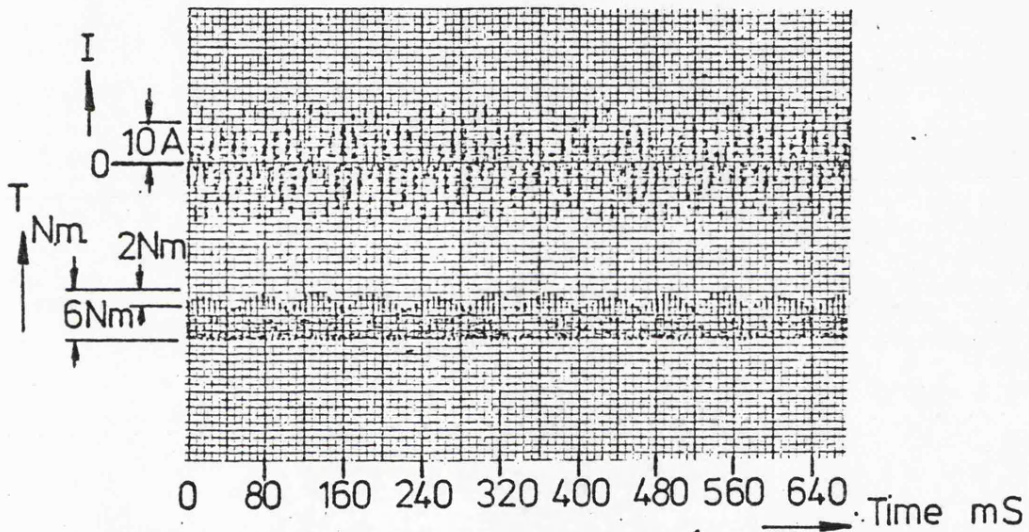


Fig 3-26 b Torque and current with $\frac{1}{3}$ sub-harmonic

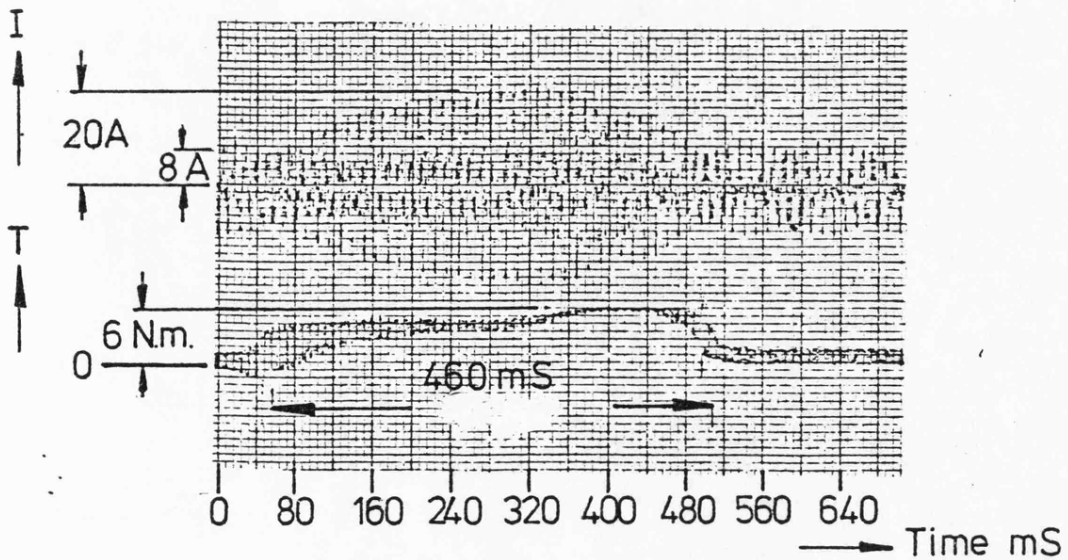


Fig3-26c Impulse torque with $\frac{1}{3}$ sub-harmonic

shows distinct amplitude modulation of period 60 ms, or sub-harmonic frequency. This profile gives a torque amplitude modulation of sub-harmonic frequency shown in the lower trace of Fig. (3.26b). It is known from communication theory that beat-frequencies will result, but here their amplitudes will not be significant. Shepherd and Munoz ⁽²²⁾ have used this modulation principle in an inverter drive to give variable-speed, beat-frequency operation.

Fig. (3.26c) shows the impulse response when the one-third sub-harmonic is present. Current amplitudes are approximately doubled and the recovery torque halved. It was, of course, impossible to stall the motor when Ward-Leonard loading was used, but the same torque impulse applied to the unloaded motor might stall it. The recovery time for the exponential current amplitude transient is approximately trebled when compared with the fundamental response. It is also interesting to note that the current and torque amplitude modulation is not so pronounced when the impulse torque is present. This may be due to magnetic saturation at high current levels. Figs. (3.27a,b and c) show impulse torque and current response to single-frequency supplies of 5, 10 and 20 Hz. It can be seen from Fig. (3.27a and b) that third harmonic distortion of the fundamental occurs when the impulse torque is applied. This is a saturation effect showing that the machine may well introduce its own harmonics into the stator current under low-frequency operating conditions. This effect would be seen at 20 Hz if the time scale was increased. The machine winding was designed to minimize third harmonic saturation effects and externally introduced third harmonic effects will be similarly reduced.

It can be concluded therefore that a higher than fundamental frequency harmonic has little effect on transient response, but that a substantial sub-harmonic may cause stalling under impulse load conditions. It will, in any case, substantially increase the recovery time.

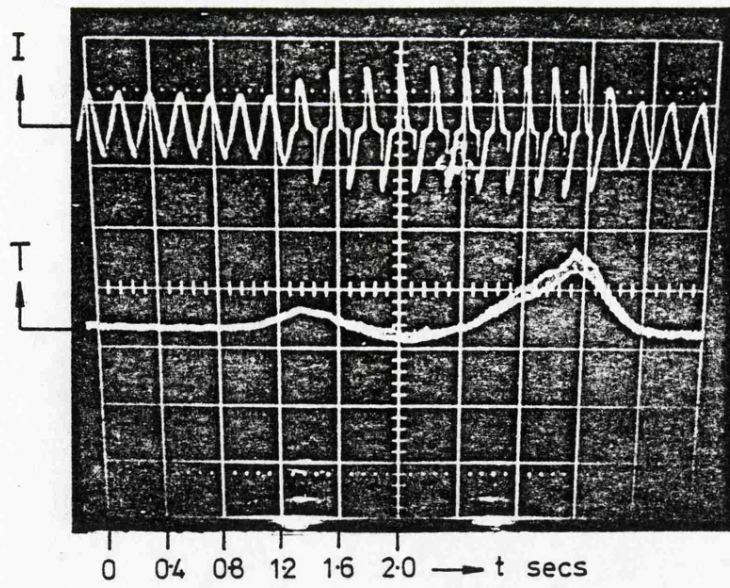


Fig.3-27a Impulse torque at 5 Hz

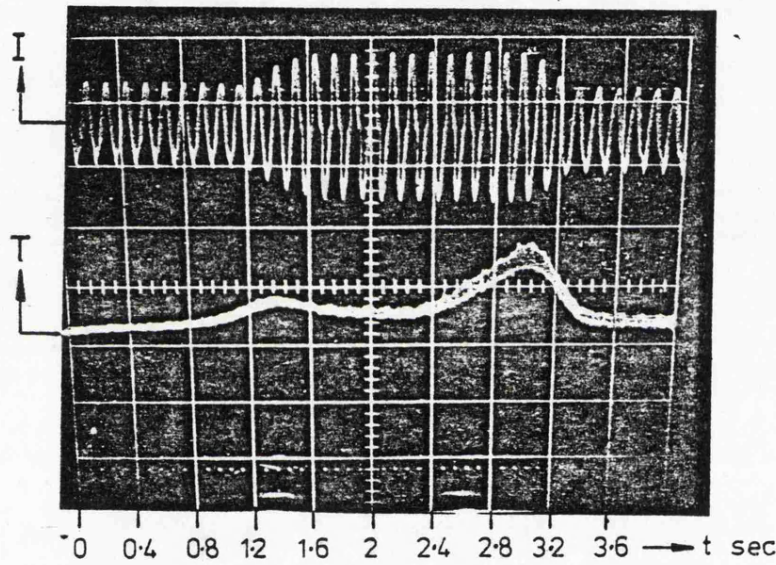


Fig.3-27b Impulse torque at 10 Hz

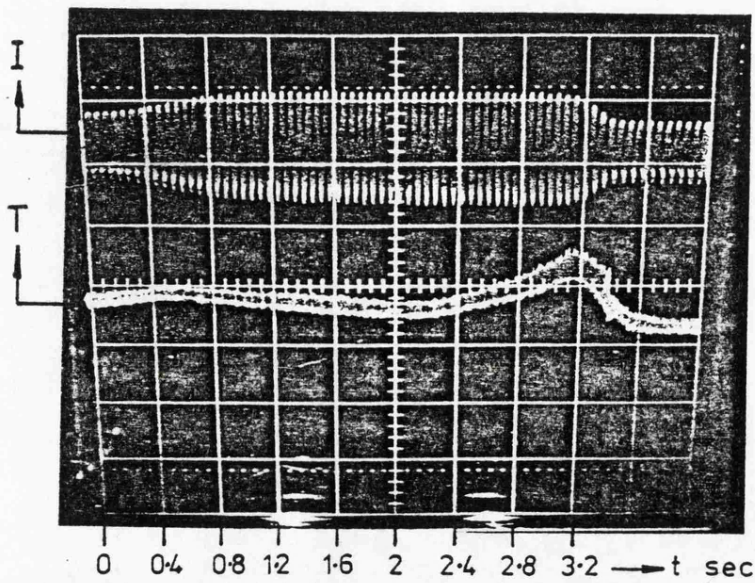


Fig.3-27c Impulse torque at 20 Hz

3.8 Effect of harmonics on run-up

The preferred method of accelerating an induction motor from standstill is to increase the stator frequency from a low value until full speed is reached. If fixed-frequency starting is unavoidable, then the acceleration time to the required speed will depend on the motor parameters. Fig. (3.28) shows measured times for acceleration from standstill to near synchronous speed for the experimental machine operating at a number of applied frequencies. The applied voltage was the voltage necessary to give a peak torque equal to the peak torque developed when the machine was fed from a 50 Hz supply of rated voltage. It can be seen that the relationship between acceleration time and frequency is not a constant, the acceleration performance falling as the applied frequency increases. The acceleration performance with additionally injected harmonics was investigated experimentally.

Fig. (3.29a) shows a 10 Hz run-up characteristic corresponding to Fig. (3.28). A 20% fifth harmonic will only add or subtract 1/25th of the fundamental torque. This makes negligible difference to the acceleration time as shown in Figs. (3.29b) and (3.29c). Acceleration times are measured on the torque characteristic in each case.

A forward one-third sub-harmonic will add to the fundamental torque at speeds below sub-harmonic synchronous speed and subtract from it beyond this point. Hence the initial torque will be increased

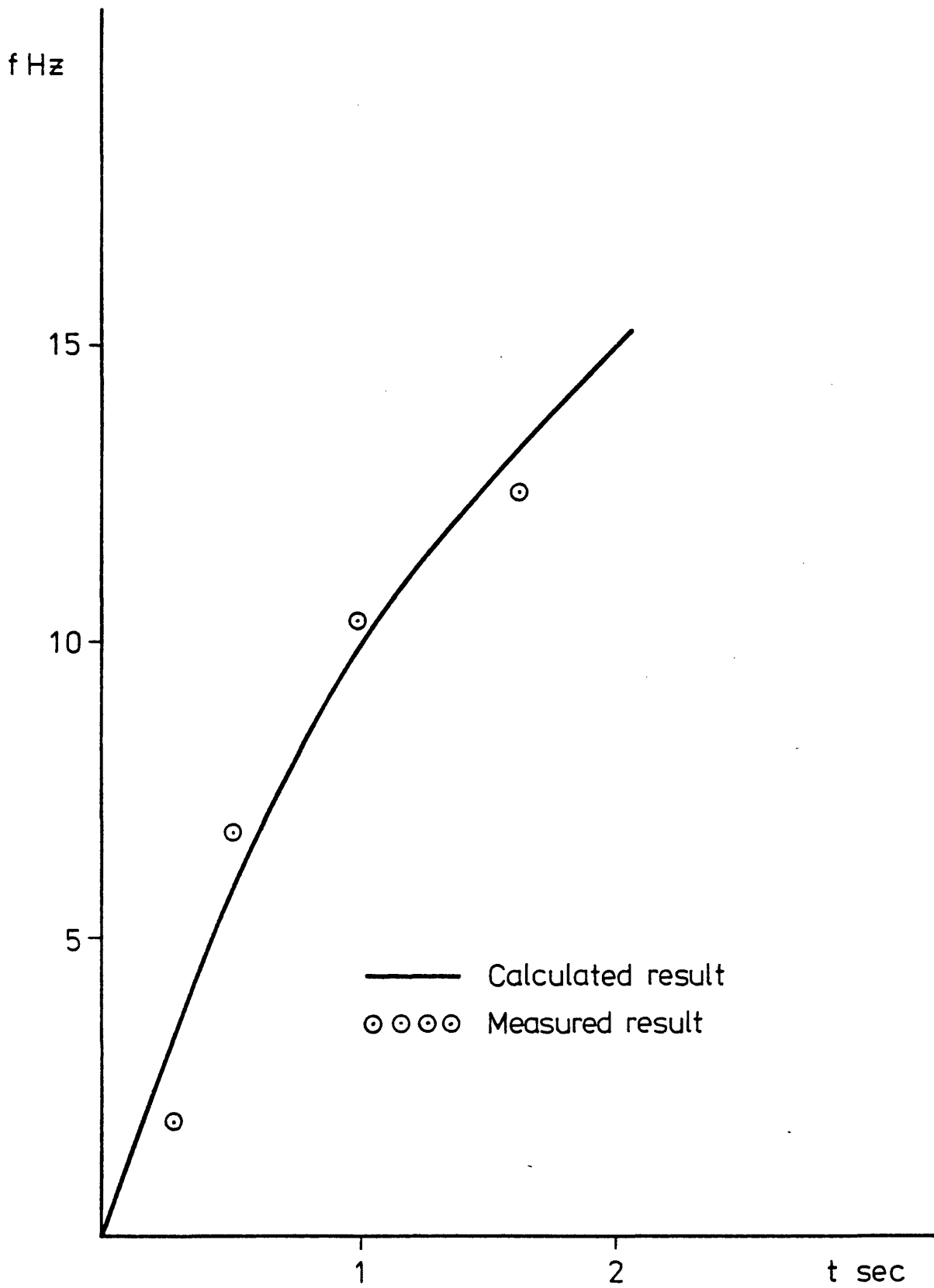


Fig.3.28 Acceleration time to full speed / frequency.

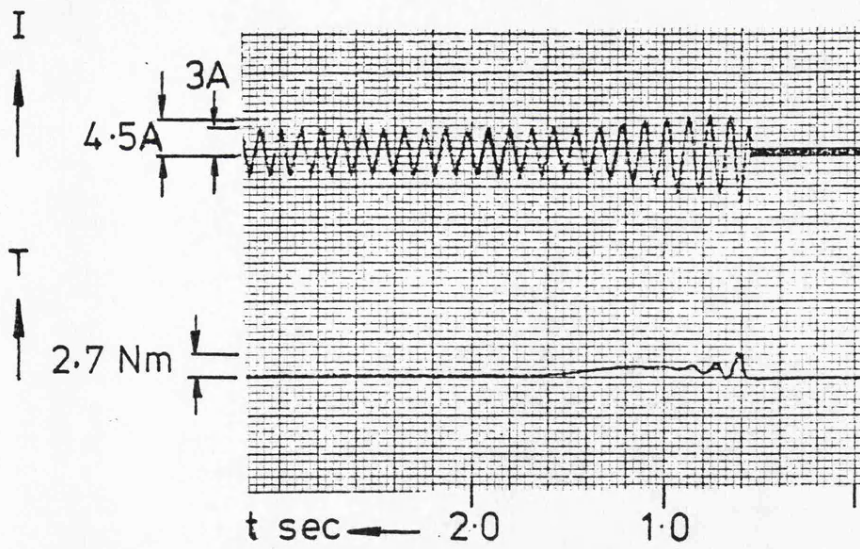


Fig 3.29c Starting 10 Hz D.O.L.

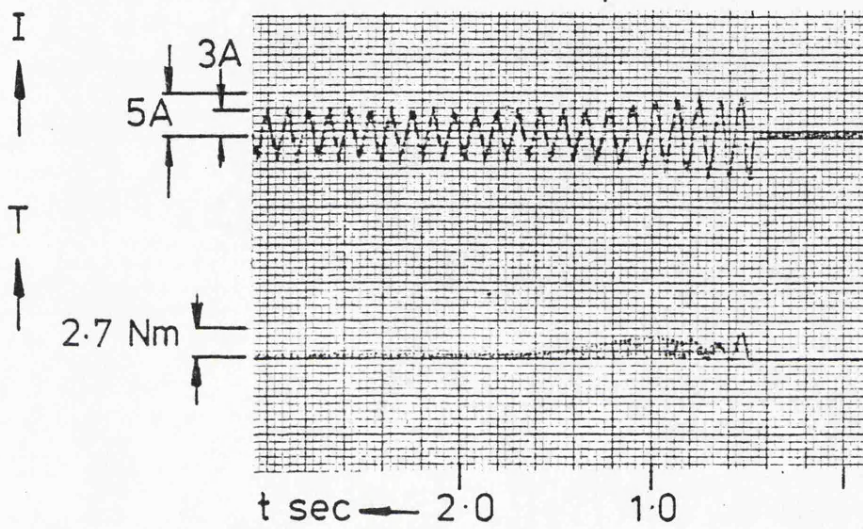


Fig 3.29b Starting 10 Hz with 20% forward 5th harmonic.

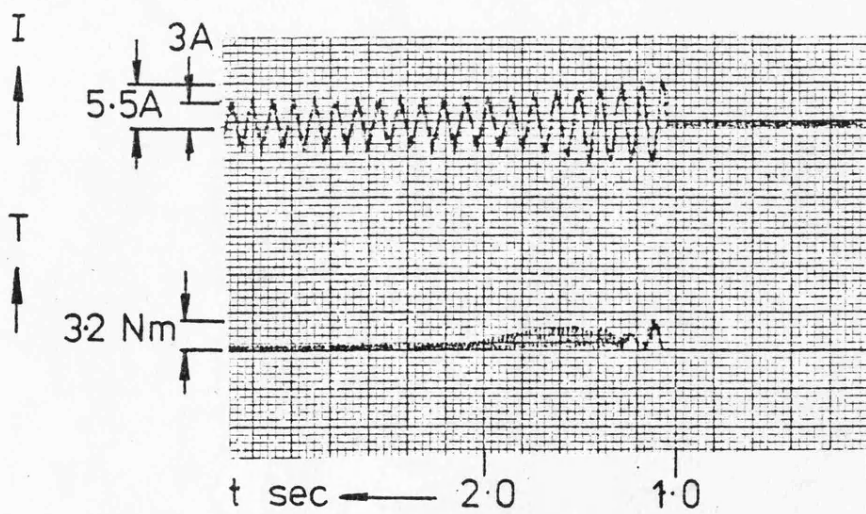


Fig 3.29c Starting 10 Hz with 20% reverse 5th harmonic.

and stiction overcome. Beyond the sub-harmonic synchronous speed, the output torque will be reduced. A one-third sub-harmonic is the most likely sub-harmonic to be encountered in a rectangular pulse inverter with a mark-space ratio of unity. The effect of such a sub-harmonic is shown in Fig. (3.30a,b and c). Here a 50Hz, direct-on-line start at 240V, gives an acceleration time of approximately 1 second. This is a smaller time than that predicted in Fig. (3.28), but here 1.0p.u torque at 10Hz was taken as 48V. The effect of stator resistance in reducing the air-gap flux is much less at 50Hz on a volts proportional to frequency supply. Fig. (3.30b) shows that the acceleration time is practically unchanged when a one-third sub-harmonic of 1p.u amplitude is superimposed on the fundamental. The amplitude modulation of the current waveform in Fig. (3.30b) seems to be dependent on the speed of the machine during acceleration reaching a steady value as shown in Fig. (3.29c). The application of full-load torque to the machine at rated speed with the positive-sequence sub-harmonic present stalled the motor. A reverse sub-harmonic gave a failure to start.

3.9 Harmonic effects on losses and efficiency

The presence of harmonics in the applied voltage results in currents at the harmonic frequencies. These currents increase the copper and iron losses, and generate heat in the winding which will cause overheating of the motor at low speeds and it becomes necessary to provide the machine with forced-cooling under these conditions.

The losses due to harmonics can be classified as follows:

a) Copper losses

The copper loss of the machine can be estimated from the expression:

$$W_c = I_{1H}^2 R_1 + I_{2H}^2 R_2 \quad , \quad (3.12)$$

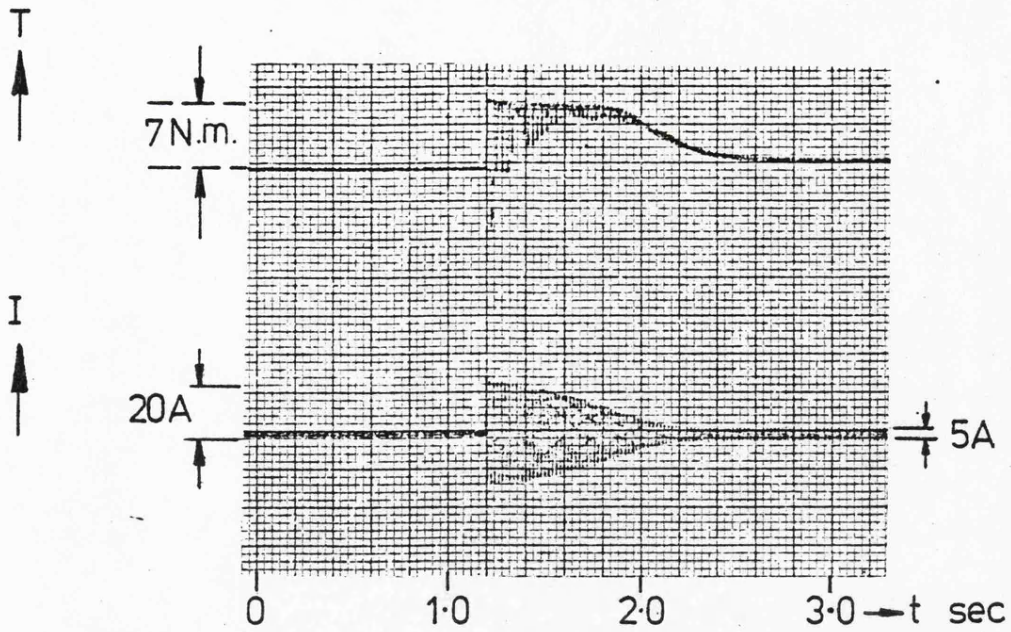


Fig.330a. 50 Hz D.O.L. Starting

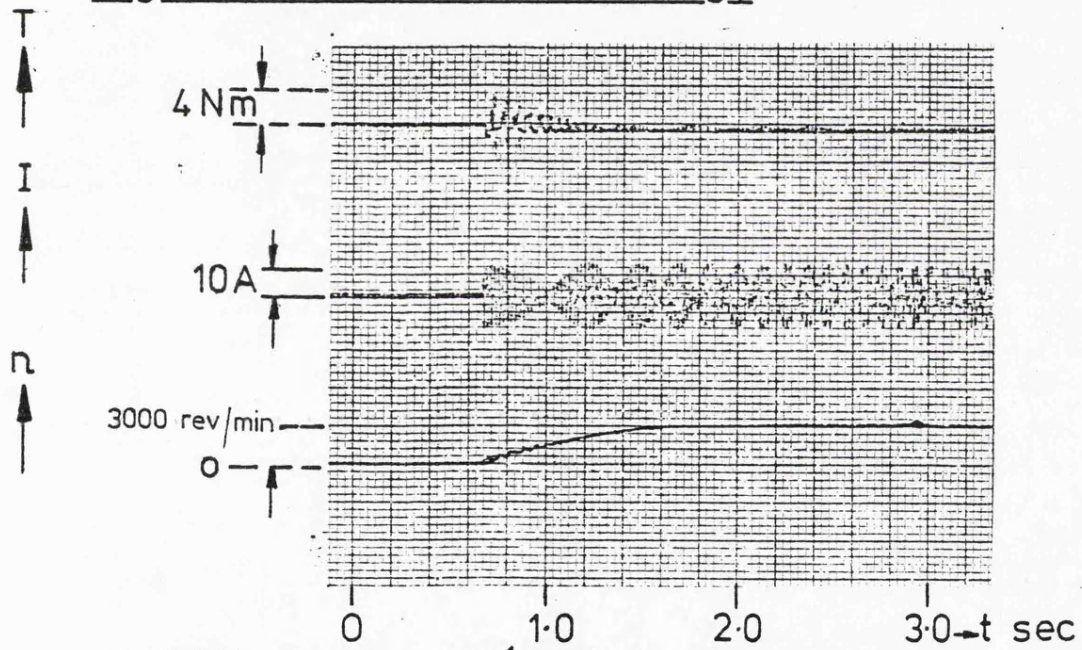


Fig.330b. 50 Hz with $\frac{1}{3}$ sub harmonic starting

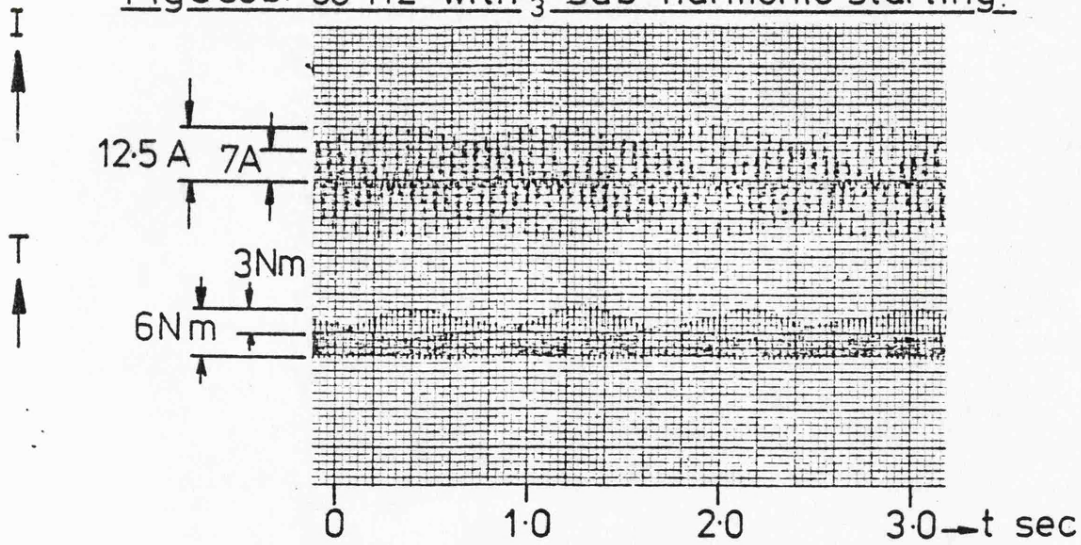


Fig.330c. 50 Hz with $\frac{1}{3}$ sub harmonic running

where I_{1H} is the rms value of the total stator current (fundamental and harmonics) and similarly I_{2H} is the rms value of the rotor current referred in stator terms. These currents can be computed from the equivalent circuit given in Fig. (2.1). Copper losses can only be estimated because they are impossible to measure in isolation from the total machine losses. Fig. (3.31) shows the computed copper losses over frequency range from 0 to 50Hz for a rectangular input voltage. The harmonics present in a rectangular input pulse increase the machine copper losses by 10% at 50Hz and up to 20% at 5Hz.

b) Iron loss

Another important loss factor is the increase of machine iron losses due to the high-frequency harmonics. This iron loss consists of two components, hysteresis loss and induced eddy current losses in the iron. An estimate of these losses in frequency terms was given in Chapter 2, section (2.4a) as:

$$W_I = K_h f B^{1.6} + K_e B^2 f^2 \quad (3.13)$$

If a ratio of harmonic frequency to fundamental frequency, λ and a ratio of harmonic amplitude to fundamental amplitude, ρ are defined, equation (3.43) can be rewritten as:

$$W_I = K'_h \lambda \rho^{1.6} + K'_e \lambda^2 \rho^2 \quad (3.14)$$

Where K'_h and K'_e are further hysteresis and eddy current loss constants obtained by experiment at 25Hz and 50Hz respectively as $K'_h = 2.69$ and $K'_e = 96$. The iron loss was estimated from equation (3.44). Fig. (3.32) shows a comparison between the iron losses of a sinusoidal supply and that of rectangular supply voltage. Experimental measurements of iron losses were made using an electronic integrating wattmeter with the

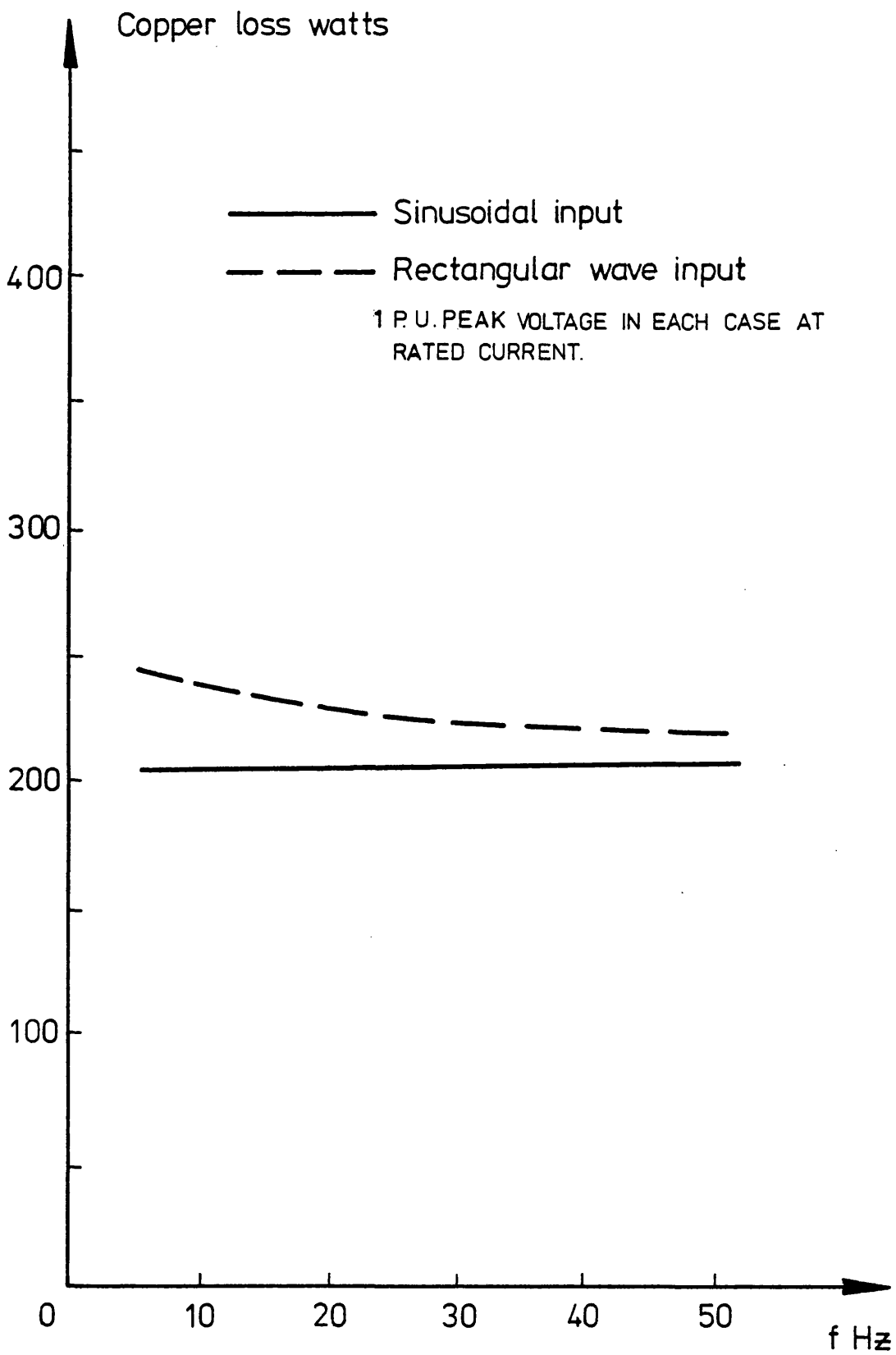


Fig 3.31 Calculated copper loss/frequency.

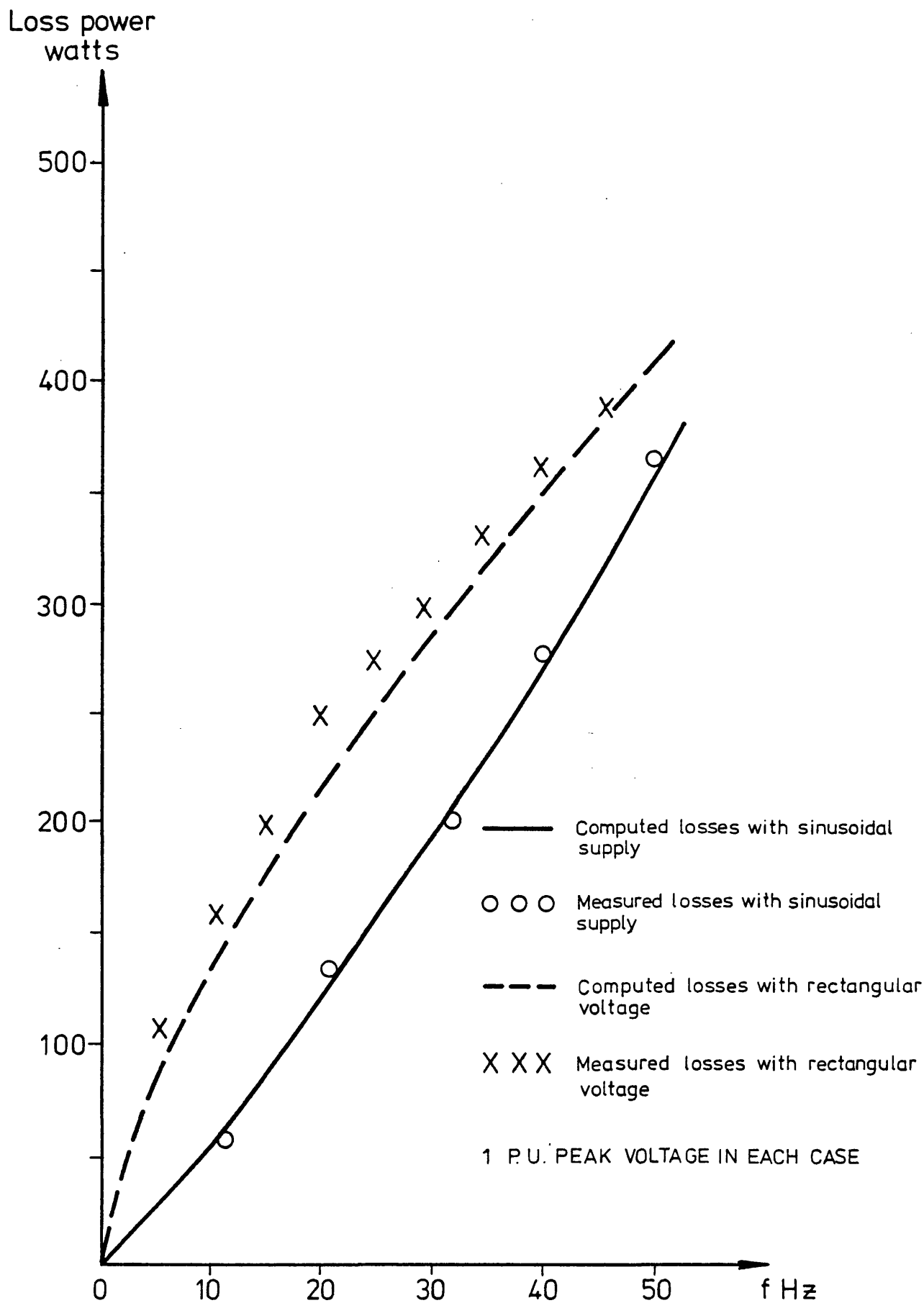


Fig. 3.32 Iron losses/ Input frequency.

machine driven at the synchronous speed related to each fundamental frequency. In each case the measured values exceed the computed loss powers. Hence only the fundamental component of rotor current will be zero at synchronous speed and the harmonic voltages will produce additional copper losses. It can be seen that the predicted and measured results correlate when a sinusoidal input is applied because the rotor copper losses will be zero in this case. Fig. (3.33) shows that at low frequencies (<10Hz) harmonics have almost doubled the iron losses. The efficiency,

$$\eta = \frac{\text{Input power} - \text{losses}}{\text{Input power}}, \quad (3.15)$$

where the losses may be defined as the sum of the copper losses, mechanical losses and iron losses. Estimates of iron loss and copper loss can be made. While the mechanical losses for the experimental machine as a function of speed can be obtained from, Fig. (2.14).

Fig. (3.33) shows computed estimates of efficiency for the experimental machine. Full-load torque is assumed to be exerted in each case, and a rectangular wave supplied to the stator of the motor. This shows that the efficiency of the experimental machine falls to 38% at 10Hz; this is compared with 47% efficiency when operating on a sinusoidal supply.

The power losses due to harmonics must be dissipated within the windings and laminations of the machine as heat. At low frequencies, the speed of the machine will be insufficient to circulate natural currents of sufficient velocity to cool the machine.

The double-layer experimental machine is fitted with external fan cooling and so thermal equilibrium can be maintained even when operating at full load with frequency at 5Hz as shown in Fig. (3.34). 60°C is specified as the maximum stator iron temperature by the manufacturer.

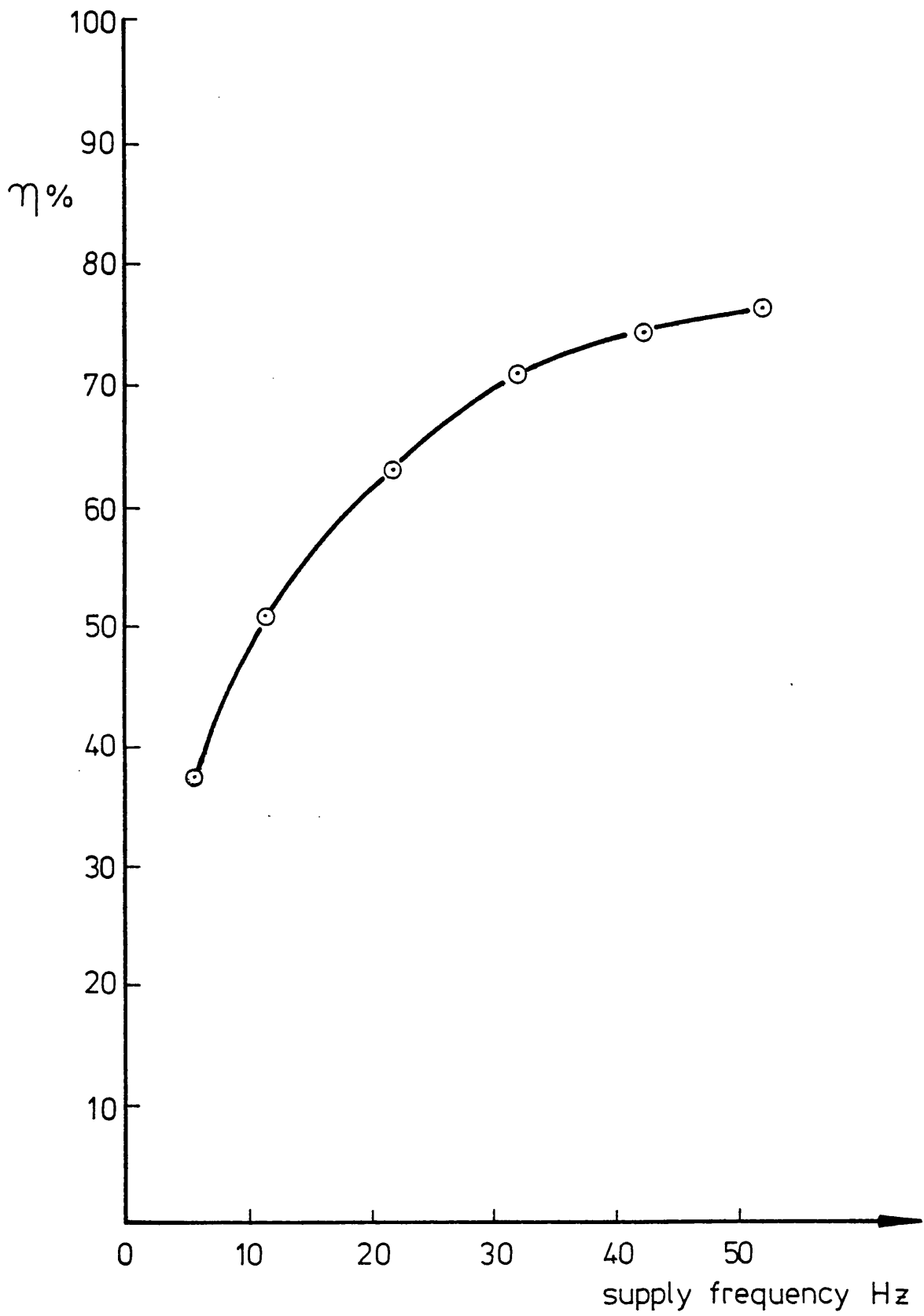


Fig. 3.33 Calculated motor efficiency / supply frequency.

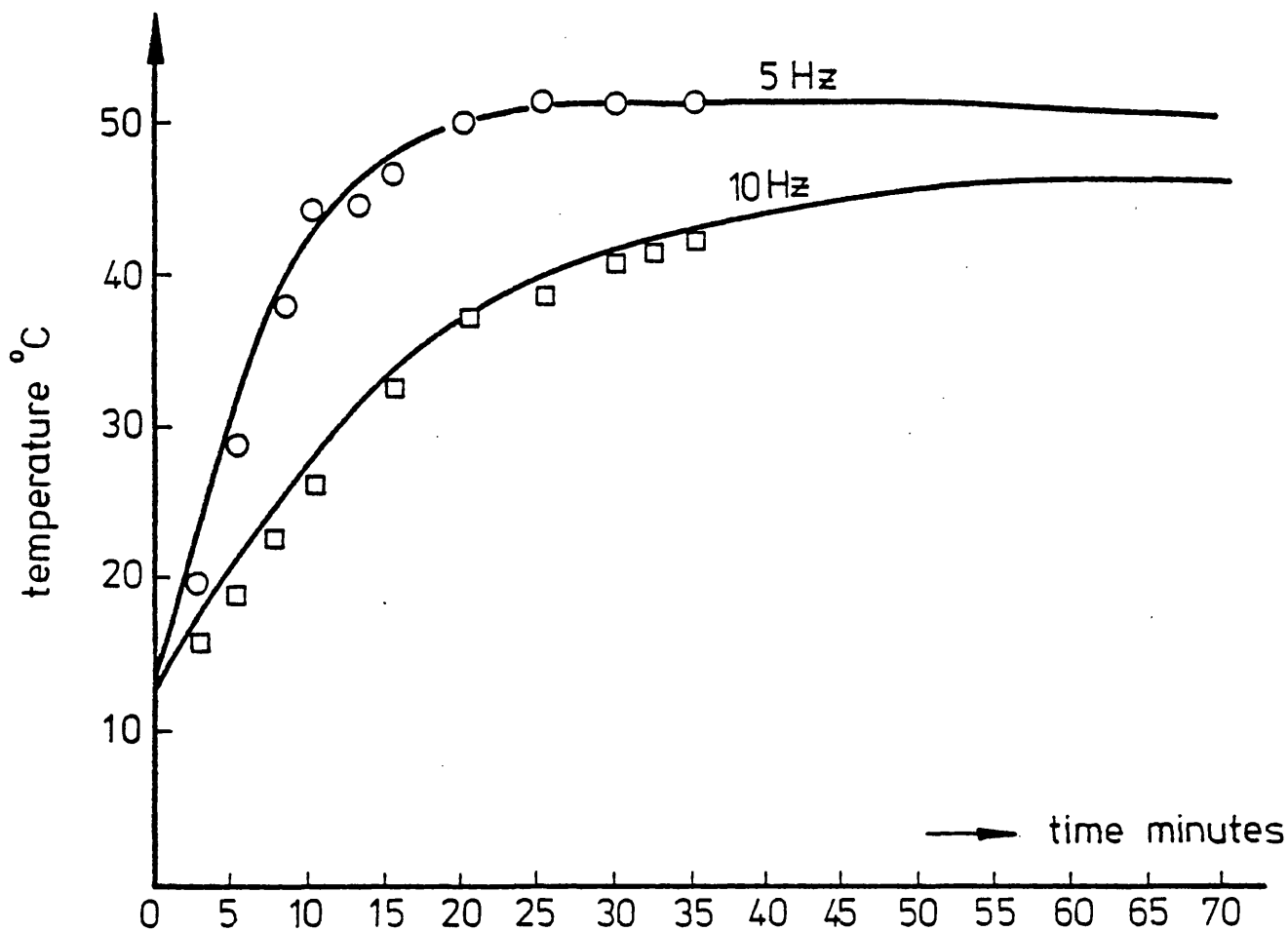


Fig 3-34 Heat runs 1 P.U. Voltage sinusoidal supply at rated current.

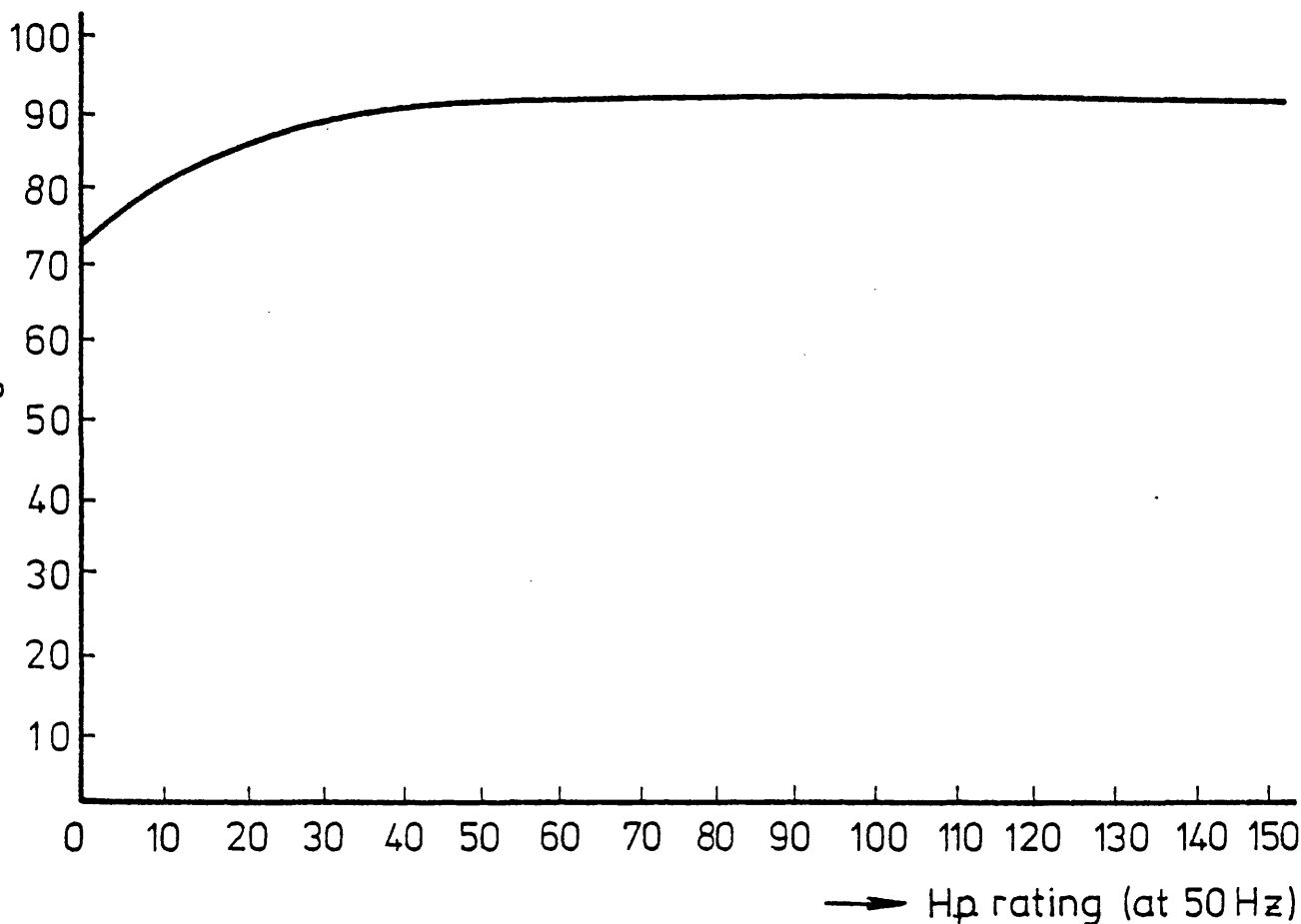


Fig 3-35 Efficiency/frame size rating of the motor. (G.E.C. Graph.)

Some estimate of the potential of the machine in a larger system can be made from a consideration of the established thermal ratings of induction motors ⁽²⁴⁾. Fig. (3.35) shows the efficiency of an induction motor operating on a sinusoidal supply related to its maximum output as specified by a typical manufacturer ⁽²⁵⁾.

3.10 Conclusions from Chapter 3

The operation of an induction motor with its stator terminals connected to non-sinusoidal supplies has been investigated. It has been seen that any particular harmonic and its multiples can be eliminated by the use of a specific controlled pulse-width, but that it is most general practice to eliminate the triplens and zero-sequence effects. Fourier analysis expresses the rectangular waveform as a fundamental frequency and a series of harmonics. The harmonic voltages present were then classified into positive-sequence, negative-sequence or zero-sequence harmonics according to the phase rotation of the resultant field. An equivalent circuit has then been used to predict the stator current and electrical torque produced by each particular harmonic. The main effects of harmonics on the performance of the motor can be summarized as follows;

1) Harmonics of greater than fundamental frequency

(a) Effect on torques: In practice, the effect of positive and negative-sequence harmonics at frequencies higher than the fundamental on torque is negligible, since the leakage reactance is much greater than the machine resistance at high frequencies. Since the leakage reactance increases with frequency, the Kth harmonic current will be $\left(\frac{1}{K}\right)^2$ x the fundamental. This means that positive and negative-sequence harmonics have little effect on steady-state performance. Zero-sequence harmonics substantially reduce the motoring torque and increases the total rms current as the fundamental frequency is decreased. Triplen harmonics

cause zero-sequence operation, and then must be eliminated from the supply. The pulse-width limited waveform of Fig. (3.2) is highly desirable in order to achieve this, but this would be at the expense of poor utilisation of electronic components.

(b) Effect on losses: The harmonics increase the copper and iron losses. This additional loss power will be dissipated as heat in the windings of the machine and its laminations. Hence additional cooling may be required, especially in low-speed operation.

(c) Effect on acceleration and impulse response: A higher than fundamental frequency harmonic has little effect on acceleration or transient response.

2) Sub-harmonics

(a) Effect on torques: A positive-sequence sub-harmonic can cause a machine accelerating from standstill at fixed fundamental frequency to "cog" at a speed near to the sub-harmonic synchronous speed. A negative-sequence sub-harmonic drastically reduces starting torque and reduces all motoring torques at higher speed. Plug-braking torques are increased. Low-speed crawling will inevitably result if the forward sub-harmonic amplitude approaches $(K) \times$ fundamental. A substantial reverse sub-harmonic will probably prevent starting.

(b) Effect on losses: Overheating will result due to increased copper loss caused by sub-harmonic currents, although the low sub-harmonic frequencies will have very little effect on the total iron loss.

(c) Effect on acceleration and impulse response: The no-load acceleration time was not noticeably affected by the presence of a positive sub-harmonic in the supply voltage, but the application of full-load torque to the machine to the motor running at full speed caused stalling. A reverse sub-harmonic gave a failure to start.

The sub-harmonic will increase the recovery time of speed from an impulse load. Hence it must be concluded that a variable-frequency supply for an induction motor drive should be free of sub-harmonics and triplens. Other harmonics can be accepted at the expense of efficiency.

CHAPTER 4A phase-controlled circulating current cycloconverter-induction-
motor drive using a rotating machine as an inter-group reactor

	<u>Page No.</u>
4.1	Introduction. 54
4.2	Cycloconverter output voltage. 55
4.3	Voltage output with circulating-current-free operation. 58
4.4	Continuous-circulating-current operation. 61
4.5	The experimental system. 62
4.6	Ramp generator board and mono-polarity board. 63
4.7	Operation of voltage loop. 64
4.8	Speed-servo. 65
4.9	Thyristor firing and pulse board. 65
4.10	Inter-group reactance. 70
4.11	The use of the machine stator as a reactor in the cyclo- converter motor drive. 71
4.12	Conclusions. 72

CHAPTER 4A Phase-controlled circulating current cycloconverter-
induction-motor drive using a rotating machine as an
inter-group reactor4.1 INTRODUCTION

It can be seen from Chapter 3 that a variable frequency supply free of sub-harmonics and with a minimum harmonic content is required for a stable motor drive. A cycloconverter can achieve this, but the limited input to output frequency ratio restricts the available speed range of the drive. This range can be extended by the harmonic cancellation achieved when a continuous circulating current can be maintained in the cycloconverter. Usually continuous circulating current can only be obtained by the use of an inter-group reactor rated for full-load current. The static reactors are expensive and a system in which the machine stator performs the reactor operation and still gives torque may be a better proposition⁽²⁶⁾. The cycloconverter⁽²⁷⁾ as a direct frequency converter without a dc link is well known as a power amplifier⁽²⁸⁾ employing phase-controlled thyristors. In an ac variable speed drive the reversibility of the cycloconverter permits regenerative braking, but the output frequency is limited by the acceptable harmonic content of the output voltage.

This chapter describes the use of an induction-motor stator as an inter-group reactor in a circulating current cycloconverter. A double-layer stator winding formed into electrically separate thyristor group circuits, magnetically coupled in the stator provides a conventional rotating field in the air-gap. This enables the double-wound stator machine to act as a reactor maintaining continuous circulating current operation in the cycloconverter and as a torque producing motor.

A closed-loop speed control system including electronic current clamping is incorporated to maintain constant speed independent of load on the divided-winding reactor machine.

4.2 Cycloconverter output voltage

The basic three thyristor per group cycloconverter element is shown in Fig. (4.1). Multiples of these elements can form polyphase frequency converters of which Fig (4.2) shows a half-wave converter. Further elements of thyristor groups can be added to give full-wave or multi-phase operation. The simple three thyristor group, half-wave, cycloconverter is studied here as the worst case of harmonic generation and to minimise the hardware cost. If the thyristor gate pulse positions are modulated and an inter-group reactor as shown in Fig. (4.1) is provided for inductive energy storage to ensure regenerative operation, the voltage and current profiles shown for unity load power-factor in Figs. (4.3a) and (4.3b) will be generated. Fig. (4.3) and the results given in this chapter are based on the traditional cosine-crossing method of pulse timing shown in Fig. (4.4) with the constraint relative group firing angles of

$$\alpha_p + \alpha_N = \pi \quad , \quad (4.1)$$

where α_p and α_N are the positive and negative thyristor group firing angles respectively. This method of pulse timing gives the best quasi-sine wave of output voltage available by natural sampling, although the output profile can be improved considerably by the use of communication sampling techniques ⁽²⁹⁾. The divided-winding stator system described in this chapter is equally applicable to either method of pulse timing.

If the voltage profiles of Figs. (4.3a) and (4.3b) are superimposed as shown in Fig. (4.5a), an instantaneous voltage difference will be observed. This voltage difference shown in Fig. (4.5b), must be

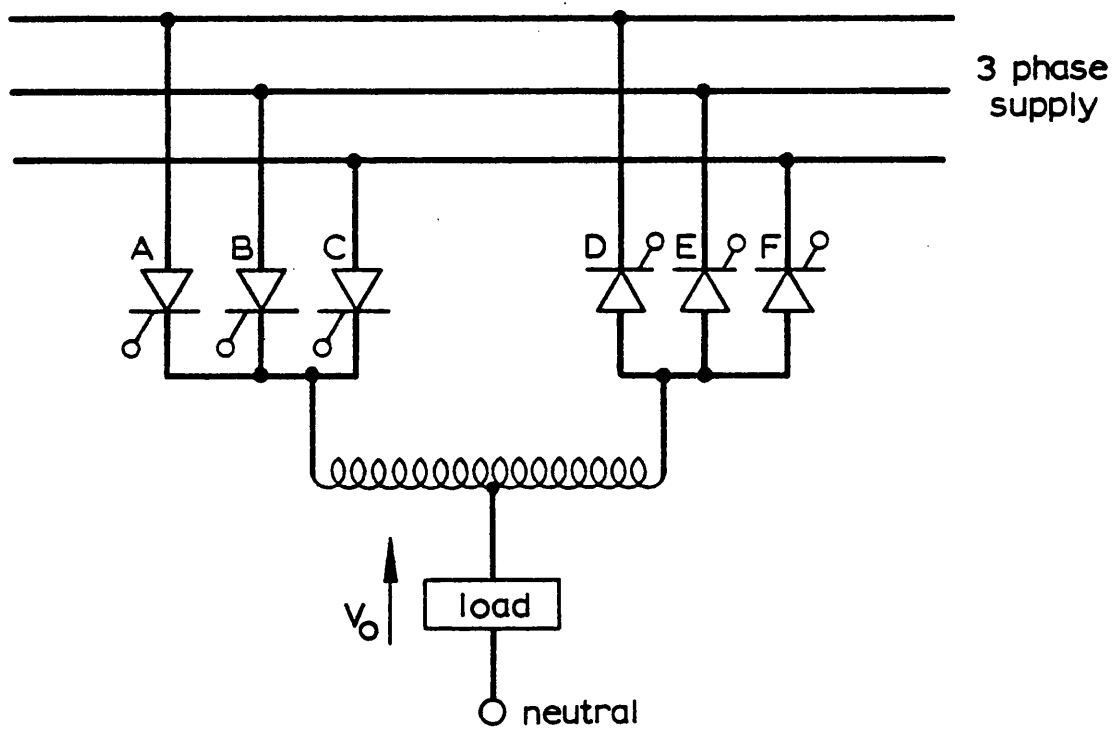
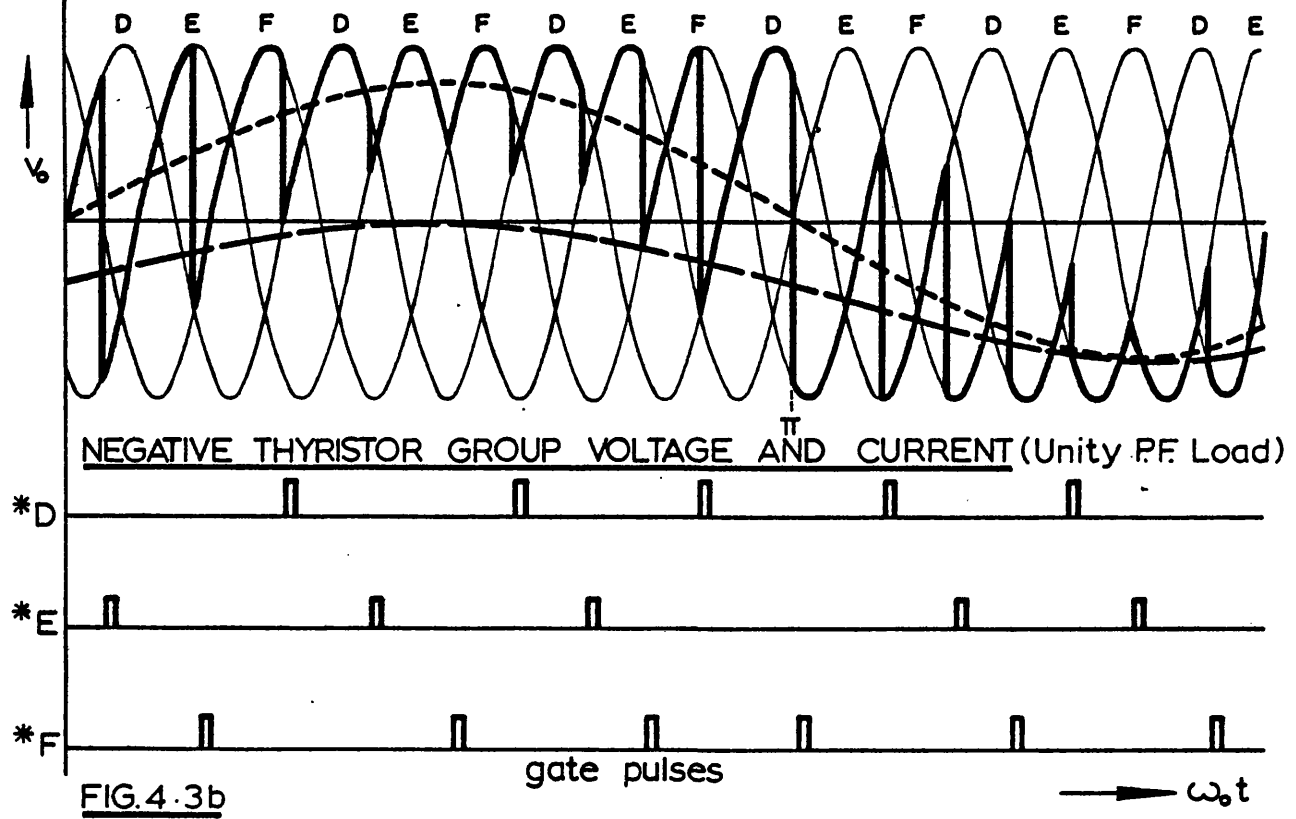
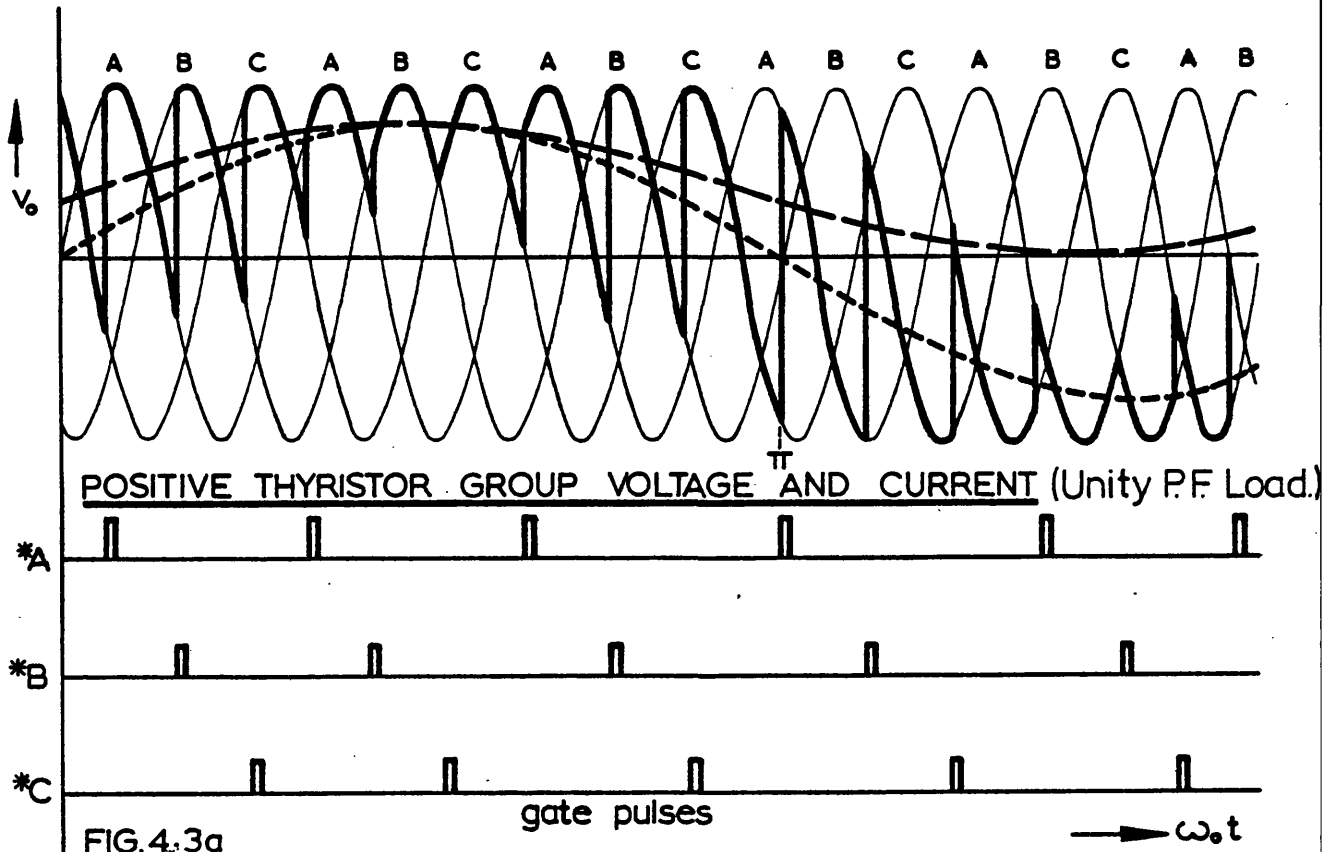


Fig 4.1. THE BASIC 3-PHASE INPUT, 1-PHASE OUTPUT
CYCLOCONVERTER UNIT



————— instantaneous voltage

- - - - - mean voltage

————— mean current

* thyristors A,B,C,D,E,F

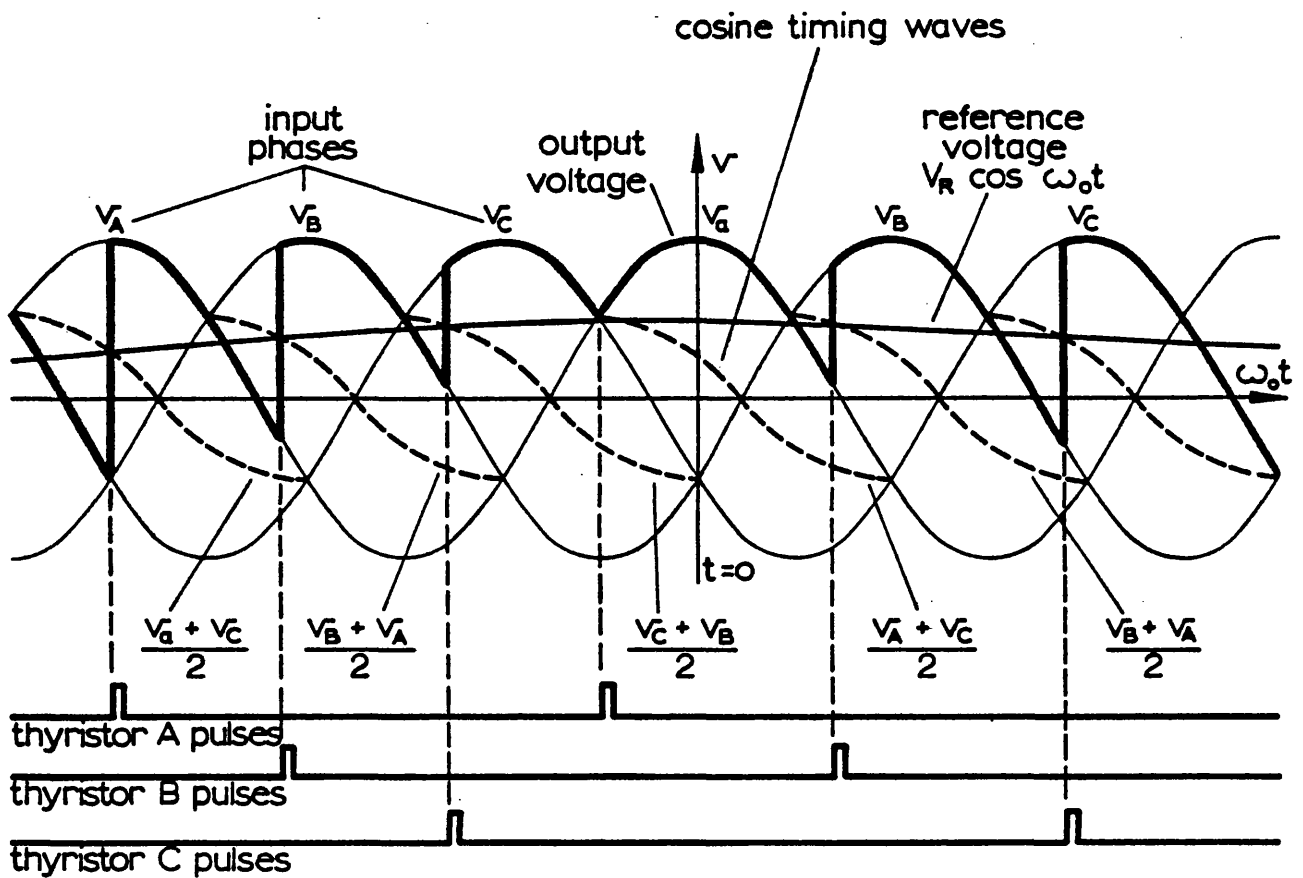


FIG. 4.4. MINIMUM INSTANTANEOUS DEVIATION FIRING SCHEME

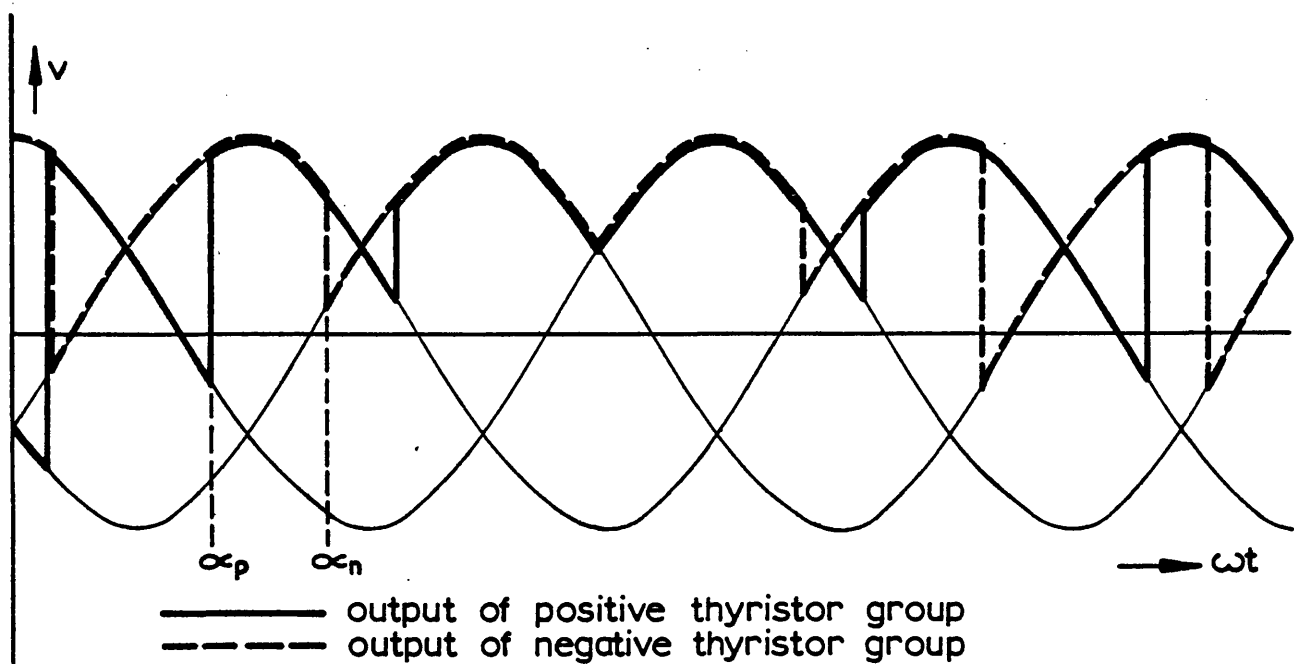


FIG. 4-5a SUPERIMPOSED POSITIVE AND NEGATIVE THYRISTOR GROUP VOLTAGES

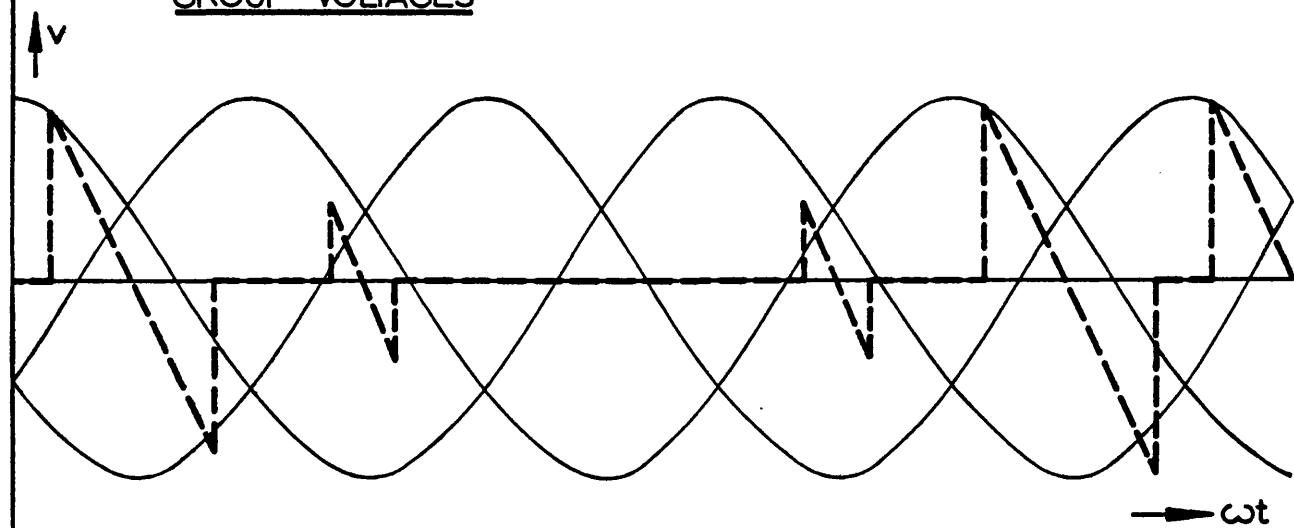


FIG 4-5b. VOLTAGE ACROSS INTER GROUP REACTOR
(difference between positive and negative thyristor group voltages)

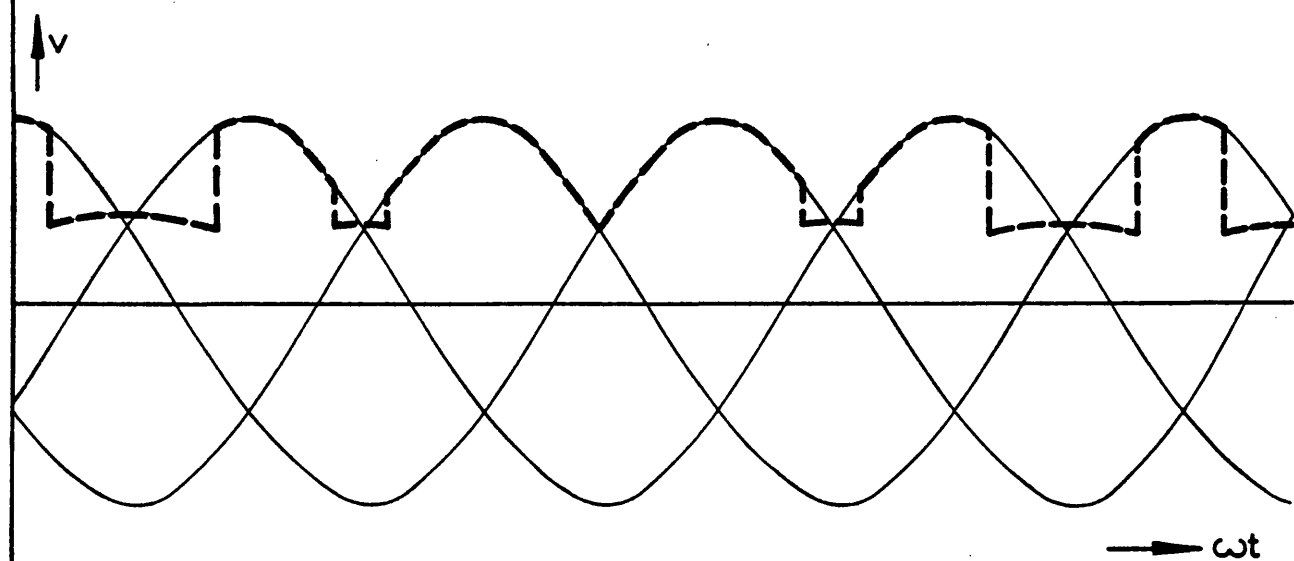


FIG. 4-5c OUTPUT VOLTAGE MEAN OF POSITIVE AND NEGATIVE THYRISTOR GROUP VOLTAGES

limited by an inter-group reactor. The mean output will now be as shown in Fig. (4.5c).

Some commercial cycloconverters dispense with the reactors by the use of integral circuit blanking ⁽³⁰⁾ to prevent the simultaneous conduction of positive and negative thyristor groups. Each group will conduct for π radians of output voltage, but the part of the output cycle over which conduction takes place varies with the fundamental displacement angle of the load current as shown in Fig. (4.6). The harmonic content of the output voltage now depends on,

- (a) the input to output frequency ratio,
- (b) the ratio of the input voltage amplitude to the control reference signal amplitude, and
- (c) the angle of displacement between the fundamental output voltage and current.

The output voltage applied to the load, V_o , is now given by

$$V_o = \frac{V_p + V_N}{2} \quad , \quad (4.2)$$

where V_p and V_N are the positive and negative group voltages respectively.

Pelly ⁽¹⁹⁾ indicates how a Fourier analysis can be carried out if the voltages V_p and V_N are multiplied by unit step-functions of length corresponding to the thyristor group conduction half-period. Each period of thyristor conduction is defined by a unit step function, $f_1(\omega t - \alpha)$, $f_2(\omega t - \alpha)$, each taking the value +1 when the associated thyristor is on and zero at all other times. V_p and V_N can be expressed as,

$$V_p = \{V_m \sin \omega t\} f_1(\omega t - \alpha_p) + \{V_m \sin(\omega t - \frac{2\pi}{3})\} f_2(\omega t - \alpha_p) + \{V_m \sin(\omega t - \frac{4\pi}{3})\} f_3(\omega t - \alpha_p) \quad , \quad \text{and}$$

$$V_N = \{V_m \sin \omega t\} f_1(\omega t - \alpha_N) + V_m \{\sin(\omega t - \frac{2\pi}{3})\} f_2(\omega t - \alpha_N) + V_m \{\sin(\omega t - \frac{4\pi}{3})\} f_3(\omega t - \alpha_N) \quad . \quad (4.3)$$

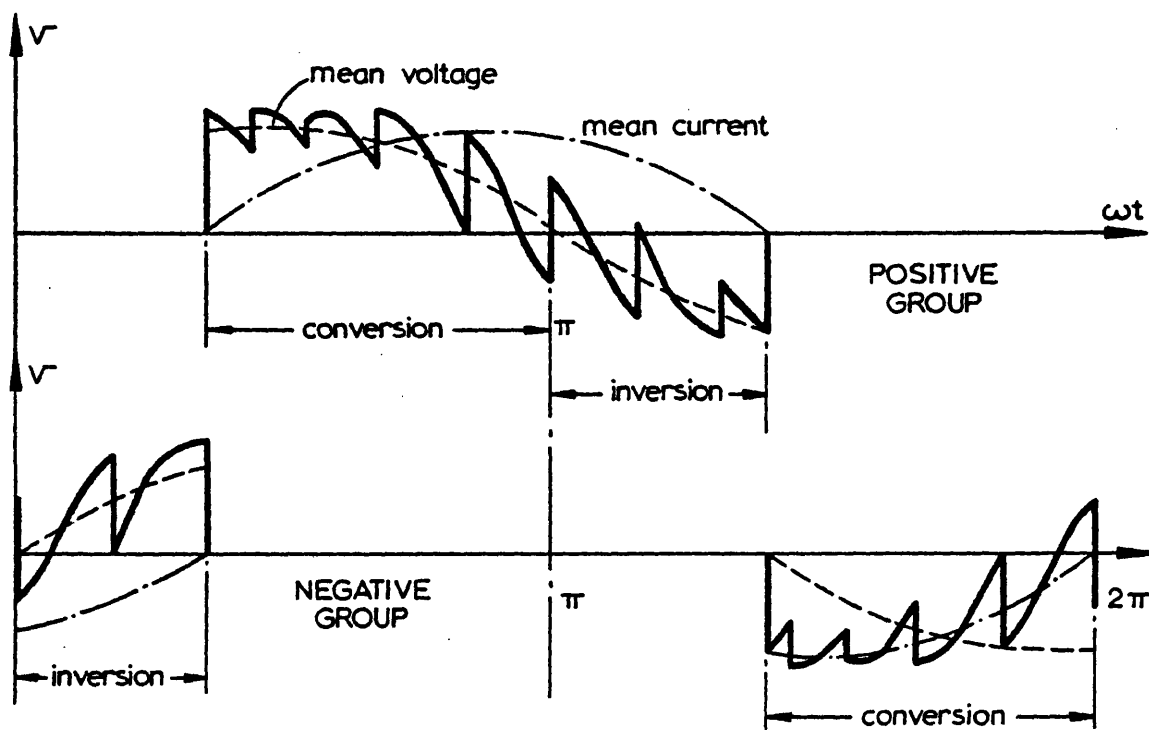


FIG.4.6 THYRISTOR GROUP VOLTAGES IN CIRCULATING CURRENT FREE MODE OF OPERATION
 (output fundamental displacement angle = $\frac{\pi}{6}$)

The conduction limits of thyristor A in Fig. (4.3) are $(\alpha_p + \frac{5\pi}{6})$ and $(\alpha_p + \frac{\pi}{6})$, while thyristors B and C have similar limits displaced forward and back by $\frac{2\pi}{3}$ radians referred to the input frequency respectively. Each step function is an even function of period 2π which may be expressed in a Fourier series as,

$$f(t) = a_0 + \sum_{n=1}^{\infty} a_n \cos \frac{2n\pi t}{T} \quad (4.4)$$

The basic cycloconverter shown in Fig. (4.1) generates its output voltage by oscillating the firing angles of the positive and negative thyristor groups in opposite relative directions about the $\alpha_p = \alpha_n = \frac{\pi}{2}$ quiescent point. For minimum maximum deviation from the output voltage mean,

$$\alpha_p = \pi - \alpha_n \quad (4.5)$$

From equations (4.2), (4.3), (4.4) and (4.5), the output voltage may now be given in terms of a firing angle function $f(\omega_0 t)$. The output voltage is now given as,

$$V_o = \frac{3\sqrt{3}V_m}{2\pi} \left[\sin f(\omega_0 t) + \frac{1}{2} \sin 3 \omega t \cos 2f(\omega_0 t) + \frac{1}{4} \sin 3 \omega t \cos 4f(\omega_0 t) + \frac{1}{5} \cos 6 \omega t \sin 5f(\omega_0 t) + \frac{1}{7} \cos 6 \omega t \sin 7f(\omega_0 t) + \dots \text{etc.} \right] \quad (4.6)$$

V_o should have the greatest possible fundamental to harmonic ratio for satisfactory operation of the motor. Ideally, the cycloconverter is a linear amplifier in which the output voltage is an amplification of an input control voltage. The control voltage needed to implement this for a sinusoidal output is

$$v_c = rV_c \sin \omega_0 t, \quad (4.7)$$

where V_c is the peak value of the control voltage and r is a dimensionless scaling factor between 0 and 1 allowing for amplitude variation. In a physical system, r is the ratio between the peak control voltage and the

peak timing voltage. The thyristor firing function is now,

$$f(\omega_0 t) = \sin^{-1}(r \sin \omega_0 t) \quad , \quad (4.8)$$

which implies that the firing angle is moved from the $\frac{\pi}{2}$ quiescent position by the angle $\sin^{-1}(r \sin \omega_0 t)$.

An inspection of equation (4.6) shows that the families of harmonics present in the output voltage can be expressed in frequency terms by the equations,

$$\frac{f_H}{f_0} = 3(2p-1) \frac{f}{f_0} \pm 2N \quad , \quad \text{where } 2N \leq 3(2p-1) + 1, \quad (4.9)$$

and

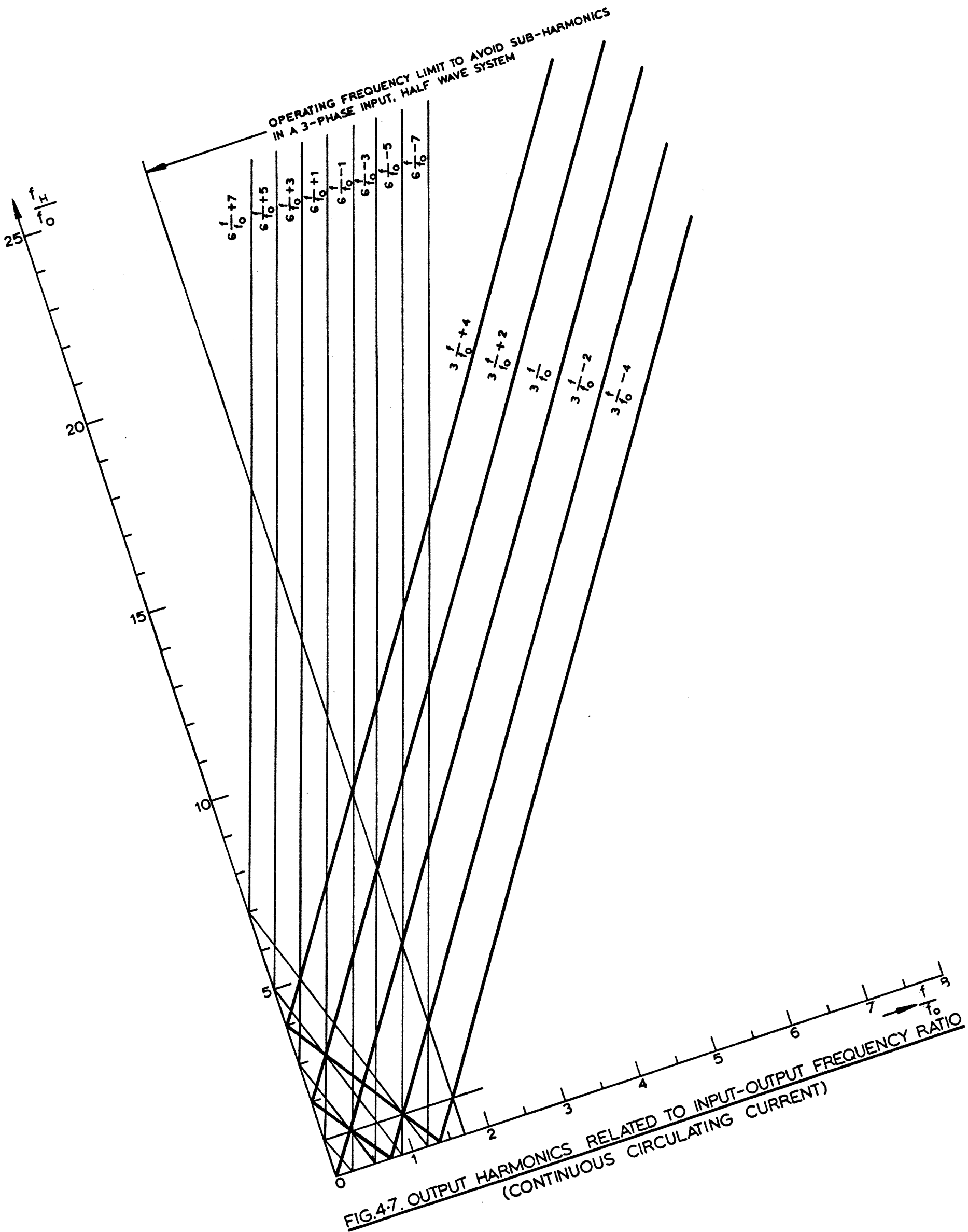
$$\frac{f_H}{f_0} = 6p \frac{f}{f_0} \pm (2N + 1) \quad , \quad \text{where } (2N+1) \leq (6p+1) \quad . \quad (4.10)$$

Fig. (4.7) shows the lowest frequency harmonic families present in the output voltage, i.e. when $p = 1$ and $N = 0, 1, 2$ etc. For any given input to output frequency ratio, f/f_0 , a vertical projection intersects the sloping lines to indicate the harmonic frequencies present, the values of which can be read off the vertical f_H/f_0 scale.

4.3 Voltage output with circulating-current-free operation

The early commercial cycloconverters operated without circulating current ⁽³¹⁾ considerable difficulty was experienced due to the mal-function of thyristor gate circuits causing line to line short-circuits. Also if reversibility and regeneration are to be achieved, the gate pulse sequence of the thyristor groups must be reversed at the instant of the commencement of induction generation by the load. Also gaps between the thyristor group conduction periods are usually introduced as an additional safety factor.

However, if "ideal" circulating-current-free operation can be achieved using modern semi-conductor technology, the instant at which each thyristor group begins to conduct is defined by the fundamental load current displacement angle with respect to the output



voltage. The output voltage harmonic content will depend on this instant and the fundamental load current displacement angle ϕ_0 as shown in Fig. (4.6), must become an additional parameter in the harmonic analysis. The positive thyristor group conducts over the interval, $\phi_0 \leq \omega_0 t \leq (\phi_0 + \pi)$, and the negative thyristor group over the interval, $(\phi_0 + \pi) \leq \omega_0 t \leq (\phi_0 + 2\pi)$. If two unit functions, $f_p(\omega_0 t)$ and $f_N(\omega_0 t)$ are used to define the positive and negative conducting periods respectively, the cycloconverter output voltage will now be,

$$V_o = V_p f_p(\omega_0 t) + V_N f_N(\omega_0 t) , \quad (4.11)$$

where each unit function is defined in a Fourier series as follows,

$$f_p(\omega_0 t) = \frac{1}{2} + \frac{2}{\pi} \left[\sin(\omega_0 t + \phi_0) + \frac{1}{3} \sin 3(\omega_0 t + \phi_0) + \frac{1}{5} \sin 5(\omega_0 t + \phi_0) \right. \\ \left. + \frac{1}{7} \sin 7(\omega_0 t + \phi_0) + \dots \text{etc} \right] , \text{ and}$$

$$f_N(\omega_0 t) = \frac{1}{2} - \frac{2}{\pi} \left[\sin(\omega_0 t + \phi_0) + \frac{1}{3} \sin 3(\omega_0 t + \phi_0) + \frac{1}{5} \sin 5(\omega_0 t + \phi_0) \right. \\ \left. + \frac{1}{7} \sin 7(\omega_0 t + \phi_0) + \dots \text{etc} \right] . \quad (4.12)$$

V_p and V_N are as previously defined in equation (4.3), the result of which combines with equation (4.12) to give the output voltage for a cycloconverter operating free of circulating current as,

$$V_o = \frac{3\sqrt{3}V_p}{2\pi} \left[\sin f(\omega_0 t) + \frac{1}{2} \sin 3\omega t \cos 2f(\omega_0 t) + \frac{1}{4} \sin 3\omega t \cos 5f(\omega_0 t) \right. \\ \left. + \frac{1}{7} \sin 6\omega t \cos 7f(\omega_0 t) + \dots \text{etc} \right] \\ + \frac{3\sqrt{3}V_N}{2\pi} \left[\frac{1}{2} \cos 3\omega t \sin 2f(\omega_0 t) + \frac{1}{4} \cos 3\omega t \sin 4f(\omega_0 t) + \frac{1}{5} \sin 6\omega t \right. \\ \left. \cos 5f(\omega_0 t) + \frac{1}{7} \sin 6\omega t \cos 7f(\omega_0 t) + \text{etc} \right] \\ \times \frac{4}{\pi} \left[\sin(\omega_0 t + \phi_0) + \frac{1}{3} \sin 3(\omega_0 t + \phi_0) + \frac{1}{5} \sin 5(\omega_0 t + \phi_0) + \frac{1}{7} \sin 7(\omega_0 t + \phi_0) \right. \\ \left. + \dots \text{etc} \right] . \quad (4.13)$$

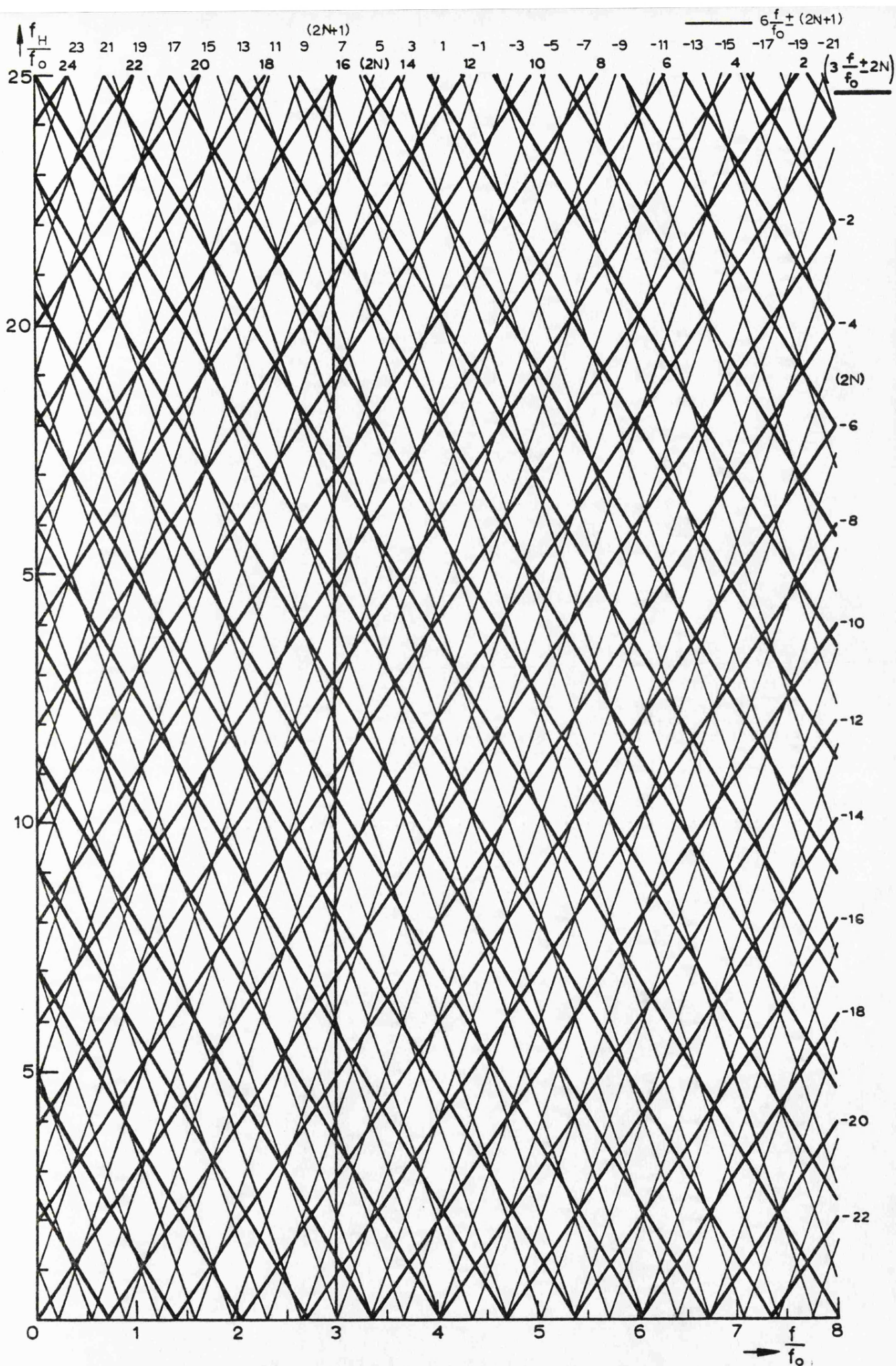


**FIG. 4. 8 OUTPUT HARMONICS RELATED TO INPUT-OUTPUT FREQUENCY RATIO
(CIRCULATING CURRENT FREE CASE)**

An inspection of equation (4.13) shows that families of harmonics present in the output voltage can be expressed in frequency terms by the equations (4.9) and (4.10) as,

$$\frac{f_H}{f_o} = 3(2p-1) \frac{f}{f_o} \pm 2N \quad (4.9)$$

$$\frac{f_H}{f_o} = 6p \frac{f}{f_o} \pm (2N + 1) \quad (4.10)$$

with the additional equation,

$$\frac{f_H}{f_o} = 12p \frac{f}{f_o} \pm (2N + 1) , \quad (4.14)$$

where p is any positive integer and $0 < N < \infty$. $f(\omega_o t)$ was defined in equation (4.8).

Fig. (4.8) gives the complete harmonic families present in the output voltage for circulating-current-free operation. The thick sloping lines represent equation (4.9) plotted for the case where $p = 1$ and the thin sloping lines represent equation (4.10) plotted for the case where $p = 1$. As no cancelling takes place, all values of N are significant.

Fig. (4.8) can be used to determine the harmonics present in the output voltage at any fixed fundamental output frequency. In Fig. (4.8) a vertical line can be drawn through the known value f/f_o and the harmonic frequencies will be indicated by the points of intersection with the sloping lines. The left hand side vertical scale gives the harmonic value at the point of intersection.

If Fig. (4.8) is compared with Fig. (4.7), it can be seen that the main bands of frequencies present in the continuous circulating current case are still present, although their amplitudes will be different. Thus the main effect of changing load power factor in a motor drive is to alter amplitudes of the harmonics but not their frequencies. It can be noted from Fig. (4.8) that sub-harmonics will be present in the output

voltage at all frequencies and that no boundary of sub-harmonic free operation can be defined for a circulating-current-free cycloconverter.

4.4 Continuous circulating current operation

A comparison of Figs. (4.7) and (4.8) shows that continuous circulating current operation is much to be preferred if it can be achieved. Considerable harmonic cancellation takes place and only the first bracketed term of equation (4.13) remains forming equation (4.6). This indicates that if continuous circulating current operation can be maintained,

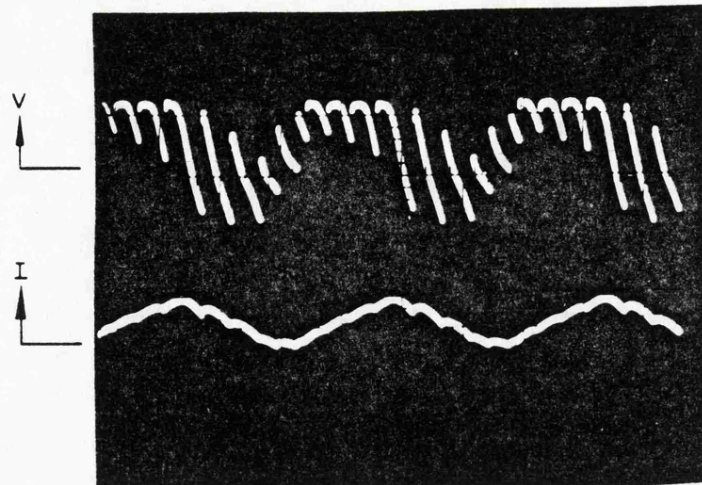
(a) the harmonic frequencies present in the cycloconverter output voltage increase as a linear function of f/f_0 . Thus operation at highest possible input to output frequency ratio is desirable, and

(b) sub-harmonics will not be produced if the input to output frequency ratio ≥ 1.66 . This defines the lowest operating frequency if motor "cogging" is to be avoided from the applied time-varying field. For a six-phase input or a three-phase full-wave system, this limit will be reduced to 1.33.

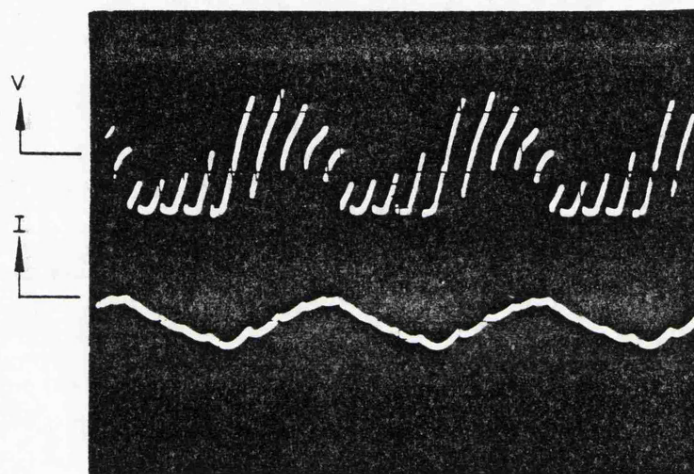
This harmonic cancellation is shown in the experimental cycloconverter in Fig. (4.9). The cycloconverter has been driven into saturation to exaggerate the harmonic content of the output.

No general harmonic amplitude pattern can be derived.

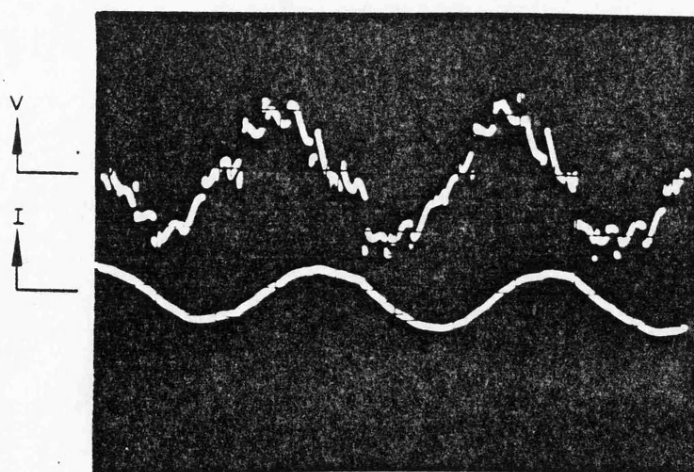
However particular cases can be computed from equation (4.13) with the aid of Fourier coefficients given in reference (27). Fig. (4.10) shows the harmonic amplitude variation caused by changing the control ratio, r . It can be clearly seen that optimum performance will be obtained when $r = 1$. Fig. (4.11) shows the correlation between computed and measured harmonic values. The measured values were obtained from a Fenlow Spectrum Analyser connected across a static L-R load.



POSITIVE THYRISTOR GROUP



NEGATIVE THYRISTOR GROUP



OUTPUT TO LOAD

FIG.4.9 OPERATION WITH CONTINUOUS CIRCULATING CURRENT

$$\frac{f_i}{f_o} = 3 \quad r = 1.0$$

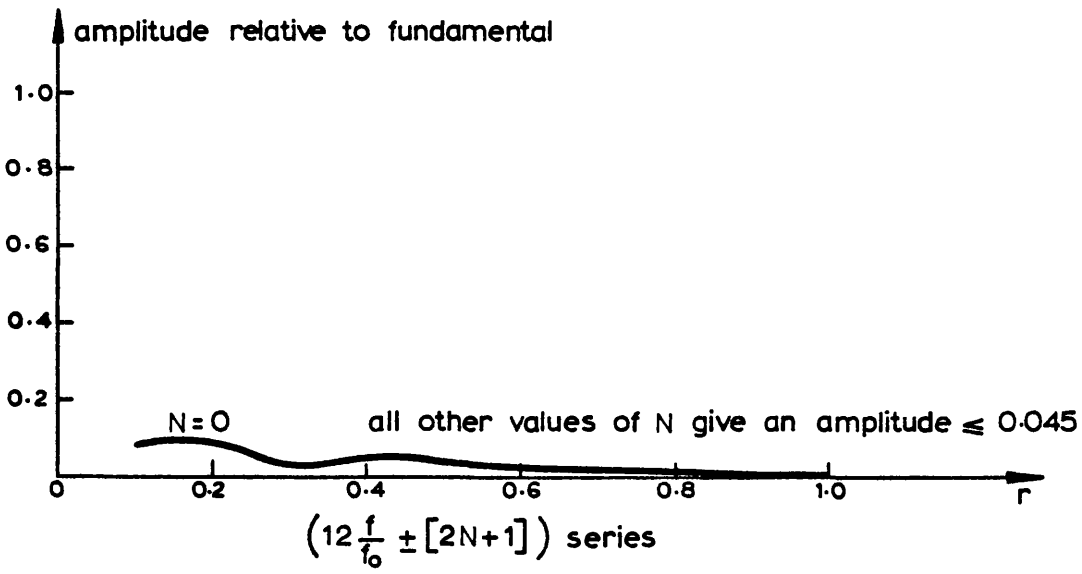
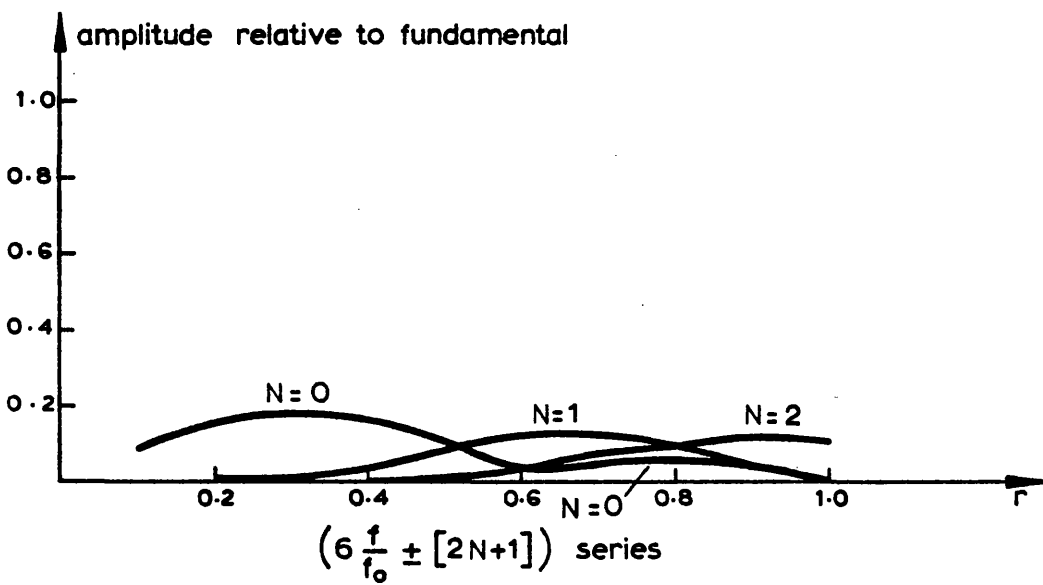
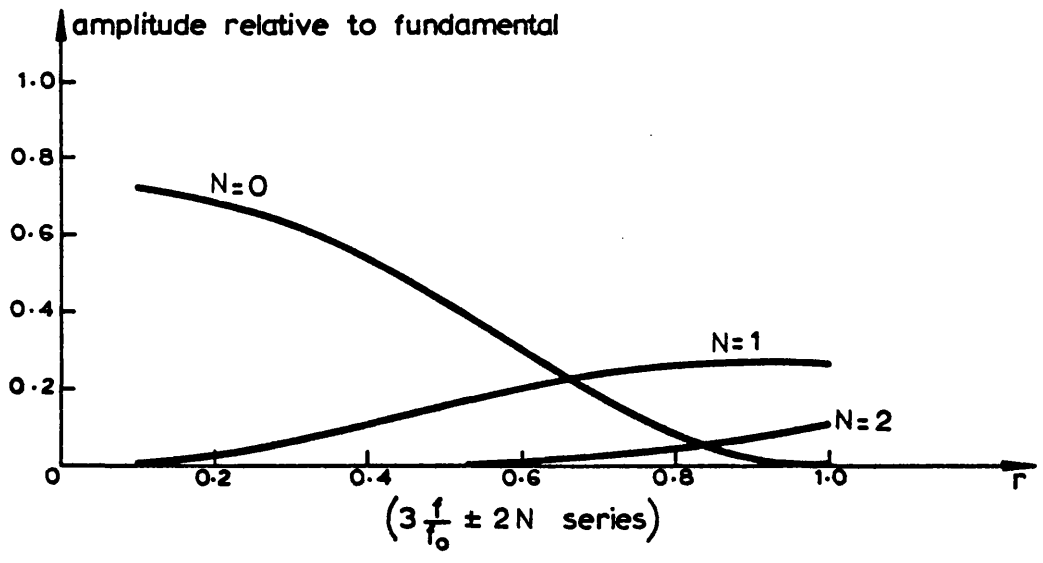


**FIG.4.10 AMPLITUDE OF HARMONICS RELATED TO OUTPUT RATIO r
3 Thyristors per group Cycloconverter operating
 with continuous Circulating Current**

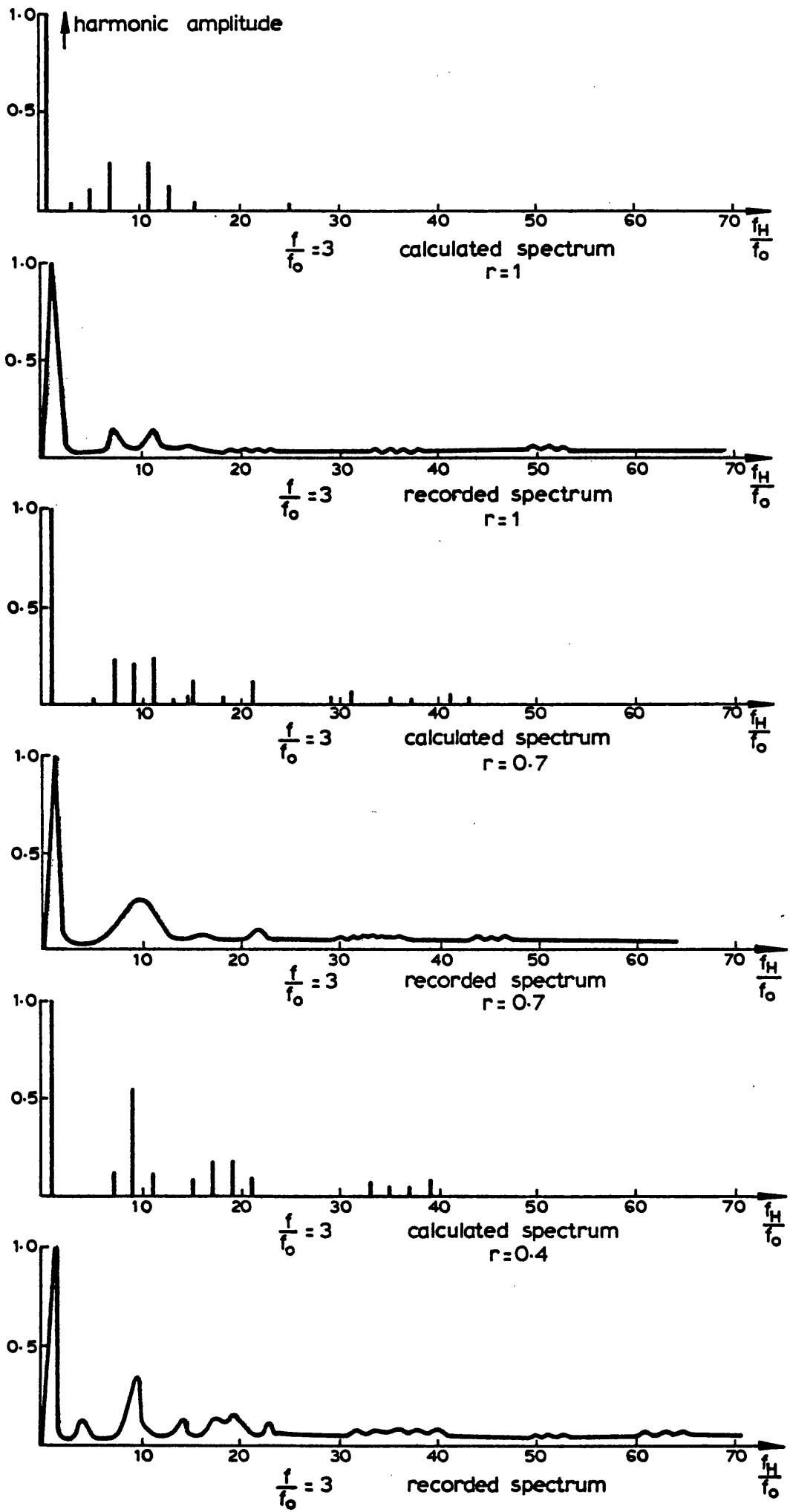


FIG.4.11 HARMONIC FREQUENCIES WITH CONTINUOUS CIRCULATING CURRENT

A further advantage of a circulating-current-cycloconverter over the circulating-current-free system is the better voltage regulation. In the circulating-current-free system, safe operation without line to line short circuits demands a gap of up to 6 ms duration between thyristor group currents. The position of this gap on the voltage wave is load dependent as shown in Fig.(4.12). This results in poor voltage regulation at low power-factor operation. The regulation of the output voltage increases with the input frequency. A continuous circulating current system has no gaps in its output waveform. It can also naturally commute at leading or antiphase fundamental current displacement angles and permits regenerative braking without pulse-circuit-modification.

4.5 The experimental system

The system constructed was generally as shown in Fig. (4.13) incorporating a cycloconverter and a divided-winding induction motor, the stator of which replaced the inter-group reactors of the conventional system. An existing frame incorporating 18 thyristors in 6 groups of 3 was used as the basis for the cycloconverter, but all control circuits and reference sources were completely redesigned and constructed by the author. A 400Hz, 3-phase, 115V supply source was used to increase the input to output frequency range to enable a wider range study to be carried out. The maximum continuous rms rating per device was 10A.

Essentially the cycloconverter is a linear amplifier giving an output proportional to the reference signal input. This reference signal input was obtained from a 3-phase, mag-slip generator with provision for separate excitation driven by a velodyne motor, the speed of which was controlled by armature voltage variation. Two feedback loops were provided;

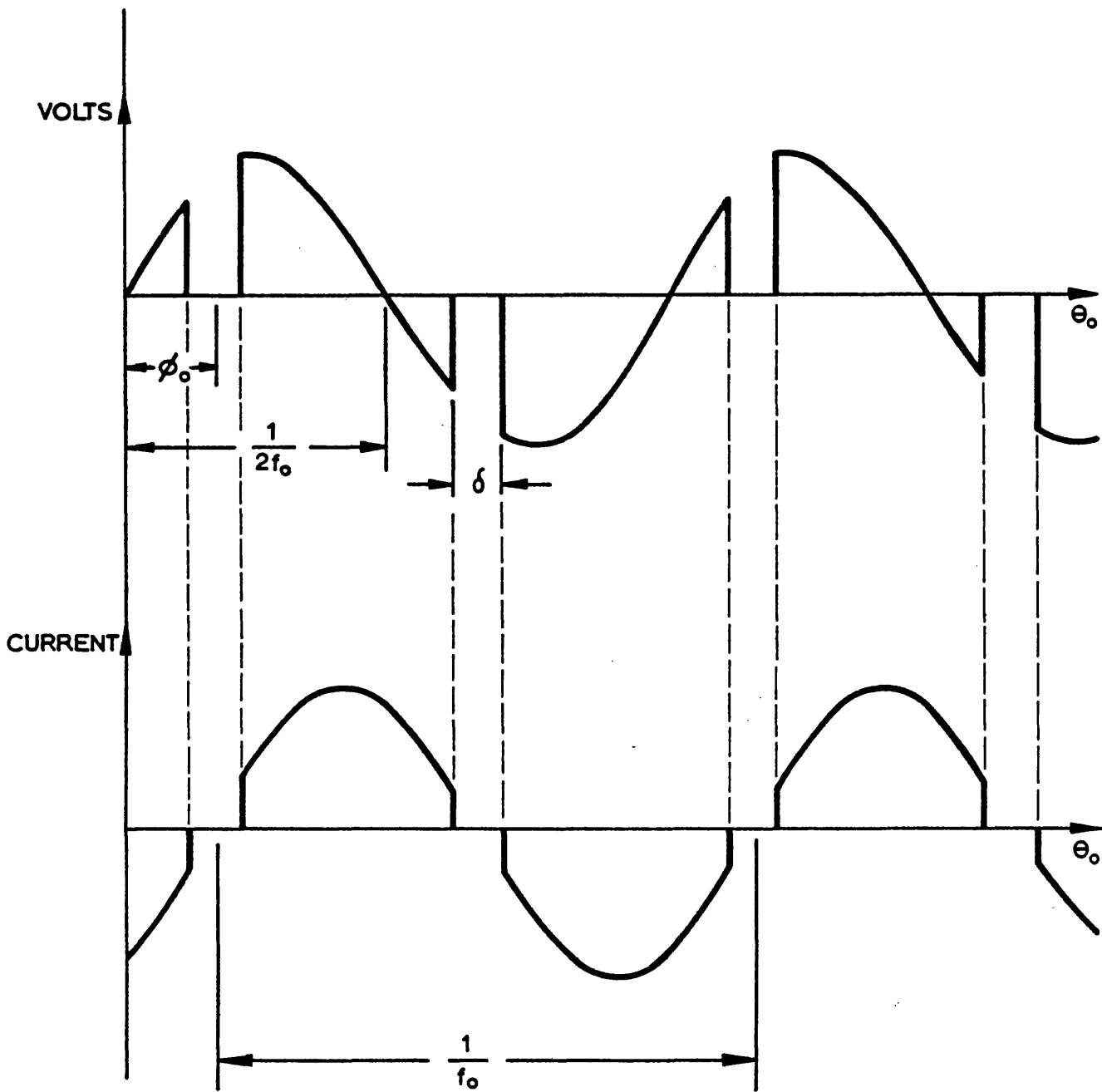


FIG.4.12 THE EFFECT OF THYRISTOR GROUP CHANGEOVER DELAY ON THE FUNDAMENTAL VOLTAGE AND CURRENT OF A CYCLO-CONVERTER OPERATING WITHOUT CIRCULATING CURRENTS

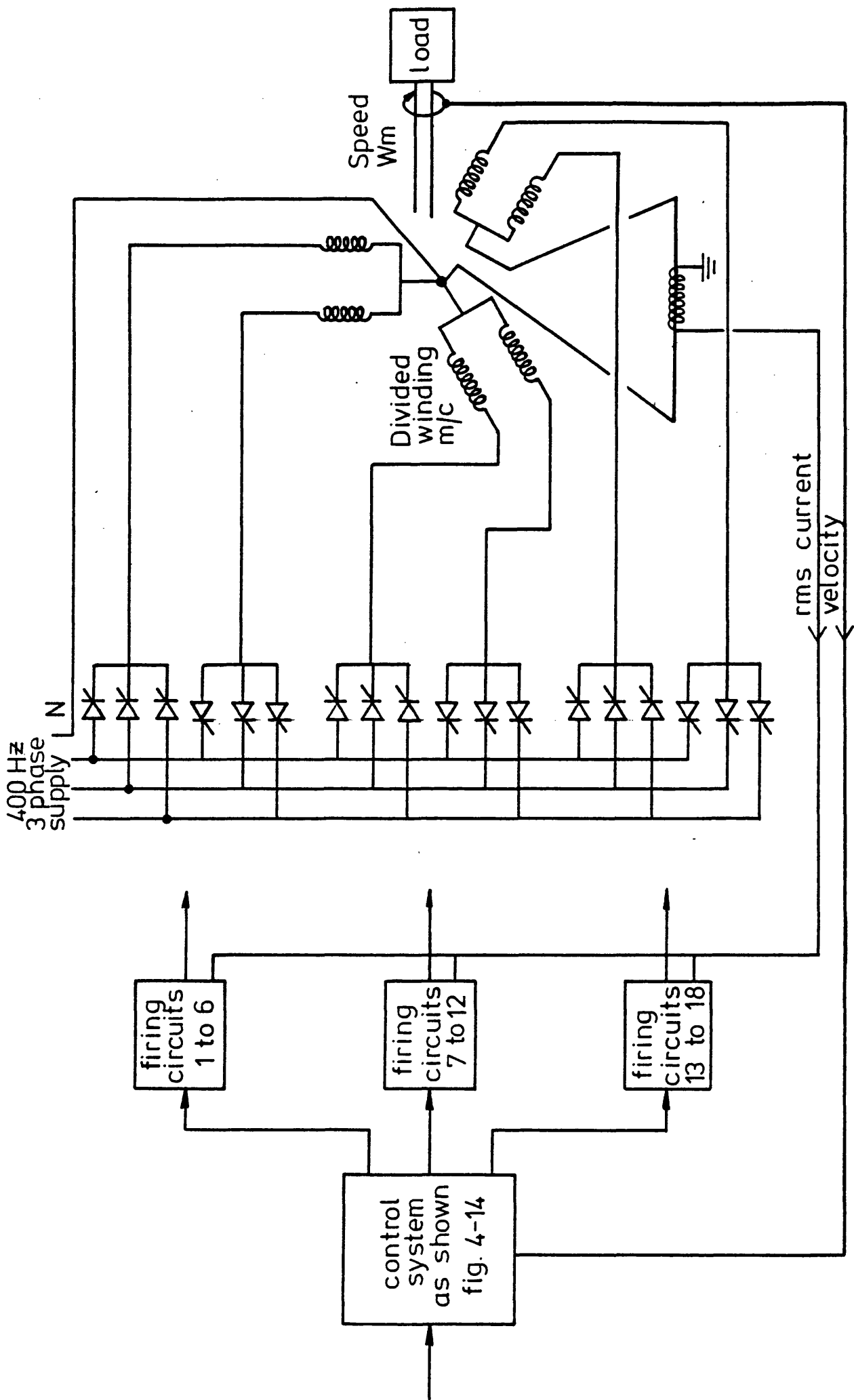


Fig 4.13. Complete cycloconverter system.

(a) a velocity-feedback signal from a tachometer which varied the velodyne speed and mag-slip frequency to give a constant induction motor speed independent of load variation and,

(b) a current level signal proportional to the rms load current which operated a current clamping circuit which prevented excessive output currents from damaging the devices.

Fig. (4.14) shows the reference generator control circuitry schematically.

The adjustable v/f control potentiometer controls the velodyne armature voltage after amplification through the ramp generator board and speed servo-board. Velocity feedback modifies the speed servo operation to give constant induction motor speed at any single setting of the demand potentiometer. The current loop signal controls the mag-slip field current through the voltage and current shaper servo current is reduced by a reduction of mag-slip voltage in the first instance. The operation of the particular parts of the control system is described in sections 4.6, 4.7, 4.8 and 4.9.

4.6 Ramp generator board and mono-polarity board

The main function of the ramp generator unit is to limit the rate of change of frequency and voltage. This means that this unit will ensure that, as the speed of the velodyne motor changes the voltage output of the mag-slip generator will always be proportional to frequency. The operation is as follows:

If the polarity of the input is negative, then the output is positive and the output current passes through diode (D_1), as shown in Fig. (4.15) hence giving an output signal of negative polarity. The diode, D_2 , passes a negative output in a similar way. A second operational amplifier operating as an integrator delays the rise of current. The purpose

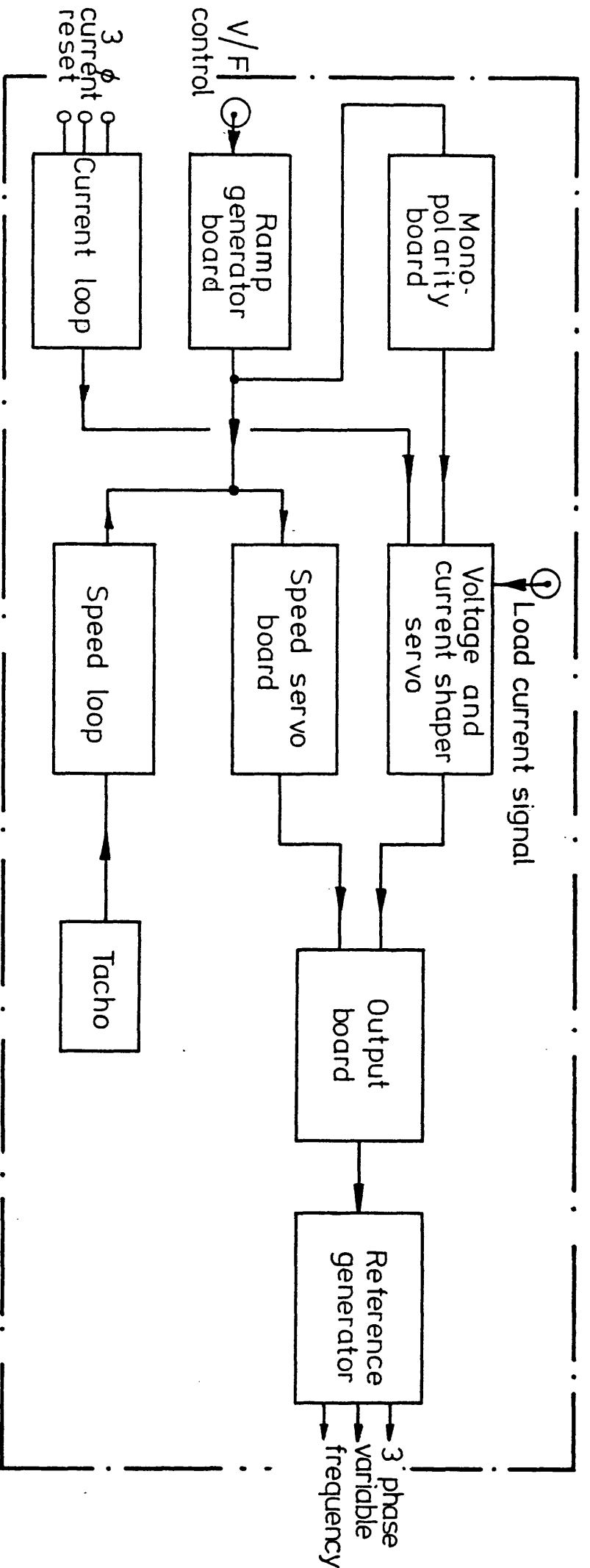
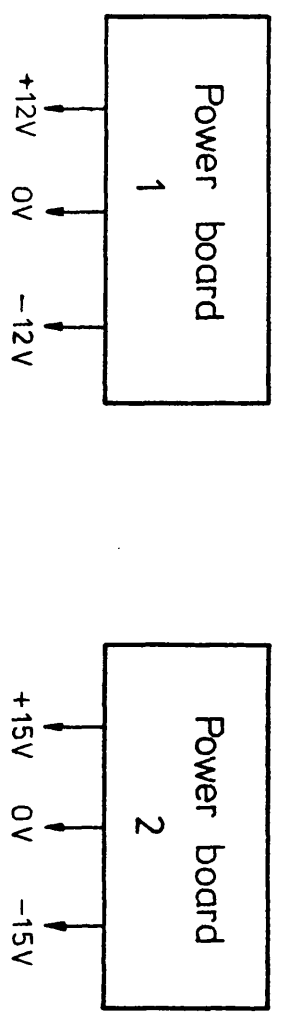


Fig. 4.14 Schematic diagram of cycloconverter control system.

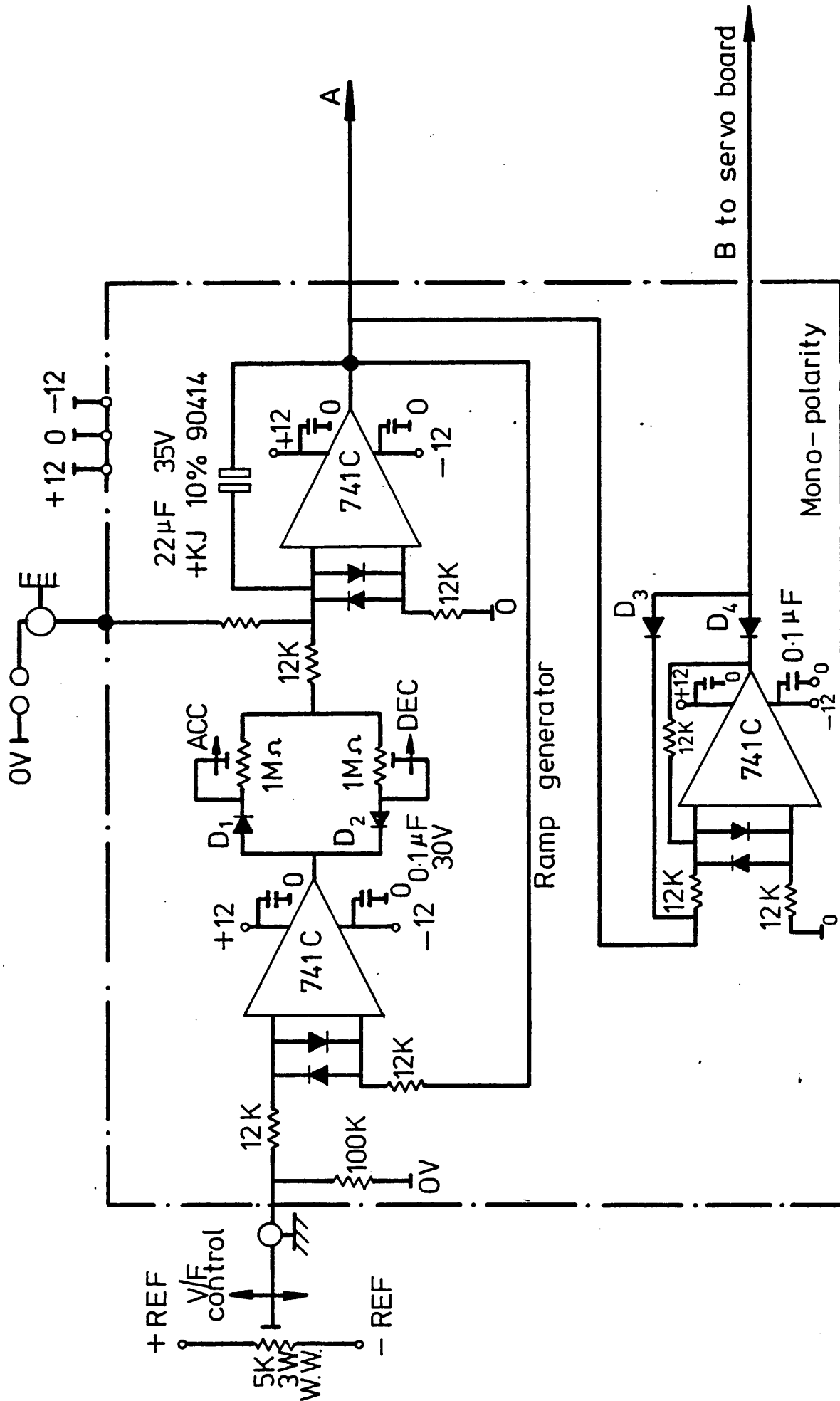


Fig.4.15 Ramp generator and mono polarity board

of the mono-polarity unit is to supply the input of the voltage shaper amplifier (A_1) as shown in Fig. (4.16) with a negative signal whatever the polarity of the input from the ramp generator. This can be explained as follows;

if a negative polarity signal voltage is fed from the ramp generator output to the mono-polarity input, a current passes through the diode D_3 to the output. This supplies the voltage shaper amplifier of Fig. (4.16) with negative input which will always keep its output voltage point below that of the current loop amplifier output and so maintains the first one in full control. This negative input will also be maintained even though mono-polarity input is supplied with positive signal, because, in this case, diode D_3 is switched off. The positive input will then switch the amplifier on giving a "negative" output which is blocked by D_3 , and thus passed to the input of the servo amplifier. Hence the mono-polarity circuit will always supply a negative input to the voltage shaper amplifier.

4.7 Operation of voltage loop (Fig. 4.16)

Voltage of negative polarity will always be supplied by the mono-polarity circuit to the input of the voltage shaper amplifier, B, and this then will be in full control as long as its output voltage point is lower than the current loop amplifier output. This will then be fed into the transistor BFY 50 and the output of the BD 203 transistor will maintain a steady, single polarity excitation to the field of the mag-slip generator.

An input v/f potentiometer controls the reference amplitude and frequency. The system operates over a relatively small low-frequency output range and so a compensating network to maintain constant air-gap flux in the machine was omitted. Excessive currents are prevented by the current clamping circuit which operates on the following principle:

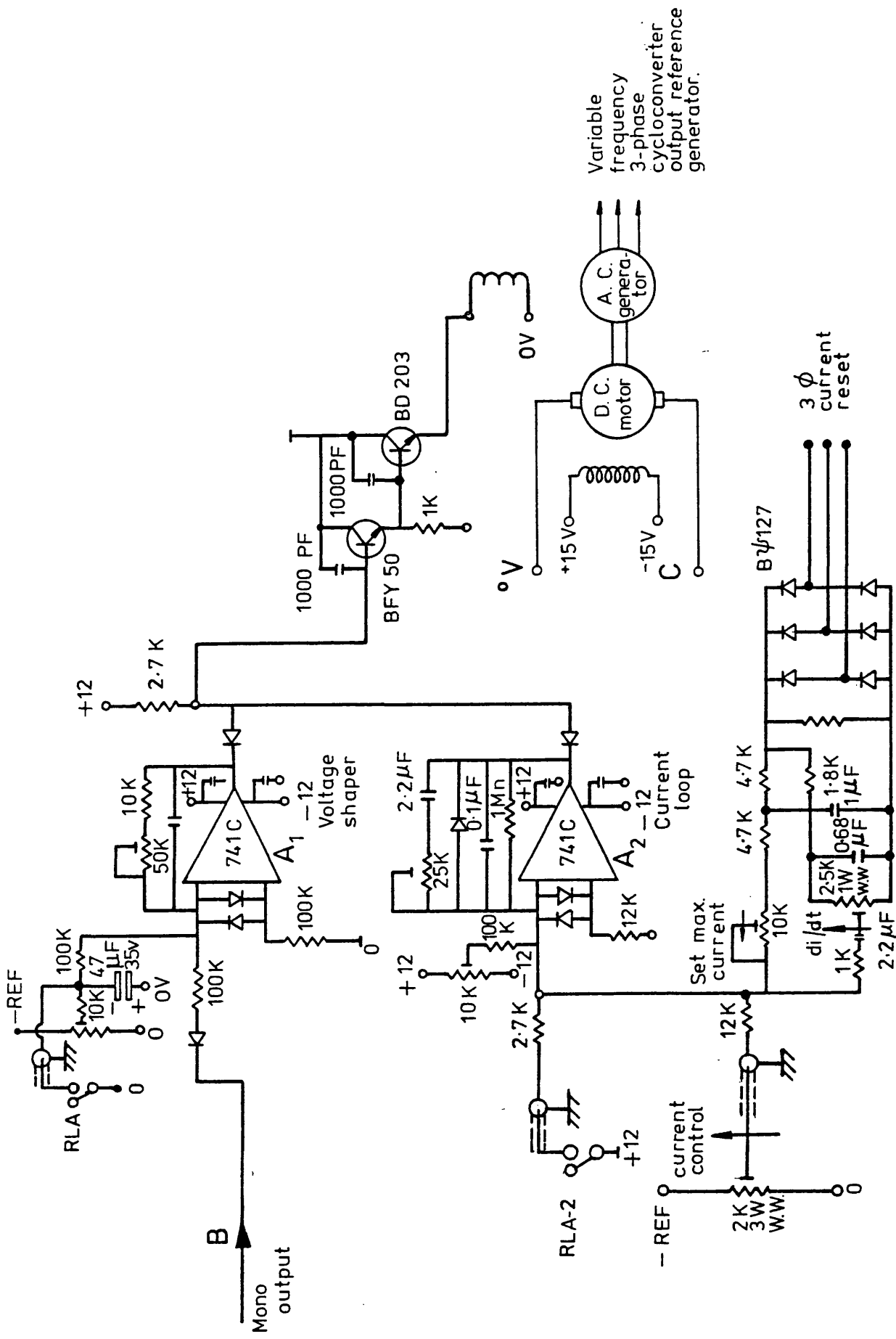


Fig.4.16. Voltage shaper and current loop circuit diagram of the servo board.

if the load current exceeds the value of the pre-set current limit, a signal is fed to the current loop amplifier (A_2) causing it to conduct. Amplifier A_2 then takes control from amplifier A_1 and reduces the field excitation of the reference generator, which in turn reduces the reference voltage amplitude and so the cycloconverter output current is limited.

4.8 Speed-servo (Fig. (4.17))

The ramp generator output may be of either polarity according to the polarity demanded by the v/f potentiometer. It is fed to the input of the speed-servo amplifier, A_3 .

The operational amplifier output is then fed through two single stages of amplification -and a push-pull amplifier to provide a controlled armature voltage for the velodyne motor driving the reference generator. Constant velodyne field excitation means that the frequency of the reference signal is directly controlled by the v/f potentiometer between velodyne armature voltage limits of +15 and -15 volts. The reference frequency is automatically adjusted by closed-loop tachometer feedback as shown in the lower part of Fig. (4.17). Here the voltage proportional to velocity is attenuated and smoothed and controlled in feedback rate, $\frac{dn}{dt}$, by the setting of the 2.5K potentiometer.

4.9 Thyristor firing and pulse-boards

For economic reasons, a 3-phase half-wave cycloconverter was constructed. In terms of output harmonic content, this is the worst possible case and so any system incorporating more thyristors will give better results. However the experimental system justifies the concept. As shown in Fig. (4.18), 18 thyristors in 6 groups of 3 are required to give a 3-phase output. Each pulse-board is timed by the phase of the input voltage appearing across the thyristor which it

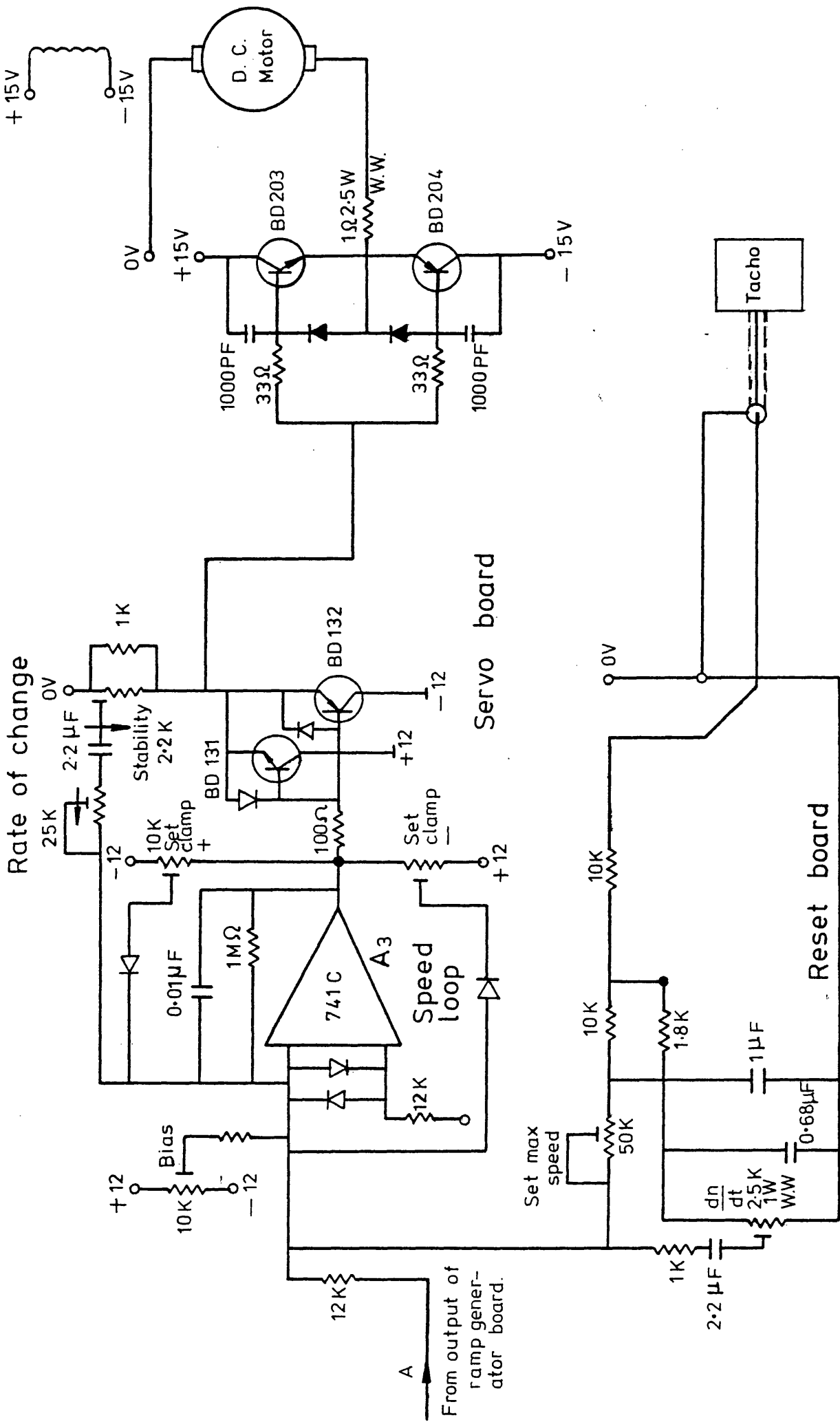


Fig. 4.17. Servo board showing speed loop.

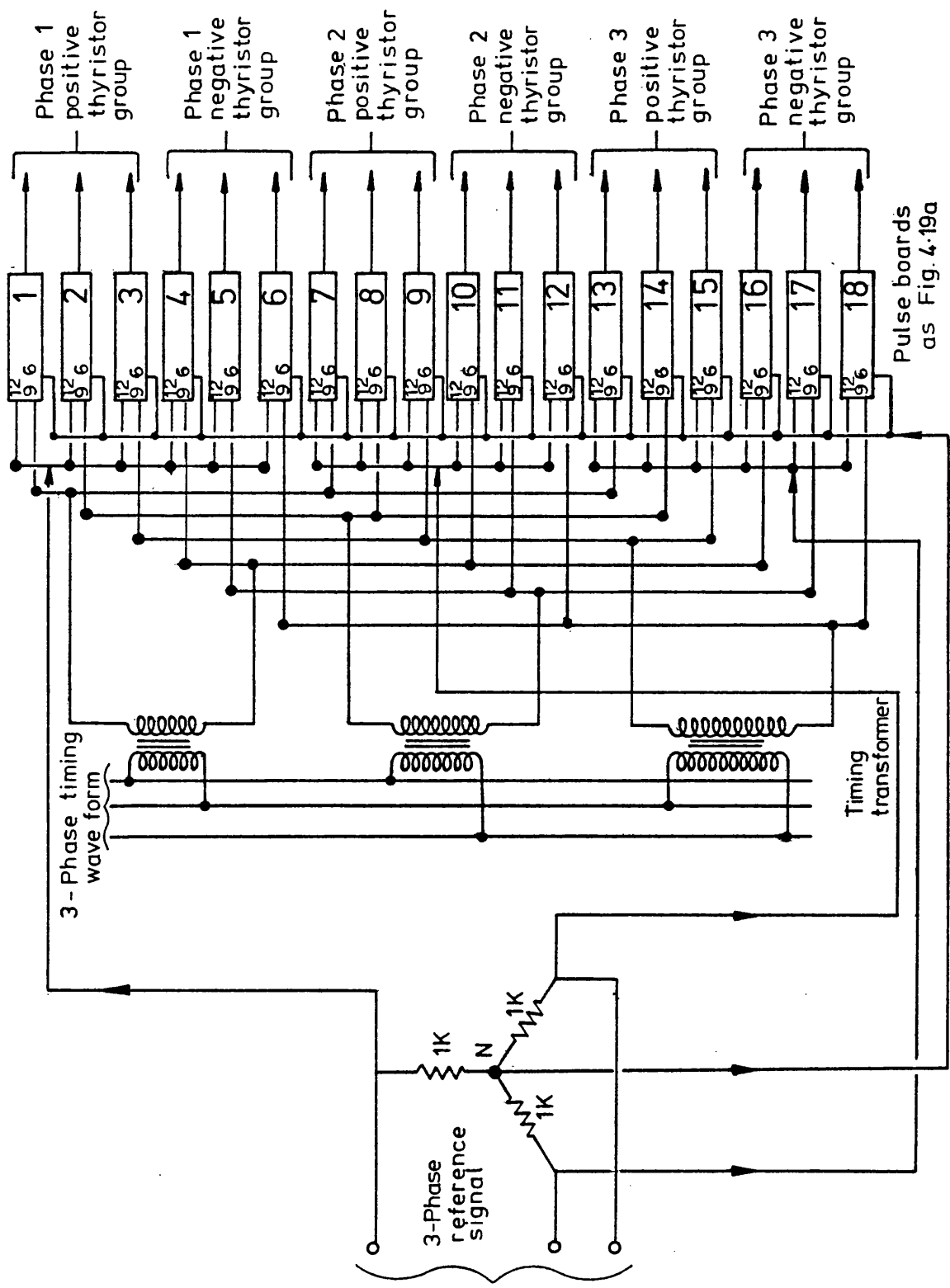
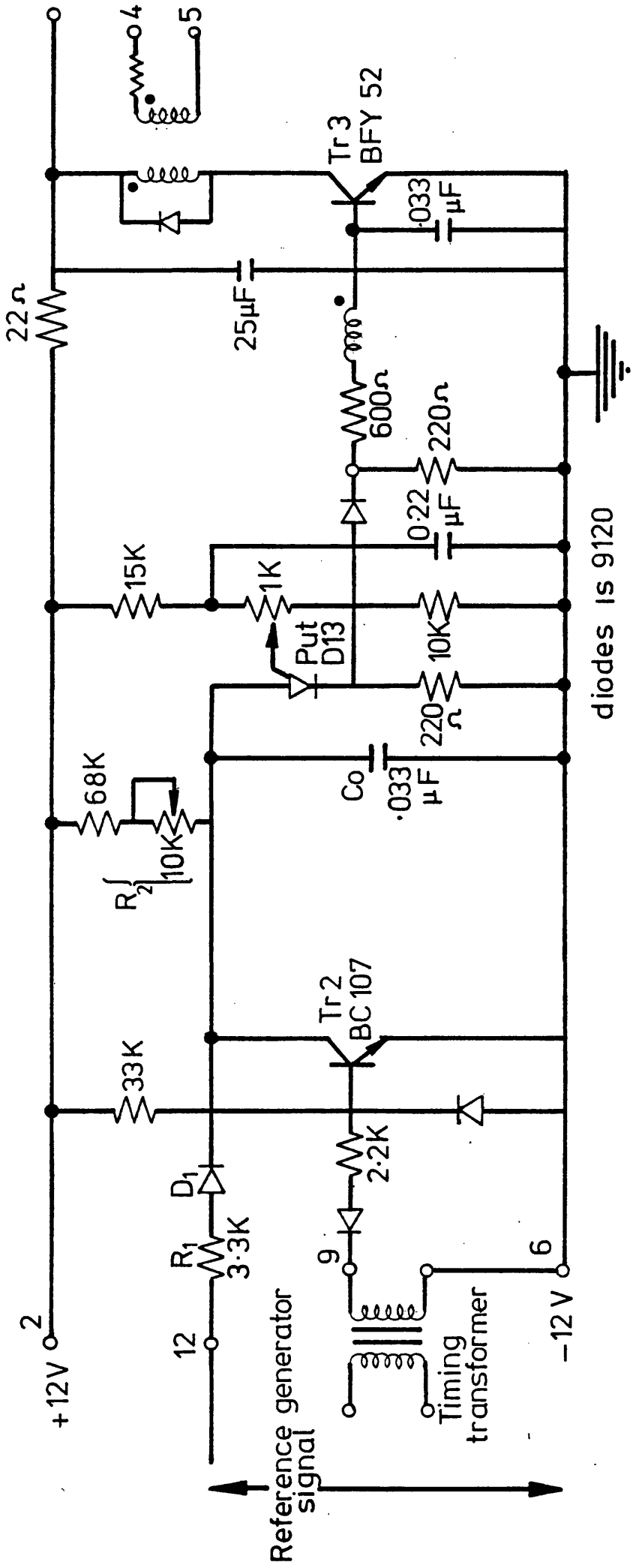


Fig. 4.18 Pulse board timing and reference control

controls. Timing signals are applied through timing transformers connected to the input mains. In this form the timing voltage amplitude will be constant and the amplitude of the output voltage will be varied by varying the amplitude of the input reference signal. As explained in section 4.7, these signals are generated by a mag-slip generator driven by a velodyne, the speed of which was controlled by the operational amplifier system described in section 4.8.

The mag-slip armature was delta connected and a star point for the reference signal was created by three star-connected resistors of $1K\Omega$. Fig. (4.18) shows that boards 1 - 6 generate the pulses which control phase-1 of the output voltage which corresponds in phase to phase-1 of the reference signal input. Similarly, boards 7 - 12 generate the pulses for phase-2 of the output which will be displaced from phase-1 by 120° , and boards 13 - 18 generate the pulses for phase-3 which will be displaced by 240° from phase-1. Phase-2 and phase-3 of the output voltage correspond to phases 2 and 3 of the reference voltage. Phase-controlled pulse-boards already in use in the laboratory were modified to accept sinusoidal modulation to time the gate pulses. If the boards are linear over the operating range, sinusoidal pulse modulation will be achieved. The pulse-board circuit is shown in Fig. (4.18a) and it operates as follows.

When the timing voltage > 0 , T_{r2} is switched on short-circuiting C_o and inhibiting all output pulses. If the timing voltage, $V_{\text{timing}} < 0$, T_{r2} is switched off and C_o charges until the voltage across C_o reaches the peak level required to fire the programmable unijunction transistor, D_{13} . In turn, D_{13} drives the switching transistor, T_{r3} hard on giving a sharp rise of current through the primary of the pulse transformer and firing the thyristor. Positive feedback was used by adding a third winding to the pulse transformer in the base load of T_{r3} in order to extend the pulse-width from $40 \mu s$ to $70 \mu s$ so that latching problems



diodes IS 9120

Fig.4.19a Pulse circuit

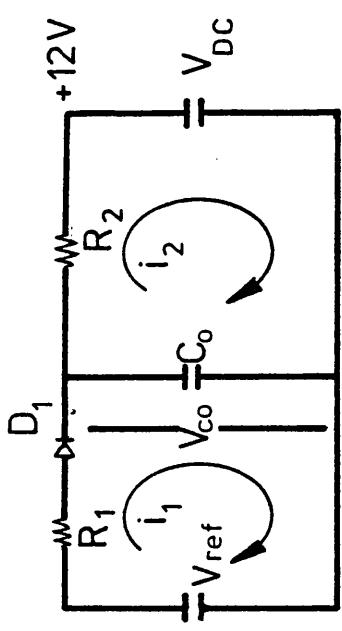


Fig.4.19b. Equivalent circuit of pulse board timing.

are avoided. Firing times are dictated by the rate of charge of C_o . The timing circuit is shown in Fig. (4.19b). The equations of the first loop of Fig. (4.19b) are as follows,

$$V_{\text{ref}} = i_1 R_1 + \frac{1}{C_o} \int_0^t i_1 dt - \frac{1}{C_o} \int_0^t i_2 dt \dots, \quad (4.15)$$

$$-V_{\text{DC}} = -\frac{1}{C_o} \int_0^t i_1 dt + i_2 R_2 + \frac{1}{C_o} \int_0^t i_2 dt \dots, \quad (4.16)$$

and
$$V_{C_o} = \frac{1}{C_o} (i_1 - i_2) t, \quad (4.17)$$

where V_{DC} is the module power supply voltage.

Equations (4.15), (4.16) and (4.17) combine to give a solution for V_{C_o} over the interval $0 \leq t \leq t_1$, shown in Fig. (4.20), for which the diode conducts, of

$$V_{C_o} = \frac{V_{\text{ref}} R_2 + V_{\text{DC}} R_1}{R_1 + R_2} (1 - e^{-t/T}), \quad (4.18)$$

where
$$T = \left(\frac{R_1 R_2}{R_1 + R_2} \right) C_o.$$

Fig. (4.20) shows the waveform for the voltage across C_o . Charging commences at the instant when the timing waveform goes negative.

The first time constant, $T = \left(\frac{R_1 R_2}{R_1 + R_2} \right) C_o$, operates until the diode is reverse biased and switched off. Then the circuit shown in Fig. (4.19) simply becomes a single loop in which V_{DC} charges C_o through R_2 . At the instant of diode switch-off, the voltage across C_o , V_{C_o} , is given by a solution of equation (4.18) at $t = t_1$. Then,

$$V_{\text{DC}} = i_2 R_2 + \frac{1}{C_o} \int_{t_1}^t i_2 dt + V_{C_o}(t_1). \quad (4.19)$$

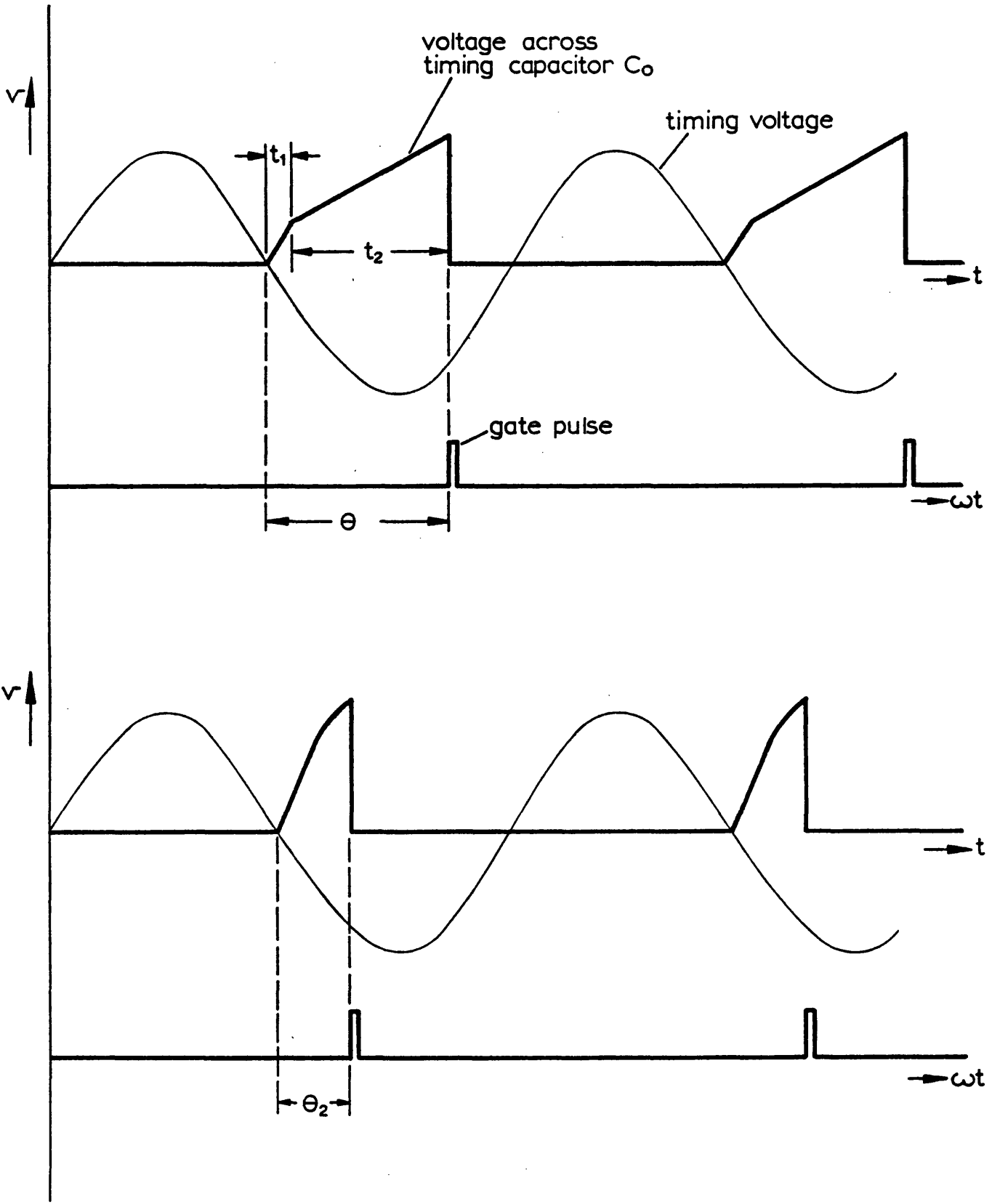


FIG. 4.20 TIMING OF FIRING PULSES.

Equation (4.17) has the solution,

$$i_2 = \frac{V_{DC} - V_{c_o}(t_1)}{R_2} e^{-(t-t_1)/C_o R_2}, \quad (4.20)$$

providing t_1 is small and $t \gg t_1$. This assumes that the initial charging time, t_1 , is within the linear charging range of C_o . The P.U.T. will conduct when V_{c_o} reaches the required peak value, V_p , where

$$V_{c_o}(t_2) = V_p = [V_{DC} - V_{c_o}(t_1)] (1 - e^{-t_2/C_o R_2}). \quad (4.21)$$

It can be seen from Fig. (4.19b) that the diode will switch off when $V_{c_o} = V_{ref}$ and hence from equation (4.18),

$$t_1 = \frac{R_1 R_2}{R_1 + R_2} C_o \ln \left[\frac{V_{ref} R_2 + V_{DC} R_1}{R_1 (V_{DC} - V_{ref})} \right], \quad (4.22)$$

and from equation (4.21)

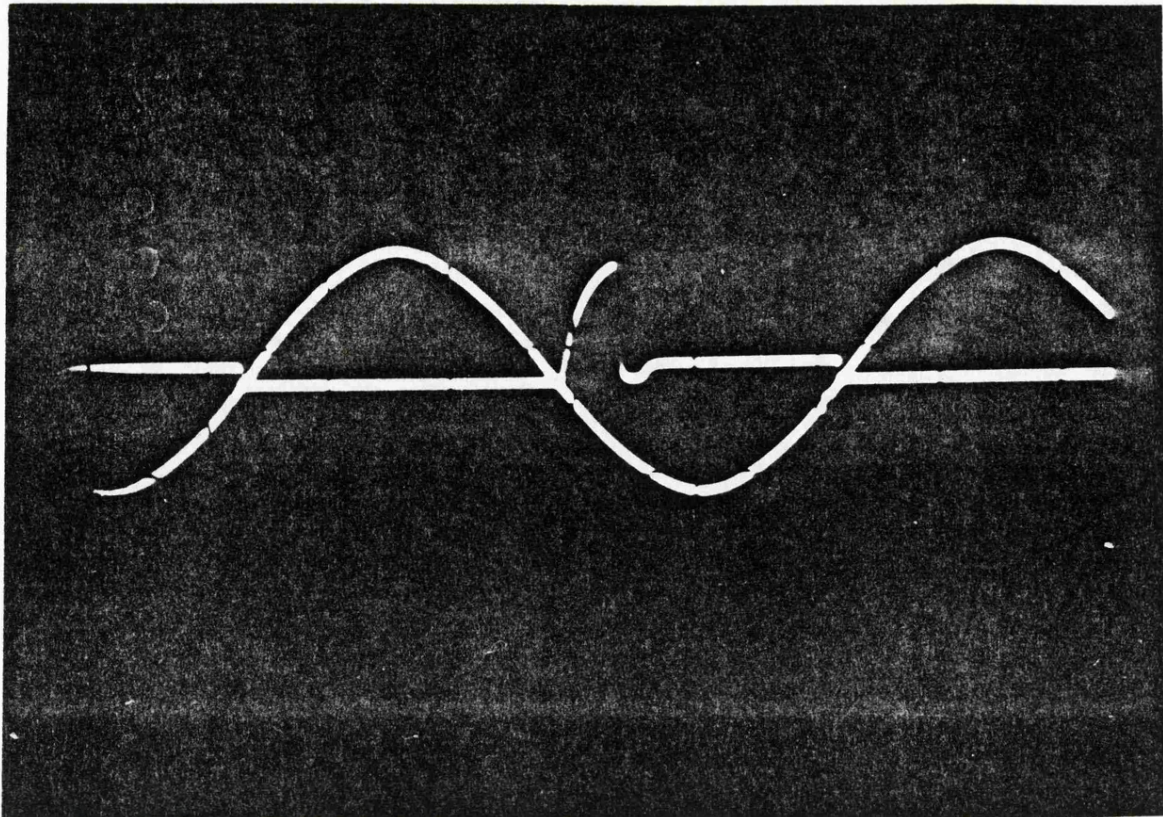
$$t_2 = R_2 C_o \ln \left[\frac{V_{DC} - V_{ref}}{V_{DC} - V_{ref} - V_p} \right]. \quad (4.23)$$

The firing angle, $\theta_1 = \alpha + \frac{\pi}{6}$, in a 3-phase input system, is then,

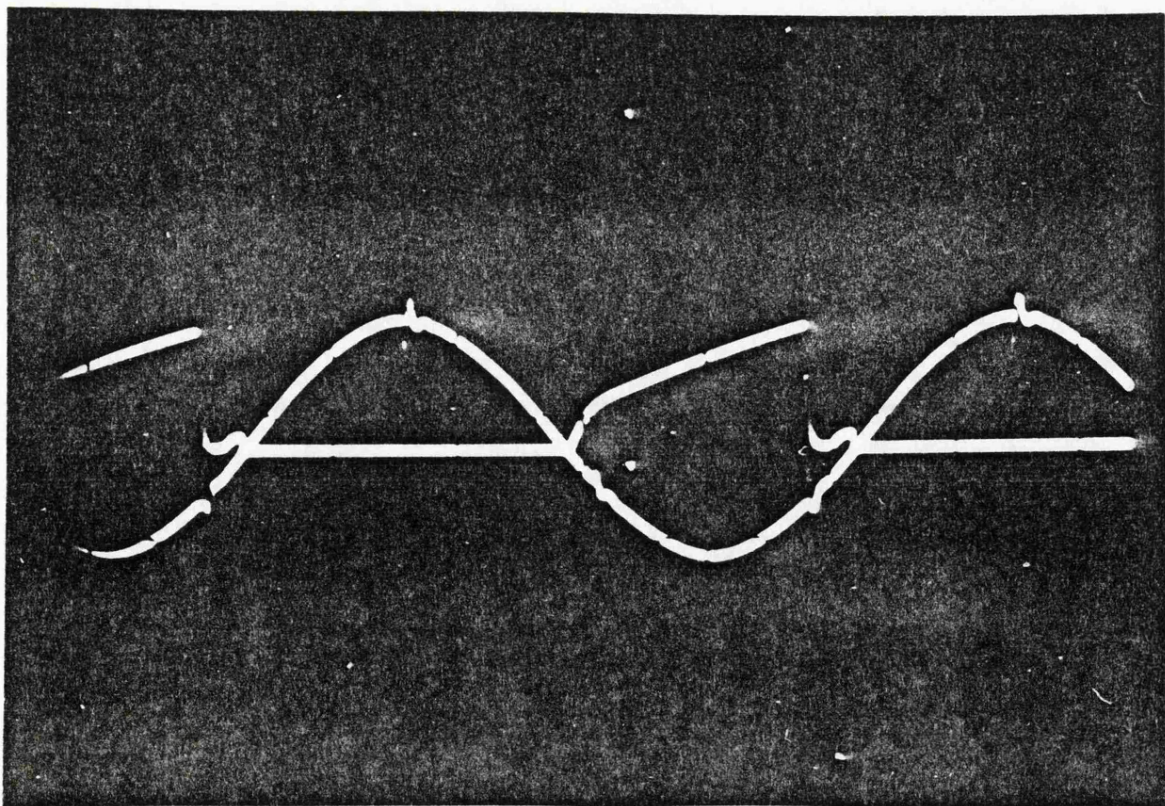
$$\theta_1 = \omega(t_1 + t_2) = \left(\frac{\omega R_1 R_2}{R_1 + R_2} \right) C_o \ln \left[\frac{V_{ref} R_2 + V_{DC} R_1}{R_1 (V_{DC} - V_{ref})} \right] + \omega R_2 C_o \ln \left[\frac{V_{DC} - V_{ref}}{V_{DC} - V_{ref} - V_p} \right] \quad (4.24)$$

Any increase in the value of V_{ref} delays the diode turn-off time causing most of the charging to occur at the initial faster rate.

V_{c_o} reaches the value of V_p sooner and the smaller firing angle shown in the lower diagram of Fig. (4.20) results. Fig. (4.21) shows the voltage across C_o obtained experimentally.



SYNCHRONISING VOLTAGE AND TIMING CAPACITOR VOLTAGE FIRING ANGLE $\theta_1=36^\circ$



SYNCHRONISING VOLTAGE AND TIMING CAPACITOR VOLTAGE FIRING ANGLE $\theta_1=156^\circ$

Fig. 4.21

The linearity of the pulse circuit was then investigated. Fig. (4.22a) compares the relationship between the firing angle and the reference voltage obtained experimentally with the computed results. The non-linearity is more pronounced at high firing angles due to the longer charging time of C_o . This non-linearity affects the cycloconverter as shown in Figs. (4.22b and c), reducing the regenerative half-cycle voltage amplitude to 0.85 x the rectified half-cycle peak.

An inspection of Figs. (4.3a and b) indicates that the cycloconverter will give zero net output under continuous circulating current conditions when the firing angle $\theta_1 = 120^\circ$. Under this condition equal amounts of power are transmitted from the source to the load (rectification) and retained from the source to the load (regeneration) and zero net output results. The pulse-boards need to be offset with a d.c. voltage to give the appropriate zero output. The reference voltage then modulates the gate signals 90° on either side of the quiescent condition for balanced operation. Ideally, the regeneration voltage envelope should correspond to the rectification voltage envelope. Due to the non-linearity of the pulse-boards, the regenerative peak is only 0.85 of the rectified peak as shown in Fig. (4.22b and c). Under these circumstances exact continuous circulating current operation would not occur and complete harmonic cancellation would not be achieved. This can be compensated for by reducing the positive reference signal amplitudes to 0.85 of the negative reference signal amplitudes. A further disadvantage compared with cosine-crossing timing is that a reduction of reference amplitude creates gaps between the positive and negative thyristor group voltage envelopes, thus preventing continuous circulating current operation over the whole output cycle. However, the adjustment of reference voltage amplitudes and the maintenance of a unit ratio of reference to timing voltage amplitude gave satisfactory

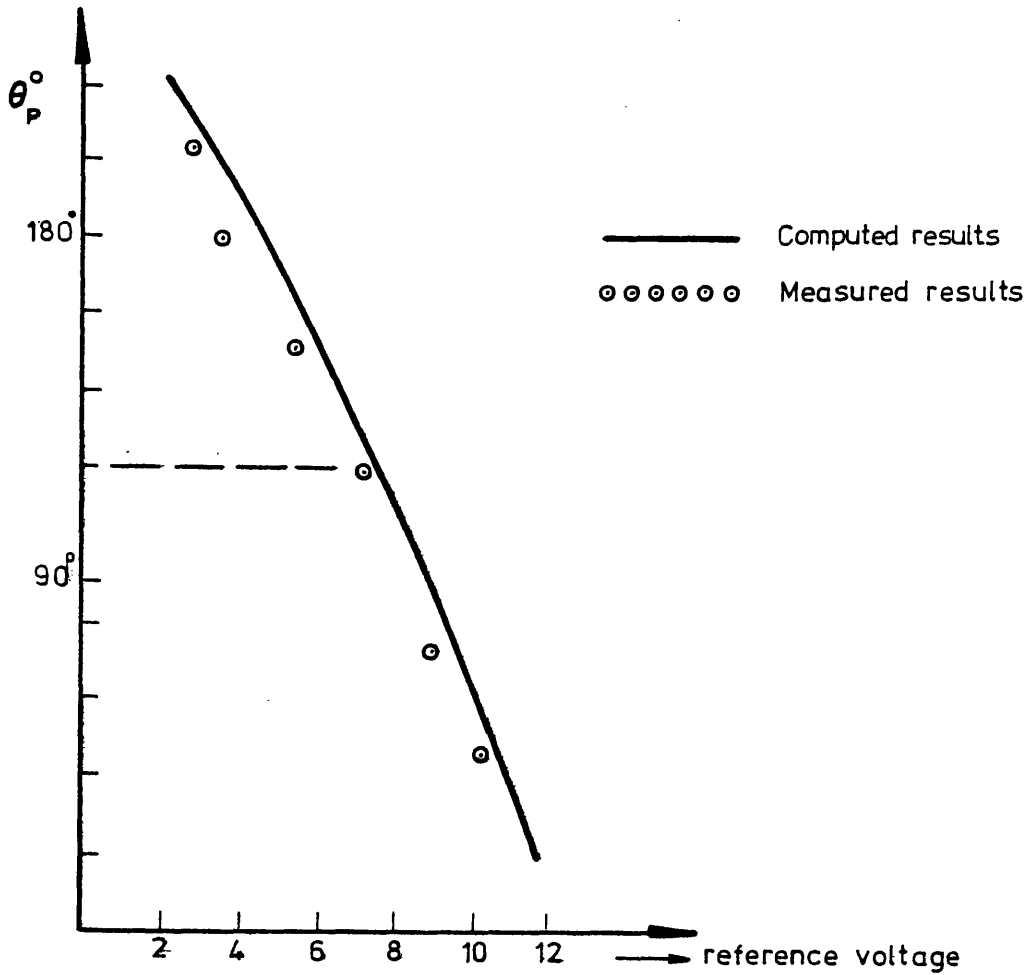


Fig.4.22a Firing circuits results.

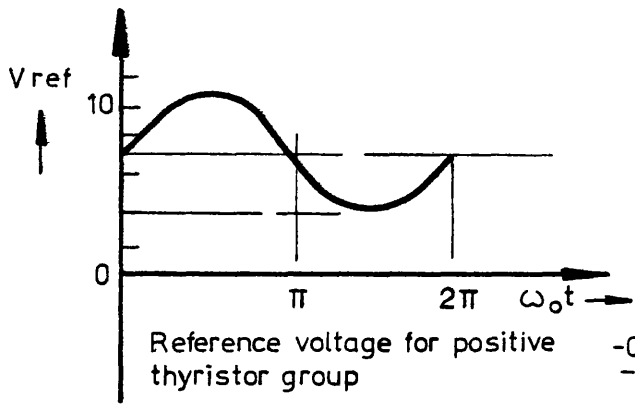


Fig. 4.22 (b)

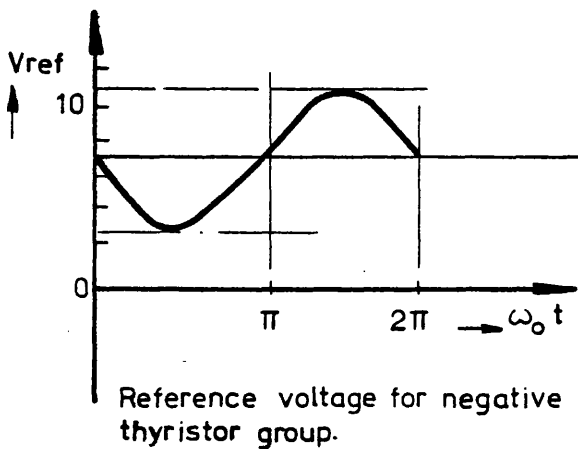
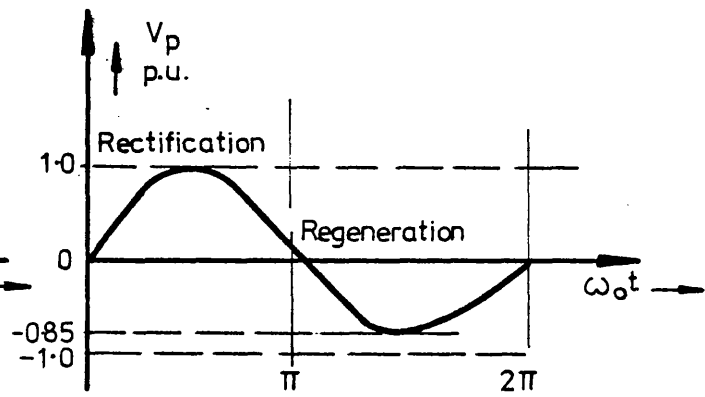
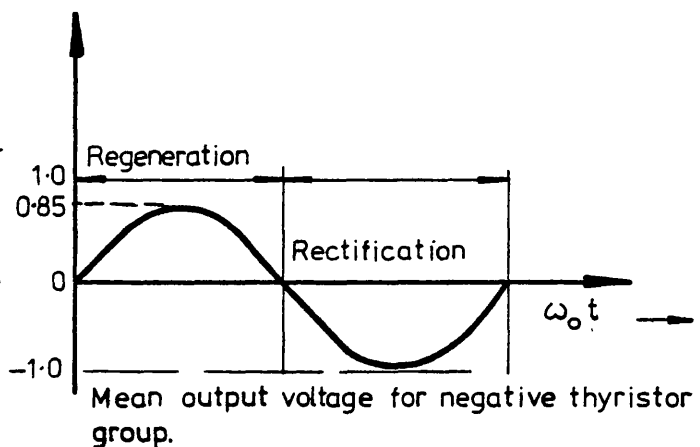


Fig.4.22 (c)



operation. Circulating current operation ceases when the current clamp operates because of reference amplitude reduction by the clamp amplifier. Normal operation is all within the range of the current limit and non-linearities caused by current clamping are removed.

4.10 Inter-group reactance

It has been shown that continuous circulating current operation gives a preferred output waveform and regulation. This operation, however requires an inter-group reactor capable of carrying the output load current. The precise value of the reactance is not critical as long as sufficient energy can be stored to maintain continuous current during the inversion or regeneration periods. However, the reactor also limits the circulating current to an acceptable value.

The largest volt-second difference between the positive and negative thyristor groups occurs when the firing angle $\alpha_p = \frac{\pi}{3}$. This volt-second difference, $\Delta\Psi$, is then,

$$\Delta\Psi = \int_0^{\pi/3} V_m \cos \omega t \cdot d \omega t - \int_{\pi/6}^{\pi/3} V_m \cos(\omega t - \frac{2\pi}{3}) \cdot d \omega t + \int_0^{\pi/6} V_m \cos(\omega t - \frac{2\pi}{3}) d \omega t , \quad (4.25)$$

as shown in Fig. (4.23). Thus,

$$\Delta\Psi = \frac{\sqrt{3} V_m}{2\omega} . \quad (4.26)$$

If the inter-group reactor has negligible resistance and an inductance $2L$, which is large compared with the supply input inductance,

$\Delta\Psi = 2LI_{cm}$, where I_{cm} is the maximum value of the circulating current.

Hence,

$$I_{cm} = \frac{\sqrt{3} V_m}{4\omega L} , \quad (4.27)$$

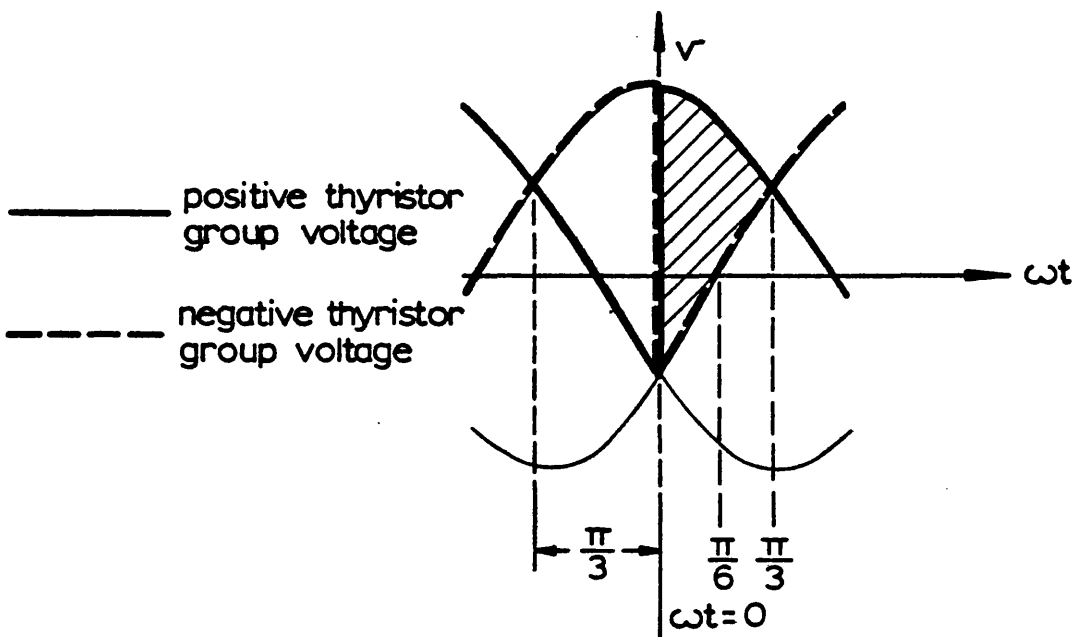


FIG.4.23 MAXIMUM VOLT-SECOND DIFFERENCE BETWEEN POSITIVE AND NEGATIVE THYRISTOR GROUP OUTPUTS IN 3-PHASE, HALF WAVE CYCLOCONVERTER

The value of the inductance L is not critical. However, the reactor must be sufficiently high to enable the stored energy of the peak circulating current, I_{cm} to be transferred from one thyristor group circuit to the other without excessive loss. The peak stored energy = $\frac{1}{2} I_{cm}^2 h$, and the required inductance, L , is seen to be a function of the maximum permissible circulating current. The conventional arrangement shown in Fig. (4.1), gives a d.c. polarised reactor and d.c. saturation must be avoided. Also only half of the reactor carries load current at any instant. This gives the useful feature that the inductance offered to the circulating current is four times that offered to the load current as shown in equation (4.25). The inter-group reactor acts as an inductive energy store maintaining continuous circulating current for the whole output range of the cycloconverter.

4.11 The use of a machine stator as a reactor in the cycloconverter induction motor drive

A static high Q centre-tapped reactor capable of handling both the energy oscillating between thyristor groups due to circulating current and the output load current will be costly and bulky. If the machine windings can be made to perform this function, a considerable saving of hardware will be made. This can easily be achieved in a double-layer stator if the layers are electrically separated. In the experimental system an experimental induction motor ⁽⁹⁾ was used with each layer of the stator winding connected as a conventional two-pole winding. The upper layer, star-connected, was connected between the positive thyristor groups and neutral, while the lower layer, identically wound was connected between the negative thyristor groups and neutral as shown in Fig. (4.24). In this way each phase of the system represents an electrically separate, magnetically coupled circuit. The winding acts as an impedance to circulating currents, while providing an alternating mmf as in a conventional machine.

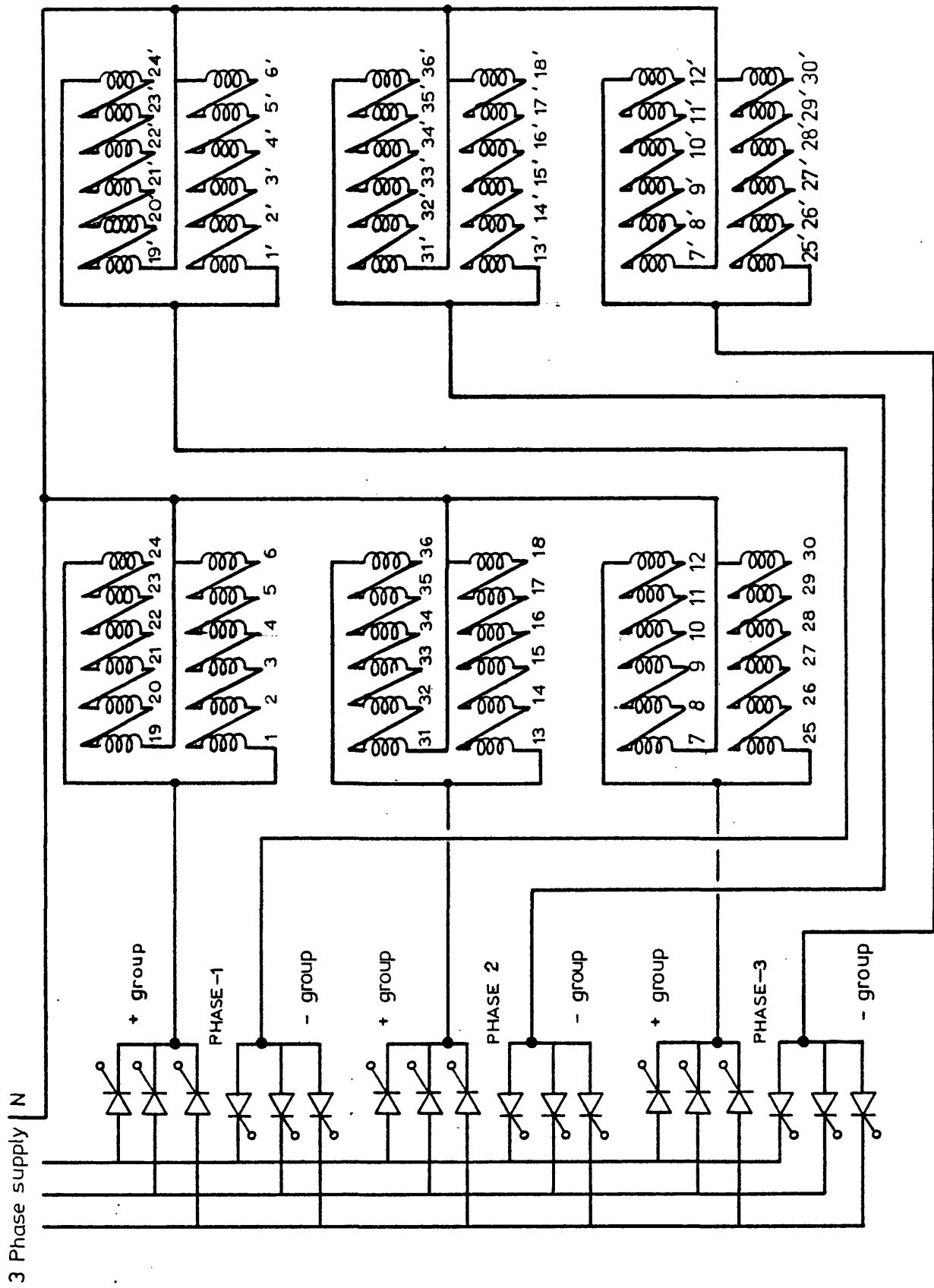


Fig. 4.24. 3-phase cycloconverter induction motor system with 2-pole divided stator winding (double layer).

Circulating-current operation may be considered if one phase of the system as shown in Fig. (4.25a) is represented by the equivalent circuit of Fig. (4.25b). Here each cycloconverter group is represented by a voltage generator in series with a diode. Continuous circulating current operation requires the simultaneous conduction of both diodes. The neutral point, N, is a zero-potential point and circulating current cannot be maintained on the principle of the inter-group reactor alone. However, it can be maintained by transformer action between the windings if the voltage envelope of the regenerative half-cycle exceeds the size of the rectification envelope. This can be achieved by attenuation of the reference voltage positive half-cycles. The instantaneous mutually induced emf's will exceed the generator emf's and continuous circulating current operation will be obtained.

The continuous current thyristor group voltages and output current and voltage have already been presented earlier in this chapter in Fig. (4.9). This shows that for a relatively small input to output frequency ratio of 6, i.e. with an output frequency of 66.6Hz for a 400Hz input, that a sinusoidal current profile results. Fig. (4.26) shows the motor stator search coil voltage of the divided winding machine at frequencies of 25, 15 and 10Hz.

4.12 Conclusions from Chapter 4

It has been shown that if the minimum output harmonic content is to be achieved in a cycloconverter, then the cycloconverter must operate with continuous circulating current. The inter-group reactor needed to maintain this continuous circulating current has been replaced by the stator of an induction motor. Two stator layers are wound identically

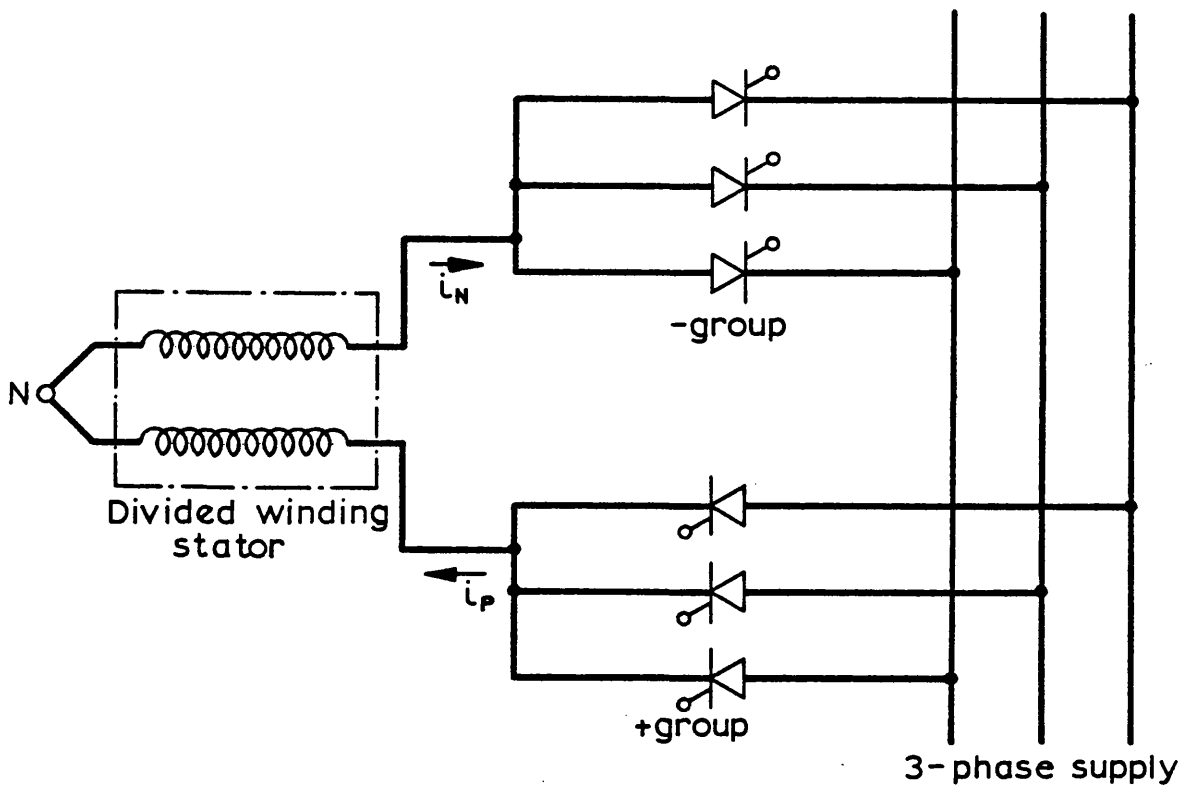


FIG.4.25a.CYCLOCONVERTER WITH SEPARATE WINDING LOAD

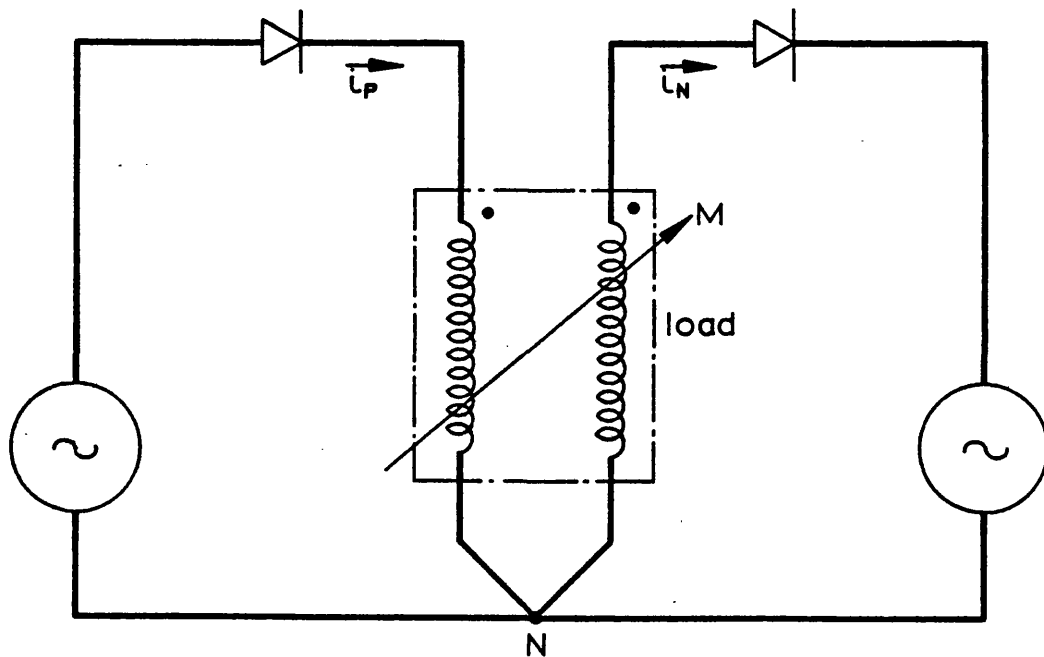


FIG.4.25bEQUIVALENT CIRCUIT OF CYCLOCONVERTER WITH SEPARATE WINDING LOAD

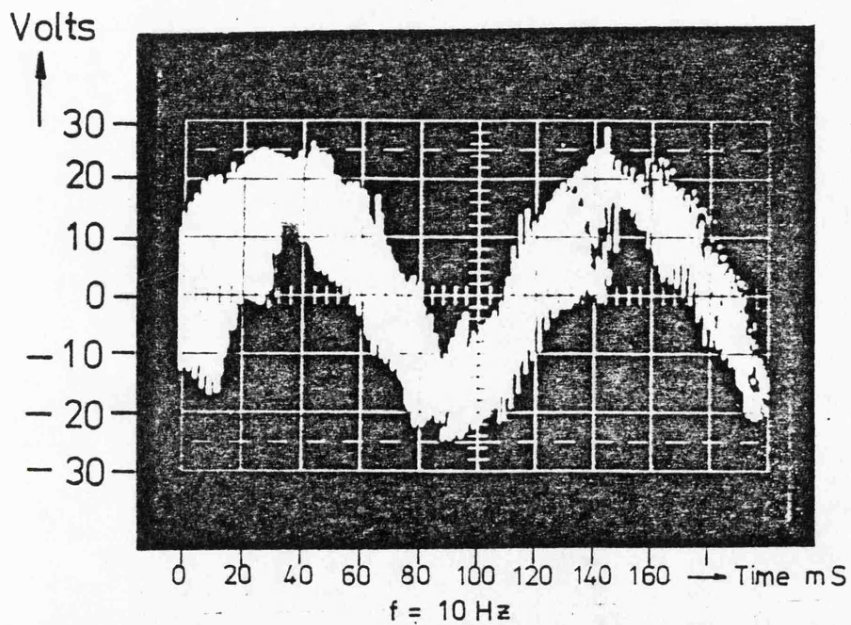
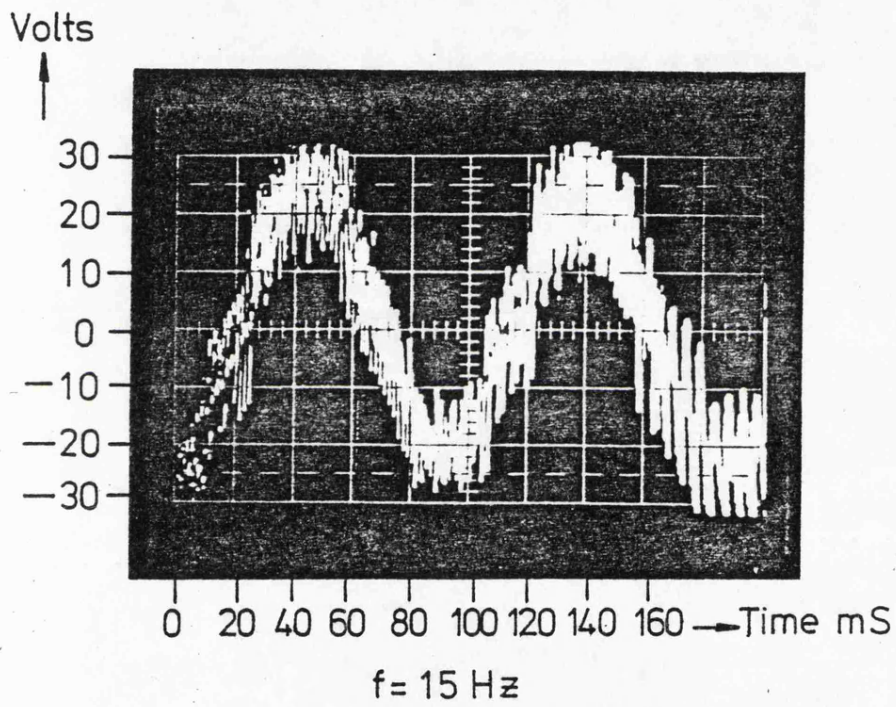
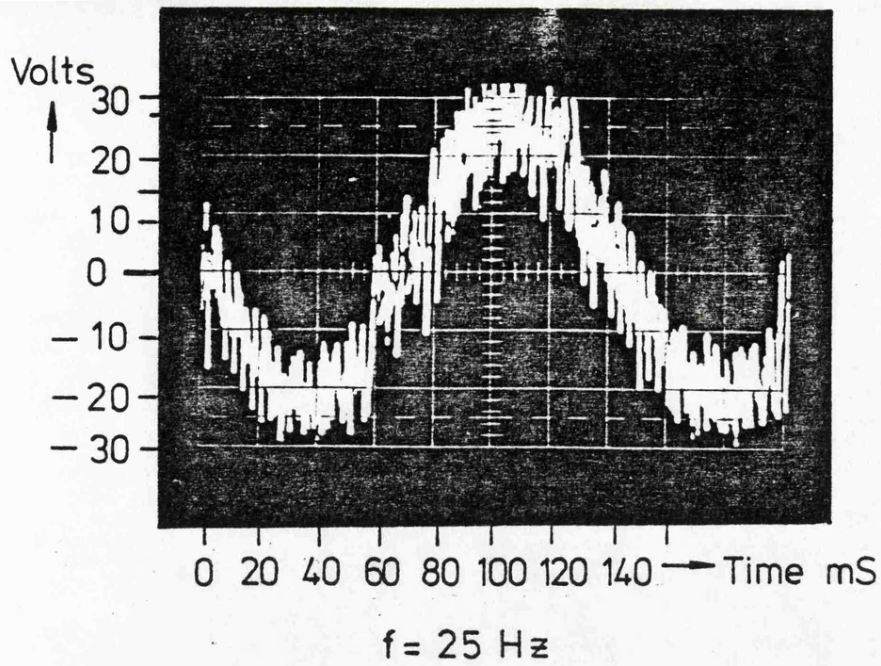


Fig. (4-26) Air gap voltage detected by search coil. (showing largest unsaturated operating condition)

as balanced 3-phase windings. They are magnetically coupled, but electrically separate. In this way, the inter-group reactor function is met, line to line short-circuit faults in the cycloconverter are prevented and the usual travelling field is set up in the machine air-gap.

An experimental system has been constructed to verify the proposal. Two electronic feedback servo-loops have been incorporated for speed control and current clamping. The behaviour and characteristics of the system can now be studied. This study is described in chapter 5.

CHAPTER 5Operation of the cycloconverter-induction motor-drive

	<u>Page No.</u>	
5.1	Introduction.	75
5.2	Single machine operation.	75
5.3	Multimachine operation.	76
5.4	Braking.	78
5.5	Variable-frequency regenerative braking.	79
5.5a	Peak torque requirements for braking.	82
5.5b	Induction generation.	84
5.5c	Reactive power requirements for induction generation.	85
5.6	Induction generation in the experimental system.	87
5.7	Small-signal perturbation model of the closed-loop system.	89
5.8	Cycloconverter-divided winding system response.	93
5.9	Conclusions from Chapter 5.	94

CHAPTER 5

Operation of the cycloconverter-induction motor drive

5.1 INTRODUCTION

It has been shown in Chapter 4 that the inter-group reactor needed to maintain continuous circulating current can be replaced by the stator of an induction motor. The experimental machine described in this work is supplied by a cycloconverter, the machine stator having its winding divided into two electrically separate, magnetically coupled circuits. To improve the overall utility of the system, standard induction motors have been connected, effectively in parallel with the divided winding machine rotor.

Possible application of a cycloconverter-induction motor drive includes crane or hoist drives, mine winders and lifts. For these operations electrical braking is an essential feature. An investigation has been carried out to determine the preferred form of braking for the system. The stability of the closed-loop system has been investigated using a small-signal perturbation model.

5.2 Single machine operation

The mode of operation using a divided-winding machine with electrically separate, magnetically coupled stator windings has been discussed in Chapter 4.

It can be seen that this operation increases the stator copper loss and reduces the overall system efficiency. This is because the stator resistance is effectively doubled, giving increased stator voltage regulation and a reduced air-gap flux. This can be compensated by increasing the cycloconverter output voltage in the feedback loop described in Chapter 4.

The steady-state operation of the divided-winding machine in the cycloconverter drive is simply the performance of a standard-winding machine

of the same frame size and rotor, but having twice the stator resistance. Equations (3.15) and (3.19) then enable the performance to be predicted if R_1 is written as $2R_1$. Figure (5.1) shows the single machine characteristics in open- and closed-loop operation over a frequency range, $3.76 < f_o < 8.75$ Hz. This shows that the machine operates throughout the load and speed range at any frequency within the range of the cycloconverter. Current clamping in the cycloconverter restricts the current at high slips and a slight fall in air-gap mmf of the divided-winding machine was observed.

Constant-speed operation under varying load conditions was obtained by a velocity feedback from the divided-winding machine to the cycloconverter reference generator giving the characteristics shown in Fig. (5.1). The increased speed to compensate for a load-dependent fall is produced by a simultaneous increase of stator volts and frequency.

5.3 Multimachine operation

Standard single-winding squirrel-cage induction motors may be additionally incorporated into the system as in a conventional cycloconverter drive. This motor was connected as shown in Fig. (5.2a). This, in effect, connects the standard machine in parallel with the divided-winding rotor. An equivalent-circuit representation for one phase is given in Fig. (5.2b).

In Fig. (5.2b), the magnetising reactance of the two machines is combined as a single term X_{oo} . The reactance parameters X_1 X_2 x_1 x_2 and X_{oo} are all frequency dependent, V_o is the cycloconverter fundamental output rms voltage and V_2 the effective air-gap voltage for both machines. Then if a rotor and magnetising admittance function is defined as,

$$Y(S_1, S_2) = \left[\frac{1}{\frac{R_2}{S_1} + jX_2} + \frac{1}{(r_1 + \frac{r_2}{S_2}) + jx_e} + \frac{1}{jX_{oo}} \right], \quad (5.1)$$

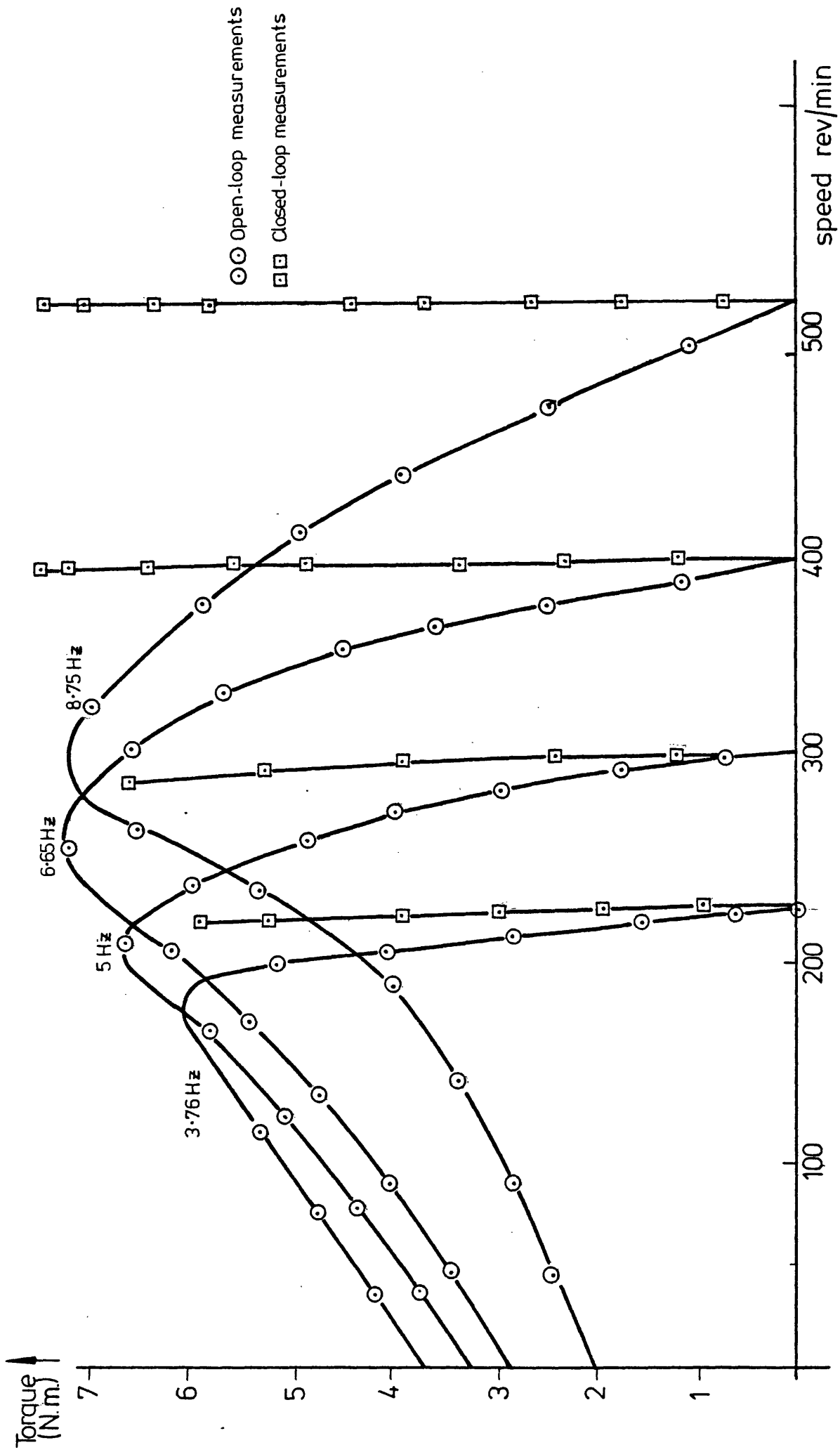


Fig. 5.1 Open and closed loop motoring characteristics divided winding machine.
Current clamp operating at 1.0 P.U. (6A)

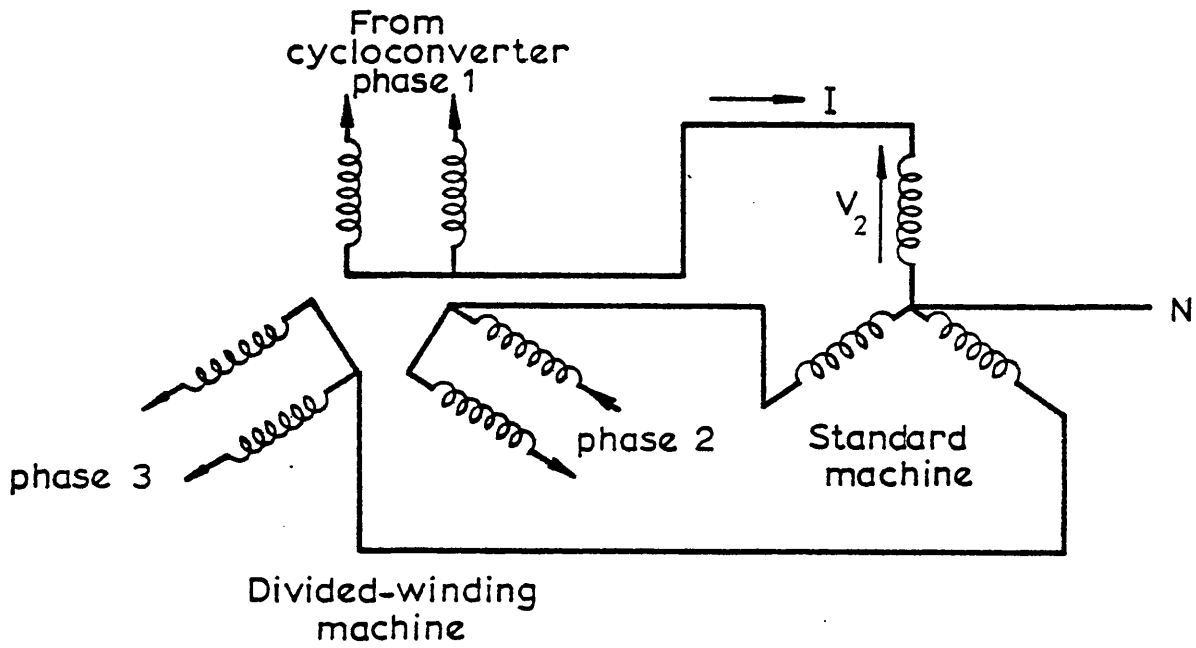


Fig.5-2a Machine schematic

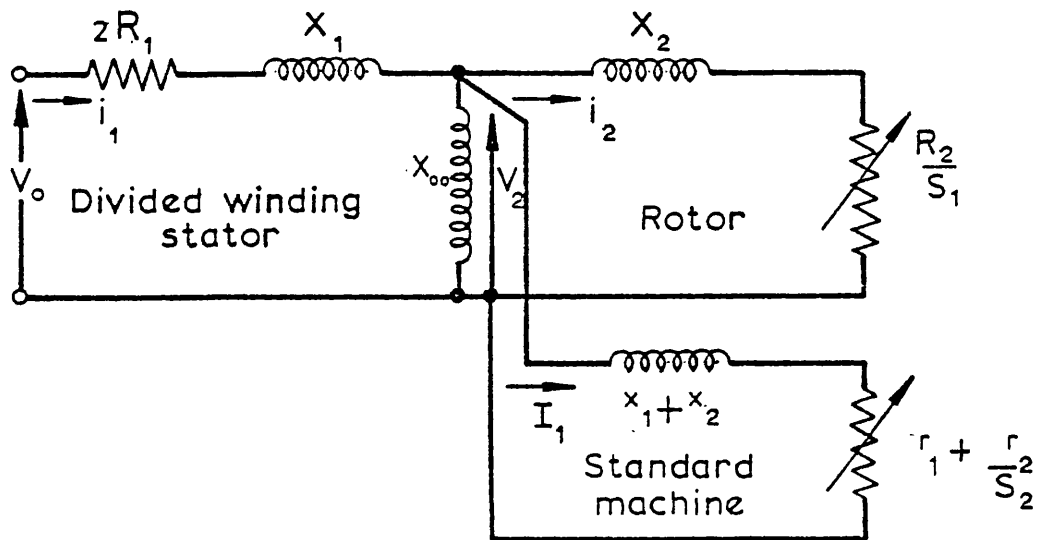


Fig.5-2b Equivalent circuit of machine combination

where $x_e = x_1 + x_2$, the system performance equations are,

$$i_1 = \frac{V_o Y(S_1, S_2)}{[1 + (2R_1 + jX_1) Y(S_1, S_2)]} , A. \quad (5.2)$$

$$V_2 = V_o - i_1(2R_1 + jX_1) , V. \quad (5.3)$$

$$i_2 = \frac{V_2}{\frac{R_2}{S_2} + jX_2} , A. \quad (5.4)$$

$$i = \frac{V_2}{(r_1 + \frac{r_2}{S_2}) + jx_e} , A. \quad (5.5)$$

$$T_{e1} = \frac{m|i_2|^2 \cdot R_2}{S_1\omega} , Nm , \quad (5.6)$$

and $T_{e2} = \frac{|i|^2 r_2}{S_2\omega} , Nm . \quad (5.7)$

Computed and experimental results for the two machine combination of Fig. (5.2a) are given in Figs. (5.3), (5.4) and (5.5a).

These results show that either or both of the machines can operate throughout the load and speed range at any frequency within the range of the cycloconverter. It can be seen that in a two machine system where the second machine has a standard connection, the loss of efficiency can be halved compared with the single divided-winding machine system. However, the loss of system efficiency is more than compensated by the use of a simple 3-thyristor group cycloconverter in the continuous circulating current mode.

The most satisfactory form of closed-loop control was achieved in the two-machine combination by velocity feedback from the divided-winding machine.

This machine was maintained at constant speed and the speed regulation of the standard machine which was effectively supplied by the

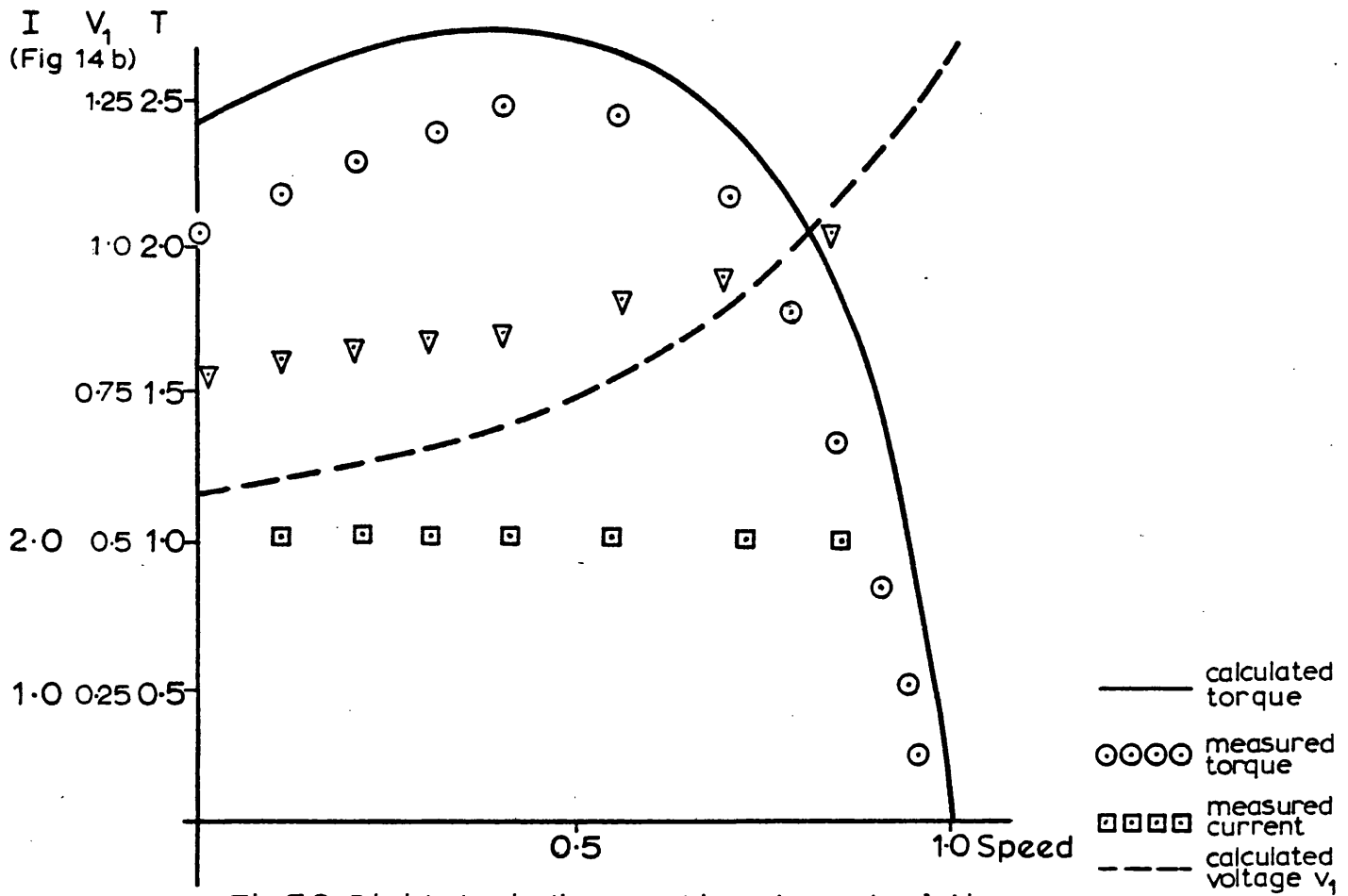


Fig.5.3 Divided winding machine characteristics,
std. machine running light.
Current unrestricted.

$f = 4.4$ Hz

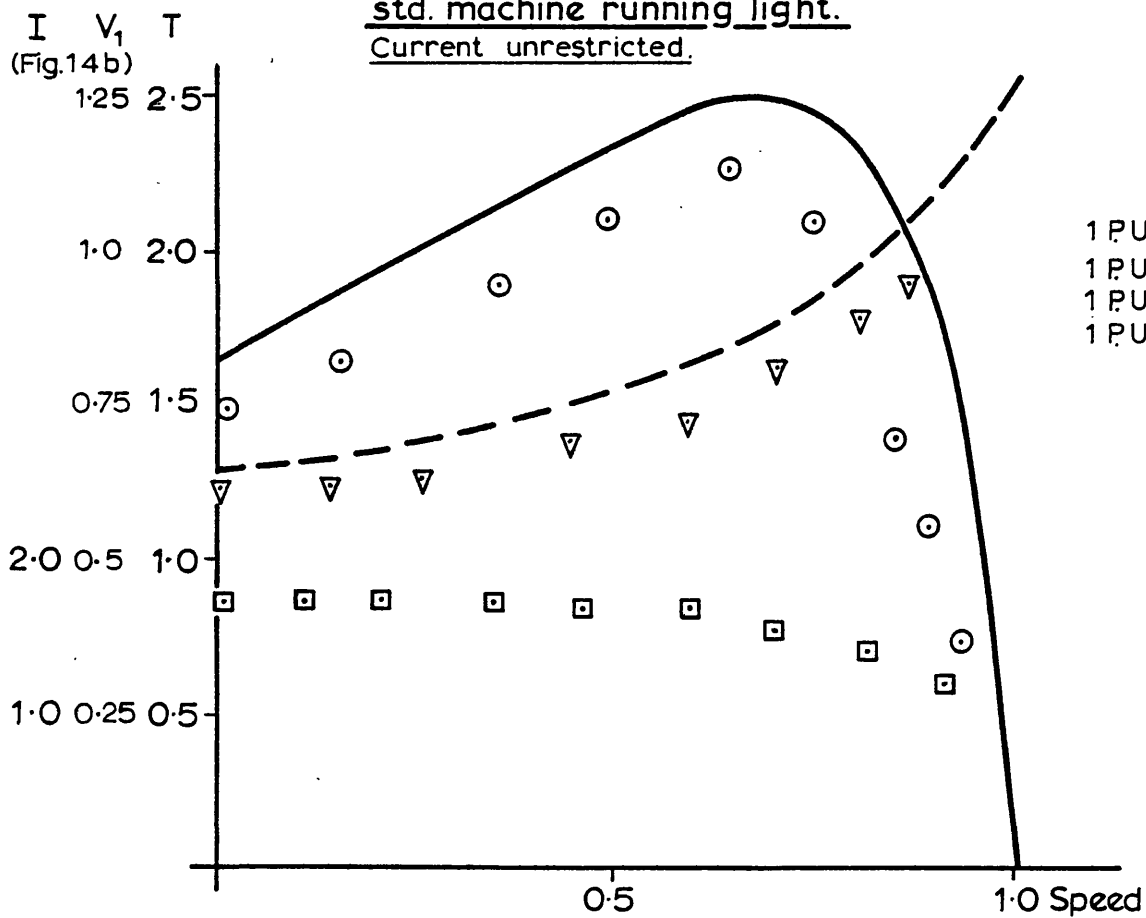


Fig.5.4 Standard machine characteristics divided
winding machine running light.
Current unrestricted.

divided-winding machine air-gap voltage was minimal as shown in Fig. (5.5b). Feedback control from the standard machine tended to overvolt the divided-winding machine causing saturation.

5.4 Braking

Increased operating speeds in transport systems and rotating drives which have duty cycles involving frequent acceleration and retardation impose severe restrictions on the braking system. To avoid the frequent replacement of brake shoes, mechanical braking should be only an emergency standby in case of power failure. It is preferable to bring the system rapidly to rest by an electrical means such as dynamic braking.

Dynamic braking implies that the kinetic energy of the machine is converted to electrical energy and dissipated as heat in the machine or its associated equipment. Braking in which the converted kinetic energy is returned to the supply is known as regenerative braking. One of the earliest forms of electrical braking used in induction motor drives is "plugging". Here a braking torque is produced by the reversal of the stator phase rotation. "Plug" braking necessitates the use of input line contactors. Unless the supply is then removed, the motor will run-up in the opposite direction. Plugging requires currents greater than the normal starting currents and stator voltage reduction may be necessary. In a cycloconverter drive, the current clamp incorporated to prevent excessive current damaging the devices restricts the plug braking torque ($\propto I^2$) to a low level. Plug braking can therefore be discounted in a cycloconverter drive.

D.c. dynamic braking ⁽³²⁾ is commonly used in induction motor drives for mine winders and winches. This method of braking effectively makes the machine operate as an alternator which dissipates the kinetic energy of the system in the rotor. D.c. dynamic braking of the induction machine is obtained by disconnecting the three-phase a.c. supply from the

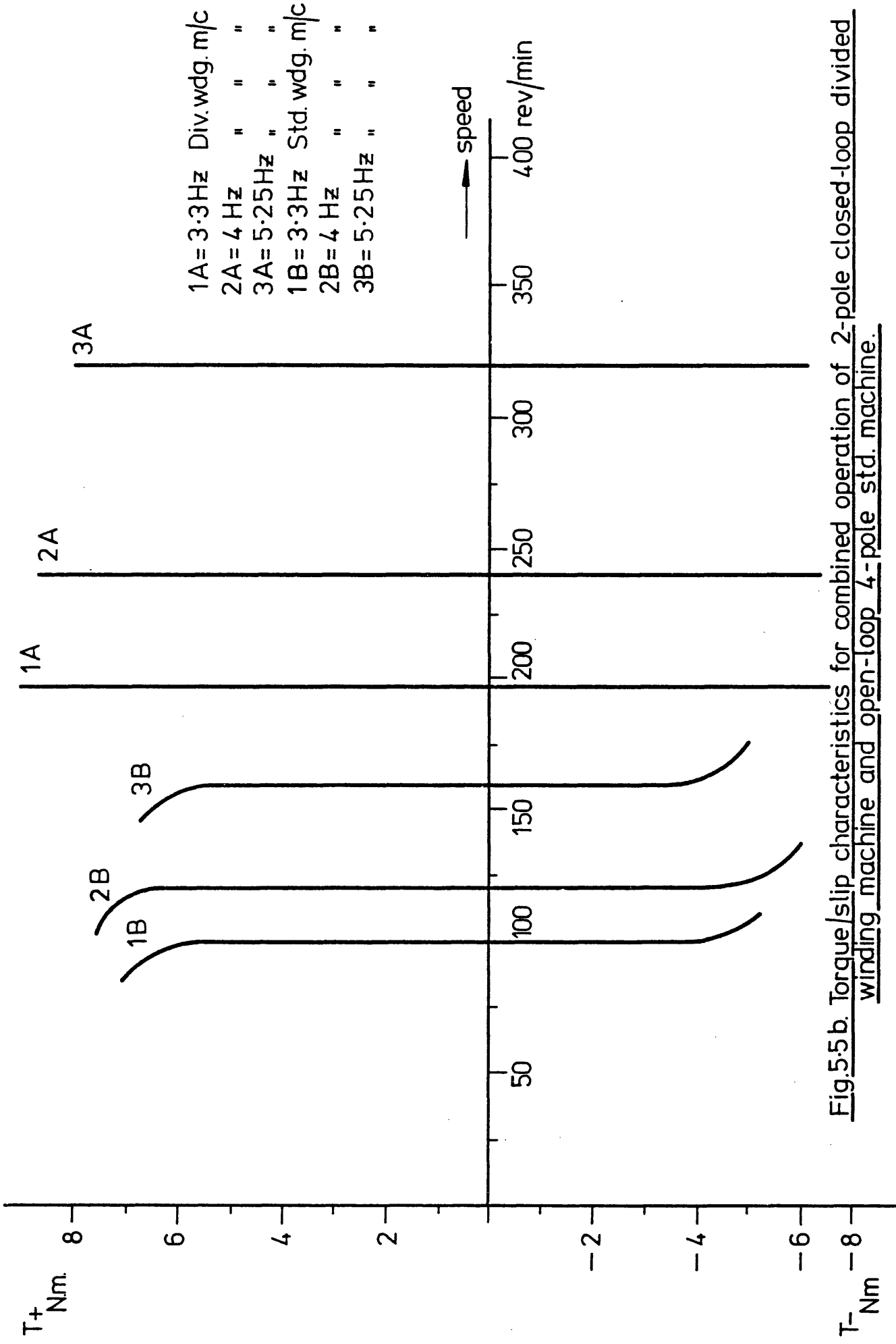


Fig 5.5 b. Torque/slip characteristics for combined operation of 2-pole closed-loop divided winding machine and open-loop 4-pole std. machine.

stator and replacing it by a d.c. supply as shown in Fig. 5.6a or, in the case of a cycloconverter, by suppressing half of the thyristor groups and driving the others into saturation. The d.c. current produces a stationary field in the air-gap, giving a synchronous speed of zero. The resulting induced voltages and currents caused by movement of the rotor dissipate the kinetic energy as heat in the rotor, and a braking torque is produced which retards the machine. The equivalent a.c. current to the d.c. input current I_D is $I_D/\sqrt{2}$ for the connection used.

In a squirrel-cage machine with a low rotor impedance, the peak braking torque obtained by d.c. dynamic braking will occur at very low speeds while the braking torque at high speeds will be small. This is shown in Fig.(5.6b) for two levels of constant current, the calculations being made from Harrison's torque equation given in reference (32). There are many methods. Two such methods are by increasing the rotor resistance and adding capacitance (33) in the rotor circuit. This is clearly impossible in a squirrel-cage machine and so d.c. dynamic braking is impractical for a cycloconverter-squirrel-cage, induction motor drive.

5.5 Variable-frequency regenerative braking

If the overall system efficiency is to be improved in a drive with frequent braking in its duty cycle, the kinetic energy of the machine must be converted to electrical energy and returned to the supply. This imposes two conditions on the system, induction generation in the rotating machine and reversibility in the cycloconverter. Also the stator frequency must be selected as a function of motor speed if peak torque braking is to be obtained at all speeds.

Fixed-low-frequency supersynchronous braking has been used for mine winders and hoists (34). The aim of this kind of braking system is to brake rapidly to a slow crawling speed and then to move slowly to the final, required position.

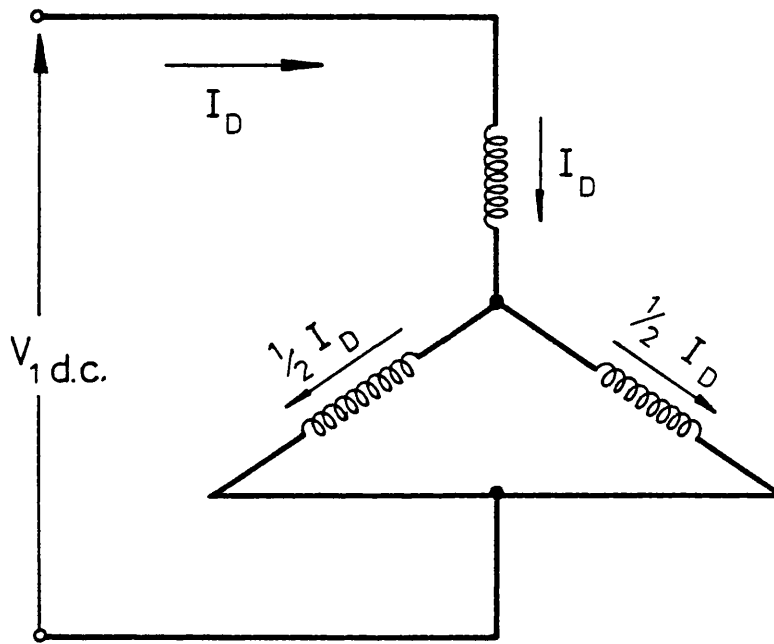


Fig. 5.6a. Stator connection for D.C. dynamic braking.

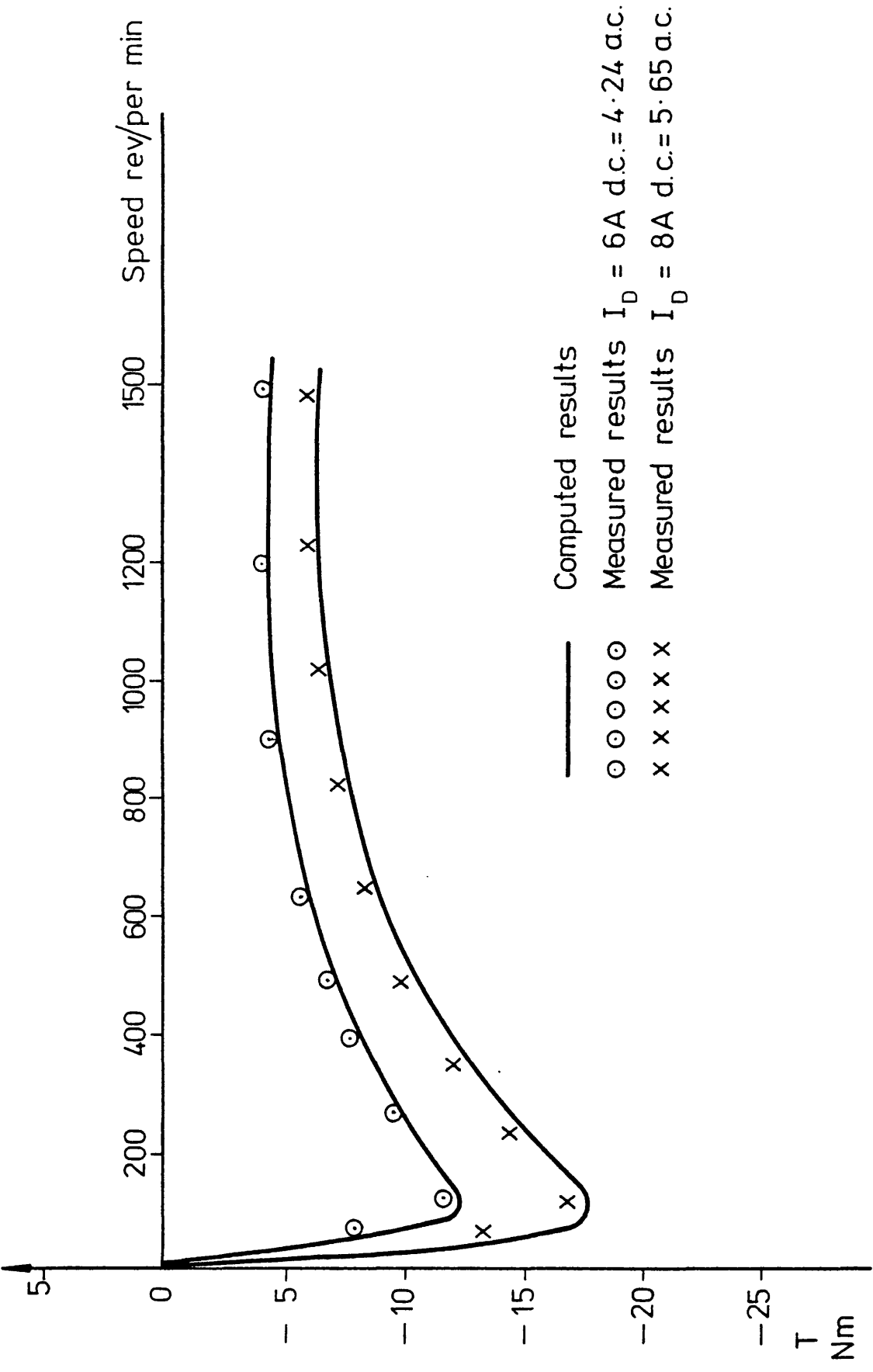


Fig. 5.6b Computed and measured d.c. dynamic braking results showing effect of variation of exciting current.

Low-frequency a.c. braking may, at certain speeds, be regenerative, and some of the kinetic energy of the rotor and the load may be returned to the supply. The range of speed over which regeneration is possible is now investigated.

If the equivalent circuit shown in Fig. (5.7) is considered, it can be seen that two operating conditions can be obtained for negative slip operation. The vector diagrams of these two conditions are shown in Figs. (5.8a) and (5.8b). In Fig. (5.8a), the phase angle between the stator voltage V_1 and the stator current I_1 is less than 90° . This condition is a dynamic braking condition where some energy is taken from the supply and the rotational energy of the motor is dissipated as heat in the rotor.

Fig. (5.8b), shows an input phase angle greater than 90° . The machine is now an induction generator and energy is now returned to the supply. Limits for each operating condition can be derived from the vector diagram of Fig. (5.8). Here a regenerative condition is defined when the input impedance has a negative real term. In terms of slip the regeneration region can be approximately defined by the slip limits, $0 > S > -\frac{R_2}{R_1}$. The system is non-regenerative when $S < \frac{R_2}{R_1}$.

In variable-frequency regenerative braking the amount of energy dissipated as heat and the amount returned to the supply depends on the relationship of the applied frequency to the motor speed. In order to recover a maximum amount of kinetic energy the stator frequency must then be varied to ensure that the motor is rotating just above synchronous speed at all points of its run-down.

A comparison of the energy dissipation in various forms of braking is useful for system evaluation.

The output power of the machine = $3I_2^2 \frac{R_2}{S} (1-S) = 2\pi nT$, where n is the rotor speed in rev/sec.

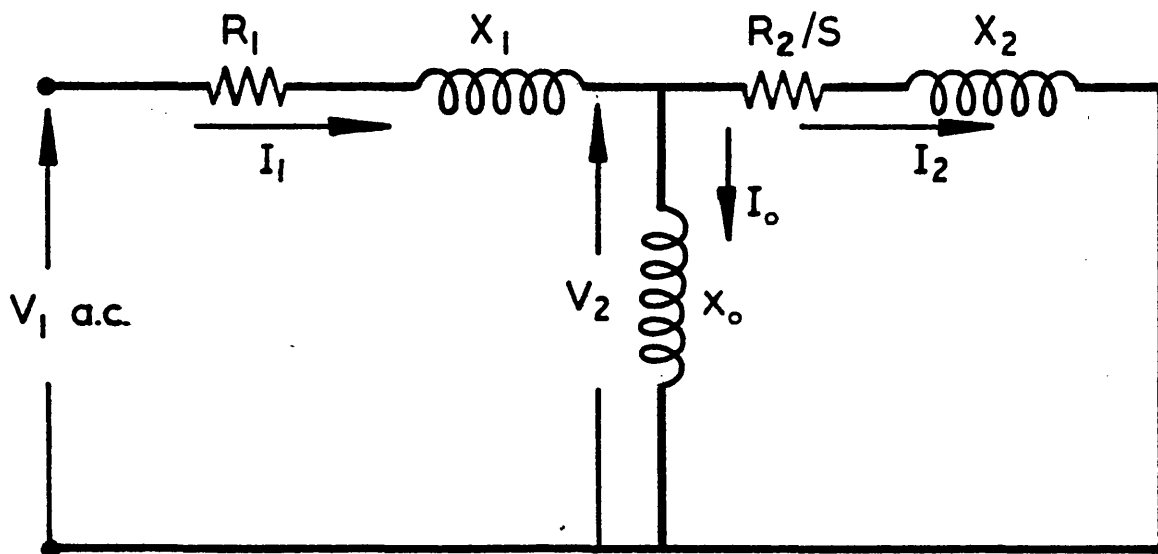


FIG.5.7 Equivalent circuit of a.c. low-frequency braking.

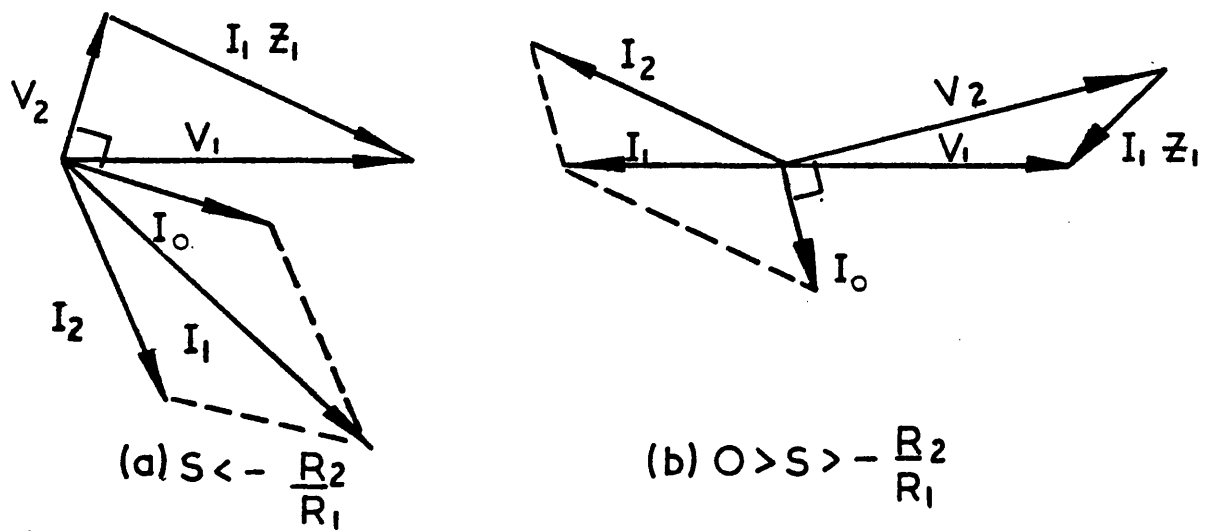


FIG.5.8 Induction motor vector diagrams

Let $U(t)$ = Energy dissipated as heat in rotor resistance in Joules,

U_{ω} = Kinetic energy of rotor at synchronous speed, and

J = Polar moment of inertia of load and rotor in Kgm.m^2 ,

then $\frac{dU(t)}{dt} = 3I_2^2 R_2$, and

$$2\pi nT = \frac{(1-S)}{S} \cdot \frac{dU(t)}{dt} \quad (5.8)$$

If the motor is running light or braking electrically,

$$T = J \frac{d\omega_2}{dt} = 2\pi J \frac{dn}{dt}, \quad \text{where } \omega_2 = 2\pi n, \text{ and}$$

$$\frac{dU(t)}{dt} = \frac{2\pi nS}{(1-S)} \cdot 2\pi J \frac{dn}{dt}.$$

$$dn = n_s dS \quad \text{where } n_s = \frac{\omega}{2\pi}, \text{ and so}$$

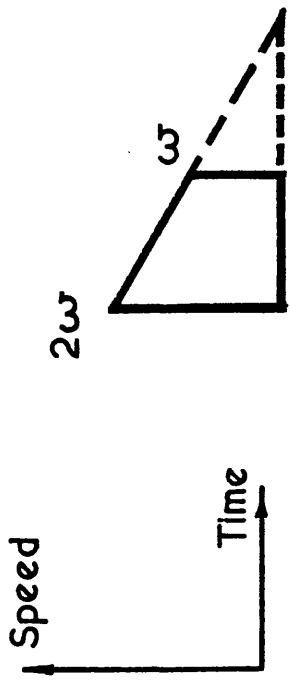
$$dU(t) = -(\omega)^2 \cdot J \cdot S dS, \quad \text{which gives the energy as}$$

$$U(t) = -\omega^2 J \int_{S_1}^{S_2} S \cdot dS = -\frac{J}{2} \omega^2 [S_2^2 - S_1^2] = -U_{\omega} [S_2^2 - S_1^2] \quad (5.9)$$

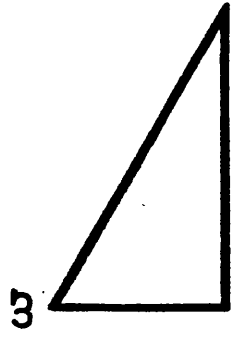
If the motor accelerates from standstill to full-speed (assumed to be synchronous speed for simplicity) on no-load, $S_1=1$ and $S_2=0$. By substitution in equation (5.9), the energy in the rotor, $U(t) = U_{\omega}$ Joules, i.e. the heat generated in the rotor circuit when running up light, is equal to the kinetic energy of the machine at synchronous speed. The rotor copper loss = $S \cdot (\text{rotor input})$ which tends to zero when the slip approaches zero.

To consider the energy returned to the supply in low-frequency a.c. braking a fixed frequency has been chosen. When this frequency has been fixed, the limits S_1 and S_2 may be put into equation (5.9). For example, if the frequency is 25Hz and the rotor is retarded from 3000 rev/min. to 1500 rev/min.,

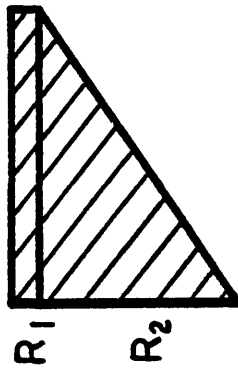
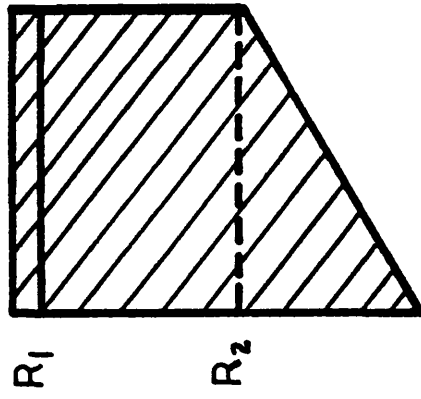
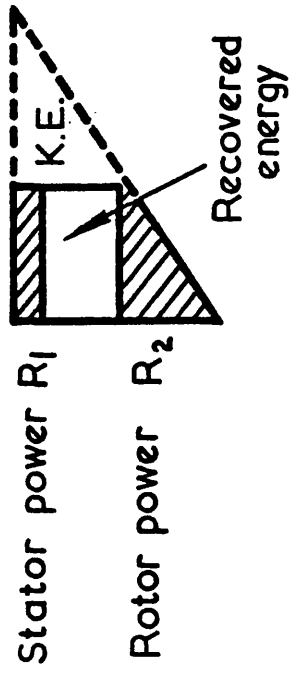
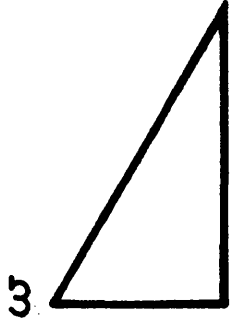
(a) Braking on A25 Hz Supply



(b) Plugging



(c) D.C. Braking



Power dissipated

FIG.5.9. Energy diagrams for braking.

for a 2-pole machine, then $S_1 = -1$, $S_2 = 0$ and the energy loss $U(t) = U_\omega$. The original speed of the machine was 2ω and hence its kinetic energy is $4U_\omega$. At ω the rotor still has U_ω Joules of kinetic energy and only U_ω Joules are dissipated as heat. Thus $(2U_\omega - \text{stator copper loss})$ Joules are returned to the supply. This is illustrated in Fig. (5.9a).

Figure (5.9b) shows the energy dissipated in order to bring the machine to rest by the method of "plugging", this is obtained from equation (5.9) by substituting $S_1 = 2$, $S_2 = 1$, which gives $U(t) = 3U_\omega$. Thus the energy wasted as heat in the rotor resistance is three times as big as the kinetic energy of the machine before braking and so this is a very wasteful method in which a lot of heat will be generated. Fig. (5.9c) shows the energy dissipated in d.c. dynamic braking. No power crosses the air-gap and the energy dissipated in the rotor is exactly equal to the kinetic energy of the machine. This analysis and the energy diagrams of Fig. (5.9) shows that controlled regenerative low-frequency a.c. braking is preferable to both "plugging" and d.c. dynamic braking, on energy consideration.

5.5a Peak torque requirements for braking

Fixed low-frequency braking has been used in the past to brake a slip-ring type induction motor, because of the possibility of controlling its rotor resistance by connecting external rotor resistance to increase the torque at large negative slips. In a squirrel-cage induction motor this is impossible. However, a relationship between frequency and speed related to peak torques can be derived as follows:

$$T_e = \frac{3V_1^2 R_2}{\left[\left(R_1 + \frac{R_2}{S} \right)^2 + (X_e)^2 \right] \omega S}, \quad \text{Nm} \quad (5.10)$$

Maximum torque occurs when $\frac{dT}{dS} = 0$ and this gives the relationship

$$S_{\max} = \pm \frac{R_2}{(R_1^2 + X_e^2)^{\frac{1}{2}}} \quad (5.11)$$

Since $S = 1 - \frac{nP}{f}$ and $X_e = 2\pi fL_e$, a relationship between speed and frequency for maximum torque can be derived as,

$$n = \frac{f}{P} \left[1 \pm \frac{R_2}{(R_1^2 + 4\pi^2 f^2 L_e^2)^{\frac{1}{2}}} \right] \quad (5.12)$$

For peak torque braking, the speed $n > \frac{f}{P}$ and so equation (5.12) becomes,

$$n = \frac{f}{P} \left[1 + \frac{R_2}{(R_1^2 + 4\pi^2 f^2 L_e^2)^{\frac{1}{2}}} \right] \quad (5.13)$$

Fig. (5.10) shows the change in the speed at which peak torque occurs on the experimental machine for open-loop, fixed-frequency operation with cycloconverter excitation. It can be seen from Fig. (5.10) that peak torque of the characteristics is not the same. This is due to stator voltage regulation described in section (2.3) at low-frequencies. To achieve a constant peak torque at all speeds, a closed-loop system was designed as shown in Chapter 4, where the stator frequency can be a controlled function of the regenerative peak speed. It can be seen from equation (5.13), that the relationship between speed and frequency for maximum regenerative braking torque is a quartic equation.

In the experimental system, a linearised approximation to the quartic equation was made as shown in Fig. (5.11). This approximation is also useful in obtaining near peak torque acceleration. The closed-loop experimental system would be also applicable to crane and winch applications where a potentially overhauling load needs to be maintained at constant speed. Fig. (5.12) shows motor and braking torques obtained at constant speeds. The relatively small braking peak torque is due to current clamping in the cyclo-

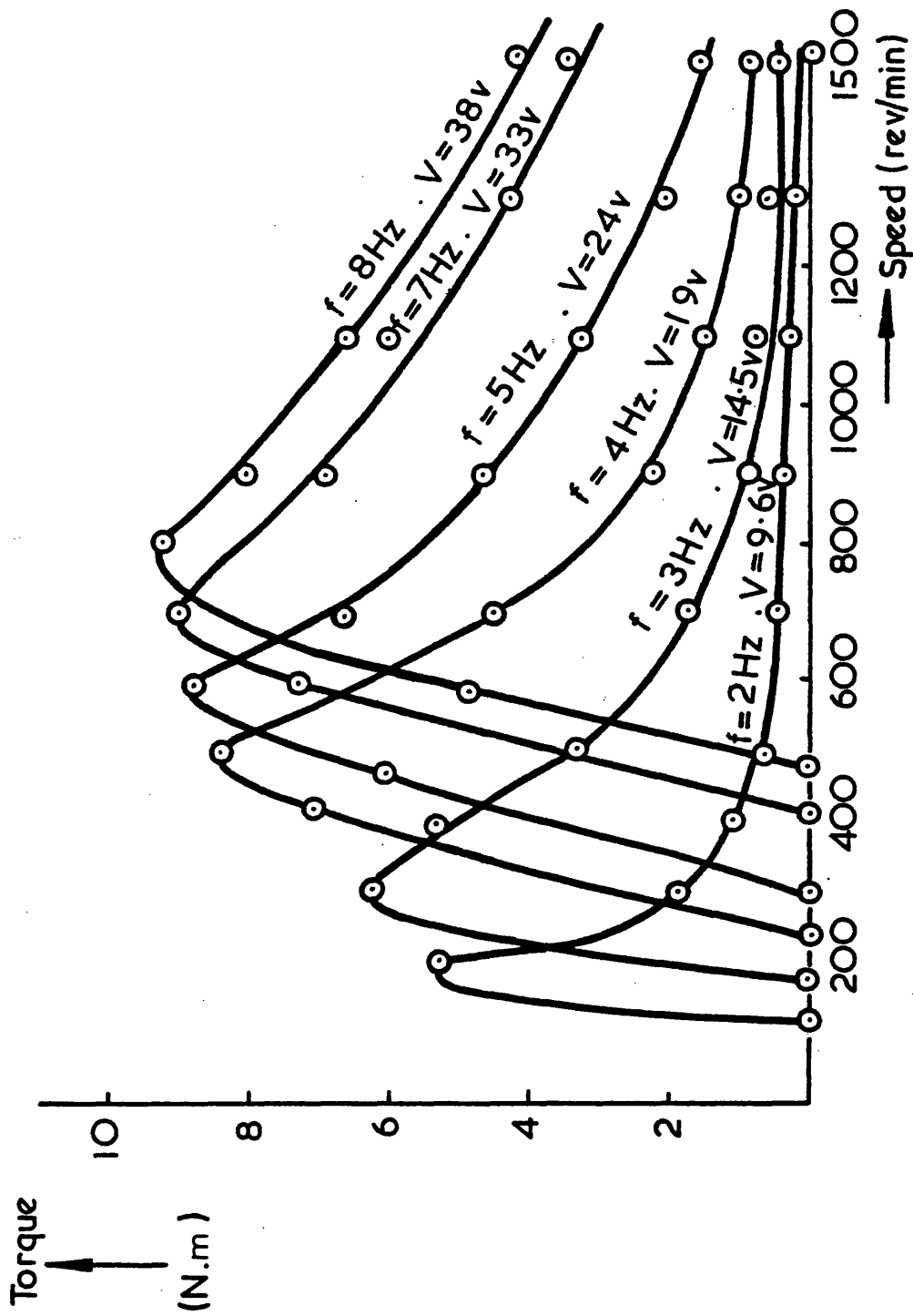


FIG.5.10 Family of measured torque-speed curves with different values of low frequency supply

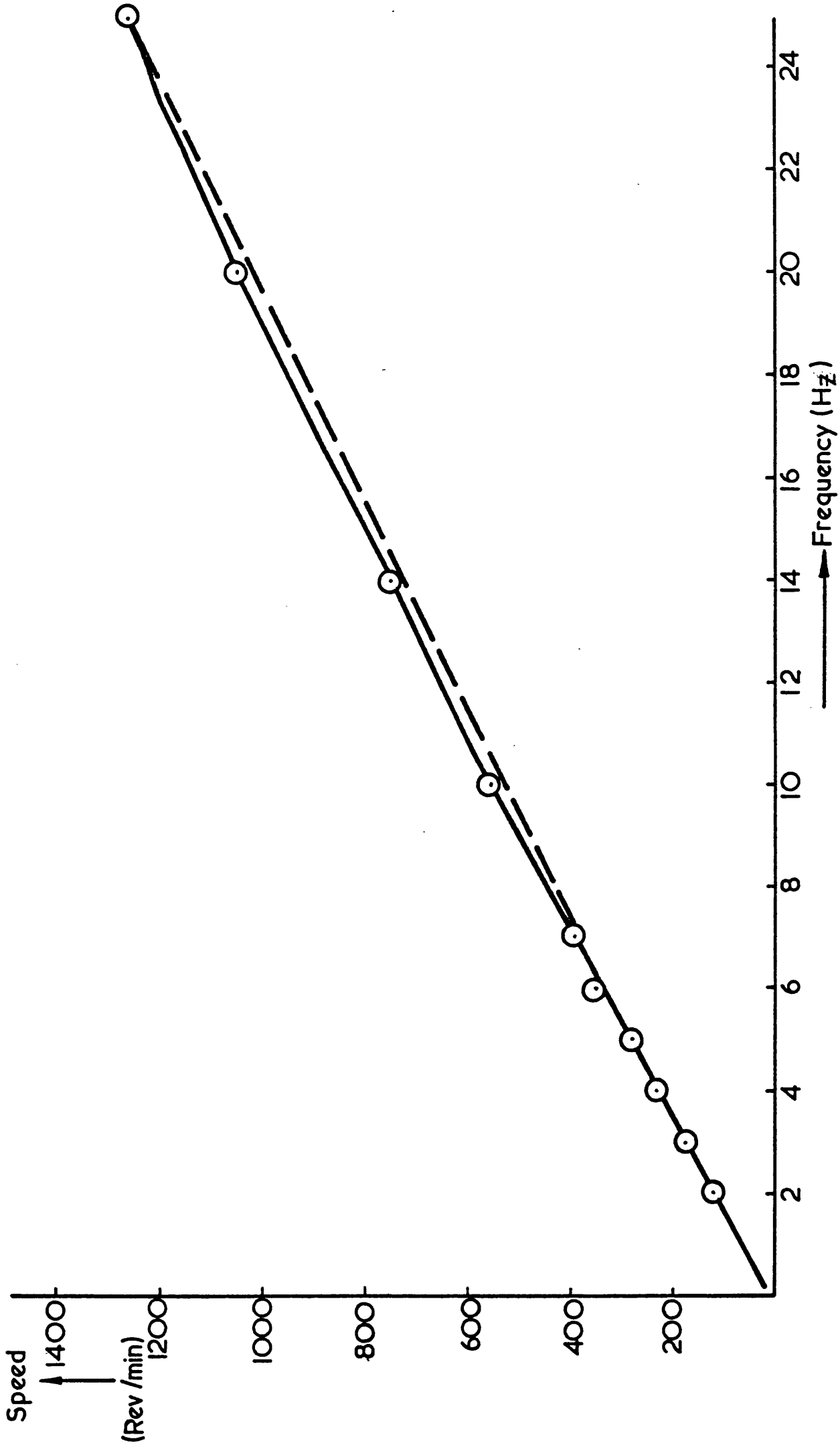


FIG.5.11 Calculated results of speed with variable low frequency supply. for peak braking torque.

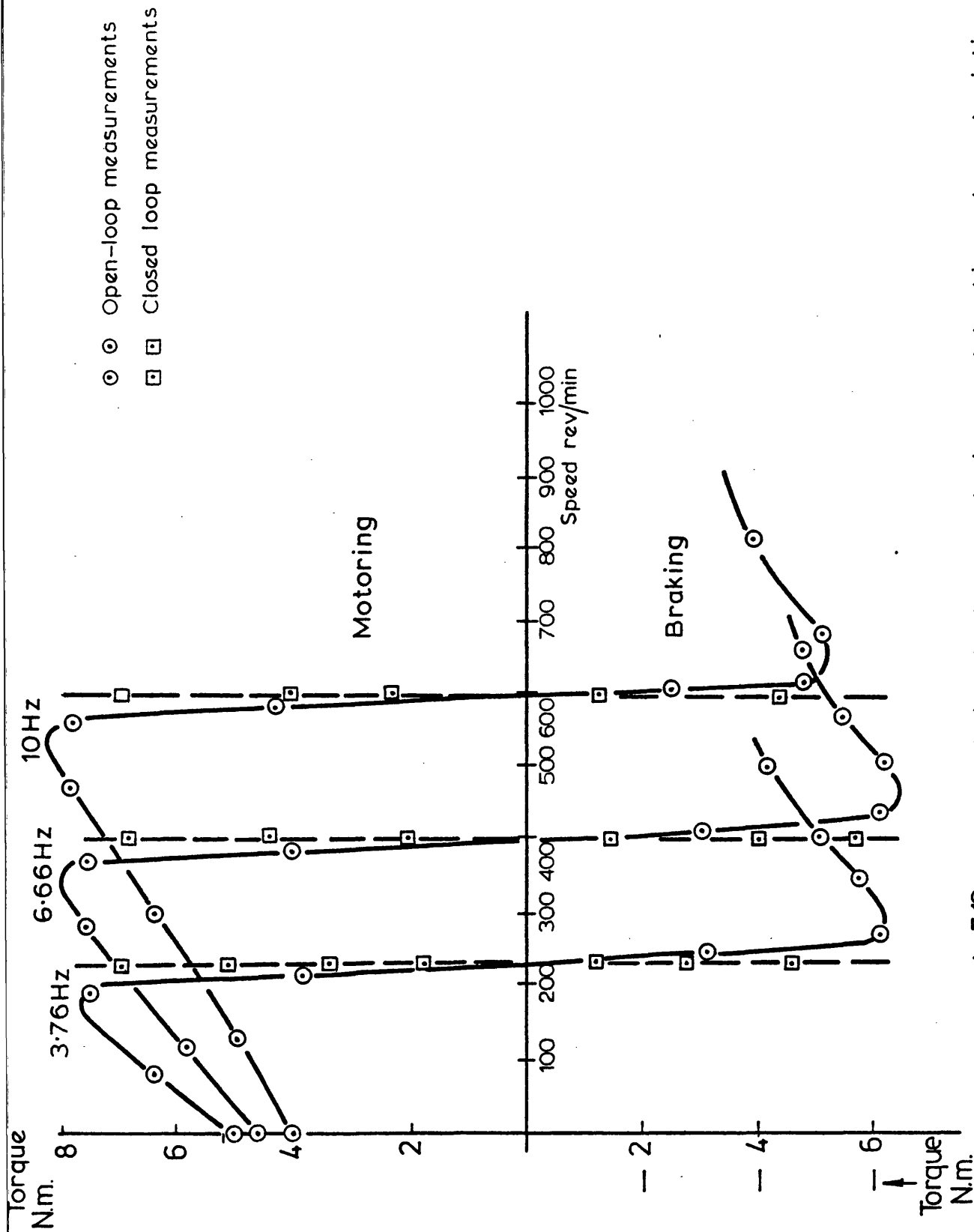


Fig. 5.12 Open and closed loop motoring and braking characteristics
divided winding machine

5.5b Induction generation

Any regenerative braking involves the operation of an induction machine as a generator ⁽³⁵⁾. The condition for induction generation is that the reactive power of the load (in this case the reactive power demanded from the mains to ensure generation) and the reactive power of the induction machine must be supplied externally ^{(36),(37)}. In past practice, capacitors have been connected to the generator terminals to provide reactive power, but the required amount of capacitance varies inversely with the supply frequency and so capacitive excitation has wide applications in aircraft systems at 400Hz, but little application at lower frequencies.

It is possible to self-excite an induction generator by a synchronous machine "floating" on the output terminals, but direct frequency control is not possible in this case, although voltage amplitude may be controlled by synchronous machine excitation control. If the induction generator output frequency is to be controlled, the excitation source must be controllable in voltage amplitude and frequency. This can be achieved by an externally driven variable-speed synchronous machine with variable excitation, but it is hardly an economic solution. The ideal excitation source is a variable-frequency generator of controllable amplitude in which the exciter current leads the voltage by 90° at all frequencies.

An investigation was carried out to determine the cycloconverter output requirements necessary to meet the reactive power demand in induction generation and braking. The possibility of exciting an externally driven induction generator by a cycloconverter as a means of low frequency power generation was also investigated and early hopes were found to be unrealisable. It has been shown in section (5.5) that induction generation can only occur in a limited slip range when the stator current is more than 90° out of phase with the appropriate stator phase voltage. If the iron loss component is neglected, an approximation of increasing validity as the applied frequency falls, it can be shown that the slip range over which generation can occur

is defined by $0 > S > -\frac{R_2}{R_1}$.

The appropriate phasor diagram is shown in Fig. (5.8b). If the slip is decreased, generation ceases and the mechanical energy applied to the machine is dissipated within the machine. Fig. (5.8a) illustrates this condition. If the slip is defined as a function of speed and frequency by,

$$S = 1 - \frac{nP}{f} , \quad (5.14)$$

the maximum attainable operating ranges may be stated as follows using the previously defined approximate slip limits,

$$\frac{nPR_1}{R_1 + R_2} < f < nP , \quad (5.15)$$

for constant speed, n , and,

$$\frac{f}{P} < n < \frac{f}{P} \frac{(R_1 + R_2)}{R_1} , \quad (5.16)$$

for constant frequency, f .

The possible operating range of speed will fall with frequency. It may be extended at the expense of efficiency if a high resistance rotor is used. Equations (5.15) and (5.16) only define possible operating ranges. If a practical system is to be implemented it is necessary to investigate the variation of the reactive power requirement over the possible operating range.

5.5c Reactive power requirements for induction generation

From a consideration of Fig. (5.7), the generator impedance,

$Z_g = R_g + jX_g$ may be expressed as,

$$Z_g = - (R_1 + jX_1) - \left(\frac{R_2}{S} + jX_2 \right) \parallel jX_o \left| \frac{R_2}{S} + j(X_2 + X_o) . \quad (5.17)$$

If $\frac{(jX_0)^2}{2j(X_2 + X_0)}$ is added to the first term and subtracted from the

second term in equation (5.17), after simplification,

$$Z_g = -R_1 - j \left[(X_1 + X_0) - \frac{X_0^2}{2(X_2 + X_0)} \right] - \frac{(jX_0)^2}{2j(X_0 + X_2)} \left[\frac{R_2/S j(X_2 + X_0)}{R_2/S j(X_2 + X_0)} \right]. \quad (5.18)$$

Z_g can be expressed as $R_g + X_g$ and $X_1 + \frac{X_0 X_2}{X_2 + X_0}$ as X_3 and equation (5.18)

simplified to give

$$R_g + R_1 + j \left(X_g + \frac{X_1 + X_0 + X_3}{2} \right) = -j(X_0 + X_1 - X_3) \left[\frac{R_2/S^{-j}(X_2 + X_0)}{R_2/S^{+j}(X_2 + X_0)} \right]. \quad (5.19)$$

Rationalising equation (5.19), evaluating the magnitudes and combining terms results in the equation of a circle,

$$(R_g + R_1)^2 + (X_g + X_1 + X_0)(X_g + X_3) = 0 \quad (5.20)$$

If the real and reactive powers of the induction generator are expressed as P_g and Q_g respectively,

$$P_g + jQ_g = \frac{V_1^2}{R_g - jX_g} \quad (5.21)$$

The combination of equations (5.20) and (5.21) (see Appendix 3) show that the locus of power and var outputs of an induction generator is defined as a circle with centre coordinates, $-V_1^2 \frac{R_1}{R_1^2 + (X_0 + X_0) X_3}$;

$$-V_1^2 \frac{[X_0 + X_1 + X_3]}{2[R_1^2 + (X_0 + X_1) X_3]} \quad \text{and a radius} \quad \frac{V_1^2 [X_0 + X_1 - X_3]}{2[R_1^2 + (X_0 + X_1) X_3]} .$$

Figure (5.13a) shows the reactive power requirement for power generation at a constant frequency of 50Hz at various voltages, while Fig. (5.13b) illustrates the requirement for a range of fixed frequencies. The calculations have been made using the parameters of the experimental machine given in Appendix (1). In each case the upper intersection of the circle and the

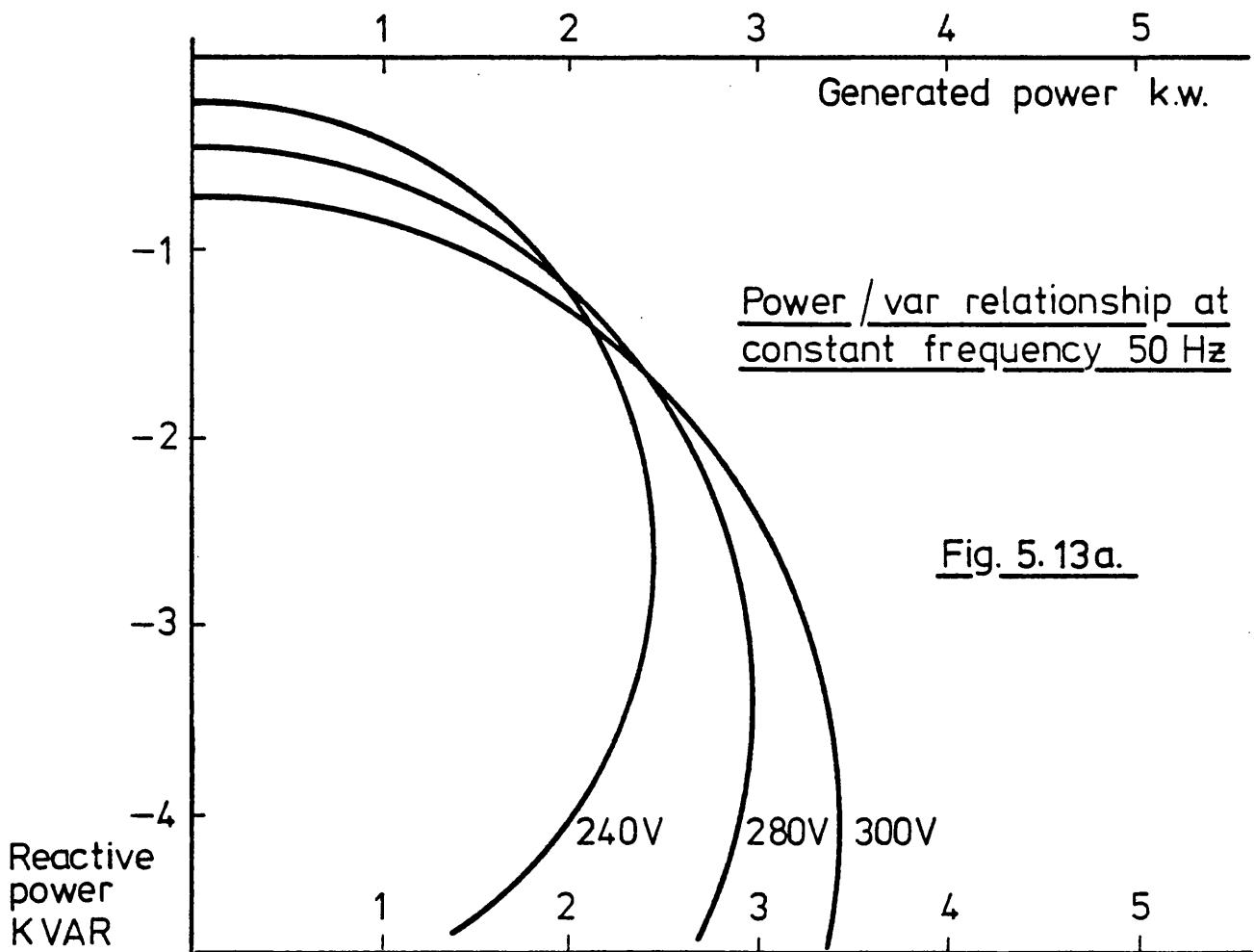


Fig. 5.13a.

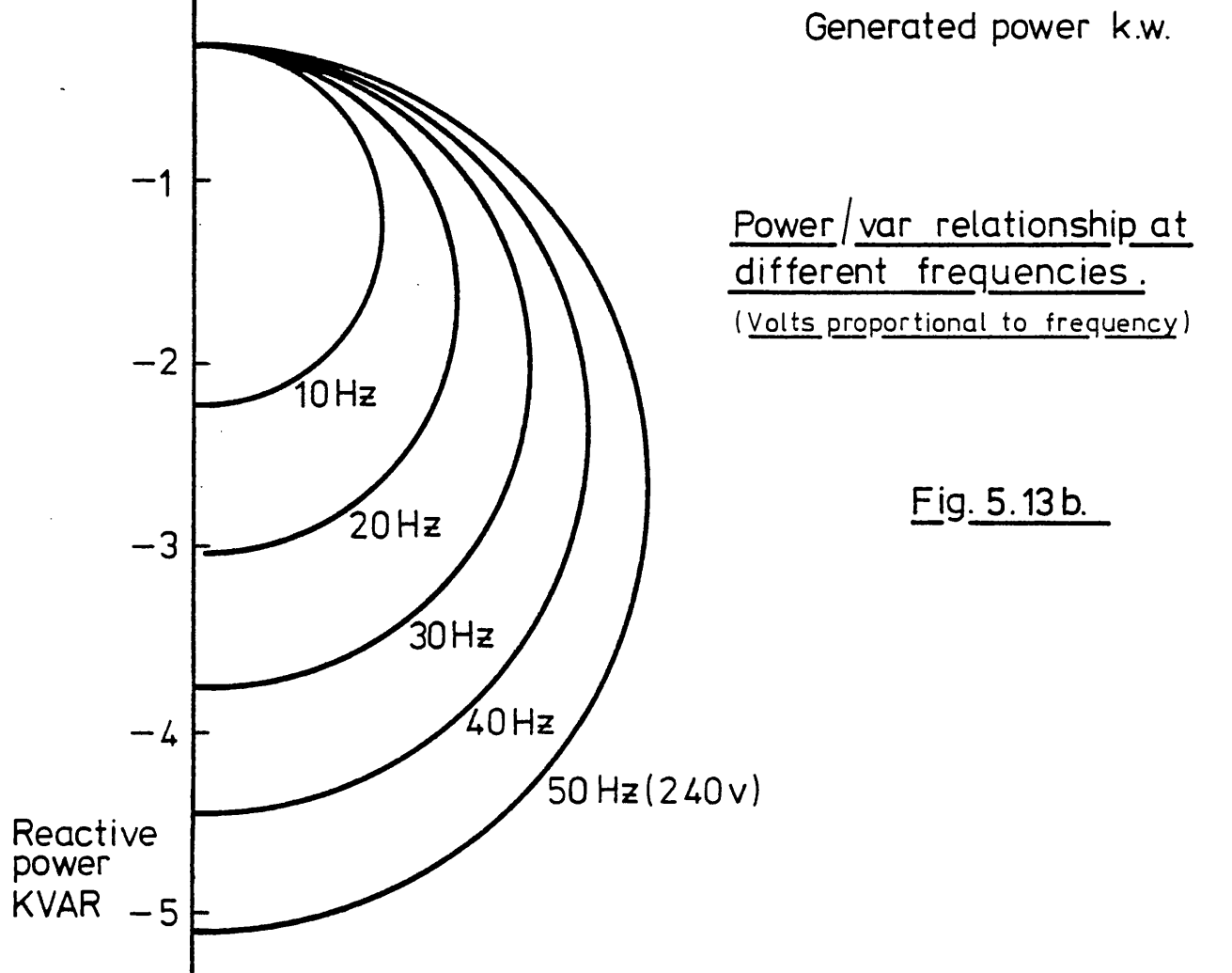


Fig. 5.13b.

vertical ordinate represents synchronous speed operation and the lower intersection an approximate slip of $-R_2/R_1$. The range of speed over which generation is possible can be increased if the stator voltage is increased, although saturation may result. It can also be seen from Fig. (5.13b) that this range decreases with frequency.

From a practical point of view, the reactive power needed to permit power generation at the high speed end of the generating range is prohibitive and a lower range limit is necessary. If this limit is fixed to give maximum power availability, the radius of the semicircle defines both the maximum available power and the required reactive power for unity power factor operation. Fig. (5.14) shows this reactive power plotted on a frequency base together with the value of capacitance needed for capacitive self-excitation. Clearly, as indicated in reference (36), capacitive self-excitation is only practical at high frequencies, of which the 400Hz aircraft system frequency is ideal. Figures (5.13) and (5.14) are conditions relating to a unity power factor load. For a lagging power-factor load, additional loading reactive power must be provided.

5.6 Induction generation in the experimental system

It has been seen in section 5.5 that the reactive component of the stator current in induction generation, $I_1 \sin \phi$, can be larger than the in-phase component $I_1 \cos \phi$. Clearly a cycloconverter excited induction generator system is not a practical proposition because the reactive power transmitted gives as large a current in the cycloconverter as direct frequency conversion and the cycloconverter would be better utilised as a direct frequency converter.

However in a cycloconverter-induction motor drive, system efficiencies may be increased considerably by regenerative braking. A continuous circulating current cycloconverter can operate with any phase displacement

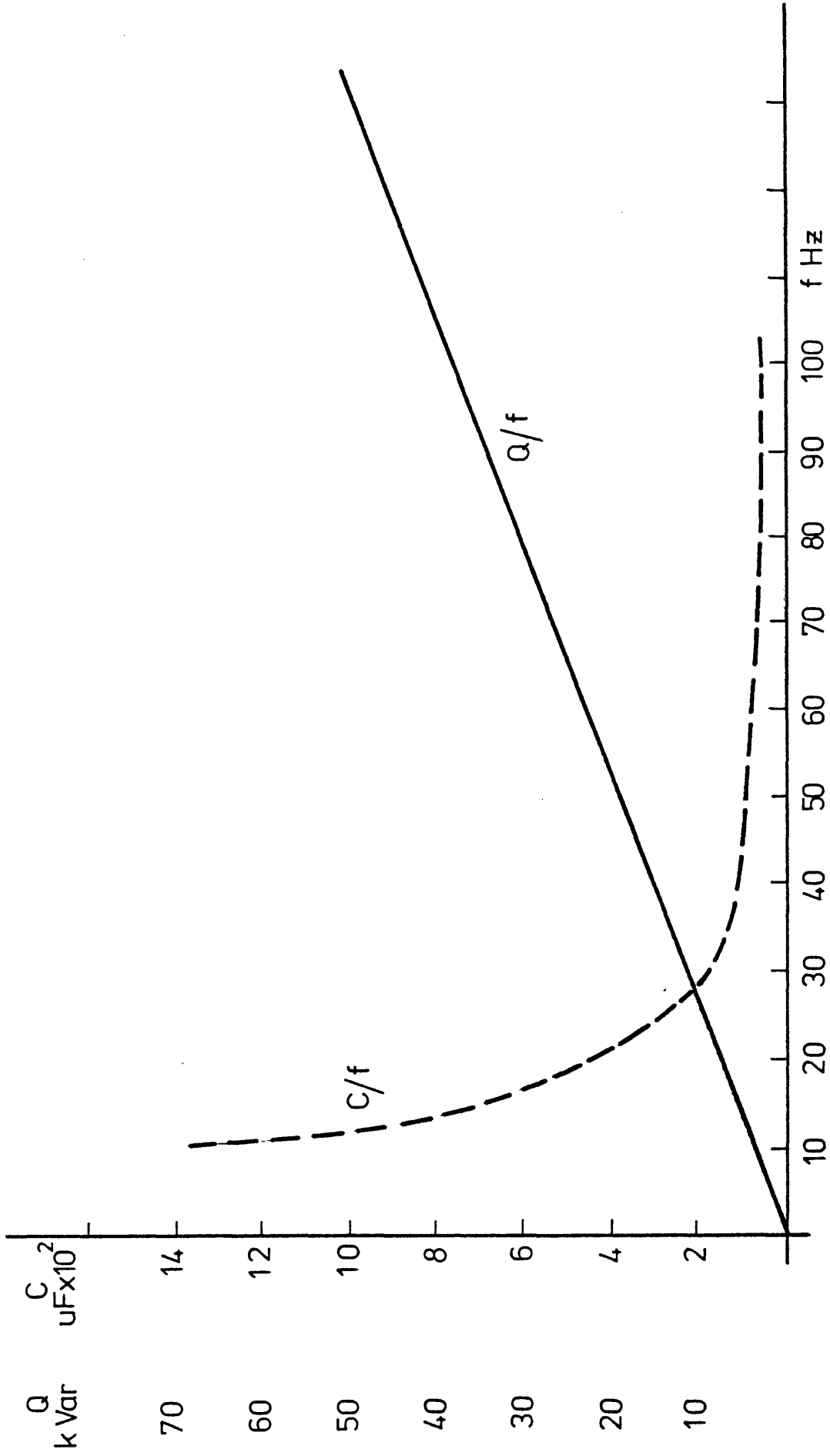


Fig.5.14. Reactive power requirement and corresponding capacitance for maximum power availability / frequency.

between output current and voltage fundamentals without gate pulse sequence changing, if the inter-group reactor can provide the energy storage capacity. Fig. (5.15) shows the measured regenerative powers in the experimental system at a series of fixed speeds with variable frequency contrasted with computed results obtained from equation (5.21). It can be seen that the range of frequencies over which generation is possible and the peak generated power increase with motor speed. The motor was driven externally in each case. Figure (5.16) shows similar results for fixed-frequency, variable-speed operation and Fig. (5.17) contrasts open- and closed-loop fixed frequency results.

The efficiency of an induction generator can approach 90% at a speed just above synchronous speed. If stator losses are neglected and all power transferred from the rotor to the stator is assumed to be available as output power, the generator efficiency will be,

$$\eta = \frac{I_2^2 R_2/S}{I_2^2 R_2(1-S)/S}, \quad (5.22)$$

and since the slip

$$S = \frac{\omega - \omega_2}{\omega},$$

$$\eta = \frac{\omega}{\omega_2}. \quad (5.23)$$

Thus the closed-loop frequency-speed relationship defined in equation (5.13) can give efficient generation and the cycloconverter provides a reversible energy flow frequency converter. If the limited frequency range of the cycloconverter can be accepted, a single electronic frequency converter can be used for motoring and braking. This contrasts favourably with the uni-directional power flow link-inverter system. Here regenerative braking can only be achieved through another anti-parallel inverter.

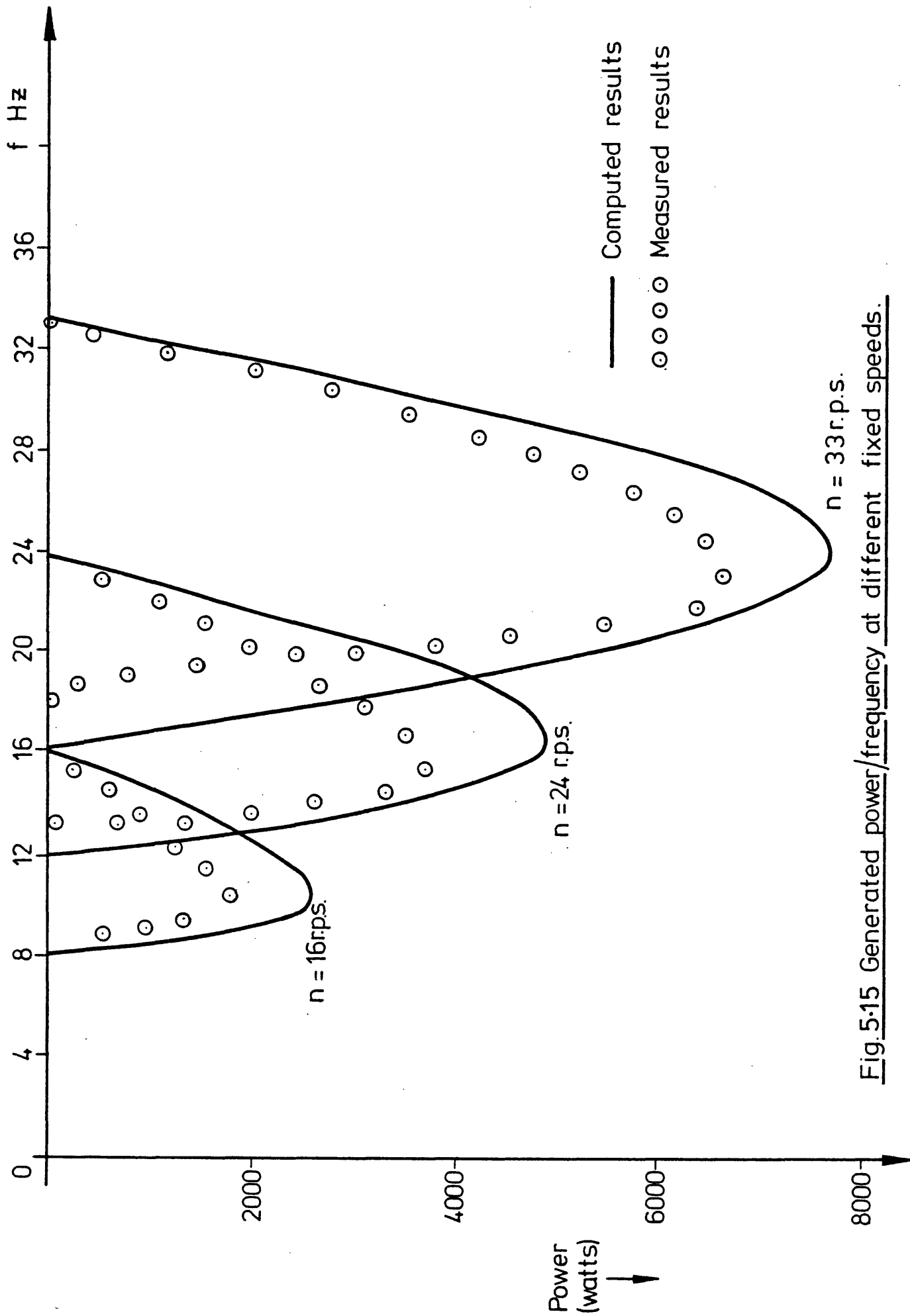


Fig. 5.15 Generated power/frequency at different fixed speeds.

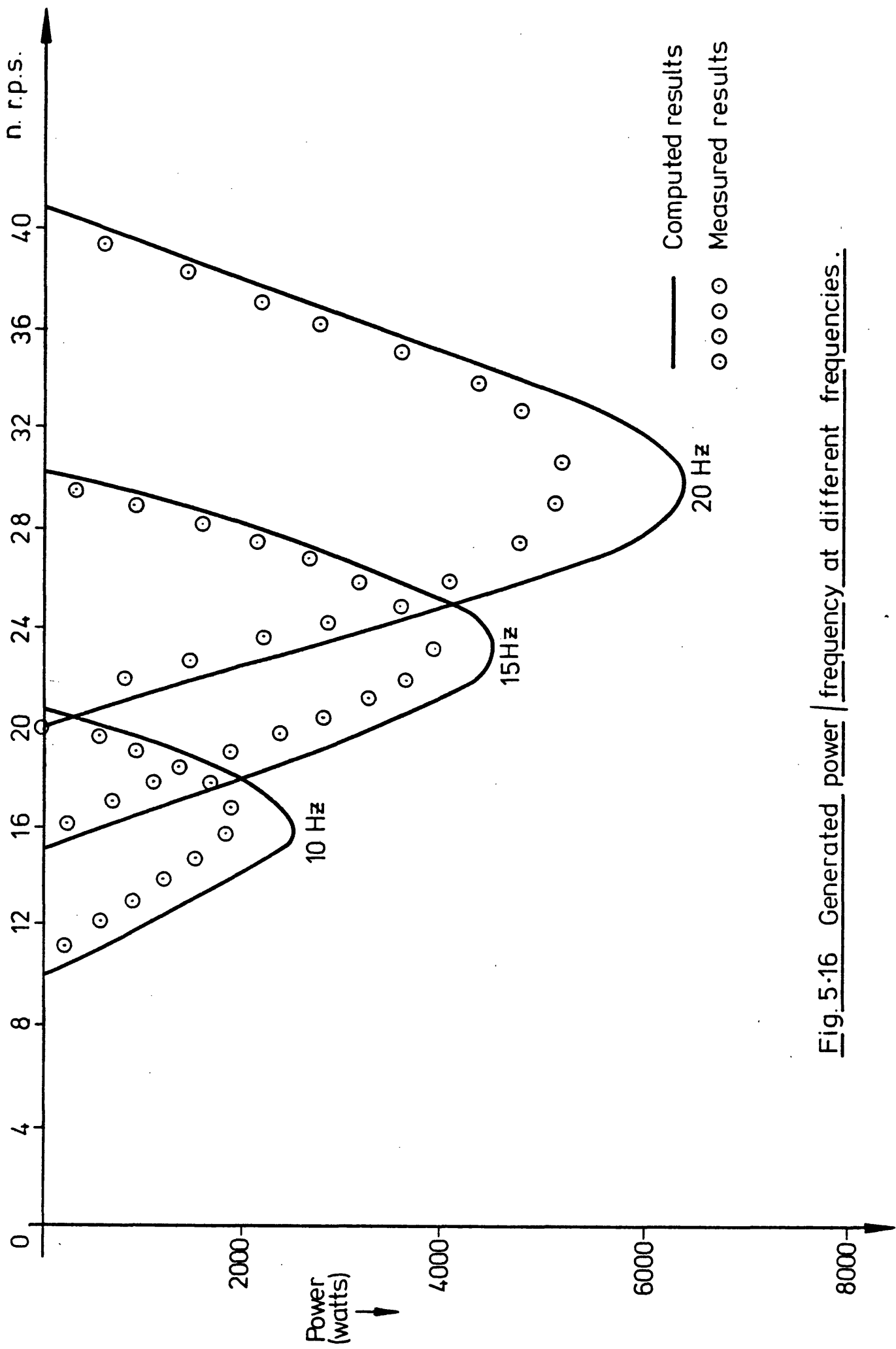


Fig. 5.16 Generated power / frequency at different frequencies.

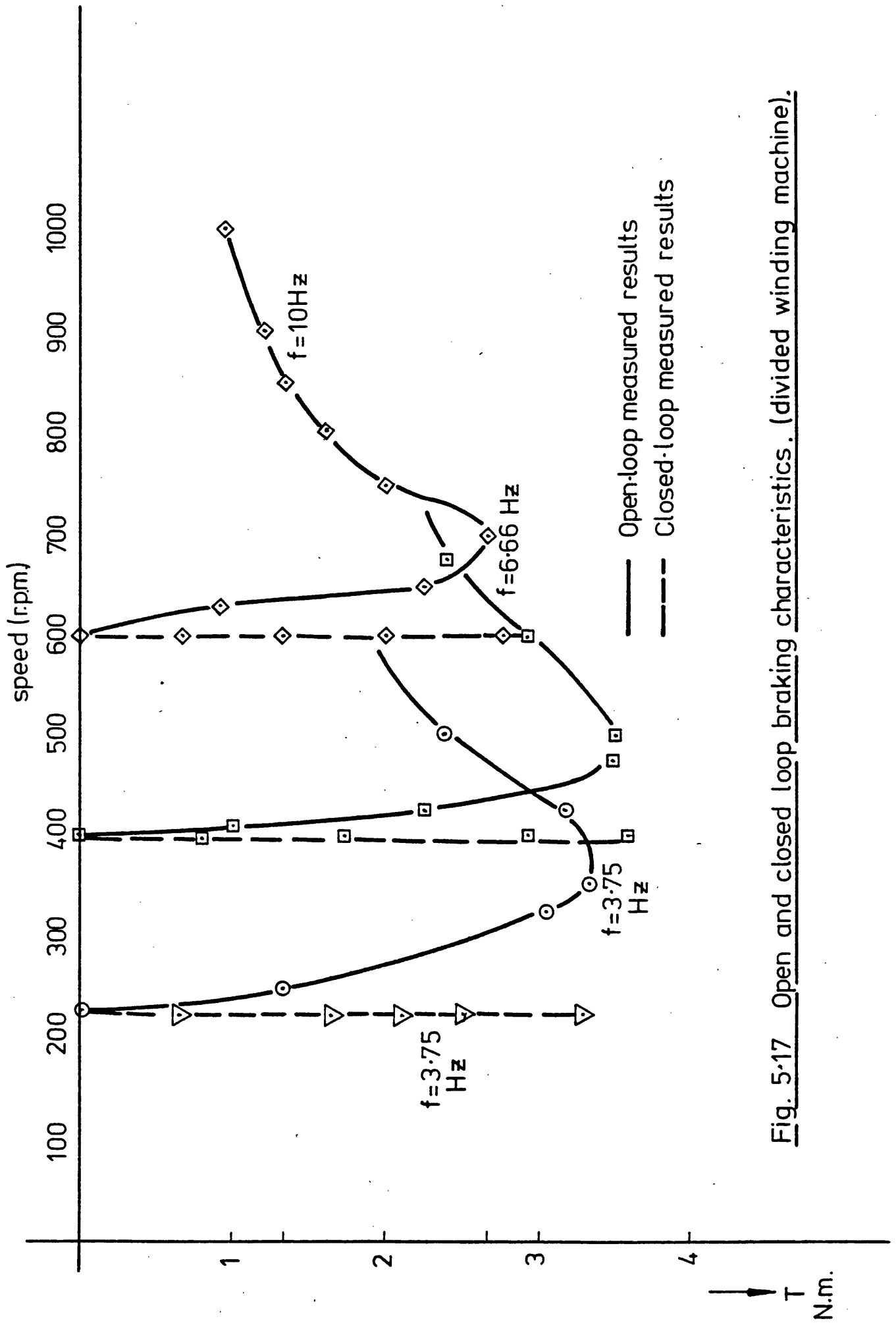


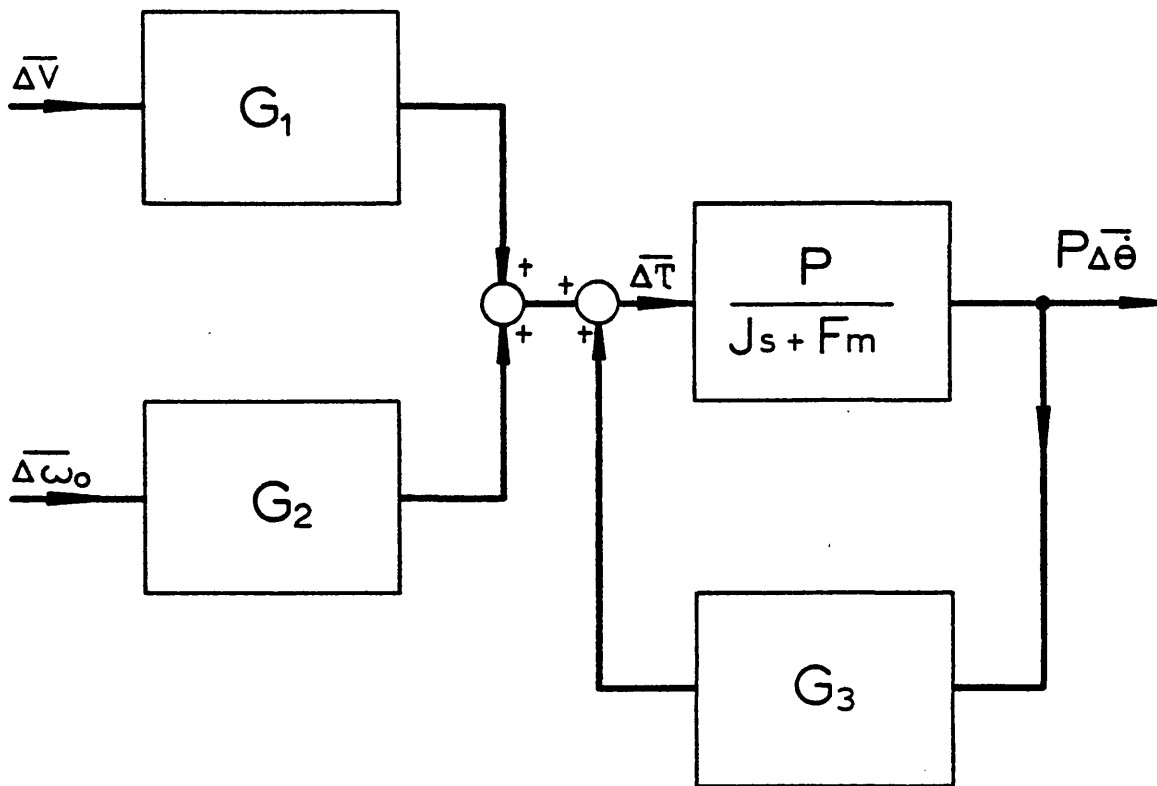
Fig. 5.17 Open and closed loop braking characteristics. (divided winding machine).

5.7 Small-signal perturbation model of the closed-loop system

The final stage of this work was to attempt to investigate the stability of the closed-loop experimental system by means of a small-signal perturbation model. Such a model requires a transfer-function block representation of an induction motor. De Carli and Murgo⁽³⁸⁾ have represented the induction motor in the block form of Fig. (5.18). Here torque variations are related to variations of voltage, frequency and speed. An open-loop representation incorporating the cycloconverter added to the induction motor is shown in Fig. (5.19). Here the time-constants of the reference generator field, $\tau_{f.g.}$, and inertia, τ_M , are the main cause of time delays in the cycloconverter transfer function. The motor transfer functions, G_1 , G_2 and G_3 are now represented in terms of the rotor-time-constant, τ_2 and the motor polar moment of inertia, J and frictional constant, F_m . Here the term, s , is the Laplace operator, and ω_{00} is the angular frequency of the stator voltage before displacement. If the stator voltage can be considered to be proportional to frequency, the block diagram is greatly simplified. Suppose a control signal $\Delta\bar{U}$ is defined so that as a result of a change in volts proportional to frequency, $\Delta\bar{\omega}_0 = K_A\Delta\bar{U}$ and $\Delta\bar{V}_1 = K_B\Delta\bar{U}$, the combined transfer function of G_1 and G_2 in Fig. (5.18) can be defined as,

$$\frac{\Delta\bar{U}}{\Delta T_e} = \frac{K_A(s^2 + \omega_{00}^2)}{(s + \tau_2)(s^2 + \omega_{00}^2)} = \frac{K_A}{(s + \tau_2)} \quad (5.24)$$

Equation (5.24) is the linearised transfer-function of a constant-flux, variable-speed induction motor drive in which the stator parameters are neglected and the slip is negligibly small, defined by Rogers⁽³⁹⁾ and Pfaff⁽⁴⁰⁾. Clearly in the case of the divided-winding machine with an effectively doubled stator resistance, this is a doubtful assumption. However the extra stator resistance may be assumed to simply attenuate the air-gap flux of the motor with no additional phase shift.



$$G_1 = \frac{\Delta \bar{T}}{\Delta \bar{V}}$$

$$G_2 = \frac{\Delta \bar{T}}{\Delta \bar{\omega}_0}$$

$$G_3 = \frac{\Delta \bar{T}}{\Delta \bar{n}}$$

FIG.5.18 BLOCK DIAGRAM OF LINEAR MODEL OF INDUCTION MOTOR

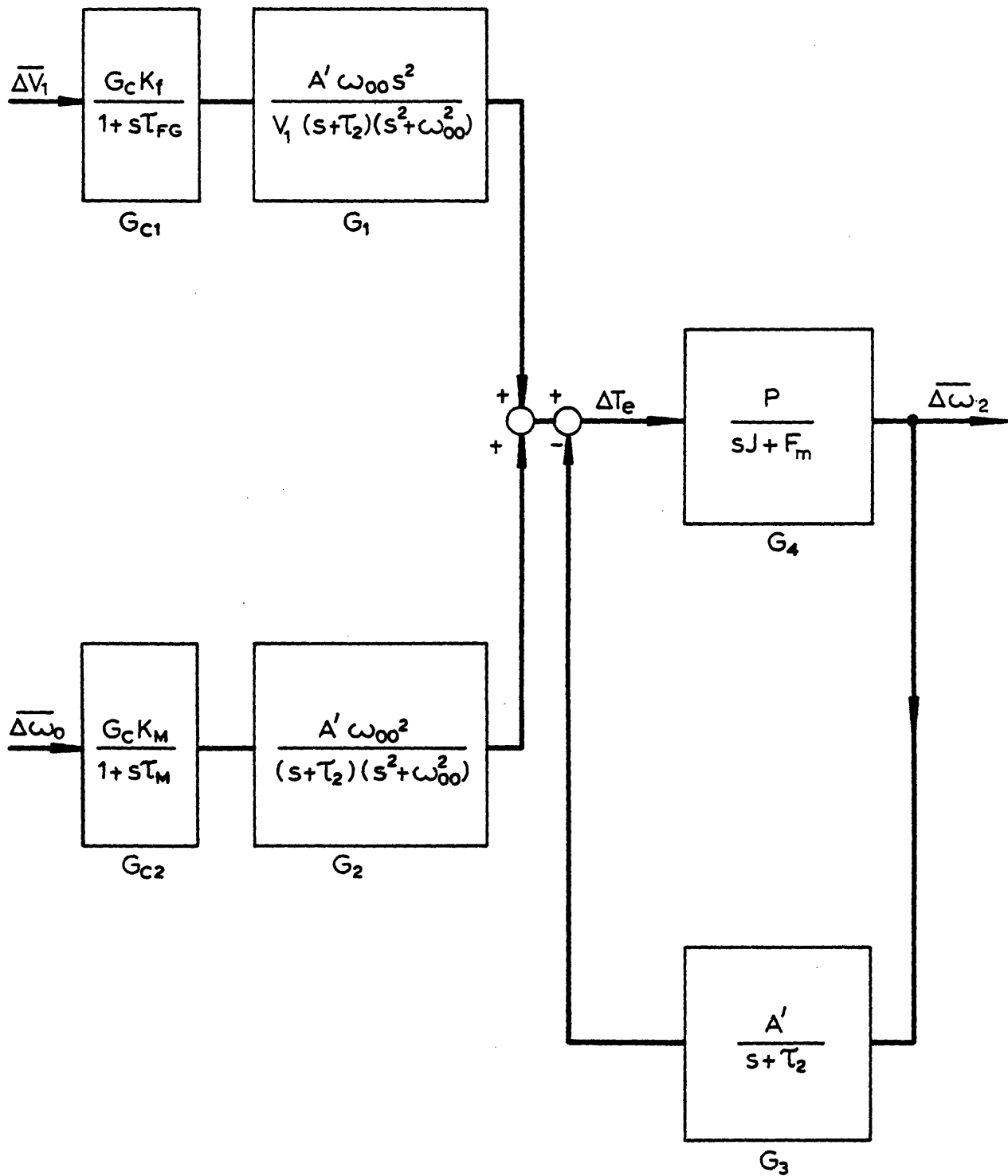


FIG.5-19 SMALL SIGNAL OPEN-LOOP CONTROL SYSTEM SHOWING TRANSFER FUNCTIONS

In the experimental system, the cycloconverter time constants are negligible compared with the inertia constant of the motor. Velocity feedback was implemented by a d.c. tachometer of transfer function

$$\frac{\Delta \bar{\omega}_2}{\Delta \bar{V}_t} = K_2. \quad \text{The tachometer output voltage was fed into a feedback amplifier of transfer function } \frac{1}{s + \frac{1}{CR_2}}. \quad \text{This capacitor } C \text{ was}$$

introduced to smooth out the tachometer commutator ripple. Thus the block diagram of the closed-loop system becomes that of Fig. (5.20), which further simplifies to the form shown in Fig. (5.21). The practical system was as shown in Fig. (5.22). It can be seen that in the form shown in Fig. (5.21), the linearised block diagram representation does not include the externally connected standard induction motor or the current clamp amplifier. Considering the block diagram of Fig. (5.21), the open-loop transfer-function can be seen to be,

$$G(s) \cdot H(s) = \frac{PA' \omega_{oo} K_2 \frac{1}{CR_1}}{\left[PA' + (s + \tau_2)(sJ + F_m) \right] \left(s + \frac{1}{CR_2} \right)}, \quad (5.25)$$

where A' is a constant, and the closed-loop transfer-function is,

$$\frac{\Delta \bar{\theta}}{\Delta \bar{U}} = \frac{PA' \omega_{oo} \left(s + \frac{1}{CR_2} \right)}{\left(s + \frac{1}{CR_2} \right) \left[PA' + (s + \tau_2)(sJ + F_m) \right] + PA' \omega_{oo} \frac{K_2}{CR_1}}, \quad (5.26)$$

which simplifies to the form of,

$$\frac{PA' \omega_{oo} \left(s + \frac{1}{CR_2} \right)}{J \left(s + \frac{1}{CR_2} \right) \left[s^2 + s \frac{(\tau_2 J + F_m)}{J} + \frac{(A'P + \tau_2 F_m)}{J} \right] + PA' \omega_{oo} \frac{K_2}{CR_1}} \quad (5.27)$$

Root-locus techniques can be used to provide an accurate solution of the system performance and also have the advantage of showing the extent of the system stability. In the system under consideration, the transient

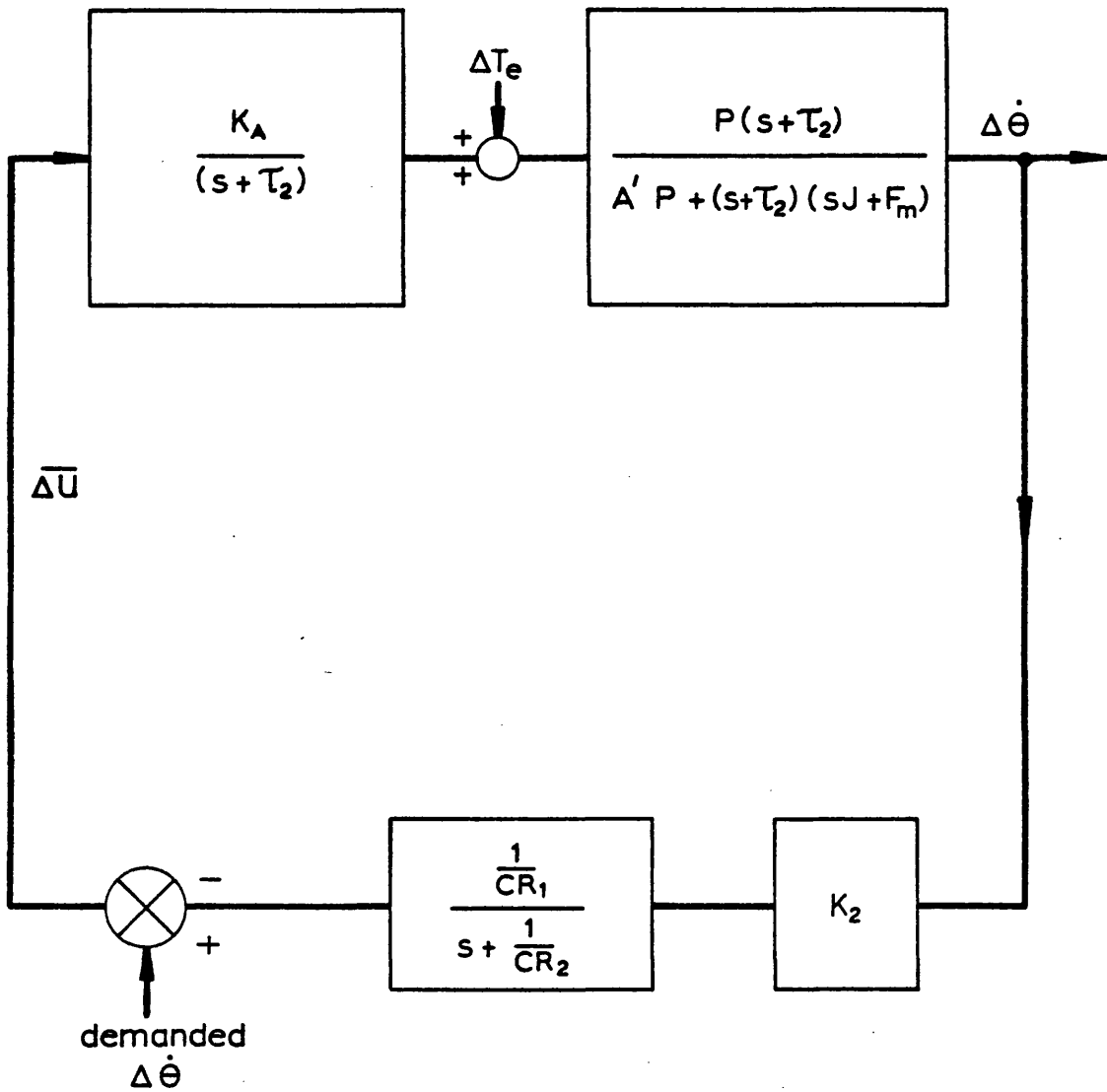


FIG. 5.20 SMALL SIGNAL CLOSED-LOOP SPEED CONTROL SYSTEM WITH VOLTAGE AND FREQUENCY CONTROL

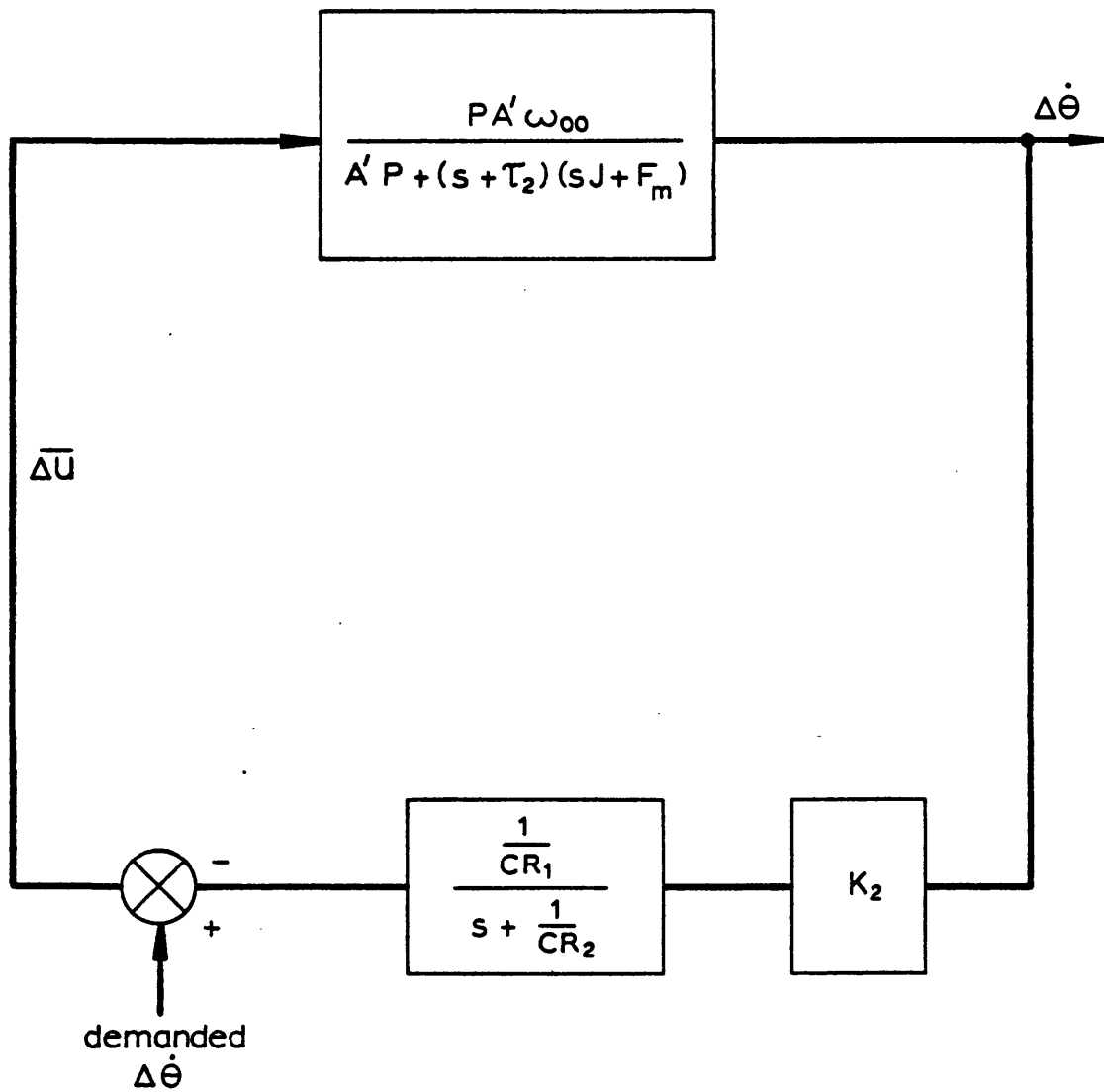


FIG.5.21 MODIFIED SMALL SIGNAL CLOSED-LOOP SPEED CONTROL SYSTEM WITH VOLTAGE AND FREQUENCY CONTROL

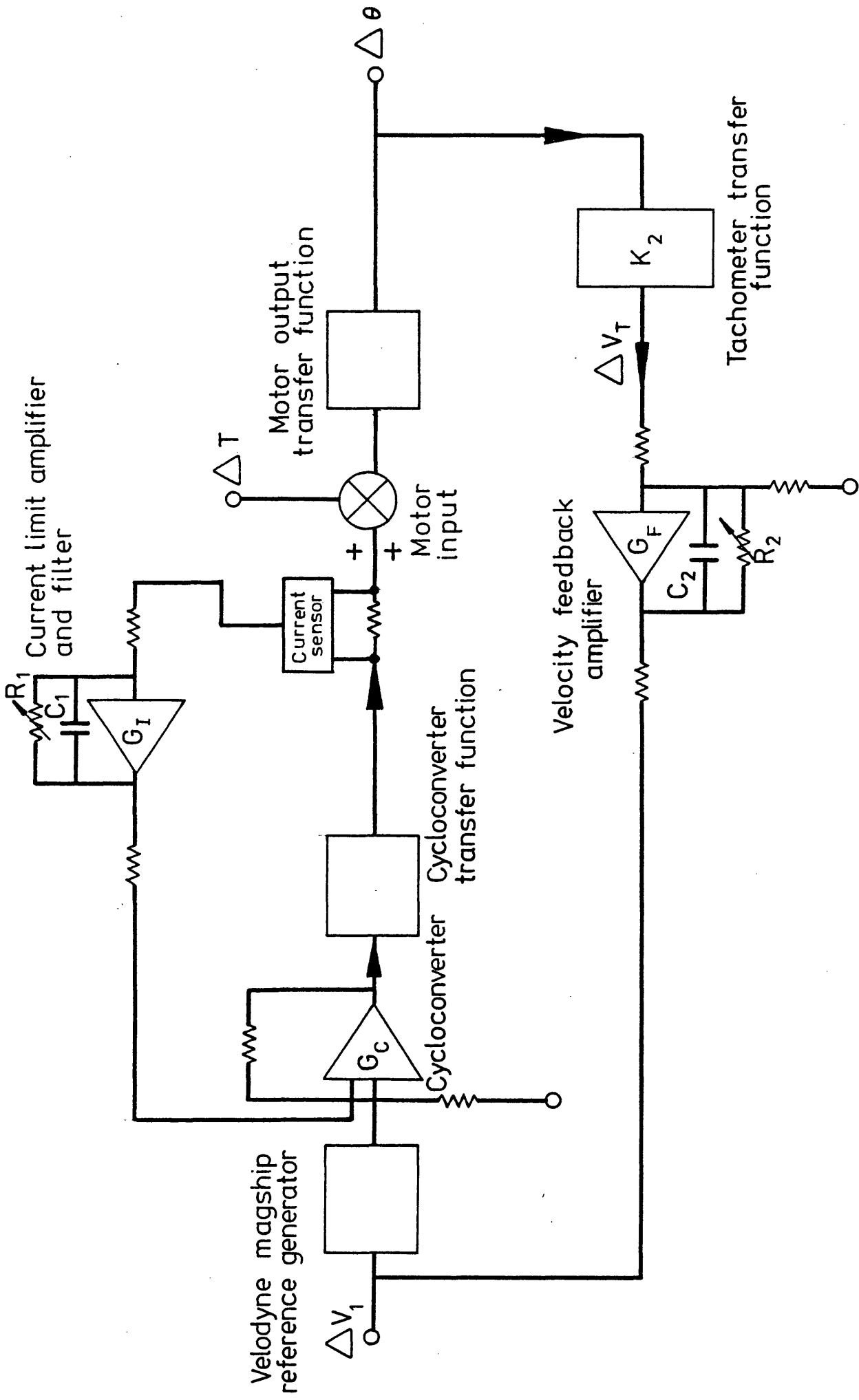


Fig.5:22 Closed loop induction motor speed control system

response is of importance rather than the frequency response, because of the inertia of the rotor and the load.

The root-locus technique is therefore chosen for this analysis. Derivation of the root-loci of the system is given in Appendix 4.

Consider the open-loop transfer function of the system given in equation (5.25), rearranged as,

$$G(s) \cdot H(s) = \frac{PA' \omega_{oo} K_2 \frac{1}{CR_2}}{J \left(s + \frac{1}{CR_2} \right) \left[s^2 + s \frac{(\tau_2 J + F_m)}{J} + \frac{(\tau_2 F_m + PA')}{J} \right]} \quad (5.27)$$

Constants, a, b and d are now defined as follows,

$$a = \frac{F_m + \tau_2 J}{J} ,$$

$$b = \frac{\tau_2 F_m + A'P}{J} ,$$

$$\text{and } d = \frac{1}{CR_2} .$$

Then equation (5.27) can be written as,

$$G(s) \cdot H(s) = \frac{PA' \omega_{oo} K_2 \frac{1}{CR_2}}{A'P + J(s + d) [s^2 + sa + b]} \quad (5.28)$$

Factorization of the second term in the denominator gives,

$$\frac{PA' \omega_{oo} K_2 \frac{1}{CR_1}}{A'P + J(s + d) \left[s + \frac{-a + \sqrt{a^2 - 4b}}{2} \right] \left[s + \frac{-a - \sqrt{a^2 - 4b}}{2} \right]} \quad (5.29)$$

In the complex plane this has the following poles.

$$\text{poles, } P_1 = -d, \quad P_2 = \frac{-a + \sqrt{a^2 - 4b}}{2}, \quad P_3 = \frac{-a - \sqrt{a^2 - 4b}}{2} .$$

The closed-loop transfer function of equation (5.26) then becomes,

$$\frac{\Delta\bar{\theta}}{\Delta\bar{U}} = \frac{PA' \omega_{oo} (s + d)}{J(s + d) [s^2 + sa + b] + g} \quad , \quad (5.30)$$

where $d = \frac{1}{CR_2}$ and $g = PA' \omega_{oo} \frac{K_2}{CR_1}$.

To obtain the poles and zeros, the denominator of equation (5.30),

$$J(s+d)(s^2+sa+b) + g = 0 \quad ,$$

and so $J[s^3+s^2(a+d) + s(b+da) + (db + \frac{g}{J})] = 0$. (5.31)

Equation (5.30) can be expressed in the form,

$$\frac{\Delta\bar{\theta}}{\Delta\bar{U}} = \frac{PA' \omega_{oo} (s+d)}{J(s+D)(s+A-jB)(s+A+jB)} \quad , \quad (5.32)$$

where A, B and D are constants. The roots of the equation are then -D and $-A \pm jB$.

The solution of the equation (5.32) gives the variation in speed, relative to a steady-state operating point for a given disturbance $\Delta\bar{U}$ in the system. Fig. (5.23a) shows the form of root-locus for experimental system with one induction machine. A full derivation of this root-locus is given in Appendix 4. This system is only conditionally stable because the loci approach the imaginary axis when the system gain, K, becomes large.

An inherently stable system could be formed by the addition of an extra s term in the numerator of the closed-loop transfer function to give

$$\frac{\Delta\bar{\theta}}{\Delta\bar{U}} = \frac{sPA' \omega_{oo} (s+d)}{J(s+d)(s^2+sa+b) + g} \quad . \quad (5.32)$$

The system root-locus will then be as shown in Fig. (5.23b) with a stability independent of gain. However, a practical solution to the problem involves the feeding of the reference generator output to the cyclo-converter through a differentiator. A practical differentiator built around an operational amplifier must incorporate a (1+s) term in the numerator

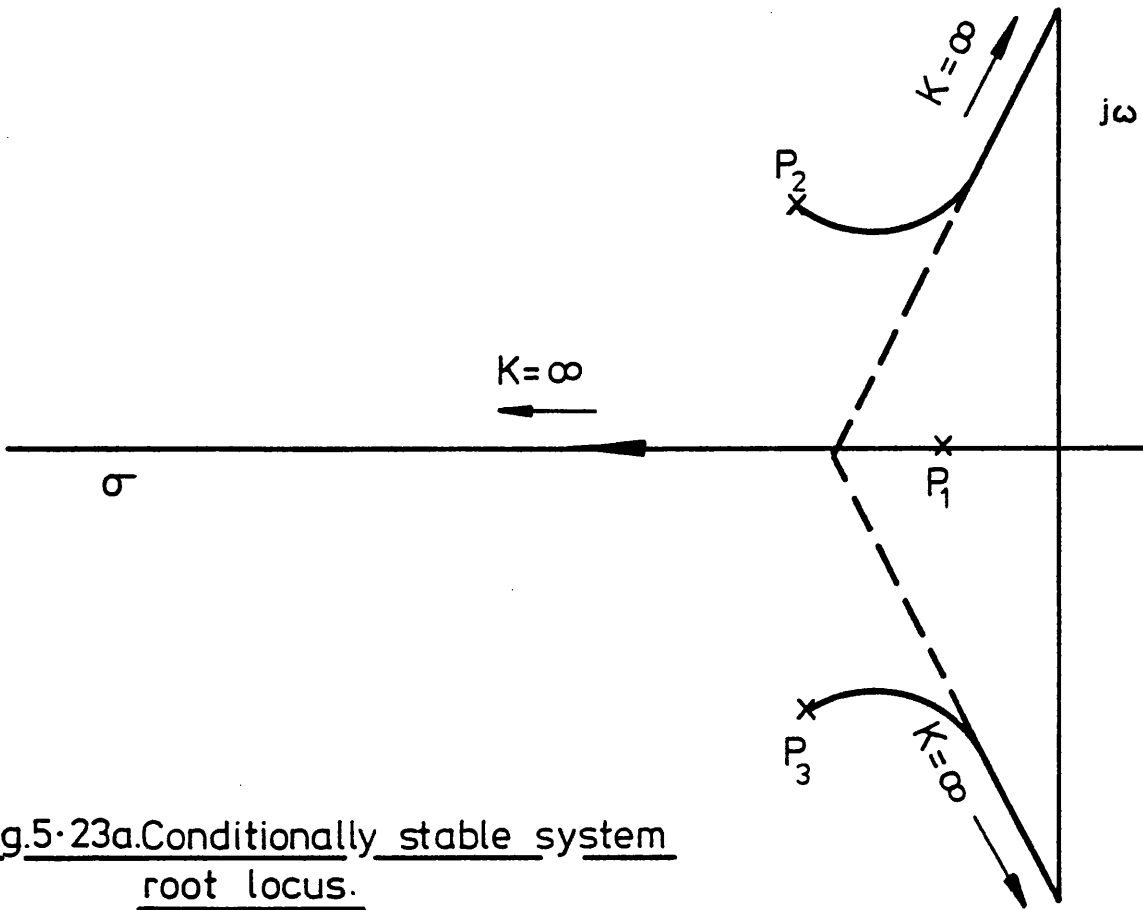
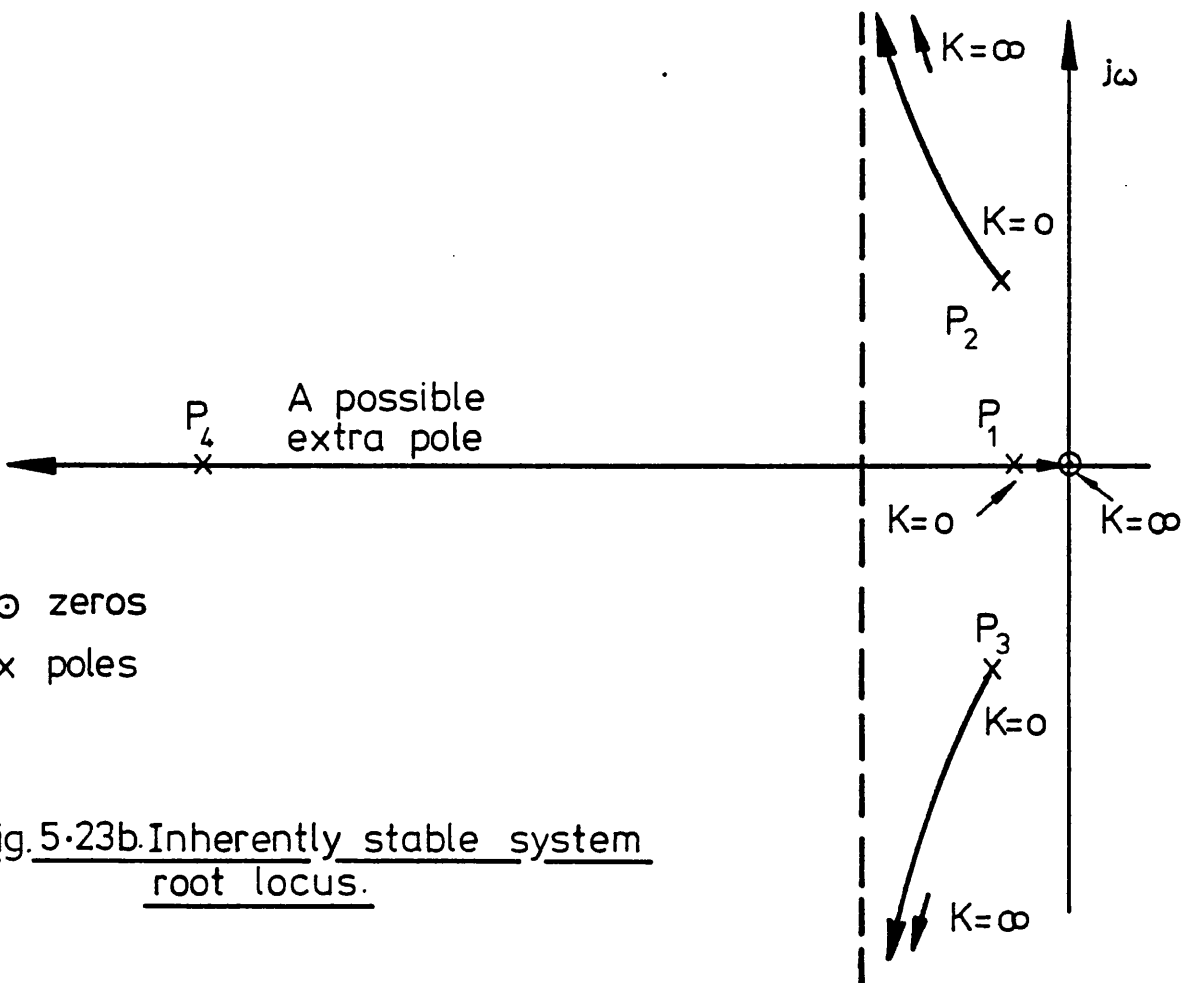


Fig.5-23a. Conditionally stable system root locus.



o zeros
x poles

Fig.5-23b. Inherently stable system root locus.

of equation (5.32), also incorporating a phase-shift. The problem is not then the inherently stable system of Fig. (5.23b). A differentiator operating on digital principles might provide a better solution.

In practice, the closed-loop system operated stably with medium to low gain. In practice, it is preferable to operate with a large generated reference voltage so that the loop gain can be reduced. This means operation at high reference generator field currents.

This small-signal perturbation study has shown that stable, small-slip operation in a system having negligible stator resistance is possible. Up to now single machine operation has been considered, but if the two conditions can be satisfied for the multi-machine system of Fig. (5.24), multi-machine stability may be possible. Here the second machine operates at the voltage necessary to maintain constant air-gap flux in the first machine. This means that the rotor of the divided winding machine is not affected by the loading of the standard induction motor. The standard induction motor is constrained by the feedback loop of the first machine to operate as if it were connected to a "hard" low-frequency supply. It then operates under open-loop conditions subject to the stability criteria discussed in Chapter 2. To achieve this type of operation completely, the stator of the divided-winding, inter-group reactor machine might be operated under cryogenic conditions.

5.8 Cycloconverter-divided winding system response

The full potential of the divided winding system can be seen when its performance is contrasted with the performance of the same machine with a standard winding operating with the same cycloconverter in the circulating-current-free mode. Figs. (5.25a) and (5.25b) contrast the response in each system to a steady increase of torque. Stability can be achieved in the divided winding system with double the rate of torque increase.

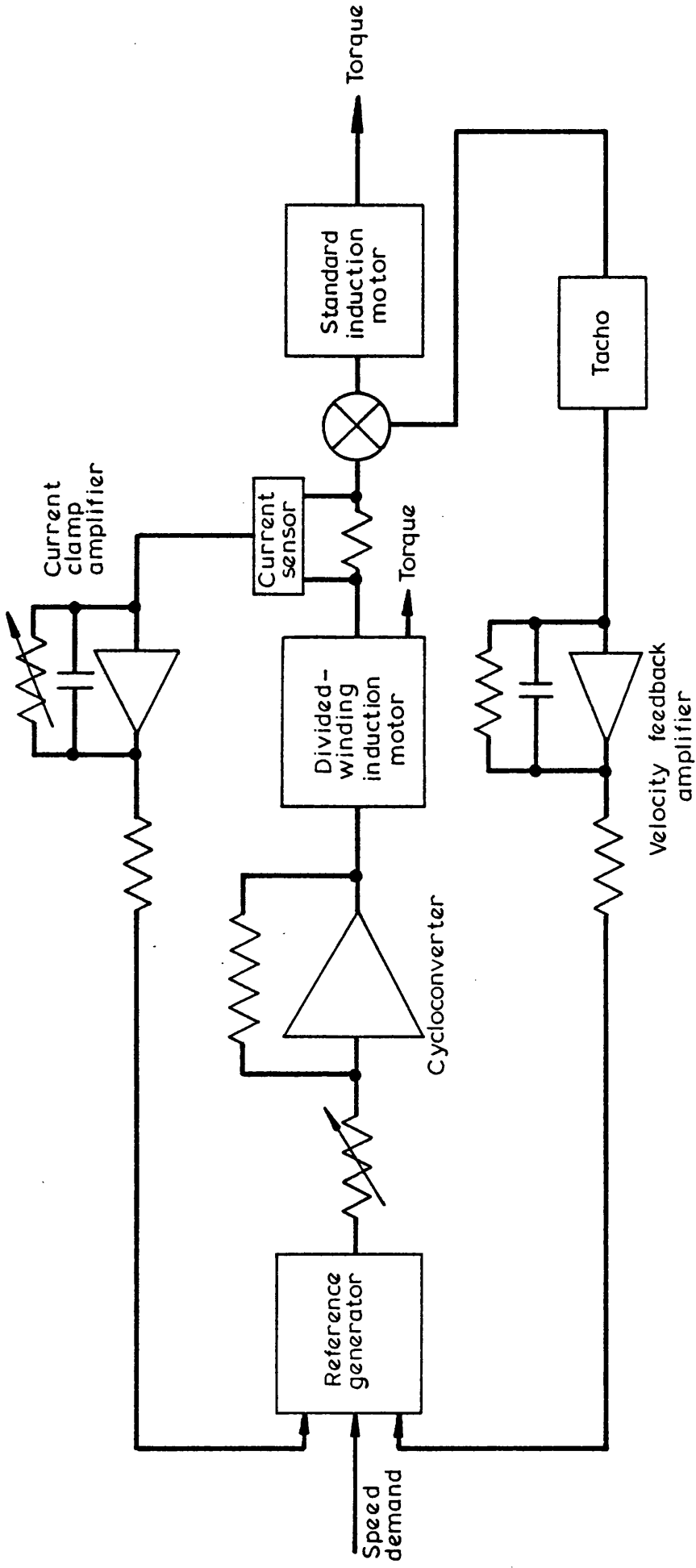


Fig.5.24 Schematic diagram of control system

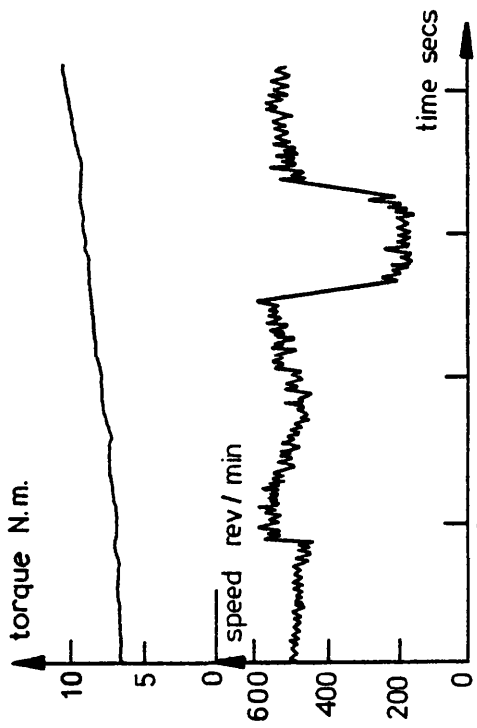


FIG.5:25a INCREASING TORQUE, CIRCULATING CURRENT FREE SYSTEM

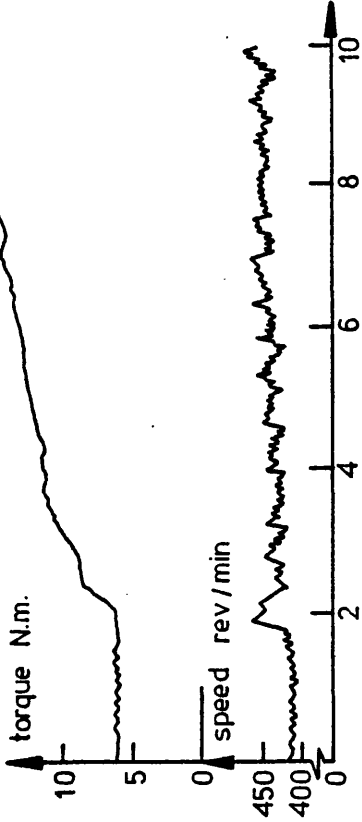


FIG.5:25b INCREASING TORQUE, DOUBLE WINDING SYSTEM.

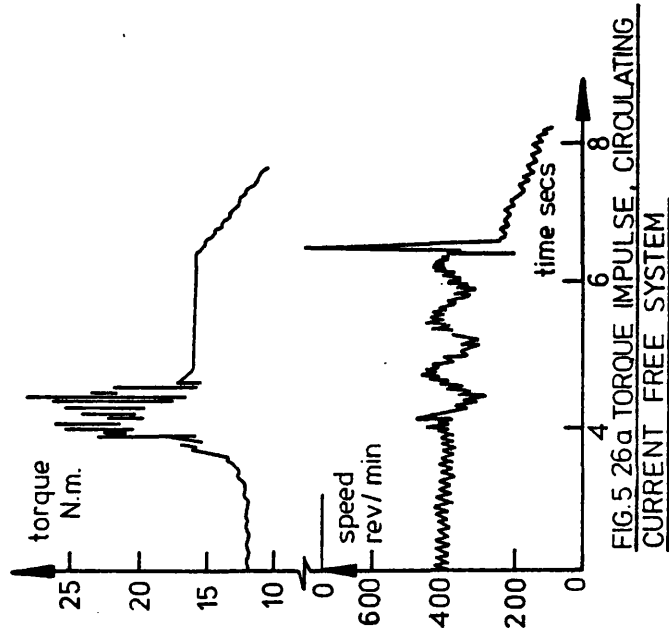


FIG.5:26a TORQUE IMPULSE, CIRCULATING CURRENT FREE SYSTEM

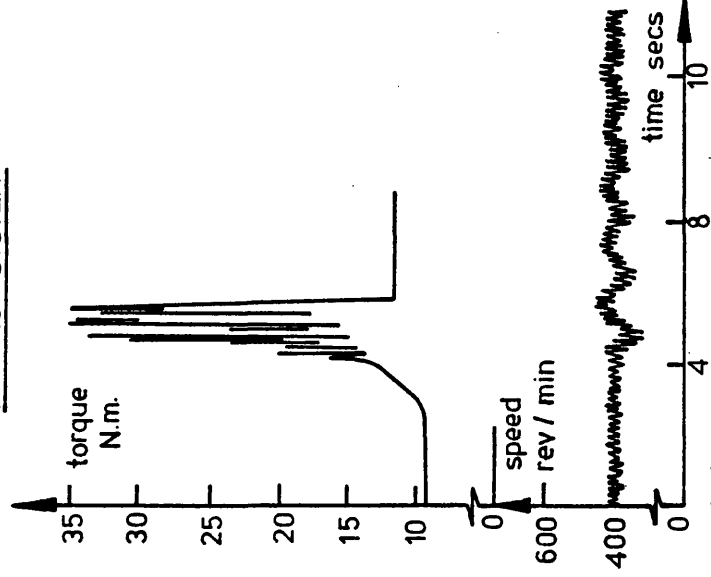


FIG.5:26b TORQUE IMPULSE, DOUBLE WINDING SYSTEM CYCLOCONVERTER INDUCTION MOTOR CLOSED - LOOP SYSTEM RESULTS

Figure (5.26a) shows that a 100% step torque increase in the circulating current free system causes oscillation and eventual pull-out due to a current requirement in excess of the clamping level, while Fig. (5.26b) shows that the divided winding system can accept 200% step torque increases and still operate stably.

5.9 Conclusions from Chapter 5

The performance of a single and a two-machine system has been investigated. This performance has been attained at the expense of poor utilisation of copper and loss of system efficiency in the single-machine system. An improvement in utilisation and efficiency can be seen in the two-machine system.

Regenerative braking can be achieved without modification to the thyristor gate circuits because the continuous circulating current cycloconverter can operate with natural commutation under leading power factor conditions.

It has been shown that regenerative braking is to be preferred in a system operating with a rapidly repeated duty cycle such as a crane or a hoist. However, induction generation imposes severe reactive power demands on the cycloconverter. Although the continuous-circulating current cycloconverter is naturally reversible in energy flow, small slip operation is vital in braking if the reactive power demand is to be tolerable. The closed-loop system meets this requirement in braking as well as acceleration.

A qualitative stability study has shown that the closed-loop system can operate stably if small-slip operation is maintained and the stator impedance is small. It has been shown that a differentiator in the reference generator circuit may improve stability.

CHAPTER 6

General Conclusions

It has been shown that an induction motor can operate stably on a sinusoidal supply at frequencies less than 5Hz. A wide range of speeds can therefore be incorporated into an induction motor drive without the need for a reduction gear. Parameter variation with frequency is insignificant, but the reduction in air-gap flux due to the stator resistance is significant at low frequencies. Closed-loop stator voltage control to maintain constant air-gap flux is desirable in a constant-torque, variable-speed drive. At low frequencies, the magnetising current forms an increasing part of the total input current and the motor efficiency is greatly reduced. This has little effect on open-loop stability.

The operation of an induction motor with its stator terminals connected to non-sinusoidal supply has been investigated. It was found that a variable-frequency source to be used in an induction motor drive must be free of sub-harmonics and triplens if "cogging" is to be avoided. The main effect of higher order harmonics is to reduce efficiency.

The inter-group reactor needed to maintain continuous circulating current in a cycloconverter has been replaced by the stator of an induction motor. This motor then produces torque and maintains continuous circulating current in the cycloconverter giving a significant reduction in harmonics compared with conventional circulating-current-free operation. Two stator layers are wound identically as balanced 3-phase windings. They are magnetically coupled, but electrically separate. Line to line short-circuit faults in the cycloconverter are prevented and the usual rotating field is set up in the machine air-gap.

The most significant part of this work is the design and construction of an experimental system to verify the proposal. Two electronic feedback servo-loops have been incorporated for speed control and current clamping.

A control system incorporating one divided-winding machine makes poor use of the copper in the machine, although the other advantages may be significant. In the experimental system, standard squirrel-cage machines have been added to produce a multi-machine drive. Better utilisation and overall efficiency result. The performance of single and two-machine systems have been investigated.

Regenerative braking can be achieved without modification to the thyristor gate circuits because the continuous-circulating-current cycloconverter can operate with natural commutation under leading power factor conditions. Although the continuous-circulating-current cycloconverter is naturally reversible in energy flow, small slip operation is vital in braking if the reactive power demand is to be tolerable. The closed loop system meets this requirement in braking as well as acceleration.

The closed-loop system can operate stably if small-slip operation is maintained and the stator impedance is small. A differentiator in the reference generator circuit may improve stability.

CHAPTER 7

Suggestions for Future Work

The advantages of the cycloconverter-induction motor drive with electrically-separate, magnetically-coupled thyristor group circuits has been clearly demonstrated in this work. To develop this system into a more economical industrial drive, further work to improve its performance and utility should be attempted. Suggestions that may achieve this are as follows:-

a) A preferred machine combination may consist of the divided-winding machine and the standard machine operating with a common shaft. In this case torque-sharing and closed-loop control are achieved and since both machines have squirrel-cage rotors, the combination will be cheaper than a cascaded slip-ring combination of similar size.

b) From the investigations carried out in this work, it has been shown that stator resistance effect becomes significant in using the divided-winding machine as inter-group reactor. This will increase the overall copper loss and dissipate more heat in the windings making extra cooling necessary. A machine operating with a cryogenic stator winding could be used in a large divided-winding machine (e.g. 1000 HP), since at cryogenic temperatures there will be no significant stator resistance.

Several standard machines can then operate from this common "reactor" with the cycloconverter maintained in the continuous circulating current mode of operation.

c) The experimental laboratory machine used as a divided-winding machine is inefficient due to the type of gramme-ring winding used which gives a large copper loss. The nature of the construction used limits the number of stator slots which impairs the air-gap flux waveform. Better results would be obtained if a commercial induction motor stator was modified to act as the reactor machine.

CHAPTER 8Acknowledgments

The author gratefully acknowledges the advice and encouragement given by Professor G.D.S. MacLellan, Head of Engineering Department of the University of Leicester. The author also wishes to record his appreciation of the continued advice which he has received from his supervisor, Dr. P.G. Holmes.

Acknowledgments are due to the University of Leicester for the provision of laboratory facilities and to the Science Research Council who partly contributed towards the cost of the materials. The author also wishes to acknowledge his warm appreciation of the financial support he has received from the Ministry of Higher Education and Research of the Republic of Iraq.

Grateful thanks are expressed to Mr. R.G. Stephens, Experimental Officer, of the University of Leicester, for his assistance relating to electronic circuitry. The assistance of the Technical staff is also warmly appreciated.

Finally, thanks are due to Miss N.I. Berridge for the preparation of diagrams used in this dissertation and to Mrs. E. Knowles who typed this script.

CHAPTER 9REFERENCES

1. Adkins, B., The general theory of electrical machines, Chapman & Hall, 1962.
2. Hancock, N.N., Matrix analysis of electrical machinery, Pergamon, 1964.
3. Rogers, G.J., Linearised analysis of induction motor transients, Proc. IEE, 12, pp.1917-26, 1965.
4. Draper, A., Electrical Machines, 2nd Edition, 1969, Longmans, pp.121-4.
5. Brown, J.E. and Grantham, C., Determination of the parameters and parameter-variation of a 3-phase induction motor having a current-displacement rotor, Proc. IEE, Vol. 122, No. 9, 1975.
6. Reference 4, pp. 133 and 134.
7. Morgan, H. and Brown, E., Reverse-rotation test for the determination of stray-load-loss in induction machine. Proc. AIEE, 1939, Vol. 58, pp.319-24.
8. Hirst, A.W., Introduction to electrical machines, Blackie, 2nd Edition, pp. 84-5.
9. Mawdsley Ltd., Handbook for the Educational Induction Motor.
10. Lawrenson, P.J. and Stephenson, J.M., Note on induction motor performance with a variable-frequency supply. Proc. IEE, 1966, 113, pp.1617-23.
11. Bowler, P., Steady-state stability criterion for induction motors. Proc. IEE, 121, 1974, pp.663-667.

12. Lipo, T.V. and Krause, P.C., Stability analysis of a rectifier-inverter induction motor drive. IEEE Trans. 1969, PAS-88, pp.55-66.
13. Fallside, F. Steady-state oscillations and stabilisation of variable-frequency inverter-fed induction motor drives, Proc. IEE, 1969, 116, pp.991-99.
14. McLean, G.W. and Alwash, S.R., Performance and design of induction motors with square-wave excitation. Proc. IEE, Vol.116, No. 8, Aug. 1969.
15. Klingshirn, A. and Jordan, E., Polyphase induction motor performance and losses on non-sinusoidal voltage sources, IEEE Trans., 1968, PAS-87, pp.624-631.
16. Jain, G.C., The effect of voltage waveshape on the performance of a 3-phase induction motor, IEEE Trans., 1964, pp.561-566.
17. Bedford, B.D., and Hoft, R.G., Principles of inverter circuits. Wiley, 1971.
18. Hennessy, J.P.D. The design of a pulse-width-modulated inverter fed induction motor drive using logic switching. Leicester University Engineering Department Report 69-27.
19. Pelly, B. Thyristor phase-controlled converters and cycloconverters. Wiley, 1971
20. Holmes, P.G. Harmonic content and regulation of a cycloconverter output at high input frequencies. Leicester University Engineering Department Report 75-17.
21. White, D.C. and Woodson, H., Electromechanical Energy Conversion. Wiley, 1966.

22. Munoz, A. and Shepherd, W., Speed-change (2:1) induction motors driven by modulated supply voltages. Proc. IEE, Vol. 122, No. 3, 1975.
23. Fitzgerald, A.E. and Kingsley, C., Electrical Machinery. McGraw-Hill, 1961.
24. Martiny, W.J., McCox, R.M. and Margolis, H.B., Thermal relationships in induction motors. Trans. AIEE, 80, pp.66-77, 1971.
25. Alger, L., The nature of induction machines. Gordon & Breach, 1965.
26. Holmes, P.G. and Smith, G.A., Cycloconverter control of asynchronous and synchronous machine in single- and doubly-fed machine systems. Proc. 8th Universities Power Conference, Bath, 1973, pp.228-233.
27. Rissik, H., The Fundamental Theory of A.C. Converters. Chapman & Hall, 1939.
28. Bland, R.J., Factors affecting the operation of a phase-controlled cycloconverter. Proc. IEE, 114, pp.1908-1916, 1967.
29. Bird, B.M. and Ford, J.S., Improvements in phase-controlled circulating current cycloconverter using communication principles. Proc. IEE, 121, pp.1146-1149, 1974.
30. Miyairi, S., and Shioya, M., Gate control circuit for thyristor cycloconverter. Electrical Engineering in Japan, 88, 1965. pp.31-41.
31. Slabiak, W. and Lawson, L.J. Precise control of a three-phase squirrel-cage induction motor using a practical cycloconverter. Trans. IEEE, IGA, 2, 1966, pp.274-280.
32. Harrison, D. The dynamic braking of induction motors. Proc. IEE, 103, A, 1956, pp.121-133.
33. Bland, T.G. and Shepherd, W., "D.C. dynamic braking of induction motors with secondary capacitors!" Proc. IEE, 122, 1975, pp.163-167.

34. Dixon, F.F. and Tiley, G.L. "Low-frequency performance of a wound-rotor induction motor for mine hoist drives". AIEE Trans., 1957, pp.1140-1145.
35. Barkle, J.E. and Ferguson, R.W. "Induction generator theory and application". AIEE Trans., 73, pp.12-19, 1954.
36. McConnell, H.M. "A self-excited induction generator with regulated voltage". AIEE, Trans., 73, pp.279-295, 1954.
37. Erdelyi, E. and Kolatorowicz, E.E., "The limitations of induction generators in constant frequency aircraft systems". AIEE Trans., 77, pp.348-352, 1958.
38. De Carli, A. and Murgo, M., Mathematical model of amplitude and frequency controlled induction motor. Vol. 6, pp.535-544, Pergamon Press, 1970. Printed in Great Britain.
39. Rogers, G.J., Linearised analysis of induction motor transients, Proc. IEE, pp.1917-26, 1965.
40. Pfaff, G., Zur dynamic des asynchromotors bei drehzahlsteuerung mittels veranderlicher speisefrequenz, ETZ-A, 85, pp.719-724, 1964.
41. D Azzo, J.J., Houpis, C.H. "Feedback control systems analysis and synthesis". Text book published by McGraw-Hill, 2nd Edition.
42. Sensicle, A. Control Theory for Engineers. Blackie, 1968.

CHAPTER 10AppendicesPage

A1	Determination of Machine Parameters.	115
A2	Stability Dependence on Slip Analysis.	117
A3	Derivation of the Centre Co-ordinates and Radius of the Power and Var Limit Circle.	120
A4	Derivation of the System root-loci.	122

CHAPTER 10Appendix 1Determination of machine parameters

The machine parameters were determined from a series of locked-rotor and running-light tests carried out over a range of frequencies from 5 to 50Hz. A variable-frequency alternator driven by a d.c. shunt motor, the speed of which is controlled by half-controlled thyristor bridge, shown in Fig. (2.5) provided the three-phase induction motor supply. The machine used as the main experimental induction motor was a Mawdsley Educational Induction Motor with a 2-pole double layer stator winding and a squirrel-cage rotor. A further 4-pole, 3-phase Y-connected, 3 h.p., 200V, 9.5A squirrel-cage machine was used for the multi-machine system of Chapter 4.

Figures (2.15) and (2.12) shows the measured values obtained by a locked-rotor test and a running-light test, of total effective winding resistance, R_e , total effective reactance, X_e , magnetising reactance, X_o , and iron loss resistance, R_o , with all values referred in stator terms. The value of stator resistance was measured on a Wheatstone Bridge. The rotor resistance per phase referred in stator terms was then obtained as

$$R_2 = R_e - R_1.$$

It was assumed that the values of stator and rotor leakage reactance referred to the stator are equal. In a squirrel cage machine, the stator to rotor turns ratio is an arbitrary constant, taken for convenience as unit.

It can be seen from Fig. (2.15) that the value of $L_e = \frac{X_e}{\omega} = \frac{X_e}{2\pi f}$ varies with frequency. The stator to rotor mutual inductance

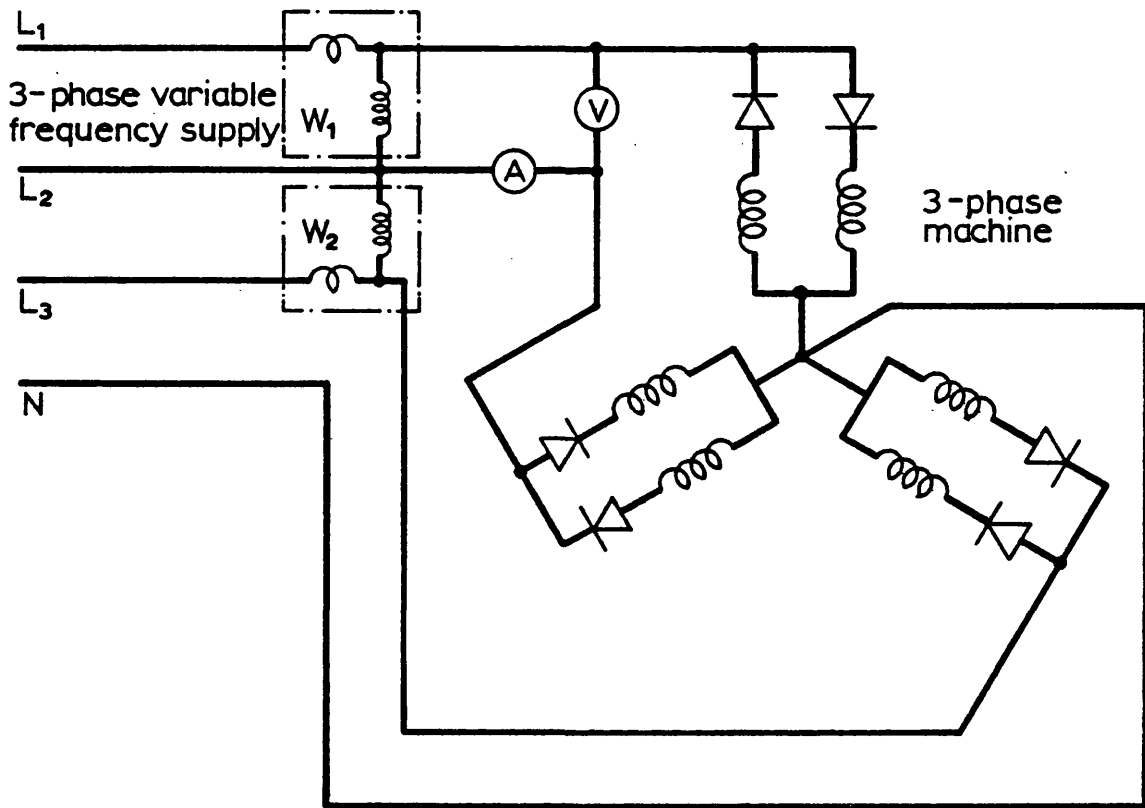


FIG.A.1. TEST CIRCUITS FOR THE DETERMINATION OF EQUIVALENT CIRCUIT PARAMETERS OF THE INDUCTION MOTORS WITH SEPARATED STATOR WINDINGS

$L_o = \frac{X_o}{\omega}$, where X_o is the value determined by experiment for one phase at 50Hz. The stator and rotor leakage inductances, $\ell_1 = \ell_2 = \frac{X_e}{2\omega}$, where X_e is the value determined by experiment for one phase at 50Hz. The 50Hz values for the two machines used are:

	Educational Induction Machine		Standard squirrel-cage Machine
R_1	0.55 Ω	r_1	0.58 Ω
R_2	1.07 Ω	r_2	0.45 Ω
$X_1=X_2$ $L_1=L_2$	0.59 Ω 0.101H	$x_1=x_2$	0.12 Ω
X_o L_o	31 Ω 0.988H	x_o	15 Ω

$$L_1 = \ell_1 + L_o ; \quad L_2 = \ell_2 + L_o.$$

All values given are referred to the stator.

Divided winding machine parameters were obtained by similar tests, but the stator windings of the machine were separated electrically and coupled magnetically as shown in Fig. (A.1). The parameters values at 50Hz are:

	Electrically separate stator windings, Educational Machine
R_1	1.1 Ω
R_2	1.07 Ω
$X_1=X_2$ $L_1=L_2$	0.59 Ω 0.101H
X_o L_o	31 Ω 0.0988H

Appendix 2

Stability dependence on slip analysis

From the equivalent circuit of Fig. (2.1) the impedance per phase is given by the equation,

$$Z = R_1 + j\omega L_1 + j\omega L_0 \frac{R_2 + j\omega_r L_2}{R_2 + j\omega_r (L_0 + L_2)}, \Omega \quad (\text{A2.1})$$

$$T_e = \frac{I_1^2 m P \omega_r L_0^2 R_2}{[R_2 + j\omega_r (L_0 + L_2)]^2}, \text{ Nm} \quad (\text{A2.2})$$

The steady state can be defined as follows;

Let power $P_e = \text{constant}$, where

$$P = V R_e I, \text{ watts} \quad (\text{A2.3})$$

where V and I are rms quantities. Then,

$$\frac{d(R_e |I|)}{dV} = - \frac{P}{V^2}, \Omega^{-1} \quad (\text{A.24})$$

Or,

$$\frac{dV}{d(R_e |I|)} = - \frac{P}{(R_e |I|)^2} \Omega.$$

Equation (A2.4) represents the small signal inphase admittance, and

$$R_e |dZ| = \frac{dV}{d(R_e |I|)}, \Omega^{-1} \quad (\text{A.25})$$

These equations show that the steady-state power relationship requires the small signal inphase admittance or impedance of the machine to be negative.

Equations (A2.1) and A2.2) were used by Bowler ⁽¹¹⁾ to provide the steady-state stability criterion which was achieved as follows;

Since the voltage to current relation in equation (A2.1) is a function of three variables,

$$dV = \frac{\partial V}{\partial I} dI + \frac{\partial V}{\partial \omega_r} d\omega_r + \frac{\partial V}{\partial \omega} d\omega, \quad V. \quad (\text{A2.6})$$

$$Z = \frac{\partial V}{\partial I} \text{ at any operating point and for small changes of slip.}$$

$$\partial V = \partial IZ. \text{ Then,}$$

$$dV = Z dI + I \frac{\partial Z}{\partial \omega_r} d\omega_r + I \frac{\partial Z}{\partial \omega} d\omega, \quad V. \quad (\text{A2.7})$$

Similarly,

$$\partial T_e = \frac{\partial T_e}{\partial I} + \frac{\partial T_e}{\partial \omega_r} d\omega_r, \quad N_m. \quad (\text{A2.8})$$

Now considering ω to be constant,

$$dV = \frac{\partial V}{\partial I} dI + \frac{V}{\partial \omega_r} d\omega_r \quad V.$$

At this steady-state operating point the torque variation was assumed to be zero as torque variation is one of the two variables which determines the steady-state. The second term in equation (A2.8), the speed, must then confirm to the bound of stability according to the sign of $R_e |dZ|$. Thus with $dT = 0$ we have from equation (A2.8),

$$d\omega_r = -dI \frac{\partial T_e}{\partial I} \cdot \frac{\partial T_e}{\partial \omega_r}, \quad \text{rad/sec.}$$

Solving equations (A2.7) and (A2.8) results in,

$$dZ = Z - I \frac{\partial Z}{\partial \omega_r} \times \frac{\partial T_e}{\partial I} \frac{\partial T_e}{\partial \omega_r}, \quad \Omega. \quad (\text{A2.10})$$

From equations (A2.1) and (A2.2) the partial derivation is,

$$\frac{\partial Z}{\partial \omega_r} = \frac{\omega L_o^2 R_2}{(R_2 + j\omega_r A L_o)^2} ,$$

where $A = 1 + \frac{L_2}{L_o} ,$

$$\frac{\partial T_e}{\partial I} = \frac{2 \text{Im} P \omega_r L_o^2 R_2}{(R_2 + j\omega_r A L_o)^2} , \quad (\text{A2.11})$$

$$\frac{\partial T_e}{\partial I} = \frac{\partial T_e}{I} , \quad (\text{A2.12})$$

and $\frac{\partial T_e}{\partial \omega} = \frac{\partial T_e}{\omega_r} \times \frac{R_2 - j\omega_r A L_o}{R_2 + j\omega_r A L_o} .$ (A2.13)

Substituting equations (A2.11), (A2.12) and (A2.13) in (A2.10) gives,

$$dZ = R_1 + j\omega L_1 + j\omega L_o \frac{R_2 - j\omega_r L_2}{R_2 - j\omega_r (L_o + L_2)} , \quad \Omega . \quad (\text{A2.14})$$

Inverting equation (A2.14) gives the small signal admittance,

$$dy = \frac{R_2 - j\omega_r A L_o}{(R_2 - j\omega_r A L_o)(R_1 + j\omega L_1) + j\omega L_o (R_2 - j\omega_r L_2)} , \quad \Omega^{-1} . \quad (\text{A2.15})$$

The real part of this equation is:

$$R_e dy = \frac{R_1 R_2^2 + R_2 \omega^2 S L_o (A L_1 + L_2) - \omega^2 L_o^2 S A (R_2 B - R_1 S A)}{[R_1 R_2 + \omega^2 S L_o (A L_1 + L_2)]^2 + \omega^2 L_o^2 (R_2 B - R_1 S A)^2} , \quad \Omega^{-1} .$$

where $B = 1 + \frac{L_1}{L_o} .$

Appendix 3

Derivation of the centre co-ordinates and radius of the power and var
limit circle

The induction generator limit circle is defined in equation (5.20) as,

$$(R_g + R_1)^2 + (X_g + X_1 + X_0)(X_g + X_3) = 0 . \quad (5.20)$$

The addition of $\frac{(X_g + X_1 + X_0)^2}{4}$ to both sides with a transposition of terms gives,

$$(R_g + R_1)^2 + \left(X_g + \frac{X_1 + X_0 + X_3}{2} \right) = -X_3(X_1 + X_0) + \frac{X_1 + X_0 + X_3}{4} = \left(\frac{X_0 + X_1 - X_3}{2} \right)^2 . \quad (A3.1)$$

A circular impedance locus can now be defined with centre co-ordinates,

$$-R_1; \quad -\frac{(X_1 + X_0 + X_3)}{2} \quad \text{and radius} \quad \frac{(X_1 + X_0 - X_3)}{2} .$$

Equation (A3.1) can now be used to introduce power and var terms as

$$P_g + jQ_g = \frac{V_1^2}{R_g - jX_g} , \quad (A3.2)$$

and then,

$$R_g = \frac{P_g V_1^2}{P_g^2 + Q_g^2} , \quad (A3.2)$$

$$\text{and} \quad X_g = \frac{Q_g V_1^2}{P_g^2 + Q_g^2} . \quad (A3.3)$$

If equations (A3.2) and (A3.3) are substituted into equation (A3.1), the limit circle equation becomes,

$$\left[\frac{P_g V_1^2}{P_g^2 + Q_g^2} + R_1 \right]^2 + \left[\frac{Q_g V_1^2}{P_g^2 + Q_g^2} + X_1 + X_0 \right] \left[\frac{Q_g V_1^2}{P_g^2 + Q_g^2} + X_3 \right] = 0 . \quad (\text{A3.4})$$

Equation (A3.4) expands to give,

$$\frac{V_1^2}{P_g^2 + Q_g^2} + \frac{V_1^2 2R_1 P_g}{P_g^2 + Q_g^2} + \frac{V_1^2 [X_1 + X_0 + X_3] Q_g}{P_g^2 + Q_g^2} + R_1^2 + (X_1 + X_0) X_3 = 0 . \quad (\text{A3.5})$$

The terms of equation (A3.5) are multiplied by $P_g^2 + Q_g^2$ and divided by $R_1^2 + (X_1 + X_0) X_3$, giving,

$$\left[P_g + \frac{V_1^2 R_1}{R_1^2 + (X_1 + X_0) X_3} \right]^2 + \left[Q_g + \frac{V_1^2 \{X_1 + X_0 + X_3\}}{2[R_1^2 + (X_0 + X_1) X_3]} \right]^2 = \frac{V_1^4 [X_1 + X_0 - X_3]^2}{4[R_1^2 + (X_1 + X_0) X_3]^2} . \quad (\text{A3.6})$$

Hence from equation (A3.6) the limit circle has centre co-ordinates,

$$-\frac{V_1^2 R_1}{R_1^2 + (X_0 + X_1) X_3} ; \quad -\frac{V_1^2 [X_0 + X_1 + X_3]}{2[R_1^2 + (X_0 + X_1) X_3]} \quad \text{and a radius,} \quad \frac{V_1^2 [X_0 + X_1 - X_3]}{2[R_1^2 + (X_0 + X_1) X_3]} .$$

Appendix 4

Derivation of the system root-loci

The root locus is a graph of the roots of the characteristic equation of a closed-loop system as a function of the gain. It is a relatively easy method of determining graphically the effect of loop gain adjustment in the system.

Suppose a simple closed-loop control system has a forward transfer function, $G(s)$, and a feedback transfer function, $H(s)$. For non-unity feedback, the open- and closed-loop transfer functions of the system will be given by $G(s)H(s)$, and $\frac{G(s)}{1 + G(s)H(s)}$, respectively. The system response is determined by the roots of the characteristic equation, $1 + G(s)H(s) = 0$. The root-locus technique is based on the fact that the poles (the roots of the characteristic equation) of the closed-loop transfer-function are related to the poles and zeros of the open-loop transfer-function and the gain.

Consider the open-loop transfer function of the cycloconverter-induction motor drive represented by Fig. (5.18), then

$$G(s)H(s) = \frac{PA\omega_{oo} K_2 \frac{1}{CR_1}}{J(s+d) [s^2 + sa + b]} \quad (A4.1)$$

The factorisation of the second term in the denominator gives,

$$G(s)H(s) = \frac{PA\omega_{oo} K_2 \frac{1}{CR_1}}{J(s+d) \left[s + \frac{-a + \sqrt{a^2 - 4b}}{2} \right] \left[s + \frac{-a - \sqrt{a^2 - 4b}}{2} \right]} \quad (A4.2)$$

In the complex plane, equation (A4.2) has the following poles and zeros;

$$\text{poles; } s = -d \quad ; \quad s = \frac{-a \pm \sqrt{a^2 - 4b}}{2} \quad ;$$

$$\text{zeros; } s = 0.$$

These poles and zeros are shown on the argand diagram of Fig. (5.23). They determine the roots of the characteristic equation and of the closed-loop system defined by $1 + G(s)H(s) = 0$. The locus that describes the roots of the closed-loop characteristic equation can be obtained by any one of a number of methods. In this work the general nature of the locus has been determined by a standard text method ⁽⁴²⁾. The rules of the method are as follows;

(a) The number of branches of the root-locus is equal to the number of poles of the open-loop transfer-function. This system has three branches.

(b) A point on the real axis lies on the locus if the total number of poles and zeros to the right of the point on the real axis is odd. There is a real axis locus between the real pole and the real zero.

(c) The locus starting points at a gain of 0 are at the open-loop poles and the locus ending points at a gain of ∞ are at the open-loop zero and infinity. This completely determines the real axis branch of the locus. Since there is only one zero, the locus end points for the branch which start at the complex poles must be at infinity.

(d) The angle which the asymptotes of the root locus make with the real axis is given by;

$$\lambda = \frac{(1+2K) 180^\circ}{\text{number of poles of } G(s)H(s) - \text{number of zeros of } G(s)H(s)}$$

(A4.3)

For the system under consideration

$$\lambda = \frac{(1+2K) 180^\circ}{3-1} = (1+2K) 90^\circ .$$

Hence, for $K = 0$, $\lambda = + 90^\circ$

$$K = \pm 1, \lambda = + 270^\circ, -90^\circ$$

$$K = \pm 2, \lambda = + 450^\circ, -270^\circ, \text{ and}$$

the asymptotes make an angle of $\pm 90^\circ$ with the real axis.

(e) The real axis intercept of the asymptotes is given by,

$$\sigma_e = \frac{\boxed{\text{sum of the real parts of all poles}} - \boxed{\text{sum of the real parts of all zeros}}}{\boxed{\text{number of poles}} - \boxed{\text{number of zeros}}}$$

for the system under consideration,

$$\sigma_e = \frac{\frac{1}{CR_2} + a}{2} = \frac{d + a}{2} .$$

(f) The angles by which the locus departs from the complex poles and zeros is given by,

$$180^\circ = \boxed{\text{All the angles of the vectors from all the other poles and zeros to the pole or zero in question}}$$

In the system under consideration the approximate angle of departure is indicated. This is sufficient to obtain the root-locus sketches given in Fig. (5.23). The exact location of the locus would have to be obtained by a numerical solution. However, the root-locus sketches give a useful qualitative analysis of the system.

Appendix 5Fig. A.2 Side view of cycloconverter and machines

Left to right torque and speed recording pen recorder, divided winding machine coupled to d.c. load machine (under bench), cycloconverter (at rear), torque transducer (on bench), Ward-Leonard loading machine, standard induction machine (rear front).

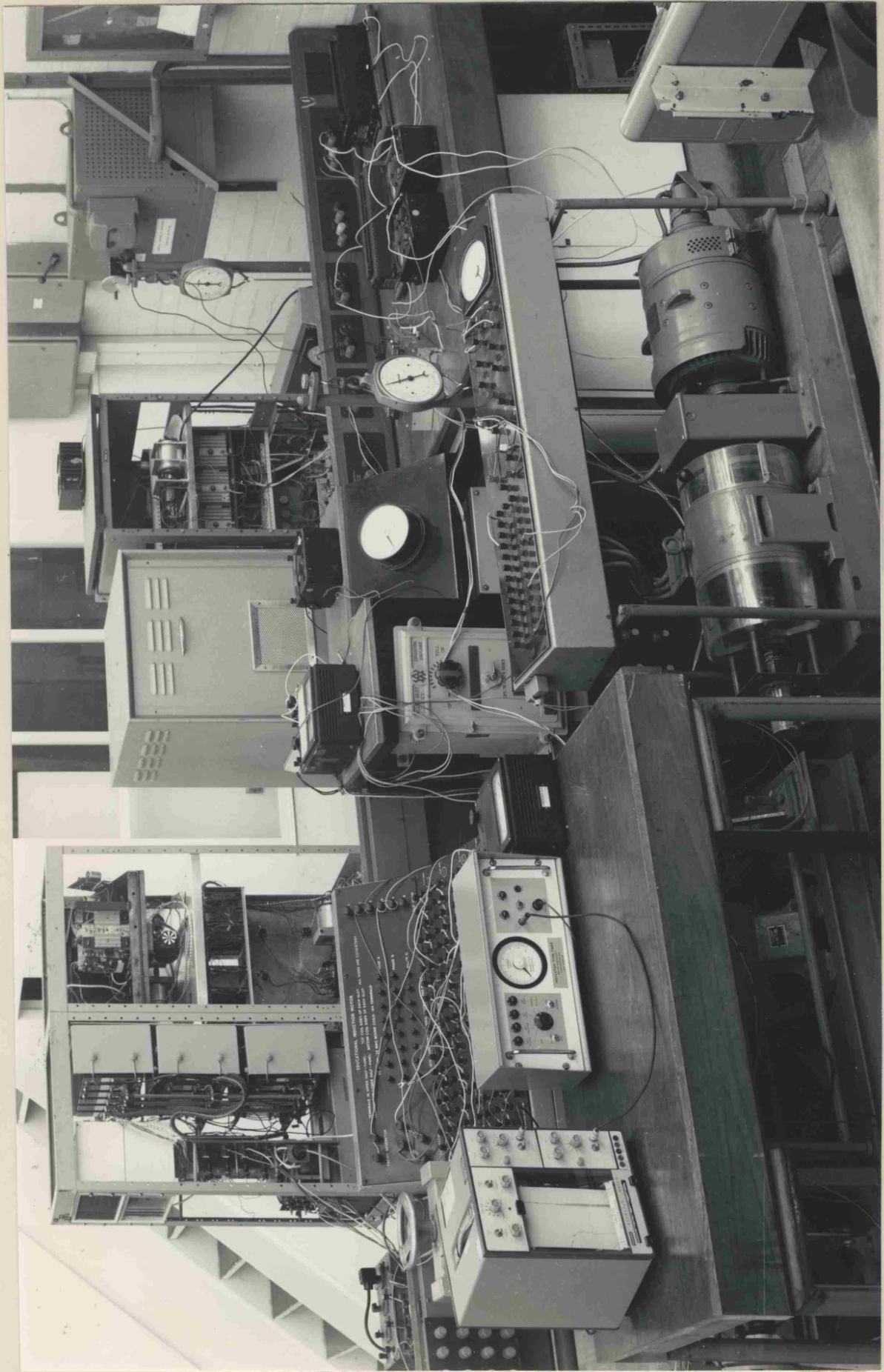
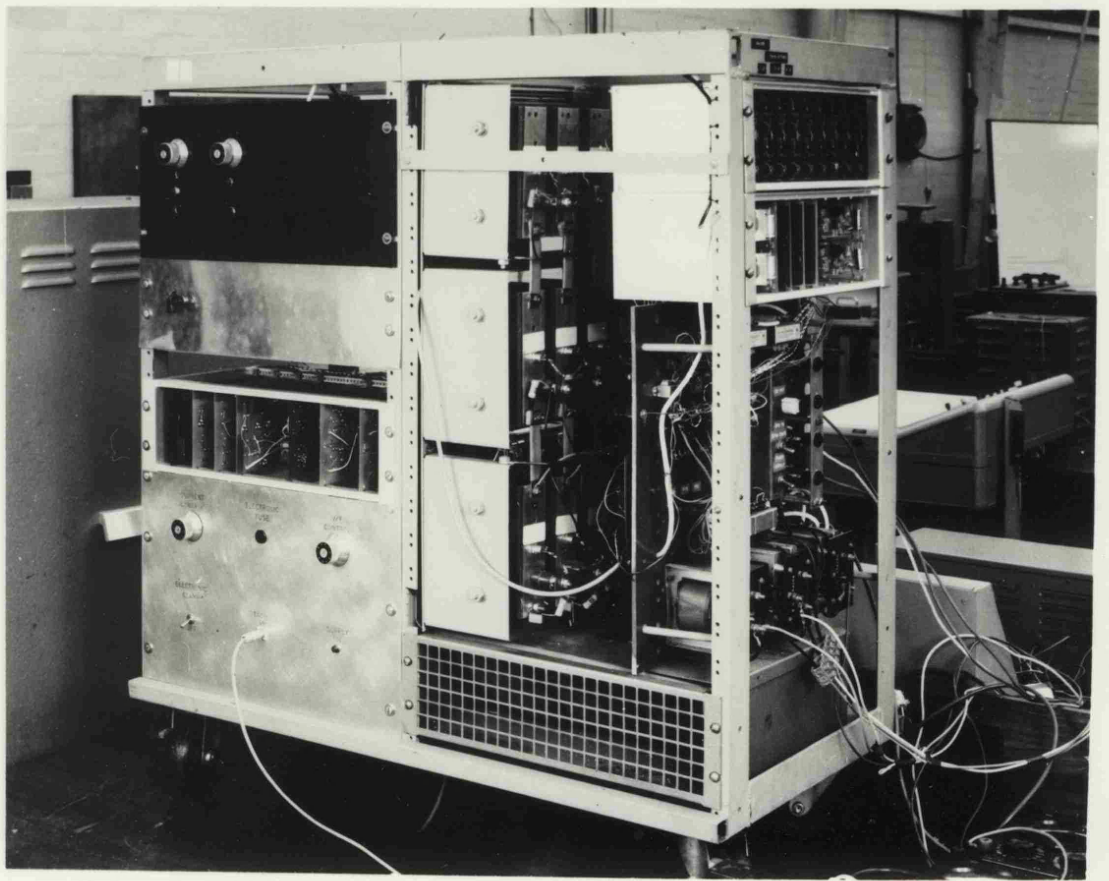
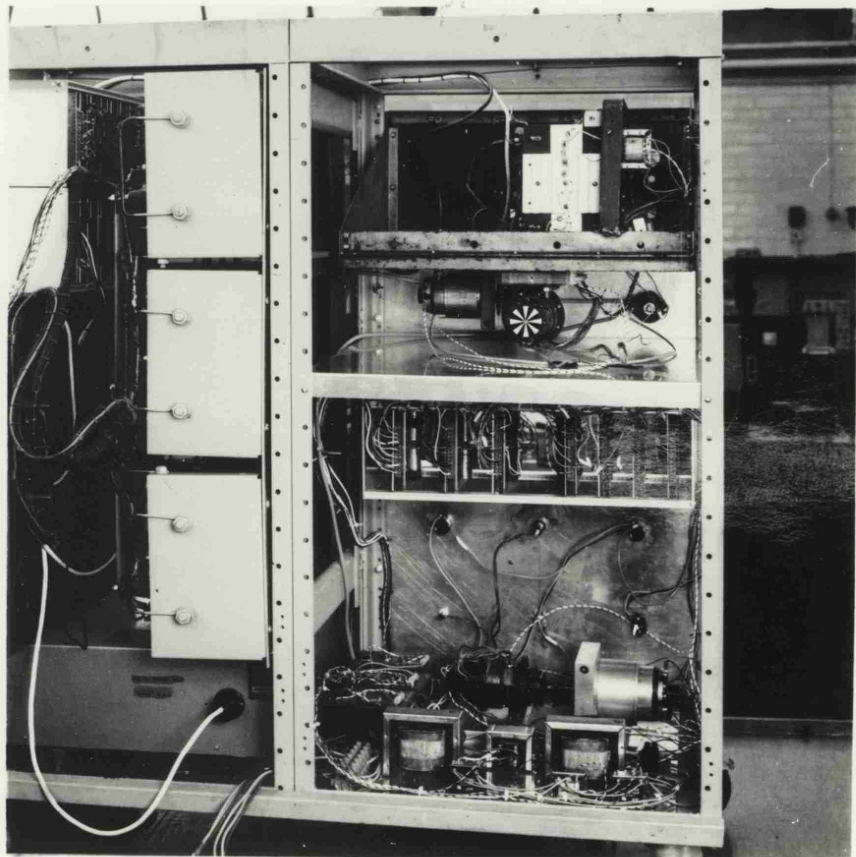


Fig. A2 Side view of cycloconverter and machines

CYCLOCONVERTER CIRCUITRY
SHOWING REFERENCE SCHEMATICS



CYCLOCONVERTER FRONT ELEVATION



CYCLOCONVERTER REAR ELEVATION
SHOWING REFERENCE GENERATORS

FIG. A 3


ABSTRACT

The cycloconverter as a direct frequency converter without a d.c. link is well known as a power amplifier in low speed a.c. drives. If continuous circulating current operation can be maintained, reversible energy flow and regenerative braking can be achieved in an induction motor drive without a change in the gate pulse sequence. Continuous circulating current operation also reduces the output harmonic content of the cycloconverter and increases the speed range of the drive.

This dissertation describes the use of an induction motor stator as an inter-group reactor maintaining continuous circulating current in the cycloconverter. The same stator winding sets up the conventional rotating air gap-flux and the reactor machine has standard torque-speed characteristics.

In the multi-machine drive designed and constructed in this work, one machine requires a special stator winding. Conventional squirrel-cage machines can then be added for tandem speed control and the utilisation of copper improved. Closed-loop speed control and air gap flux control are incorporated on the reactor machine. The standard induction motors added in addition to the reactor machine are shown to be essentially operating under open-loop conditions but a "hard supply" is maintained by closed-loop control.